# Coexistence of communication systems based on enhanced multi-carrier waveforms with legacy OFDM Networks

Quentin Bodinier

**ANNÉE 2017**

UNIVERSITÉ DE RENNES 1

UNIVERSITE BRETAGNE LOIRE

**THÈSE / UNIVERSITÉ DE RENNES 1**
*sous le sceau de l'Université Bretagne Loire*

pour le grade de

**DOCTEUR DE L'UNIVERSITÉ DE RENNES 1**

*Mention: STIC – Télécommunications/Traitement du Signal*

**École doctorale MATHSTIC**

présentée par


# Quentin Bodinier

Préparée à l'UMR 6164 - IETR (Équipe SCEE)
Institut d'Électronique et de Télécommunications de Rennes
au sein de CentraleSupélec


---

# Coexistence of Communication Systems Based on Enhanced Multi-Carrier Waveforms with Legacy OFDM Networks

**Thèse soutenue à Rennes le 29 novembre 2017**

devant le jury composé de :

**Ana Isabel Pérez-Neira**
Pr. à UPC, Barcelone / *rapportrice*

**Jean-Marie Gorce**
Pr. à INSA Lyon / *rapporteur*

**Sofie Pollin**
Ass. Pr. à KU Leuven/ *examinatrice*

**Nicola Marchetti**
Ass. Pr. à Trinity College Dublin / *examinateur*

**Jean-Baptiste Doré**
Ing. R&D, Ph.D., à CEA LETI / *examinateur*

**Didier Le Ruyet**
Pr. à CNAM, Paris / *examinateur*

**C. Faouzi Bader**
Ass. Pr. à CentraleSupélec / *encadrant*

**Jacques Palicot**
Pr. à CentraleSupélec / *directeur de thèse*

# Remerciements

Comme tout travail personnel, ce manuscrit ne l'est que très peu; il est d'abord et avant tout le reflet de moments partagés, de rencontres fortuites et d'idées échangées avec les personnes dont j'ai eu la chance de croiser le chemin au cours de ces dernières années.

Mes premiers remerciements vont à mon encadrant, Carlos Faouzi Bader, pour m'avoir donné l'opportunité d'effectuer un stage d'abord, puis une thèse au sein de l'équipe SCEE de CentraleSupélec. De Carlos je retiendrai d'abord la sincère bienveillance et la volonté de me faire profiter d'autant d'opportunités que possible. Auprès de lui, j'aurai aussi appris une intransigeance qui me pousse encore aujourd'hui à toujours relever mon niveau d'exigence envers mon travail. Enfin et surtout, je retiendrai son amitié, sa confiance et sa joie sincère à voir ses étudiants réussir. Pour tout cela, je lui suis infiniment reconnaissant.

Je tiens à remercier Jean-Marie Gorce et Ana Perez Neira d'avoir rapporté ma thèse, ainsi que Sofie Pollin, Didier Le Ruyet, Nicola Marchetti et Jean-Baptiste Doré de l'avoir examinée. Je suis honoré par leur lecture de mon travail et leur participation à mon jury.

Je remercie aussi Jacques Palicot, pour avoir accepté de diriger ma thèse, et étend mes remerciements aux membres de l'équipe SCEE. J'ai une pensée particulière pour Vincent Gouldieff, Vincent Savaux, Malek, Amor, Pascal, Lilian, Rami, Muhammad, Navik, Haïfa et tous les autres que j'aurais pu oublier, en espérant qu'ils ne m'en tiennent pas rigueur. Je remercie aussi particulièrement Karine Bernard, notre secrétaire, pour son soutien.

Ma thèse fut pour moi l'occasion de voyager, à Barcelone tout d'abord, au CTTC, où j'ai eu la chance d'être accueilli un mois au sein du groupe d'Ana Perez Neira dans le cadre du programme Newcom#. Je suis très reconnaissant envers Ana Perez Neira de m'avoir accueilli, puis d'avoir accepté de rapporter ma thèse. Je remercie aussi Marius Caus ainsi que Musbah Shaat pour leur accueil et leur collaboration fructueuse lors de mon séjour Barcelonais.

J'ai aussi eu la grande chance de travailler à plusieurs reprises avec le laboratoire CONNECT au Trinity College Dublin, depuis mon stage de master alors que le laboratoire se nommait encore CTVR, jusqu'à nos différentes visites mutuelles tout au long de ma thèse. Je remercie Linda Doyle d'avoir créé une équipe aussi ouverte et accueillante, qui m'a fait me sentir chez moi dès mon premier jour en tant que simple stagiaire lors de l'été 2014. Mes

remerciements vont ensuite bien sûr à Luiz Da Silva, pour son accueil répété, ses conseils éclairés lors de nos collaborations, et sa sincérité. CONNECT a de la chance d'avoir quelqu'un d'aussi brillant et bienveillant à sa tête. Je ne pourrais bien sûr pas oublier Nicola Marchetti. Merci à lui pour son amitié, les parties de ping-pong, et sa participation à mon jury de thèse. Merci à Hamed Ahmadi, mon responsable de master à Trinity College, pour son amitié et sa confiance répétée à de multiples reprises depuis. Merci à Arman pour notre collaboration fructueuse et pour m'avoir appris les mille et une façns de marquer depuis le gardien au baby-foot. Merci aussi à Conor, à qui je dois une grande partie des résultats présentés dans cette thèse. J'ai apprécié chacunes de nos collaborations, et chacun de nos whisky partagés, à Dublin comme à Washington DC. Merci enfin à Danny d'être un vrai Irlandais, à Francisco pour son amitié, et à Jacek pour les bons moments partagés à Dublin comme à Kuala Lumpur.

Je ne pourrais terminer ces remerciements sans un mot pour ma famille. Je pense d'abord à mes parents, qui m'ont toujours soutenu et encouragé à entreprendre de nouveux défis. Merci de m'avoir poussé à toujours accomplir plus que je ne pensais le pouvoir. A ma soeur Julie ensuite, dont je suis très fier d'être le petit frère. Je lui souhaite beaucoup de bonheur, entourée de son mari Aurélien et de Nathan, qui fait de moi un oncle comblé.

Merci enfin à Inès, pour sa tendresse et son soutien inconditionnels, qui m'ont porté jusqu'à l'écriture de ces lignes. N'hebek.

## Abstract

Future wireless networks are envisioned to accommodate the heterogeneous needs of entirely different systems. New services obeying various constraints will coexist with legacy cellular users in the same frequency band. This coexistence is hardly achievable with OFDM, the physical layer used by current systems, because of its poor spectral containment. Thus, a myriad of multi-carrier waveforms with enhanced spectral localization have been proposed for future wireless devices. In this thesis, we investigate the coexistence of new systems based on these waveforms with legacy OFDM users. We provide the first theoretical and experimental analysis of the inter-system interference that arises in those scenarii. Then, we apply this analysis to evaluate the merits of different enhanced waveforms and we finally investigate the performance achievable by a network composed of legacy OFDM cellular users and D2D pairs using one of the studied enhanced waveforms.



## Résumé

Les futurs réseaux sans fil devront être conçus pour répondre aux besoins hétérogènes de systèmes entièrement différents. De nouveaux services soumis à des contraintes variées coexisteront avec les utilisateurs actuels sur la même bande de fréquences. L'OFDM, la couche physique utilisée par les systèmes actuels, souffre d'un mauvais confinement spectral et ne permet pas cette coexistence. De nombreuses nouvelles formes d'onde avec une localisation spectrale améliorée ont donc été proposées. Nous étudions la coexistence de nouveaux systèmes basés sur ces formes d'onde avec des utilisateurs OFDM préexistant. Nous fournissons la première analyse théorique et expérimentale de l'interférence inter-système qui se produit dans ces scenarios. Nous appliquons ensuite cette analyse pour évaluer les performances de différentes formes d'ondes avancées et nous étudions finalement les performances d'un réseau où des utilisateurs cellulaires OFDM coexistent avec des paires D2D utilisant l'une des formes d'ondes améliorées étudiées.

# List of Figures

# List of Tables

# Nomenclature

**Acronyms and abbreviations**

| | |
|---|---|
| 3G | 3rd generation of communication networks |
| 3GPP | 3rd Generation Partnership Project |
| 4G | 4th generation of communication networks |
| 5G | 5th generation of communication networks |
| 5GNOW | 5th Generation Non-Orthogonal Waveforms for Asynchronous Signalling |
| ACCENT5 | Advanced Waveforms, MAC Design and Dynamic Radio Resource Allocation for Device-to-Device in 5G Wireless Networks |
| AI | Artificial Intelligence |
| AIM | Asynchronous Interference Modeling |
| ANR | Agence Nationale de la Recherche |
| AWGN | Additive White Gaussian Noise |
| BER | Bit Error Rate |
| BLT | Balian-Low Theorem |
| CDMA | Code Division Multiple Access |
| CFO | Carrier Frequency Offset |
| COQAM | Circular OQAM |
| CP | Cyclic Prefix |
| CR | Cognitive Radio |
| CU | Cellular User |
| CUE | Cellular User Equipment |

| | |
|---|---|
| CVX | Matlab Software for Disciplined Convex Programming |
| D2D | Device To Device |
| DSA | Dynamic Spectrum Access |
| DUE | D2D User Equipment |
| DVB-T | Digital Video Broadcasting-Terrestrial |
| EMPhAtiC | Enhanced Multicarrier Techniques for Professional Ad-Hoc and Cell-Based Communications |
| EPA | Extended Pedestrian A |
| ETU | Extended Typical Urban |
| EVM | Error Vector Magnitude |
| f-OFDM | Filtered OFDM |
| FB-MC | Filter Bank Multi-Carrier |
| FBMC/PAM | Filter Bank Multi Carrier with PAM |
| FDMA | Frequency Division Multiple Access |
| FFR | Fractional Frequency Reuse |
| FFT | Fast Fourier Transform |
| FMT | Filtered Multi-Tone |
| GFDM | Generalized Frequency Division Multiplexing |
| GUI | Graphical User Interface |
| ICI | Inter Carrier Interference |
| IFFT | Inverse Fast Fourier Transform |
| IoT | Internet of Things |
| IQR | Inter-Quartile Range |
| ISI | Inter Symbol Interference |
| ISM | Industrial, Scientific and Medical |
| ITU-R | International Telecommunication Union Radiocommunication Sector |
| LO | Local Oscillator |
| LPWAN | Low Power Wide Area Network |
| LTE | Long Term Evolution |

| | |
|---|---|
| LTE-M | LTE for Machines |
| LTE-U | LTE Unlicensed |
| M2M | Machine to Machine |
| MAC | Medium Access Control |
| METIS | Mobile and wireless communications Enablers for the Twenty-twenty Information Society |
| MMSE | Minimum Mean Square Error |
| MNO | Mobile Network Operator |
| MTC | Machine Type Communications |
| NB-IoT | Narrow Band-IoT |
| NMSE | Normalized Mean Square Error |
| OFDM | Orthogonal Frequency Division Multiplexing |
| OFDM/OQAM | Offset QAM OFDM |
| OFDMA | Orthogonal Frequency Division Multiple Access |
| OOB | Out Of Band |
| OSA | Opportunistic Spectrum Access |
| PAM | Pulse Amplitude Modulation |
| PAPR | Peak to Average Power Ratio |
| PHY | PHYsical |
| PHYDYAS | PHYsical layer for DYnAmic Spectrum access and cognitive radio |
| PLC | Power Line Communication |
| PPM | Parts Per Million |
| PPP | Poisson point process |
| PROFIL | Evolution de la PROfessional Mobile Radio large bande basée sur la modulation FILter Bank MultiCarrier |
| PSD | Power Spectral Density |
| PUSCH | Physical Uplink Shared Channel |
| QAM | Quadrature Amplitude Modulation |
| QoSMOS | Quality of Service and MObility driven cognitive radio Systems |

| | |
|---|---|
| RA | Resource Allocation |
| RB | Resource Block |
| SC-FDMA | Single Carrier FDMA |
| SCEE | Signal, Communications and Embedded Electronics |
| SINR | Signal to Interference plus Noise Ratio |
| SMS | Short Message Service |
| SNR | Signal to Noise Ratio |
| SU | Secondary User |
| TDMA | Time Division Multiple Access |
| TO | Timing Offset |
| TSE | Time-Spectral Efficiency |
| TVWS | TV White Space |
| UE | User Equipment |
| UF-OFDM | Universal Filtered OFDM |
| UFMC | Universal Filtered Multi-Carrier |
| VR | Virtual Reality |
| Wi-Fi | Wireless Fidelity |
| WONG5 | Waveforms MOdels for Machine Type CommuNication inteGrating 5G Networks |
| ZF | Zero Forcing |

**General notations**

| | |
|---|---|
| (x.x) | Reference to equation (x.x) |
| [xx] | Citation referring to [xx] in bibliography |
| **bold** | Emphasis |
| *italic* | Term referring to a specific notion in the literature |

### Mathematical notations

| | |
|---|---|
| $\cdot * \cdot$ | Convolution product |
| $\hat{\cdot}$ | Estimate of $\cdot$ |
| $\mathfrak{I}\{\cdot\}$ | Imaginary part of $\cdot$ |
| $\lfloor x \rfloor$ | Integer part of $x$ |
| $\lfloor x \rfloor^+$ | $\max(0, \lfloor x \rfloor)$ |
| $\lvert\cdot\rvert$ | Absolute value of $\cdot$ |
| $\mathbb{N}$ | Set of natural integers |
| $\mathbb{R}$ | Set of real numbers |
| $\mathbb{Z}$ | Set of all integers |
| $\mathbf{X}$ | Matrix |
| $\mathbf{x}$ | Vector |
| $\mathbf{X}^H$ | Hermitian Matrix of $\mathbf{X}$ |
| $\mathcal{F}\{\cdot\}$ | Fourier Transform of $\cdot$ |
| $\mathcal{X}$ | Set |
| $\mathfrak{R}\{\cdot\}$ | Real part of $\cdot$ |
| $x$ | Scalar |

### Units

| | |
|---|---|
| dB | decibel |
| Hz | hertz |
| s | second |

# Contents

# Résumé étendu en français

## Chapitre 1: Introduction générale

Alors que les usages des technologies de communication sans fil se multiplient, les réseaux de télécommunication font face à une hétérogénéité d'usages sans précédent. Jusqu'ici, chaque génération de réseaux a été mise en point en réponse à des usages spécifiques, mais la 5G devra répondre à des besoins diversifiés. En effet, au côté des utilisateurs cellulaires classiques apparaissent de nouveaux types d'objets communiquant, à l'aune de ce qu'il est désormais devenu courant d'appeler l'Internet des Objets. Il est évident que les besoins d'un utilisateur cellulaire, concentré principalement sur l'obtention d'un débit de plus en plus important, sont intrinsèquement opposés à ceux d'un objet connecté, pour lequel les contrainte ne s'expriment pas tant en débit à atteindre qu'en autonomie et en durée de vie à supporter.

La communauté scientifique s'accorde à dire que les réseaux actuels, basés sur une structure centralisée et parfaitement synchronisée, ne sont pas à même de satisfaire les besoins hétérogènes d'utilisateurs coexistant de manière non coordonnée et asynchrone. En particulier, il est connu que la couche physique des réseaux actuels, basée sur l'*Orthogonal Frequency Division Multiplexing* (OFDM) qui souffre d'une très mauvaise localisation fréquentielle, est très peu résistante aux asynchronismes et nécessite donc que des mesures de resynchronisation soient mise en place par le réseau, généralement par un échange de signaux pilotes qui nuisent à l'efficacité spectrale du réseau.

Afin de dépasser les limitations de l'OFDM, un grand nombre de travaux se sont concentés sur l'élaboration de nouvelles formes d'onde basées sur des bancs de filtres (FB-MC), mieux localisées en fréquence et donc mieux adaptés à la coexistence entre utilisateurs asynchrones sur des bandes spectrales adjacentes. En particulier, de nombreuses recherches ont étudié la possibilité d'insérer des communications 5G basées sur les FB-MC dans des espaces fréquentiels laissés libres par les utilisateurs OFDM classiques. Dans ces travaux, nous nous penchons sur ce problème et proposons d'étudier la thèse suivante: *La coexistence asynchrone et non coordonnée entre communications OFDM classiques et nouveaux utilisateurs peut être*

*facilitée si ces derniers utilisent des formes d'onde FB-MC.* En particulier, nous présentons les contributions suivantes:

1. Nous menons une analyse détaillée de l'interférence émergent entre un système OFDM et un système FBMC coexistant. Nous remettons en cause les modèles couramment utilisés dans la littérature et proposons un modèle analytique exact de l'interférence créee par un utilisateur FB-MC sur un utilisateur OFDM.
2. Nous présentons un banc de test de radio logicielle que nous utilisons pour démontrer la validité de notre modèle théorique.
3. Nous évaluons les performances de multiples formes d'onde FB-MC dans un contexte de coexistence spectrale, et démontrons que les gains apportés par l'utilisation de formes d'onde FB-MC pour la coexistence avec des systèmes OFDM ont été largement surévalués dans la littérature.
4. Nous appliquons ces résultats à un scénario de coexistence entre utilisateurs D2D et utilisateurs cellulaires classiques.

## Chapitre 2: Contexte et problématique

Dans ce chapitre, nous introduisons les notions de traitement de signal et communication numériques nécessaires à la compréhension des travaux présentés dans la suite de ce document. Nous y présentons notamment les principes fondamentaux des formes d'onde multiporteuse telles que l'OFDM et de la modélisation des canaux de propagation radio.

Nous introduisons ensuite deux scénarios de coexistence actuels. Tout d'abord, nous présentons le cas des *TV White Spaces* comme exemple des scénarios de Radio Intelligente et de coexistence. En particulier, nous montrons que l'OFDM ne peut pas être facilement utilisée dans ces scénarios, ses émissions hors bande ne respectant pas les masques spectraux imposés par les utilisateurs primaires. Nous présentons ensuite le cas de l'insertion de communication directe entre utilisateurs, *Device to Device* (D2D). Ce type de déploiement, que nous étudions largement dans ces travaux, entraîne nombre de problématiques liées à l'asynchronisme entre utilisateurs qui en résulte, ce qui en fait un parfait cas d'application pour les formes d'onde FB-MC.

Dans la suite de ce chapitre, nous nous attelons à décrire et comparer les différentes formes d'onde FB-MC étudiées dans cette thèse, présentant à la fois leur modèle mathématique commun et leurs performances théoriques. Ce tour d'horizon nous permet d'identifier trois problèmes de recherches ouverts que nous nous proposons de résoudre, à savoir:

1. Etant donné un déploiement où un utilisateur FB-MC et un utilisateur OFDM coexistent sur des fréquences adjacentes, comment modéliser l'interférence qu'ils créent l'un sur l'autre ?

2. En appliquant la réponse à la question précédente à un scénario de radio intelligente dans lequel l'utilisateur primaire utilise l'OFDM, quels sont les gains à espérer si le réseau secondaire utilise les FB-MC ?

3. Enfin, dans le cas où des utilisateurs secondaires D2D coexistent de manière asynchrone avec un réseau OFDM, quels sont les gains que permet d'obtenir l'utilisation des FB-MC par les D2D ?

## Chapitre 3: Etat de l'art et contributions

Ce chapitre est dévolu à l'étude de l'état de l'art concernant les trois questions introduites en fin de chapitre 2. Nous nous intéressons tout d'abord aux méthodes de modélisation de l'interférence entre systèmes coexistant présentée dans la littérature. Nous identifions deux aproches de modélisation de l'interférence entre systèmes coexistant: la plus couramment répandue tout d'abord, basée sur l'étude de la densité spectrale de puissance (DSP) du signal intérférent, dont nous montrons qu'elle ne prend pas en compte de potentiels asynchronismes entre les systèmes; puis, une approche alternative, modélisant l'asynchronisme entre utilisateur secondaire et primaire uniquement dans le cas où ceux-ci utilisent la même forme d'onde. Cette étude nous permet d'affirmer qu'aucun modèle n'étudie de manière satisfaisante la coexistence asynchrone entre un utilisateur FB-MC et un utilisateur OFDM.

Nous étudions ensuite les différentes études expérimentales reportées dans la littérature, et démontrons que la plupart repose sur des métriques haut niveau et qu'aucune d'entre elles n'est capable de fournir de résultats reproductibles au niveau de la couche physique permettant d'appréhender de manière claire l'interférence crée par un émetteur FB-MC sur un récepteur OFDM. Enfin, nous montrons que la majorité des travaux étudiant des scénarios de radio intelligente et/ou de communication D2D néligent l'importance de la forme d'onde exploitée par les utilisateurs primaires, se concentrant uniquement sur les caractéristiques des transmissions secondaires. Ces différentes observations servent de base à nos travaux, dont les résultats sont présentés dans les trois chapitres suivants.

## Chapitre 4: Analyse de l'interférence entre CP-OFDM et formes d'onde FB-MC

Dans ce chapitre, nous introduisons tout d'abord la modélisation du système que nous nous proposons d'étudier afin d'analyser l'interférence générée entre un utilisateur FB-MC et un utilisateur OFDM coexistant. Nous présentons ensuite notre modèle mathématique générique des formes d'onde FB-MC, et sa paramétrisation correspondante pour chaque forme d'onde particulière étudiée. Nous présentons ensuite notre approche basée sur l'observation de l'amplitude moyenne du vecteur d'erreur (EVM). Nous démontrons par simulation que les résultats basés sur l'observation de l'EVM diffèrent drastiquement des résultats de la littérature basés sur la DSP, montrant un niveau d'interférence jusqu'à 60 dB plus élevé qu'attendu.

Après avoir expliqué en détail les raisons des limitations du modèle basé sur la DSP, nous détaillons notre raisonnement mathématique et présentons une forme analytique générique permettant d'approximer avec un très bon niveau de précision l'interférence créée par n'importe quelle forme d'onde FB-MC sur un récepteur OFDM. Nous pratiquons d'abord notre analyse sur canal Gaussien, puis l'étendons au cas des canaux faiblement sélectifs en fréquence. Dans ces deux cas, nous démontrons la validité de notre approche théorique par simulation. Nous nous proposons ensuite de valider expérimentalement nos résultats. Pour ce faire, nous présentons un banc de test de radio logicielle basée sur trois plateformes *Universal Software Radio Peripheral* (USRP), l'une jouant le rôle d'utilisateur secondaire FB-MC tandis que les deux autres établissent une chaîne de transmission OFDM. Les résultats expérimentaux que nous montrons, obtenus à l'aide d'un logiciel développé par nos soins, attestent une fois de plus la validité de notre analyse théorique.

## Chapitre 5: Etude de scénarios de radio intelligente impliquant une coexistence avec des systèmes CP-OFDM primaires

Dans ce chapitre, nous nous basons sur les résultats obtenus au chapitre 4 pour étudier un scénario de radio intelligente classique, où un utilisateur secondaire FB-MC coexiste avec un utilisateur primaire OFDM. Plus particulièrement, nous nous intéressons à trois problèmes classiques et, pour chacun de ces problèmes, comparons les résultats obtenus grâce à notre modèle basé sur l'EVM à ceux prédits par le modèle basé sur la DSP de la littérature.

Tout d'abord, nous nous penchons sur le dimensionnement des bandes de garde nécessaires au respect d'une contrainte d'interférence établie par l'utilisateur primaire. Nous montrons que malgré la localisation spectrale avancée des formes d'onde FB-MC, celles-ci ne peuvent que très peu réduire le besoin en bandes de garde, ce qui contredit la littérature pertinente.

Nous observons des résultats de même nature dans un scénario où l'utilisateur secondaire est capable d'adapter son allocation de puissance afin d'optimiser son débit tout en limitant l'interférence créée sur l'utilisateur primaire. Enfin, nous montrons que, bien que l'efficacité temporelle améliorée de certaines formes d'onde FB-MC leur permettent de mieux exploiter certaines opportunités de transmission de courte durée, les gains restent faibles par rapport à ceux présentés dans la littérature. Dans l'ensemble, ces trois études démontrent que dans le cas où un seul utilisateur secondaire est considéré, l'utilisation des FB-MC revêt peu d'intérêt.

## Chapitre 6: Etude de communications D2D asynchrones dans les réseaux 5G

Dans ce dernier chapitre de contributions, nous étendons nier.otre étude à un scénario impliquant de multiples utilisateurs secondaires. Pour ce faire, nous considérons un scénario où un cluster d'utilisateurs D2D coexiste avec un réseau cellulaire OFDM en réutilisant une partie des ressources spectrales de ce dernier. Nous démontrons que dans un tel cas, le problème d'optimisation du débit des utilisateurs D2D est rendu complexe par les liens d'interférence entre paires d'utilisateurs asynchrones. Dans le cas où ces derniers utilisent les FB-MC plutôt que l'OFDM, ces liens d'interférence sont rendus négligeables. Nous montrons que le processus d'allocation de ressources peut dès lors être grandement simplifié dans le cas où les D2D utilisent les FB-MC.

Forts de ce résultat, nous étendons notre étude en menant une campagne de simulations système nous permettant de mesurer les performances atteignables par le réseau lorsque les utilisateurs D2D utilisent différentes formes d'onde FB-MC. Nous montrons que l'utilisation de formes d'onde FB-MC est particulièrement intéressante dans les cas où les D2D sont distribués en clusters denses, et que ces formes d'ondes permettent de faciliter la coexistence entre utilisateurs D2D et cellulaires.

## Chapitre 7: Conclusions et perspectives

Les travaux de cette thèse s'inscrivent dans une longue lignée de recherches sur les formes d'onde alternatives à l'OFDM. Nous nous sommes particulièrement intéressés aux cas de coexistence hétérogène entre systèmes FB-MC et OFDM. Nous avons proposé le premier modèle analytique de l'interférence causée par les formes d'onde FB-MC sur un récepteur OFDM. Ce faisant, nous avons démontré que contrairement aux résultats disponibles dans la littérature, l'utilisation de FB-MC ne réduit que très peu l'interférence causée sur les utilisateurs OFDM.

# Chapter 1

# General Introduction

**Contents**



## 1.1 Background and Motivations

### 1.1.1 From 4G to 5G: a road towards heterogeneity

What a century to live in ! As digital technology becomes ever more pervasive, we are surrounded by new exciting applications which can only awaken everyone's inner child: Internet of things (IoT) , Virtual Reality (VR), 8K video streaming, Artificial Intelligence (AI), Big Data, and so much more. But this abundance of new technologies is not just exciting. It will be disruptive and profoundly affect the way we live, make business, think and relate to each other. Though all these technological fields may seem uncorrelated at first glance, it soon appears that they all rely on one key element : information. Without falling into the cliché "data is the new oil", we can clearly identify that information, under different forms, is becoming the main source of value, to such an extent that companies whose only assets are their user base are now more valued than former leading industrial giants. Following this, all the new technologies that are being put under the floodlights can be seen as ways to produce (Internet of Things, Crowd-sourcing), process (Big Data, Artificial Intelligence) or consume (Virtual Reality, Video streaming) information.

All these arising applications are bound to affect the telecommunication networks needed to transmit the associated information in a twofold way. On the one hand, the abundance of new usages and data-greedy applications will increase the global burden of communication networks. This implies that new techniques are needed in order to improve their raw performance, through the enhancement of well known metrics such as the achievable data rate or spectral efficiency. Even though this is a significant challenge, it is an iterative one, well in line with the classical issues that have been tackled at each shift from one generation of communication networks to the next. On the other hand, the fact that future networks will need to cope with a wide array of applications makes them holistically different from the current systems. There is a major consensus that the next generation of wireless networks (5G) will not be an incremental step on top of 4G, but that networks will need to be fully redesigned to cope with new requirements, in particular with the unprecedented heterogeneity it will bring, [1, 2]. Indeed, communication networks have typically been dimensioned to answer a single specific use-case in the form of cellular communications. Therefore, wireless networks which have so far accommodated *homogeneous* users will have to answer *heterogeneous* needs and use cases in the near future, in particular with the development of 5G.

As a matter of fact, each generation of wireless networks was specifically thought and designed to tackle one particular application : in short, the first generation was designed to support voice communication, the second introduced additional services like Short Message Service (SMS), and the third generation (3G) enabled mobile web browsing. Finally, the main goal of 4G networks has been to increase the data rate compared to 3G systems in order to enable more bandwidth-consuming use-cases such as video streaming or online playing. It is clear that each of these steps was focused on increasing the connectivity between the core network and the users mobile terminals, as the latter have long been the only devices connected to the network. However, as stated here above, this paradigm is currently changing: as information exchanges become ever more ubiquitous, the use cases involving wireless networks are multiplying. IoT is probably the most telling example, with thousands of objects being progressively connected to the Internet through wireless networks. It is clear that the new communications introduced by IoT obey a set of constraints which are entirely different than those which must be met by classical cellular communications to enable applications such as phone calls or video streaming. Therefore, the variety of new use cases will translate to a myriad of different communication types with heterogeneous goals and constraints.

As a case in point, we present in Fig. 1.1 in the form of a radar chart a non-exhaustive list of potential use cases that 5G networks are expected to enable [2–4]. For each of the considered use-cases, we rate the relevance of five particular technical issues : the necessity to achieve a high data rate, the communication latency, energy efficiency, robustness of communications to asynchronism and the distance coverage that is necessary. This figure illustrates clearly the fact that future networks will have to deal with a myriad of heterogeneous communication

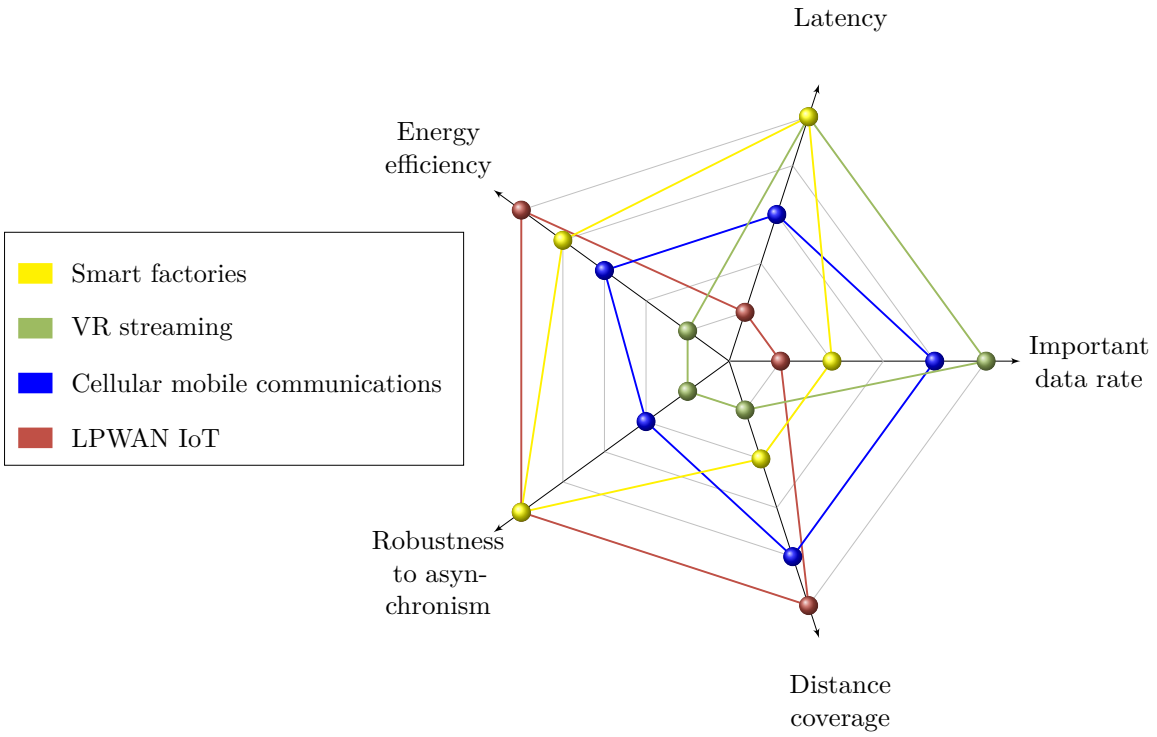


Figure 1.1: Radar chart representing some of the foreseen 5G use cases and the relevance of several technical challenges for each of them from 1 (hardly relevant) to 5 (key issue). It appears clearly that different use cases need to fulfill different and sometimes opposed constraints. For example, low power wide area networks (LPWAN) IoT and VR streaming, which are obviously holistically different applications, have entirely opposed constraints: in the case of VR streaming, communications would typically be happening at short range, and the key design factors are the high needed data rate and the latency which should be kept very low. On the opposite, LPWAN IoT networks are composed of battery-powered nodes that transmit sparse short packets at random times. Moreover, their signal has to be received by a gateway which can be multiple kilometers away. Therefore, the main constraints on these systems are their energy efficiency, their robustness to asynchronism and their distance coverage, while latency and data rate are not relevant. These extreme examples illustrate the fact that 5G networks will need to encompass use cases that are opposed both in terms of objectives and constraints.

types which obey different constraints that are even in some cases contradictory. For example, classical cellular mobile communications obey to moderate constraints in terms of latency, robustness to asynchronism or energy efficiency and distance coverage. Some other use cases have more extreme constraint sets in which some parameters are key issues while some others are irrelevant. For example, the rate and latency are not an issue for LPWAN IoT networks, whereas energy efficiency is critical as IoT nodes are expected to be able to last ten years on a single battery. In the case of some critical machine type communications (MTC), for example in smart factories for autonomous manufacturing control, latency and robustness to asynchronism are key issues, while the constraint on energy efficiency can be relaxed. Finally, if we consider an extreme case of high rate media delivery, for example VR streaming, the main issues lie in achieving an extremely high data rate as well as a very low delay in order to ensure a satisfying user experience. Obviously in that case, neither distance coverage nor energy efficiency are limiting parameters.

### 1.1.2 Coexistence in heterogeneous networks

Having clearly stated that the wireless networks of tomorrow will have to deal with heterogeneous applications, it is crucial to fully understand what the main consequences of this new paradigm will be. To do so, one must wonder if such heterogeneous needs can be fulfilled by a unique integrated flexible network or if the future landscape of wireless networks will be composed of several different specialized networks, each of them serving a peculiar need. In the recent years, there has been a new push from standardization committees to integrate new services in current long term evolution (LTE) networks, with the 3GPP most famously proposing new standards in the form of narrow-band IoT (NB-IoT) and LTE-M, [5, 6]. Nevertheless, one is forced to concede that most normalization efforts have so far been weakened by the abundance of arising standards that have been developed by private interests and which, for some of them, have been crowned with commercial success. There again, IoT gives the most telling example, as dozens of standards have already been effectively deployed, some of them such as Sigfox or LoRa being very well established. This shows that, given the heterogeneity of needs of future communications and the current landscape, it is unlikely that wireless networks will converge towards a single normalized and centralized architecture. In fact, there is a growing consensus that future networks will need to be versatile to take advantage of the different technologies being under development [1, 7, 8].

If the wireless networks of tomorrow are to be composed of different systems serving different needs, this brings in the issue of the *coexistence* of all these systems. In particular, one has to wonder where in the radio spectrum to accommodate the services which will be newly introduced in the future. On this peculiar issue of spectrum repartition, regulation agencies have so far adopted a rather conservative stand and the current situation can be

roughly sketched as follows : most of the radio spectrum is granted to a sole entity, for example a mobile network operator (MNO), which enjoys an exclusive right to exploit the frequency bands that have been allocated to them. Only portions or the radio spectrum are effectively free of licensing and can be used by virtually anyone. Industrial, Scientific and Medical (ISM) bands are of course the main examples of such free bands. Interestingly, this freedom of exploitation has given rise to an important deployment of technologies, the leading example being of course Wi-Fi, operating in 2.4 GHz and 5 GHz ISM bands. One can also think of the multitude of home automation standards operating at 434 MHz or the currently leading LPWAN solutions, SigFox and LoRa which both operate in the 868 MHz band in Europe.

To summarize, at least as far as civilian communications are concerned, we clearly see two different types of ecosystems and actors: on one side, the "exclusive" ecosystem of MNOs which each own a certain part of the spectrum and are therefore intrinsically protected from potential interferers, whereas on the other side, a lot of independent players coexist in a "cohabitation" environment, mainly on the ISM bands. A fundamental observation which is at the core of this thesis is that, under the new impulse imposed by the fore-coming heterogeneity, this bipolar situation will soon come to an end. As a matter of fact, the border between these two worlds has already started fading, as some new initiatives are currently emerging. The most famous example of this evolution is the definition of the LTE-unlicensed standard (LTE-U) by the 3GPP, which aims at deploying LTE services, in particular small cells, in the 5GHz ISM band [9]. This will create new, unprecedented coexistence issues between LTE and other standards such as Wi-Fi.

In this thesis, we make a strong case that in the future wireless networks, coexistence issues are bound to multiply. This is due to different reasons, both technical and economic, which we summarize shortly here. First, as we previously mentioned, some private operators have not waited for standardization and new use cases foreseen for 5G are already being deployed in the ISM bands. Nevertheless, because these bands represent a small aggregated bandwidth, uncoordinated services deployed in them may be subject to high interference and the ISM spectrum may well be insufficient to cope with the massive rise in communication volume that we expect to see. This gives a significant motivation to allow the coexistence of wireless services in other bands than the ones that are currently dedicated to ISM. Furthermore, the ever increasing role of unlicensed bands faces historical MNOs with a fierce and unprecedented competition. Indeed, their historical business model is quite simple: MNOs used to buy spectrum licenses at very high cost in spectrum auctions and, in turn, make profit out of that spectrum by giving a right to use it to end users, typically through a monthly subscription. However, an increasing share of communications are now taking place away from the bands these MNOs own, which clearly represents a shortfall for the latter [10]. Moreover and quite ironically, the spectrum that MNOs have paid a fortune for is, on average, largely underused

at a given time and place [11–13]. This represents a high opportunity cost, and we therefore assert that it is in the best interest of MNOs, in the future, to allow coexistence of different wireless communication systems in the spectral bands they own.

### 1.1.3 Thesis scope

Based on the discussion presented here above, in this thesis, we are interested in the coexistence of heterogeneous communication systems, and we aim in particular at evaluating whether it is feasible to insert new services in spectral bands that are so far reserved for classical cellular communications. This kind of coexistence can be enabled through different approaches. For example, coexistence between WiFi and LTE-U is made possible thanks to intricate sensing algorithms at the MAC level [14].

One key assumption of the presented work is that, if legacy cellular networks allow 5G services to reuse part of their allocated band, there can be no intricate cooperation or synchronism procedure being involved, as this would dramatically increase the global amount of overhead signaling in the network. However, orthogonal frequency division multiplexing (OFDM) the waveform that is used at the PHY layer of most currently deployed standards (LTE, Wi-Fi, digital video broadcasting terrestrial (DVB-T)) is known to be very sensitive to asynchronism [15, 16] and therefore perform poorly in scenarios where multiple systems coexist without synchronization [17]. The main drawback of OFDM that has been pointed out lies in its very high out-of-band (OOB) emissions [18]. Overall, the limitations of OFDM have been the subject of a wide range of recent works in the last decade as both the research community and industrials have clearly identified its weaknesses in the asynchronous coexistence scenarios that will, as we justified here above, multiply in the coming years. Therefore, a significant amount of new waveforms with enhanced spectral localization compared to OFDM have been proposed to replace the latter. In fact, changing the waveform used by future communication systems has been a very prolific stream of research in the course of the development of 5G, [19].

In the context of this thesis, we focus particularly on filter bank multi-carrier (FB-MC), a family of waveforms that has drawn a significant amount of attention in the recent years [20–22]. These waveforms are capable of achieving very advantageous spectral localization and are therefore thought to be particularly well adapted for asynchronous coexistence scenarios, as we exemplify in Fig. 1.2 in which we present a typical coexistence scenario in which an *incumbent* wireless system leaves part of, its allocated band unused, leaving a free space in the spectrum which could potentially be reused by another *secondary* system to establish communication. However, if the secondary system uses OFDM, its large sidelobes leak onto the band reserved to the incumbent system, whereas if a FB-MC waveform is used instead, the secondary signal can be effectively contained in the band that is reserved to the former.

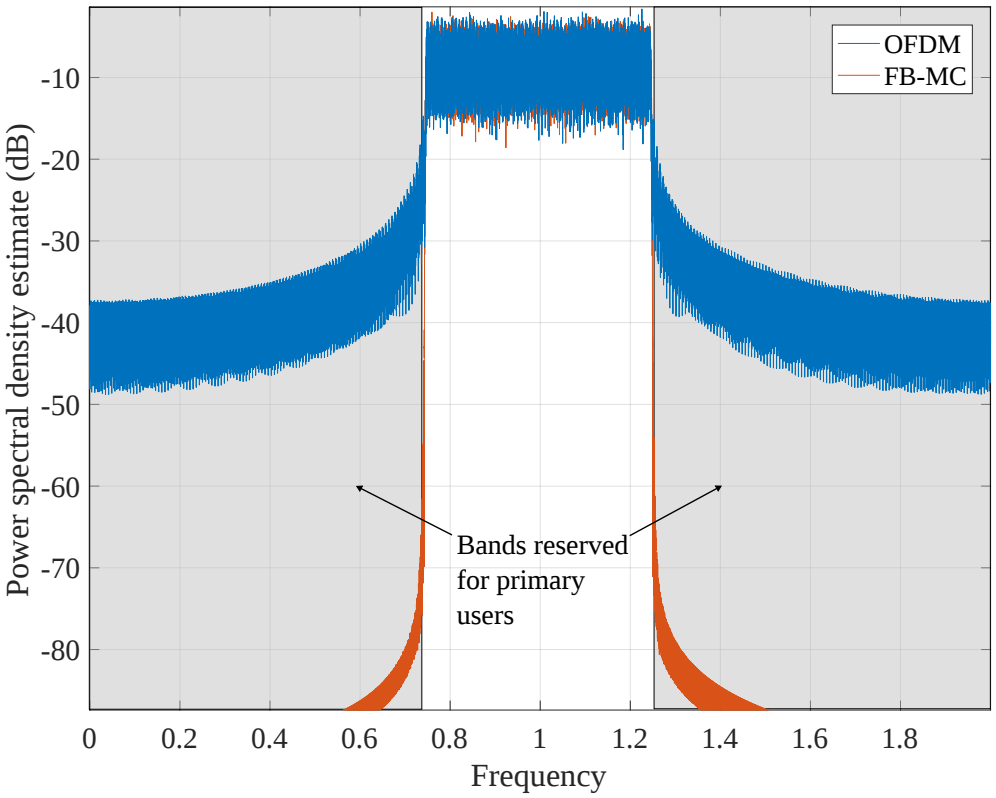


Figure 1.2: Typical example of the alleged superiority of FB-MC to OFDM in coexistence scenarios: in such a setup, in which a system occupies only part of the spectral band while leaving portion of it unused, OFDM fails to efficiently use the freed space because of its high out of band emissions. On the contrary, some FB-MC waveforms, thanks to their enhanced spectral localization, effectively contain their emissions in the band they are assigned. FB-MC based systems are therefore thought to be more efficient to reuse parts of the spectrum left free by incumbent licensed users.

In conclusion, the core assessment at the root of the work presented in this document is that wireless networks of tomorrow will be heterogeneous ones, in which multiple different systems will coexist in an asynchronous and uncoordinated manner on the same spectral band. In particular, we assert that future services introduced with 5G deployments will most likely coexist with legacy users on the spectral bands currently used for today's communications, either LTE-A cellular communications, Wi-Fi or DVB-T. In fact, we can model all these networks as OFDM-based incumbent systems, in which we try to insert new 5G secondary services. Moreover, based on the observation that OFDM is not well adapted for insertion of secondary systems because of its poor spectral localization, we are interested in seeing what are the gains to achieve if the newly introduced services rely on an alternative FB-MC waveform in replacement to OFDM. Therefore, we formulate the following thesis:

*"Asynchronous and uncoordinated coexistence of legacy OFDM-based communications and new services can be facilitated if the latter use enhanced FB-MC waveforms."*

## 1.2 Objectives and Contributions

In the present document, we propose to evaluate the thesis stated here above to either confirm or invalidate it and quantify the gains that are achievable if future wireless services that will coexist with current cellular communications are based on a FB-MC waveform in replacement of OFDM. To do so, we pursue the following objectives:

1. We thoroughly analyze inter-system interference that is created when a FB-MC system and an OFDM one coexist on the same spectral band. We make the observation that the models currently available in the literature to perform this analysis are not satisfying and inaccurate. Based on this, we provide the first exact model of interference arising between and OFDM and FB-MC users coexisting the same band of the radio spectrum.

2. In order to confirm our analysis which differs from the results so far available in the literature, we design and implement a software radio testbed able to rate with an unmatched accuracy the interference caused by an FB-MC system on an OFDM receiver. We show that empirical results validate our analysis.

3. Based on the derived interference model, we evaluate the performance of several FB-MC waveforms in the context of multiple typical coexistence scenarios. Based on our study, we are able to determine that the gains brought by FB-MC in the context of coexistence with OFDM legacy systems have been highly overestimated in the literature.

4. We apply the derived results to the specific use-case of coexistence of device-to-device (D2D) communications with classical cellular devices. D2D is one of the use cases to be implemented in 5G which is likely to involve significant issues in terms of asynchronous coexistence, which makes our work particularly relevant to that kind of application. On this topic, we are able to demonstrate that using enhanced FB-MC waveforms instead of OFDM for D2D communications can significantly facilitate the necessary resource allocation procedures. Besides, we study the coexistence of D2D and cellular systems for a large number of FB-MC waveforms through system-level simulations.

## 1.3 Thesis outline

This thesis is composed of six chapters in addition to the present one, which follow a linear progression as detailed here:

### Chapter 2: Background and problem statement.

In this chapter, we introduce the different notions that are necessary to build our work upon and we review the different works available in the literature on the topics of interest to this thesis. We explain the concept of multicarrier waveforms, in particular OFDM and OFDMA systems and the networks that rely on that technique. Furthermore, we introduce cognitive radio and how it relates to the problem studied in this thesis. Based on this, we explain the impulse from the community in favor of new waveforms with enhanced spectral localization. We therefore give an in-depth review of FB-MC waveforms that have been proposed in 5G and that we will study in this thesis. Building on the laid out background, we present at the end of this chapter the main research problems that are still open and that we propose to answer.

### Chapter 3: Related work and contributions

In this chapter, we review the works available in the literature that are directly relevant to the open problems pointed out in Chapter 2. In particular, we give an in-depth review of works addressing the issue of interference modeling between coexisting systems. By presenting the shortcomings of the different approaches of the literature, we lay the basis of the work undertaken in this thesis, and detail the organization of our study.

### Chapter 4: Analysis of interference between CP-OFDM and FB-MC waveforms

This chapter presents the core contributions of this thesis. We analyze in details the interference that arises between one user that uses OFDM and a user that uses FB-MC. To do so, we present a generic system model that we use to derive the closed-form expressions of interference. Furthermore, we validate these closed-forms through an experimentation on a software radio testbed, and compare our results with the models available in the literature. The main contributions of this chapter are therefore as follows:

- We give analytical expressions of the interference arising between FB-MC and OFDM users coexisting on adjacent resources of the same spectral band.
- We validate these expressions for a large number of FB-MC waveforms.
- We present a software radio testbed which we use to validate our analysis.

The works detailed in this chapter have been presented in conference papers [C2, C4][1] and partially in [C5], as well as in one journal article [J2]. They have also been the subject of one demonstration [D1], and have been partially included in one technical deliverable [TR1].

### Chapter 5: Coexistence with CP-OFDM incumbent systems in CR setups

In this chapter, we build upon the interference model derived in Chapter 4 to quantify the performances achieved by one FB-MC secondary user when coexisting with OFDM incumbent systems, according to the specific FB-MC waveforms. In particular, we study the three following problems: first, we establish the size of the guard band that is necessary between the secondary and the incumbent to offer a satisfying level of protection to the latter. Then, we consider a rate optimization problem in which the secondary systems aim at finding the optimal power allocation that maximizes their achieved rate while respecting a maximum interference constraint on the incumbent. Finally, we consider a scenario in which the secondary system aims at maximizing the total amount of data it can transmit in a given time frame, and compare the results achieved by different FB-MC waveforms. The works we present in this chapter have been published in a condensed version in two conference papers [C3, C5] and partially in [C6]. Presented results have also been included in two technical deliverables [TR1, TR2].

### Chapter 6: Asynchronous D2D operation in 5G networks

In this last contribution chapter, we apply the different studies led in Chapters 3 and 4 to evaluate the performances achieved by a network in which two services coexist on the same spectral band. Namely, we study the coexistence of FB-MC based D2D users with cellular devices which can be seen as OFDM incumbent systems. In addition to studying the performance of such a network through extensive simulations both in the mono-cellular and multi-cellular context, we explore how the change of waveform at the PHY layer can be beneficial at the MAC layer, in particular to simplify the resource allocation procedure. The works presented in this chapter are the fruit of a close collaboration between SCEE and CONNECT research center, Trinity College Dublin, Ireland. They have been presented in one conference paper [C1], one journal article currently under review [J1], and have been included in [TR2].

[1] All the publications of the author are listed in Appendix D

### Chapter 7: Conclusions and perspectives

In this final chapter, we summarize the work we have undertaken and we recall our main contributions. Furthermore, we also point out its limitations which pave the way to further research directions that we have not yet undertaken. Finally, we conclude by discussing the future perspectives for enhanced multicarrier waveforms.

### Appendices

In addition to the main content, this manuscript contains four appendices:

- **Appendix A** details some mathematical derivations related to chapter 4.
- **Appendix B** briefly presents the testbed on which the experiment presented in chapter 4 is run.
- **Appendix C** presents the structure of the network-level simulator used in section 6.3.
- **Appendix D** lists the publications the author has contributed to during his Ph.D.

# Chapter 2

# Background and problem statement

**Contents**



## 2.1 Introduction

In this chapter, we introduce notions that are fundamental to fully comprehend the works reported in this thesis. We organize our presentation as follows : in section 2.2 we review some digital communication basics, with a particular focus on multi-carrier waveforms, especially OFDM and its application in some current wireless networks. In section 2.3 we introduce in details the idea of coexistence in wireless networks and the concepts of cognitive radio

and opportunistic spectrum access. We explain the shortcomings of OFDM in coexistence scenarios and particularly in two scenarios that we will tackle in this thesis, namely cognitive radio (CR) networks and coexistence of D2D communications with cellular devices. Having detailed the limitations of OFDM, we introduce in section 2.4 the different enhanced multi-carrier schemes that we will consider in this thesis. Finally, we conclude this chapter in section 2.5 by laying out the different research questions that we propose to answer in this thesis.

## 2.2 Review on current wireless networks

### 2.2.1 Digital communications background

Before coming to the core contents of this chapter, we introduce some key necessary notions related to digital communications, with a particular focus on multicarrier waveforms.

#### Digital communication chain

Though there exists a multitude of different types of digital transmission techniques, they all share a common architecture which we detail in the following. We represent in Fig. 2.1 the generic diagram corresponding to the digital transmission chain of a user $i$. First, bits corresponding to the data to transmit are generated and form the vector $\mathbf{b}_i$. Note that one of the main issues in digital communication lies in the fact that bits directly generated from data are usually not independent and identically distributed (i.i.d.) as real data exhibits a significant amount of correlation. Think for example of the bits encoding two adjacent pixels of a same picture. However, as Shannon famously taught us in [23], it is crucial to transmit i.i.d data to achieve the full capacity of the wireless channel. The task of ensuring that transmitted data is in fact i.i.d. is performed in wireless devices through the interleaver and scrambler processing stages. These elements are out of scope of this thesis, and we therefore assume that the bits transmitted by user $i$, $\mathbf{b}_i$, are in fact i.i.d. In particular, this means that we do not consider any coding technique all throughout our study.

The generated bits are then mapped onto a complex constellation and packed into a vector of complex symbols $\mathbf{d}_i$ which is itself composed of i.i.d. elements. The latter are then modulated to a signal $\mathbf{s}_i$ by the waveform modulation block. This processing stage is at the core of the present thesis and will therefore be discussed in details later in this chapter. Note that, in this thesis, we will refer to some of the signals presented in Fig. 2.1 both in their discrete sampled version and in their continuous version. For example, $s_i$ is the continuous time counterpart of the discrete signal $\mathbf{s}_i$ defined as $s_i(t)|_{t=n\tau_s} = \mathbf{s}_i[n]$ where $\tau_s$ is the used sampling period. Once modulated, the transmit signal passes through an RF processing chain

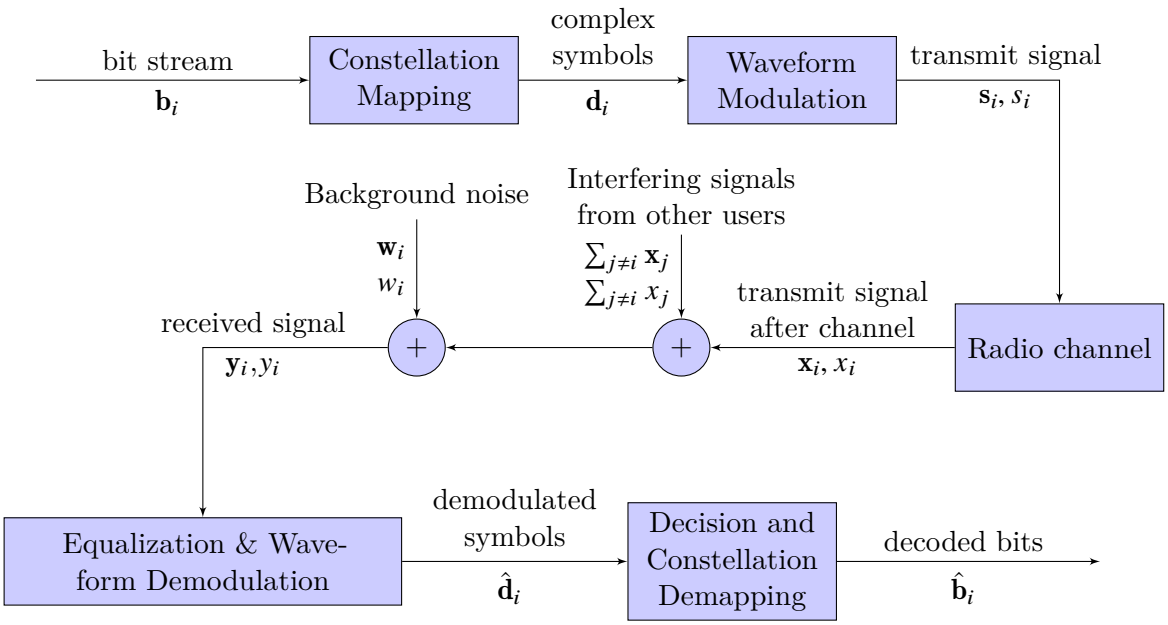


Figure 2.1: Block diagram of the generic digital communication system where we only represent processing blocks that are relevant in this thesis.

that is out of the scope of this thesis and therefore not represented. Moreover, we devise all our analysis at the baseband level, and therefore do not consider any carrier frequency. Besides, note that, in this thesis, we do not consider multi-input multi-output (MIMO) and therefore assume that both the transmitter and receiver use only one antenna.

Once transmitted, the signal propagates through the wireless channel the modeling of which we will detail in the next subsection. Moreover, as we see in Fig. 2.1, all signals from potential neighboring users add up to the useful signal and may interfere onto the latter. At the reception stage, the electronic noise is classically modeled as a white gaussian process which adds up to the total received signal. At the receiver end, we once again omit all RF architecture. Furthermore, all throughout this thesis, we assume that the receiver and transmitter of interest are perfectly synchronized, both in time and frequency. Therefore, though we acknowledge that synchronization acquisition is a key issue in wireless systems implementation, we deliberately leave it out of the scope of this study.

In Fig. 2.1, we represent in a single block the equalization and waveform demodulation because these two operations can be performed jointly. The goal of the waveform demodulation is to perform the opposite operations to those performed at the waveform modulation level in order to retrieve the complex symbols that have been transmitted. However, these symbols are affected by the propagation through the channel. The purpose of the equalization procedure is to revert the effects of the latter. Note that, usually, the transfer function equivalent to the channel is not known at the receiver and must be estimated. Nevertheless, channel estimation

is a complex procedure that is dependent on the used waveforms and has fostered a wide range of works, that are out of the scope of this thesis. All along our study, unless stated otherwise, we will therefore consider that channel estimation is perfect. We will introduce classical equalization procedures later in this chapter.

After the equalization and demodulation procedures, the receiver of user $i$ obtains the vector of demodulated symbols $\hat{\mathbf{d}}_i$. The demodulated symbols can be expressed as

$$\hat{\mathbf{d}}_i = \mathbf{d}_i^{\text{opt}} + \boldsymbol{\eta}_i, \tag{2.1}$$

where $\mathbf{d}_i^{\text{opt}}$ represents the optimal values that would be achieved in absence of any noise or interference and $\boldsymbol{\eta}_i$ is the error vector of user $i$. There exists a variety of metrics to study the latter. In this thesis, we will mainly use error vector magnitude (EVM) and the normalized mean square error (NMSE) defined as

$$\mathbf{EVM}_i = \sqrt{\frac{|\boldsymbol{\eta}_i|^2}{P_{\text{opt}}}}, \tag{2.2}$$

$$NMSE_i = E\left\{\mathbf{EVM}_i^2\right\}, \tag{2.3}$$

where $P_{\text{opt}}$ is the power of the optimal reference signal, which is typically equal to the variance of the reference constellation. The EVM is a vector that represents the power of the error vector relative to $P_{\text{opt}}$. NMSE is a measure that represents the average relative power of the error vector. It is a key metric, as it is directly related to the performances of the receiver. Typically, the knowledge of the statistical distribution of $\boldsymbol{\eta}_i$ and the NMSE is sufficient to predict the bit error rate (BER) achieved by the system in function of the type of decision that is performed at the next stage of the receiver. Note that, all throughout this thesis, we consider that the receiver performs a hard decision on the demodulated symbols. After this step, the symbols are finally demapped to retrieved the estimated bit stream $\hat{\mathbf{b}}_i$.

### Wireless channel modeling

Propagation through wireless channel is usually modeled through three different phenomenons. First, *pathloss* represents the overall loss of power due to propagation of the radio wave. Typically, pathloss is modeled as a value that is deterministically dependent of the traveled distance. For example, in free space, the power of signals emitted from an isotropic antenna is known to be decreasing with the square of the distance. Of course, free space is merely a theoretical concept and, at least in the kind of cellular communications considered in this thesis, the received power decreases more rapidly than with the square of the distance. In fact, there is a number of works that have investigated how to model the average pathloss as a function of the surrounding environment. In particular in this thesis, when needed, we will

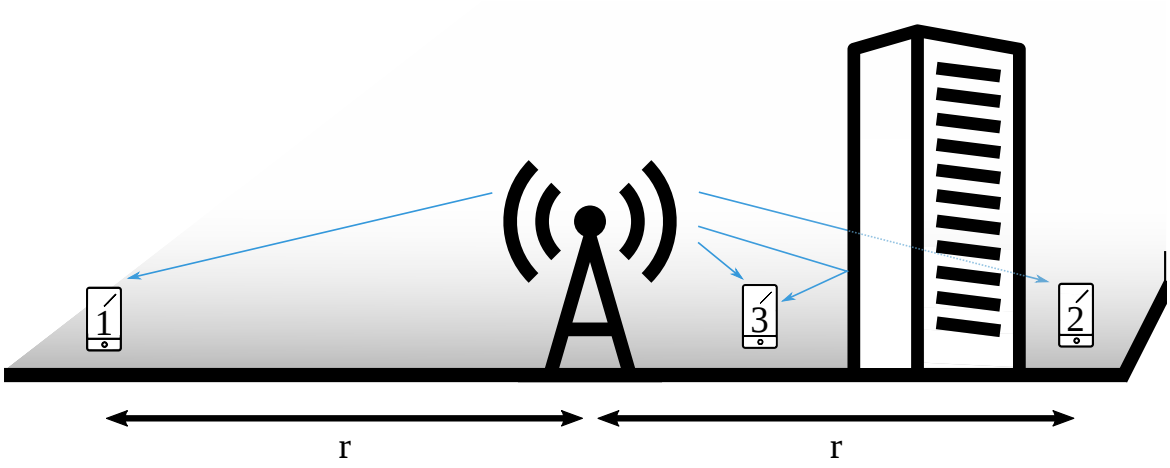


Figure 2.2: Representation of the three different channel propagation effects. Mobile devices 1 and 2 are at the same distance of the base station, and therefore experience the same pathloss. However, one of them is shadowed by a building and should therefore receive a lower signal power. This is modeled by the shadowing random process, which adds a log-normal distributed random variable to the received power. Mobile 3 experiences multi-path transmission as it receives multiple reflected copies of the same signal which incurs fading and frequency selectivity of the channel.

rely on WINNER II channel models [24] which have been extensively used and validated in the literature. In addition to the deterministic pathloss which represents the average loss of power as a function of the distance, channel models introduce the notion of *shadowing*. Shadowing represents the random attenuation due to the random spatial distribution of surrounding blocking objects such as buildings, and is modeled as a centered log-normal random variable.

Accounting for pathloss and shadowing, the signal power in dB received by a user at distance $r$ is expressed as

$$P_{r_{\mathrm{dB}}} = P_{t_{\mathrm{dB}}} + \underbrace{\alpha(f_c) + 10\beta \log 10(r)}_{\text{pathloss}} + \underbrace{\gamma}_{\text{shadowing}}, \tag{2.4}$$

where $P_{t_{\mathrm{dB}}}$ is the transmit power in dB, $\alpha(f_c)$ is a pathloss component that depends on the used carrier frequency $f_c$, $\beta$ is the factor representing how pathloss evolves as a function of $r$ (typically, $\beta = 2$ in free space) and $\gamma$ is a centered normal random variable. Pathloss and shadowing are large-scale phenomenons that only affect the received signal power, without incurring any distortions on the signal itself, at least with the models considered in this thesis. We will consider these effects only in the network level studies we will lead in Chapter 6.

In cellular environments, transmit signals experience multiple reflections on the surrounding environment. Therefore, each receiver receives multiple delayed and attenuated copies

| $l$ | $\tau_l$ (ns) | $\sigma_l^2$ (dB) |
|---|---|---|
| 0 | 0 | 0 |
| 1 | 30 | -1 |
| 2 | 70 | -2 |
| 3 | 90 | -3 |
| 4 | 110 | -8 |
| 5 | 190 | -17.2 |
| 6 | 410 | -20.8 |

(a)

| $l$ | $\tau_l$ (ns) | $\sigma_l^2$ (dB) |
|---|---|---|
| 0 | 0 | -1 |
| 1 | 50 | -1 |
| 2 | 120 | -1 |
| 3 | 200 | 0 |
| 4 | 230 | 0 |
| 5 | 500 | 0 |
| 6 | 1600 | -3 |
| 7 | 2300 | -5 |
| 8 | 5000 | -7 |

(b)

Table 2.1: Examples of available models for (a) extended pedestrian A (EPA), and (b) extended typical urban (ETU) channels [26].

of the same useful signal. Thus, propagation through the channel can be modeled as a convolution with a filter $h$ defined as

$$\forall t, h(t) = \sum_{l=0}^{L-1} h_l \delta(t - \tau_l), \tag{2.5}$$

where $L$ represents the total number of paths traveled by the transmit signal, $\delta$ is the dirac function and $\tau_l$ and $h_l$ are respectively the delay and gain associated with the $l$-th path. Note that in fact it is more accurate to represent the channel as a finite impulse response (FIR) filter $\mathbf{h}$ as follows:

$$\forall n, \mathbf{h}[n] = \sum_{l=0}^{L-1} h_l \delta[n - k_l], \tag{2.6}$$

where $k_l$ is the delay expressed in samples corresponding to the delay $\tau_l$. The factors $h_l$ are modeled as central normally distributed random variables of variance $\sigma_l^2$ and $|\mathbf{h}|$ follows therefore a Rayleigh distribution [25]. Note that (2.5) and (2.6) assume a time-invariant channel. In reality, the channel impulse response varies in time because of the movements of users and their surrounding environment, however, these effects are out of the scope of this thesis.

As for the pathloss and shadowing effects, extensive studies have been led to design models that are as realistic as possible in different scenarios. In this study, we will rely on the widely used ITU-R channel models [26] which give tabulated values of delays $\tau_l$ and

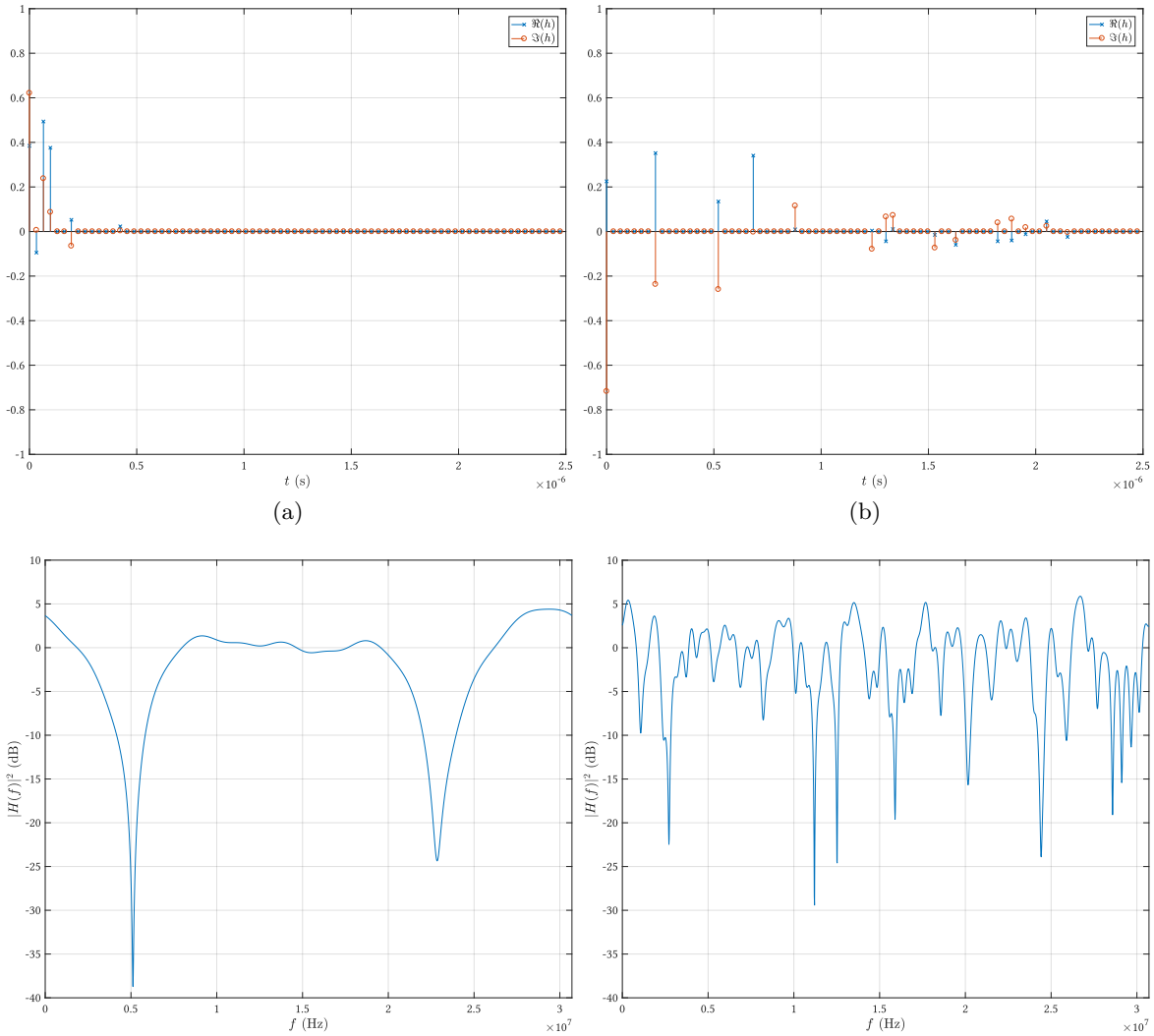


Figure 2.3: Time and frequency response of a channel realization corresponding to (a) EPA and (b) ETU channel models. Higher path delays along the time axis incur higher, steeper variations in the frequency domain.

average power $\sigma_l^2$ for a various number of scenarios. In Table 2.1 we present two examples that are given in [26] in the form of the extended pedestrian A (EPA) and extended typical urban (ETU). Furthermore, we represent the time and frequency responses of one channel realization corresponding to each of these channel models in Fig 2.3. As is widely known and as it is shown in that figure, the multi-path channel translates into frequency selectivity, a phenomenon known as *fading*.

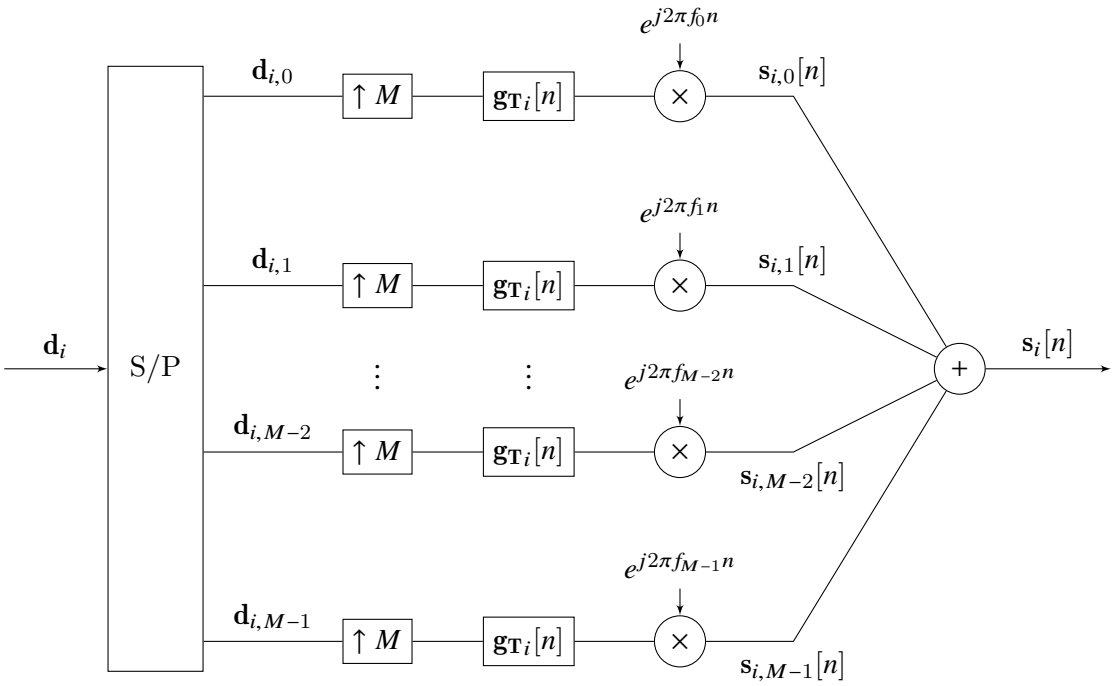


Figure 2.4: Detailed structure of a multicarrier waveform modulation block. The data vector $\mathbf{d}_i$ is split up into $M$ parallel data streams called subcarriers. On each subcarrier $m$, data is oversampled of a factor $M$, multiplied by the transmit filter $\mathbf{g}_{\mathbf{T}i}$ and modulated at carrier frequency $f_m$. The transmit signal is finally obtained as the sum of all subcarriers.

### 2.2.2 Multicarrier systems

#### Generic mulitcarrier structure

Fading is the channel effect that has fostered the wide adoption of multicarrier systems in current wireless communication systems. Indeed, when transmitting a broadband signal over a multipath wireless channel, the frequency variations shown in Fig. 2.3 incur harmful distortions, as different harmonics of the signal will experience different gains. Multicarrier techniques offer a practical solution to that problem by transmitting multiple signals called subcarriers that are narrow enough in frequency to assume that the channel is flat on each of them. Therefore, the effects of the channel propagation come down to a simple scalar multiplication on each subcarrier.

Multicarrier modulation is achieved by multiplexing data on different subcarriers and applying a filter on each obtained data stream. A generic multicarrier modulation scheme is presented in Fig. 2.4 where we see that the complex data vector $\mathbf{d}_i$ is divided into $M$ parallel data streams $\mathbf{d}_{i,m}$ by the serial to parallel converter. Then, each subcarrier $m$ undergoes a multiplication with the transmit prototype filter $\mathbf{g}_{\mathbf{T}i}$ and is modulated to its target frequency

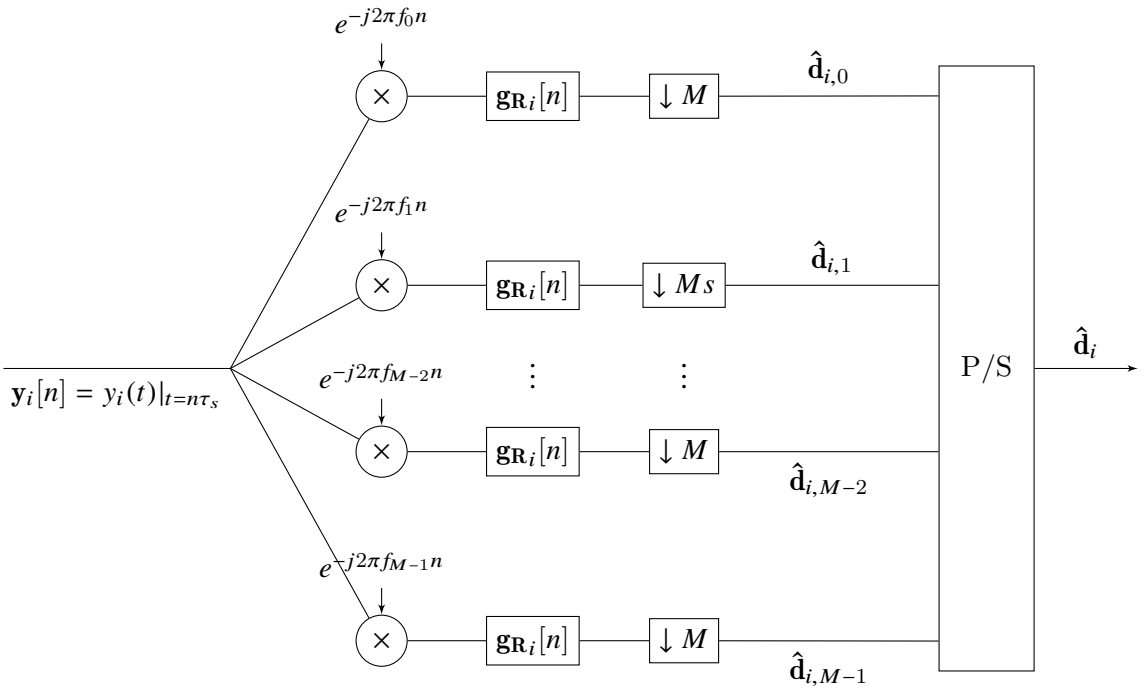


Figure 2.5: Detailed structure of a multicarrier waveform demodulation block. The received signal is split up into $M$ streams that are brought back to baseband frequency. On each subcarrier, the obtained signal is multiplied by the received filter $\mathbf{g_R}_i$ and downsampled. The demodulated symbols are then retrieved by passing through the parallel to serial converter.

$f_m$. The obtained multicarrier signal, after summation of all subcarriers, is given by

$$\forall n,\ \mathbf{s}_i[n] = \sum_k \sum_{m=0}^{M-1} \mathbf{d}_i[kM+m] \times \mathbf{g_T}[n-kM] e^{j2\pi f_m n}. \tag{2.7}$$

We also frequently refer to the analog expression of (2.8) in continuous time:

$$\forall t \in \mathbb{R},\ s_i(t) = \sum_k \sum_{m=0}^{M-1} \mathbf{d}_i[kM+m] \times g_T(t-kT_s) e^{j2\pi f_m t}, \tag{2.8}$$

where $T_s = M\tau_s$ is the time-symbol and $g_T$ is the continuous version of the transmit prototype filter defined such that $g_T(t)|_{t=n\tau_s} = \mathbf{g_T}[n]$. The multicarrier generic demodulator, not accounting for the channel equalization procedure, is represented in Fig. 2.5, where we show that the received sampled signal is processed through an architecture that is the exact reflection of the transmitter's. After sampling the receive signal $y(t)$ and obtaining $\mathbf{y}[n] = y(t)|_{t=n\tau_s}$, the multicarrier receiver yields the demodulated symbols as

$$\forall k, m,\ \hat{\mathbf{d}}_{i,m}[k] = \sum_n \mathbf{y}_i[n] \mathbf{g_R}_i[n-kM] e^{-j2\pi f_m n}. \tag{2.9}$$

Finally, the whole vector of demodulated symbols is obtained by defining $\forall n, \hat{\mathbf{d}}_i[n] = \hat{\mathbf{d}}_{i,m}[k]|_{n=kM+m}$.

### OFDM

OFDM is the most basic example of multicarrier modulation that exists, as it relies on very simple rectangular prototype filter such that

$$\mathbf{g_T}[n] = \begin{cases} \frac{1}{\sqrt{M}}, & n \in [0, M-1] \\ 0, & \text{elsewhere} \end{cases} \tag{2.10}$$

$$\mathbf{g_R}[n] = \begin{cases} \frac{1}{\sqrt{M}}, & n \in [0, M-1] \\ 0, & \text{elsewhere.} \end{cases} \tag{2.11}$$

Furthermore, in OFDM, subcarriers are critically separated in frequency so that $f_m = \frac{m}{M}$, which guarantees subcarrier orthogonality. With this particular set of filters and parameters, multicarrier modulation and demodulation operations boil down to simple Fourier transformations, as was clearly identified by Weinstein and Ebert in [27]. Thus, OFDM can be easily implemented through the use of (inverse) fast Fourier transform ((I)FFT) which benefit of a very low complexity. The OFDM transmission emission and reception operations can in fact be easily expressed as

$$\mathbf{s}_i = \mathbf{F}_M^{\mathbf{H}} \mathbf{d}_i, \tag{2.12}$$

$$\hat{\mathbf{d}}_i = \mathbf{F}_M \mathbf{y}_i, \tag{2.13}$$

where $\mathbf{F}_M$ is the $M \times M$ Fourier matrix and $\mathbf{F}_{\mathbf{M}}^{\mathbf{H}}$ the hermitian matrix of $\mathbf{F_M}$, that is to say the inverse $M \times M$ Fourier matrix.

Note that these two last expressions incur a perfect reconstruction in the case where the received signal $\mathbf{y}_i$ is exactly equal to the modulated signal $\mathbf{s}_i$. This is of course not the case in reality as the modulated signal propagates through the wireless channel and $\mathbf{y}_i = \mathbf{s}_i * \mathbf{h}$. As explained in the former section, propagation through the multi-path channel generates multiple delayed copies of the transmit signal. This would in turn create harmful inter-symbol interference (ISI) between subsequent OFDM symbols and hinder the QAM demodulation procedure. Furthermore, the distortions to the transmit signal caused by the fading channel have to be compensated for at the receiver to retrieve the modulated data. A convenient way of solving both these problems is to add a cyclic prefix (CP) to the modulated symbols, which serves two purposes: first, acting as a guard interval, that is discarded at the receiver side, it can efficiently remove ISI if it is longer than the maximum delay incurred by the transmission channel. Furthermore, it makes the convolution with the channel circular, which allows for

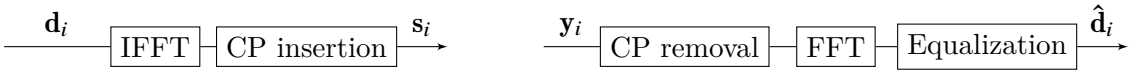


Figure 2.6: Detailed implementation of CP-OFDM transmission and reception chains.

easy frequency domain equalization at the receiver, even in the presence of small timing offsets. With the addition of a sufficiently long CP, the effects of the channel can therefore be compensated and the demodulated symbols at the OFDM receiver can be obtained as [28]

$$\hat{\mathbf{d}}_i = \mathbf{B}(\mathbf{H}_f \mathbf{d}_i + \mathbf{w}_i), \tag{2.14}$$

where $\mathbf{H}_f$ is the $M$ square diagonal matrix composed of the channel coefficients on each subcarrier. $\mathbf{B}$ is the equalization matrix which can be designed in different ways. The two most widely used techniques are zero-forcing and minimum mean square error (MMSE) equalization [25]. With zero forcing (ZF) equalization, the equalization matrix is defined as

$$\mathbf{B}_{\mathrm{ZF}} = \mathbf{H}^{-1}. \tag{2.15}$$

However, inverting the channel can enhance noise because of the possibly small values taken by $\mathbf{H}^{-1}$. MMSE equalization removes this issue by defining the following equalization matrix:

$$\mathbf{B}_{\mathrm{MMSE}} = \left(\mathbf{H}^{\mathbf{H}}\mathbf{H} + \frac{1}{\mathrm{SNR}}\mathbf{I}_M\right)^{-1} \mathbf{H}^{\mathbf{H}}, \tag{2.16}$$

where SNR is the received signal to noise ratio.

The CP-OFDM transmission and reception chain is detailed in Fig. 2.6. A convenient way to represent the CP addition to the OFDM system is by representing it directly in the used transmit and receive prototype filters as follows:

$$\mathbf{g}_{\mathbf{T}}[n] = \begin{cases} \frac{1}{\sqrt{M}}, & n \in [-N_{\mathrm{CP}}, M-1] \\ 0, & \text{elsewhere} \end{cases} \tag{2.17}$$

$$\mathbf{g}_{\mathbf{R}}[n] = \begin{cases} \frac{1}{\sqrt{M}}, & n \in [0, M-1] \\ 0, & \text{elsewhere,} \end{cases} \tag{2.18}$$

where $N_{\mathrm{CP}}$ is the number of used cyclic prefix samples. The CP-OFDM transceiver chain described in this section has proven to be very effective and has been has been widely used in different multi-user contexts which we detail in the following.

#### OFDM-based multiuser schemes

In order to accommodate multiple users on a same frequency band, there exists a number of techniques which all aim at making users signals orthogonal in a certain space. The most evident solution, called time division multiple access (TDMA) is to assign different time slots to different users so that they are orthogonal in time. Another possibility, used in code division multiple access (CDMA) 3G communication systems, is to precode users data with orthogonal codewords in order to achieve orthogonality in a certain codespace. Both TDMA and CDMA are out of the scope of this thesis in which we focus on frequency division multiple access (FDMA). In FDMA, each user gets assigned a certain set of the spectrum band in such a way that they do not significantly interfere onto one another. Orthogonal FDMA (OFDMA) is a special kind of FDMA technique which takes advantage of the orthogonality between OFDM subcarriers. In OFDMA, instead of being assigned different parts of the spectral band, every user $i$ can transmit on a specific set of subcarriers $\mathcal{M}_i$ so that $\forall n, \mathbf{d}_{i,m}[n] \neq 0 \iff m \in \mathcal{M}_i$.

OFDMA has proven to be an effective way of multiplexing users on a same spectral band as it leverages the orthogonality between OFDM subcarriers to ensure orthogonality between adjacent users. However, one of the caveats of OFDM lies in its high peak to average power ratio (PAPR) which prevents devices to function with satisfying energy efficiency [29]. The energy efficiency of base stations is an important aspect for MNOs, as their power consumption importantly affects their energy bill [30]. Nevertheless, MNOs have so far decided that the advantages of OFDM exceed this drawback and use OFDM in conjunction with some PAPR reduction techniques in the downlink of the cellular networks. However, energy efficiency represents an even greater challenge for battery-powered devices such as mobile phones, as it directly affects their battery life. In turn, the uplink of LTE cellular networks relies on a slightly modified version of OFDMA called single-carrier FDMA (SC-FDMA). In this scheme, the transmitted symbols are spread on multiple subcarriers through the use of a DFT. Therefore, the SC-FDMA transmit signal resembles a single-carrier one and thus achieves lower PAPR, which translates into enhanced energy efficiency for mobile devices.

## 2.3 Arising coexistence issues

### 2.3.1 Coexistence and cognitive radio

As we explained in the introduction chapter of this thesis, we foresee that, in the future, new services will coexist on the same spectral bands as legacy systems, in particular DVB-T2 and LTE networks which are both based on OFDM. This foreseen coexistence will trigger a crucial turning point in the history of wireless networks as we should see the first industrial

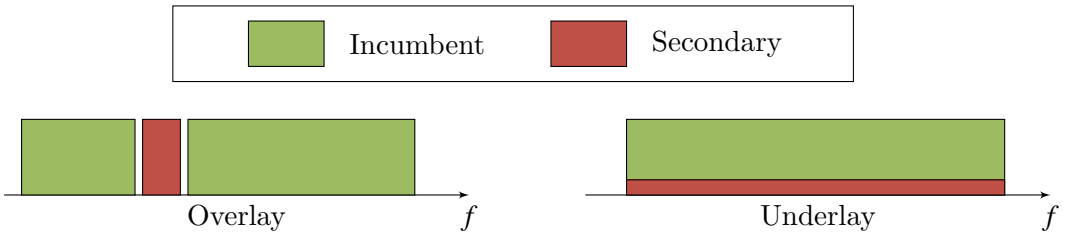


Figure 2.7: Illustration of overlay OSA and underlay. In underlay, secondary devices transmit at low power on the same band as incumbent systems. In overlay OSA, secondary devices detect and exploit white spaces left free by incumbent.

deployments of opportunistic spectrum access (OSA) systems. OSA [31] is a dynamic spectrum access (DSA) scheme in which secondary users (SU)s reuse some part of the spectrum left free by incumbent systems, usually called a *white space*, in an overlay fashion, with opposition to underlay in which secondary systems would transmit on the same spectral resources as incumbent users at very low transmit power to avoid interference to the former.

OSA creates unprecedented issues, which can be summed us as

1. *Detection:* How to detect white spaces that offer an opportunity for secondary transmission ?

2. *Exploitation:* Once a white space is detected, how to use it in the most efficient manner ?

These two issues have been widely tackled in the context of CR which was defined by Mitola in his Ph.D. thesis [32]. Recently, CR has become to start a reality thanks to the increased computation capabilities and the advent of software radio [33]. In Mitola's mind, the CR concept was not limited to the issue of OSA, but rather defined a new paradigm in which radio devices are able to adapt to and learn from their environment to meet the instantaneous needs of users. Nevertheless, it is fair to say that CR has mainly been studied as a way to enable OSA and the intricate "cognitive cycle" defined by Mitola is usually reduced to two major capabilities in the context of OSA: sensing, which aims at resolving challenge 1 here above, and exploitation, which tackles challenge 2 [11, 34].

Sensing is a broad research issue that has fostered a wide range of research works [35, 36], but it is out of the scope of this thesis. In fact, all throughout our discussion, we will assume that secondary systems are aware of the presence of white spaces and their position in the spectrum, as our work focuses on the exploitation part. In particular, we will study how the waveform modulation stage as depicted in Fig. 2.4 can affect the exploitation capabilities of secondary systems.

Indeed, to be able to fully exploit detected spectral opportunities, secondary devices must be capable of aggregating spectrum in a flexible manner. Furthermore, in order to

reduce the interference they cause to incumbent users, they should be able to transmit with very high spectral localization. Besides, because coordination between coexisting systems is limited in CR setups, secondary devices should be robust to asynchronism between users [2]. Unfortunately, though OFDM can benefit from a great flexibility due to its multi-carrier nature, it is known that it suffers from very poor spectral localization [18] and is very sensitive to asynchronism [15, 28, 37]. Therefore, it is expected to perform poorly in the CR context and, by extension, in the asynchronous coexistence scenarios that 5G will bring to life [2, 17, 38]. The quest for new enhanced waveforms capable of accommodating these setups has therefore been a major research topic in the last decade. We will present some of these waveforms in section 2.4. In order to better exemplify the shortcomings of OFDM though, we present in the following two key coexistence scenarios of interest to this thesis.

### 2.3.2 Foreseen coexistence scenarios

OSA and CR are well-traveled roads, but both these concepts have lost some of their initial popularity as it has long been unclear in what particular context they would be applicable. Interestingly though, the concepts of CR and OSA have infused and the core ideas behind them are now fully part of many current wireless network designs, though the terms of CR and OSA themselves may not be directly used. Nowadays, there are multiple examples of research areas in which CR and OSA are involved even though they are not always cited as such. In particular, we will focus on two contemporary and vivid research challenges, namely the exploitation of TV White Spaces and the insertion of D2D links in cellular networks and underline the role of the secondary PHY for each of them.

#### TV White Spaces: a paramount example of CR application

Following the shift from analog TV to fully digital transmission in, the last decade, a large amount of frequencies previously reserved to analog TV transmission have been reassigned to other services. Furthermore, as new digital broadcasting standards are much more spectrally efficient than legacy analog transmission, there are usually an important number of TV channels that are left unused at a given time and space. These unused parts of the TV spectrum are referred to as TV White Space (TVWS) and have fostered a great deal of research after the Federal Communications Commission (FCC) authorized unlicensed devices to operate in TV broadcast bands [39, 40].

In addition to the obvious commercial potential linked with the exploitation of TVWS, they represent the first credible and promising field of application for CR and OSA. Indeed, enabling secondary networks to operate in TV bands raises a number of issues that are directly related to the two problems of OSA tackled here above and the CR concept has

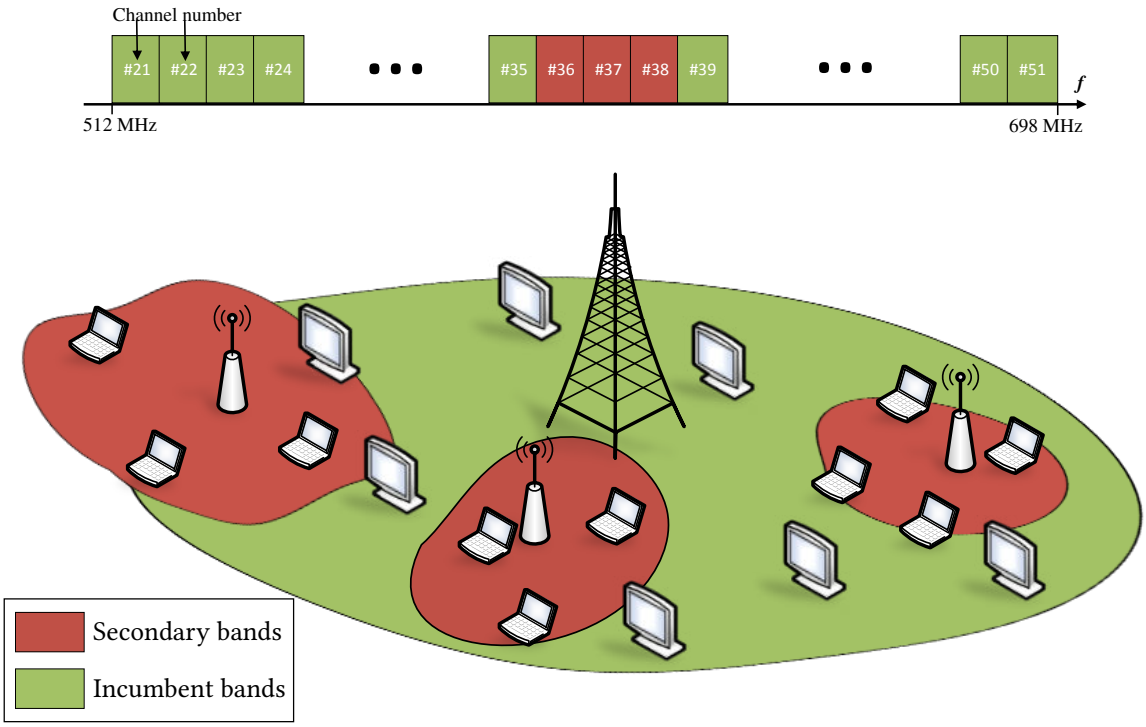


Figure 2.8: Example of a TV white space deployment, in which a secondary wireless network is established in the channels not used by the incumbent TV broadcast transmitter.

therefore been extensively applied in the context of TVWS [41–44]. In this particular context, secondary systems must be introduced without harmfully interfering onto incumbent devices which can be TV receivers, wireless microphones and even mobile devices operating in directly adjacent 4G bands [45].

This set of constraints clearly establishes a CR scenario in which secondary users must detect TVWS to avoid incumbent users and then exploit the detected white space in the best possible way. On the matter of detection, a clear consensus has emerged in favor of a combination between pure sensing and geo-location database aided detection [42]. As far as exploitation of TVWS is concerned, one of the main challenges to overcome lies in the necessity for secondary transmissions to fit into stringent spectrum masks that have been defined by the FCC to ensure that no harmful interference is created to adjacent incumbent users [40, 41].

As we represent in Fig. 2.9, the requirements on the OOB emissions of secondary TVWS devices are too stringent for OFDM to be efficiently used by secondary devices. Therefore, a number of studies that we will detail later on in this chapter have proposed to use alternative waveforms with enhanced spectral localization instead of OFDM to facilitate the exploitation of TVWS [46, 47]. In Europe, this line of research has particularly been led by the ICT-

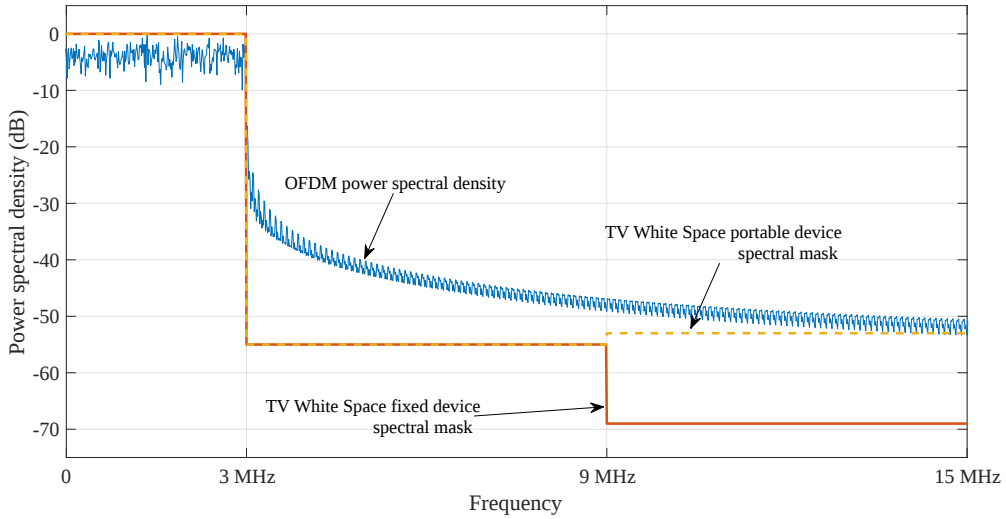


Figure 2.9: Spectral masks defined for portable and fixed TVWS secondary users as per [40]: OFDM does not properly fit into the set requirements because of its high out-of-band (OOB) emissions.

QoSMOS project[1] [48]. The limitations of OFDM caused by its poor spectral localization that we exemplified here in the context of TVWS apply of course in any CR setup [17].

### D2D communication in LTE bands

The high OOB emissions of OFDM are the roots of many of its disadvantages. Nevertheless, looking at the PSD of OFDM only does not tell the whole story about its coexistence capabilities. In fact, two OFDM based systems are fully capable of coexisting provided that they achieve proper synchronization. For example, in the uplink of cellular systems, the base station ensures that user terminals transmitting on adjacent spectral resources are synchronized in both time and frequency so that they do not interfere onto each other. Of course, in the CR context, no synchronization is bound to be established between the incumbent and secondary devices as they are not supposed to cooperate, and studying the PSD of the secondary looks as an appropriate way of roughly estimating how it will interfere on the incumbent in such an asynchronous setup.

Interestingly, there is a growing number of applications which, though they cannot be exactly classified as CR setups, will potentially involve asynchronism between coexisting users. As a matter of fact, maintaining synchronism between users in a wireless networks is a computation-costly and spectrum consuming task. In current LTE cellular networks, inter-user synchronization is achieved by a combination of pilot signaling and intricate

[1] Quality of Service and MObility driven cognitive radio Systems - http://www.ict-qosmos.eu

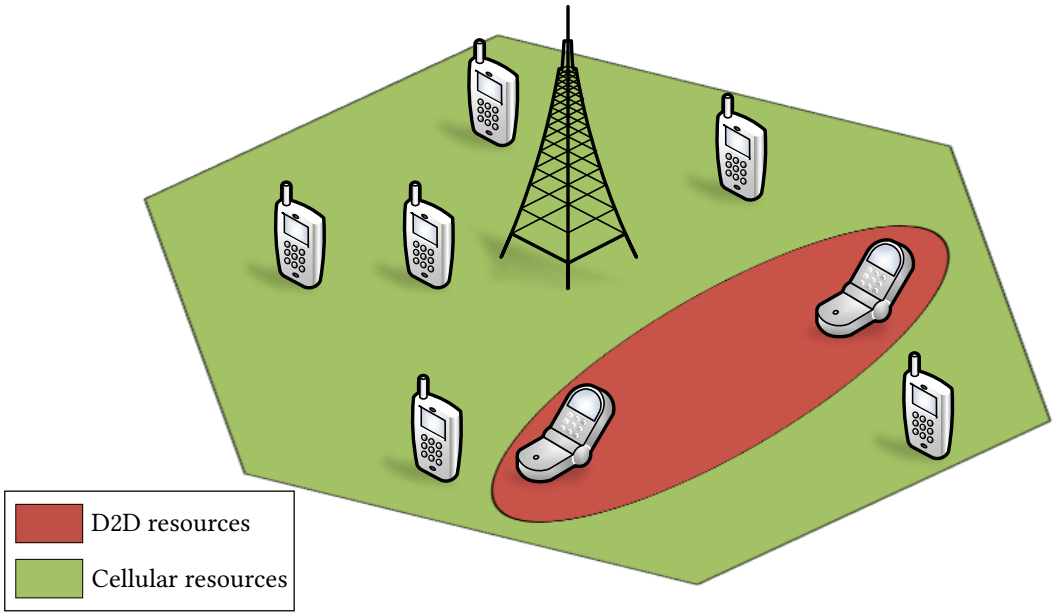


Figure 2.10: Coexistence of D2D communications and classical user equipments in cellular networks.

algorithms. In the downlink of LTE networks, around 3% of transmitted symbols are reserved for synchronization signals [1]. Furthermore, the carrier frequency offset (CFO) of each user in the uplink of cellular networks is estimated and compensated for at the base station, which increases the computational burden of the latter. Moreover, inter-user synchronization is achievable in star-shaped cellular networks in which every node is connected to the central node, i.e. the base station. However, in the context of 5G, where the number of devices will dramatically increase and networks will adopt more complex, not star-shaped structures, inter-user synchronization could prove to be hardly achievable.

D2D communication, which is currently being standardized for 5G is a typical example of how future networks will be not fully star-shaped, but will also introduce direct links between nodes. Indeed, D2D communication enables multiple UEs to communicate directly to each other by short-cutting the base station, as is represented in Fig. 2.10. This paradigm is expected to bring in multiple benefits by reducing the latency between involved devices and relieve the base station of part of its communication burden so that more cellular users could be accommodated at the same time. In this thesis, we are particularly interested in D2D communications partly because of our involvement in the French project ACCENT5[2] funded by Agence Nationale de la Recherche (ANR), which aims at facilitating the coexistence between D2D and cellular communications.

[1] The exact proportion varies according to the frame configuration. An extremely good resource on LTE frame configuration is http://niviuk.free.fr/lte_resource_grid.html

[2] Full project title: *Advanced Waveforms, MAC Design and Dynamic Radio Resource Allocation for Device-to-Device in 5G Wireless Networks* - http://accent5.fr

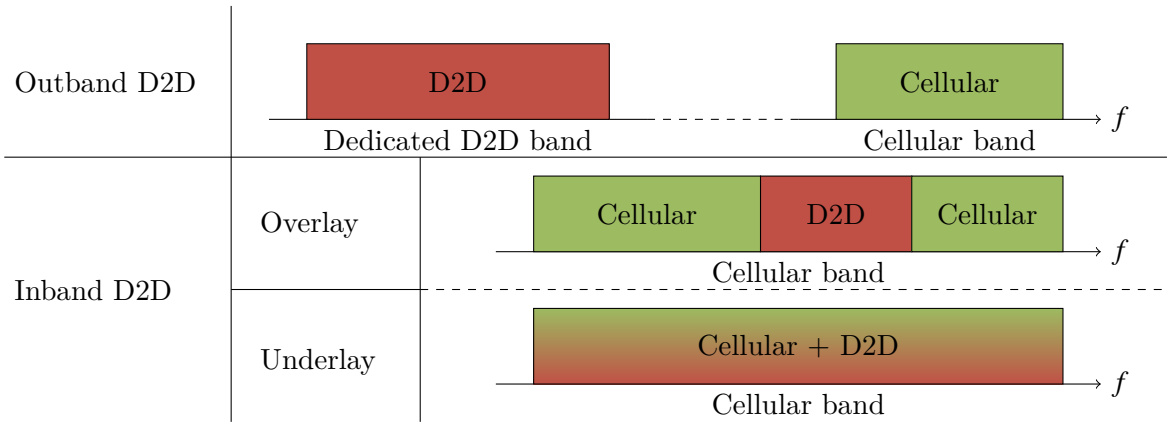


Figure 2.11: Typical classification of D2D spectrum allocation schemes [49]. Outband D2D is out of the scope of this thesis and our work will focus on inband D2D.

One key issue to tackle lies in knowing where in the spectrum to accommodate D2D pairs. On this matter, literature usually classifies different approaches according to the taxonomy represented in Fig. 2.11. In outband D2D, D2D devices are accommodated on a spectral band different to that of the cellular users. This scheme therefore avoids interference between D2D and cellular users. In fact, outband D2D does not raise any issues that are relevant to this thesis and we therefore focus on inband D2D. Interestingly, the D2D literature has adopted the CR taxonomy presented in Fig. 2.7, as it differentiates between overlay D2D and underlay D2D [49]. In overlay D2D, the assumption is that D2D devices are assigned resources that are orthogonal to the resources used by cellular users and that no interference arises between the two types of users. However, this orthogonal separation limits the rate that D2D users can achieve as they can only access a small portion of the cellular band. Therefore, most works have focused on underlay D2D in which D2D pairs reuse RBs that are already assigned to CUs. Indeed, this scheme allows D2D devices to reuse the whole cellular spectrum [50, 51].

An assumption that is widely shared in works on underlay D2D is that D2D devices only interfere with cellular users that transmit on the same resource block as they are [49, 52]. However, this is only the case if the D2D and cellular users are perfectly synchronized, which may, as we discussed here above, be difficult to achieve [53, 54]. In fact, the first 3GPP standards on D2D that have been designed involve a significant amount of signaling overhead between D2D users and the base station, even though data is directly transmitted between devices forming a D2D pair [55].

Because synchronization between all cellular and D2D devices may be difficult and/or too computation-costly to achieve, we foresee network deployments in which this synchronization is not perfect. In such scenarios, the distinction between overlay and underlay is not clear. Indeed, in the absence of synchronization between adjacent users, orthogonality between

them is lost and leakage occurs, meaning that a user active on a specific RB will also interfere on adjacent RBs [28, 56]. We therefore see clearly that such an asynchronous coexistence scenario can be tackled with the tools usually dedicated to CR setups. In fact, the will to limit cooperation between D2D pairs and the cellular network has given rise to the idea of *cognitive D2D* [57], in which D2D pairs are modeled as secondary and cellular users as incumbent. With this approach, it is clear that OFDM will suffer exactly the same limitations in the context of D2D communication as in that of TVWS. Therefore, it is relevant to study the advantages of adopting a new waveform alternative to OFDM to perform D2D communication, and some works have indeed tackled that specific problem [58–62]. We will review these works in detail in chapter 3.

## 2.4 Enhanced waveforms for 5G

### 2.4.1 Designing new waveforms: objectives and constraints

Because of the numerous shortcomings of OFDM previously mentioned, the design of new waveforms with intrinsic filtering properties which achieve advantageous spectral localization, flexibility and robustness to asynchronism has been identified as one of the key research topics to be addressed in order to fully accommodate all potential 5G use cases [2, 7, 19]. Actually, given the myriad of different multi-carrier schemes that have been proposed, it is difficult to compare them in a fair and extensive manner. Nevertheless, a significant amount of works have aimed at doing so in the last few years [19, 56, 63–70]. In fact, the design of new waveforms able to exploit the radio spectrum in an optimal manner has been identified as a strategic axis of research by the French and European authorities, which have funded a large number of projects to achieve this objective.

In Europe, research on waveforms was kick-started by Project PHYDYAS[1]. In this project, Bellanger *et. al.* proposed a first FB-MC waveform architecture that achieved high spectral localization and was later widely reused in other projects [21]. Project EMPhAtiC[2] further investigated the use of enhanced waveforms for emergency communications [71], while the 5GNOW[3] project aimed at designing different types of enhanced waveforms suited for asynchronous communication [38]. Finally, the METIS[4] project explored how new waveforms can be integrated with other components of the radio chain [72].

[1] PHYsical layer for DYnAmic Spectrum access and cognitive radio - http://www.ict-phydyas.org

[2] Enhanced Multicarrier Techniques for Professional Ad-hoc and Cell-based Communications - http://www.ict-emphatic.eu

[3] 5th Generation Non-Orthogonal Waveforms for Asynchronous Signaling - http://5gnow.eu/

[4] Mobile and wireless communications Enablers for the Twenty-twenty Information Society - http://www.metis2020.com

In France as well, the leading research funding administration, ANR (Agence Nationale de la Recherche), has financed several projects that aim at designing and analyzing new waveforms. In particular, project PROFIL[1] followed the research initiated by EMPhATiC and WONG5[2] studies waveform dedicated to machine-to-machine (M2M) communications. Finally, as we mentioned in the former section, the work presented in this manuscript has been part of the ACCENT5 project, which investigates how new waveforms can facilitate D2D communication.

All enhanced waveforms that have been proposed, in part in the projects mentioned above, have been designed to overcome the flaws of OFDM. In particular, the main objective these waveforms pursue is to enable asynchronous communication and coexistence between uncoordinated systems on the same spectral band. This means that all these waveforms involve some filtering operations to improve their spectral localization and reduce their sensitivity to asynchronism. However, spectral localization and robustness to asynchronism cannot be the only waveform design criteria. Indeed, a waveform that would be perfectly robust to asynchronism but not time and spectrally efficient would have limited interest. Therefore, in addition to the novel requirements in terms of asynchronism and spectral localization, newly proposed waveforms should preserve the benefits of CP-OFDM. In particular, CP-OFDM can be implementable with very low complexity and enables direct equalization in the frequency domain. Furthermore, it is directly applicable to MIMO, which is a key requirement for the 5G air interface [1, 19].

Any multi-carrier modulation scheme obeying the signal model defined in (2.8) constitutes a Gabor family with parameters $\Delta T$ and $\Delta F$ which respectively represent the time and frequency spacing between adjacent symbols. Given a Gabor family of density $\rho = \frac{1}{\Delta T \Delta F}$, it is proven by the Balian-Low theorem (BLT) [73, 74] that it is not feasible to achieve at the same time:

1. Optimal symbol density $\rho = 1$,
2. Complex orthogonality between transmit symbols,
3. Good localization both in time and frequency.

This set of constraints is a key design issue that limits the performance achievable by any multi-carrier waveform. Typically, any multi-carrier scheme achieves only two of the above criteria at the same time. For example, OFDM achieves optimal symbol density and complex orthogonality between transmit symbols. However, it fails to provide satisfying levels of

[1] Evolution de la PROfessional Mobile Radio large bande basée sur la modulation FILter Bank MultiCarrier - http://www.agence-nationale-recherche.fr/?Projet=ANR-13-INFR-0007

[2] Waveforms MOdels for Machine Type CommuNication inteGrating 5G Networks - http://www.wong5.fr/

frequency localization. In the following, we review FB-MC schemes which focus on the latter aspect, at the expense of either symbol density or orthogonality.

### 2.4.2 Linear FB-MC

The idea behind FB-MC, originally proposed in [75, 76] is to replace in (2.8) the rectangular filter used by OFDM systems by enhanced prototype filters which offer both time and frequency localization. The set of transceive filters used by any linear FB-MC system can therefore be summarized as

- $\forall n \in \mathbb{Z}, f_{n,\mathrm{T}}(t) = f_{\mathrm{T}}(t) = \begin{cases} g(t), & t \in \left[-\frac{T_g}{2}, \frac{T_g}{2}\right] \\ 0, & \text{elsewhere} \end{cases}$
- $\forall n \in \mathbb{Z}, f_{n,\mathrm{R}}(t) = f_{\mathrm{R}}(t) = \begin{cases} g^*(-t), & t \in \left[-\frac{T_g}{2}, \frac{T_g}{2}\right] \\ 0, & \text{elsewhere} \end{cases}$

Note that these systems usually use real symmetric filters so that $g^*(-t) = g(t) \forall t \in \mathbb{R}$.

Based on this generic structure, a significant amount of FB-MC waveforms have been designed. In the following, we present the specific examples of FB-MC waveforms that we will consider in this thesis.

#### Filtered Multi-Tone (FMT)

As we explained here above, the BLT dictates that any multi-carrier waveform with satisfying time and frequency localization cannot achieve optimal symbol density and complex orthogonality between them. A first possibility is therefore to preserve symbol orthogonality by reducing their density. It is the solution favored in FMT systems [77, 78], in which the orthogonality between subcarriers is ensured by inserting a guard band between each of them.

Though this added guard band between subcarriers enables FMT systems to transmit orthogonal symbols with satisfying frequency localization, it significantly reduces their spectral efficiency, as the symbol density of their lattice is lower than 1.

#### Offset QAM OFDM (OFDM/OQAM)

The main problem of FMT being the spectral efficiency loss caused by insertion of a guard subcarrier, the goal of OFDM/OQAM [20, 79] is to remove the latter. However, without these guard bands, as stated by the BLT, complex orthogonality between symbols cannot be achieved. Therefore, the key idea behind OFDM/OQAM is to abandon complex orthogonality

and content oneself with orthogonality in the real domain. To achieve this, OFDM/OQAM systems transmit real symbols drawn from a pulse amplitude modulation (PAM). A $\frac{\pi}{2}$ phase difference is then added between subsequent symbols and they are transmitted at twice the symbol rate $\frac{2}{T}$. As a result of this, orthogonality in the real domain is achieved.

Nevertheless, this scheme suffers certain core issues related to its real domain-only orthogonality. In particular, it suffers from intrinsic interference that is purely imaginary. This interference is usually dealt with at the receiver by taking the real part of the received signal. However, this intrinsic interference usually makes it more challenging to achieve satisfying channel estimation and equalization [80, 81], and the applications of MIMO techniques to OFDM/OQAM usually require some additional precoding steps with increase the overall complexity of the transmission system [82, 83].

#### FBMC-PAM

One of the problems of OFDM/OQAM lies in the doubling of the symbol rate. A recent alternative, called FBMC-PAM or Lapped FBMC [84] consists in doubling the number of subcarriers and multiplying each symbol by a certain phase factor $\phi_{m,n} = (n - \frac{1}{2} + \frac{M}{2})(m - \frac{1}{2})$. As a result, this modulation also achieves real orthogonality. Furthermore, the multiplication by the phase factor depicted here above acts equivalently as filtering the transmit signal by a sine filter which achieves a good trade-off between time and frequency localization.

### 2.4.3 Circular convolution based filter banks

One of the main drawbacks of linear convolution based filter banks is that they incur a delay in the transmission because of the linear convolution with prototype filter $g$. Therefore, following an idea first coined as "tail biting" in [85], circular convolution based filter banks are based on convolution with circularly shifted versions of the prototype filter $g$. Based on this idea, two main waveforms have been proposed.

#### GFDM

In GFDM [85, 86], complex symbols are modulated per block of $N_\mathrm{b}$ and a CP of length $T_\mathrm{CP}$ is added between every subsequent block. Therefore, from an initial prototype filter $g$, GFDM systems define a set of $N_\mathrm{b}$ filters defined as, $\forall n \in [0, N_\mathrm{b} - 1]$,

$$\tilde{g}_n(t) = \begin{cases} g(t - nT \mod N_\mathrm{b}T), & t \in [-T_\mathrm{CP}, N_\mathrm{b}T] \\ 0 & \text{elsewhere.} \end{cases} \tag{2.19}$$

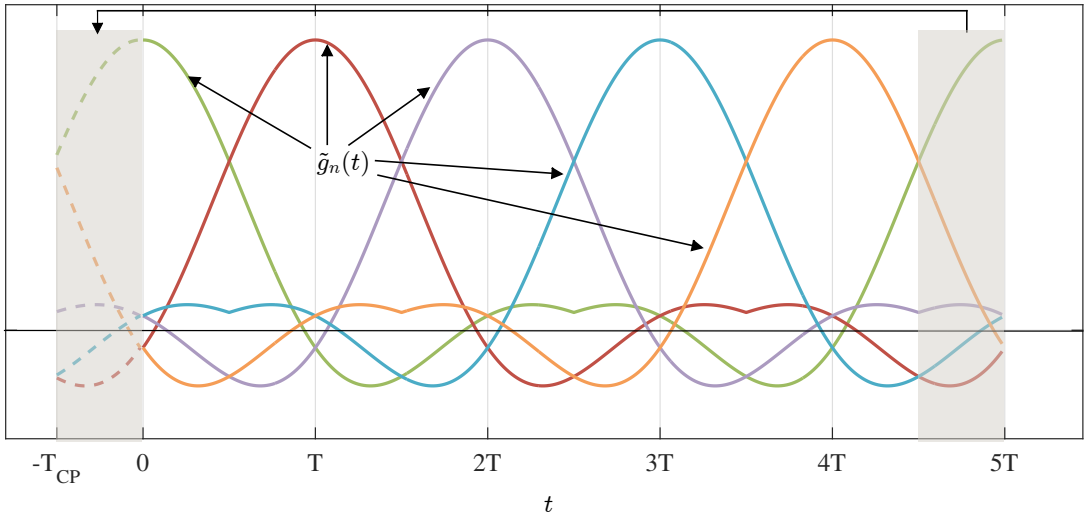


Figure 2.12: GFDM prototype filters $\tilde{g}_n(t)$ obtained from an original RRC prototype filter $g$ with roll-off 0.25, $N_b = 5$ and $T_{CP} = \frac{T}{4}$.

An example of how this applies is given in Fig. 2.12 where we plot the 5 prototype filters defined from an initial prototype filter $g(t)$ in the case where $g$ is a root-raised cosine (RRC) filter with roll-off 0.25, $N_b = 5$ and $T_{CP} = \frac{T}{4}$.

### COQAM

GFDM suffers from the same limitations imposed by the BLT as linear convolution based FB-MC. Therefore, GFDM based systems need to compensate for ICI through specific receiver schemes. However, these may result in complex receiver architectures [87]. Another possibility is to get rid of ICI by adapting the OQAM modulation to GFDM, a proposal called COQAM [88, 89]. This system is essentially similar to GFDM, the only difference lying in the fact that, as it is based on OQAM, real symbols are transmitted at half the symbol rate.

Note that, because of the circular convolution they perform, GFDM and COQAM have poorer spectral containment than linear convolution based FB-MC waveforms. To solve this problem, a number of research works have proposed to add windowing and/or filtering on top of GFDM or COQAM modulations [86, 88]. We will deliberately ignore these solutions in our analysis, as we are interested in studying how the intrinsic filtering properties of the presented waveforms may improve coexistence with CP-OFDM based users.

### 2.4.4 Band-filtered waveforms

All waveforms presented here above perform a filtering on each subcarrier of the transmit signal. This ensures that every subcarrier is well localized, which enables an efficient and dynamic aggregation of the available spectrum. However, in most cases, spectrum is not allocated with a subcarrier-level granularity. For example, in LTE cellular networks, MAC layer procedures do not treat every available subcarrier independently, but rely on resource blocks that are composed of 12 subcarriers. Therefore, it may be useless to design multicarrier schemes in which every subcarrier achieves high levels of frequency localization. Rather, it may be sufficient to ensure that the groups of subcarriers that are assigned to different users are well localized.

Therefore, in addition to the waveforms presented here above, a number of multicarrier schemes which filter groups of subcarriers together have been proposed in the literature. Among them, two main proposals have been investigated: filtered OFDM (f-OFDM) [90] and Universal Filtered Multi-carrier (UFMC), also called UF-OFDM [91].

#### UFMC

In UFMC, also known as UF-OFDM [91–94], subcarriers are packed in groups and each group of subcarriers is then filtered individually in the time domain. Most woks on the topic propose to use Chebyshev filters in order to control the level of the out of band ripples. Furthermore, the CP used by classical OFDM is abandoned and replaced by zero-padding corresponding to the length of the filter used to filter each band. Doing so, it is ensured that the transmit signal is freed of ISI and ICI.

Most works on the subject of UFMC consider that subcarriers are packed in groups of 12 because this value corresponds to the definition of an LTE resource block. This ensures potential retro-compatibility with OFDM based legacy receivers. However, this means that UFMC relies on a prototype filter that may be unnecessary long, which can be detrimental to its time-spectral efficiency.

#### f-OFDM

f-OFDM [90, 95–98] is very close to UFMC. As its name indicates, f-OFDM simply relies on adding a filtering stage in the time domain after the CP addition stage. Contrary to what some works have pretended [90], f-OFDM is not strictly speaking a *new* waveform: most current OFDM systems already apply some filtering at the edge of their band to ensure that they fit in specified spectral masks. However, this filtering was usually performed in downlink, for example to ensure that the signal of one MNO would not affect neighboring competitors.

The novelty of the f-OFDM approach lies in the fact that the signal of each user is processed through a filter that corresponds to its allocated bandwidth in a flexible manner.

Furthermore, in f-OFDM, it is possible to use long filters so that subsequent symbols may overlap, which is bound to create ISI/ICI. However, the latter can be kept low by using appropriate filters. On the other hand, allowing subsequent symbols to overlap is advantageous in terms of time/spectral efficiency, as it reduces the amount of interval time wasted during subsequent symbols.

### 2.4.5 Comparison criteria

#### Selected waveform parameters

The enhanced waveforms we introduced in the previous section achieve different performance according to the specific parameters they rely on. In particular, the used prototype filter is bound to affect the performance achieved by each scheme in a significant manner. It is impossible to investigate the performance achieved by each waveform for each possible set of parameters. Therefore, all throughout this thesis, we will select waveform configurations that are consistent with the literature.

Besides, in order to enable us to compare the studied waveforms in a fair manner, it is necessary to define at least one parameter that will be common to all of them. In this thesis, we will therefore consider that all waveforms we study use the same subcarrier spacing $\Delta F$. All other parameters can be defined with regards to the latter, as we present in Table 2.2. It is not the purpose of this thesis to give an extensive and comprehensive description of each of the waveforms we will study, and we refer the curious reader to the references provided in the former section for more details on each specific scheme. However, some parameters selected in our analysis deserve some more in-depth explanation, which we provide here.

In order to provide comparisons that are as fair as possible, we selected - when relevant - parameters that ensure that different waveforms have the same spectral efficiency. This is why the guard band of FMT is set to have a width equal to a ninth of the subcarrier spacing. It is also why the length of the guard interval used by CP-OFDM, UFMC and f-OFDM are set to have equal values. However, this reasoning does not apply to all waveforms under study. First, OFDM/OQAM and FBMC-PAM do not use any guard interval and are the only considered waveforms that achieve an optimal Gabor density $\rho = 1$. Second, one of the heralded advantages of circular FB-MC waveforms is their capability to reduce the size of the guard interval by only inserting one every $N_b$ symbols. Therefore, we set GFDM and COQAM to use a CP that has the same absolute length than CP-OFDM.

Table 2.2: Waveform configurations considered throughout the thesis

| | **Waveform** | **Parameters** | | | |
|---|---|---|---|---|---|
| | | Prototype filter | Subcarrier spacing | Time symbol | Guard interval |
| Linear FB-MC | CP-OFDM | Rectangular | $\Delta F$ | $T = \frac{1}{\Delta F}$ | Cyclic prefix, $T_{CP} = \frac{T}{8}$ |
| | FMT | RRC filter, rolloff 0.22, duration 6T | $\Delta F$ | $T = \frac{1}{\Delta F - W_{GB}}$ | Guard band, $W_{GB} = \frac{\Delta F}{9}$ |
| | OFDM/OQAM | PHYDYAS filter, duration 4T | $\Delta F$ | $T = \frac{1}{\Delta F}$ | None |
| | FBMC-PAM | Sine filter, duration 2T | $\frac{\Delta F}{2}$ | $T = \frac{1}{\Delta F}$ | None |
| Circular FB-MC | GFDM | RRC filter, rolloff 1, duration 5T | $\Delta F$ | $T = \frac{1}{\Delta F}$ | Cyclic prefix, $T_{CP} = \frac{T}{8}$ |
| | COQAM | Phydyas filter, duration 4T | $\Delta F$ | $T = \frac{1}{\Delta F}$ | Cyclic prefix, $T_{CP} = \frac{T}{8}$ |
| Band-filtered | UFMC | Chebyshev, $-60$ dB attenuation, Length $T_{ZP}$ | $\Delta F$ | $T = \frac{1}{\Delta F}$ | Zero Prefix $T_{ZP} = \frac{T}{8}$ |
| | f-OFDM | Truncated sinc filter with $T_w = \frac{T}{2}$ | $\Delta F$ | $T = \frac{1}{\Delta F}$ | Cyclic prefix, $T_{CP} = \frac{T}{8}$ |

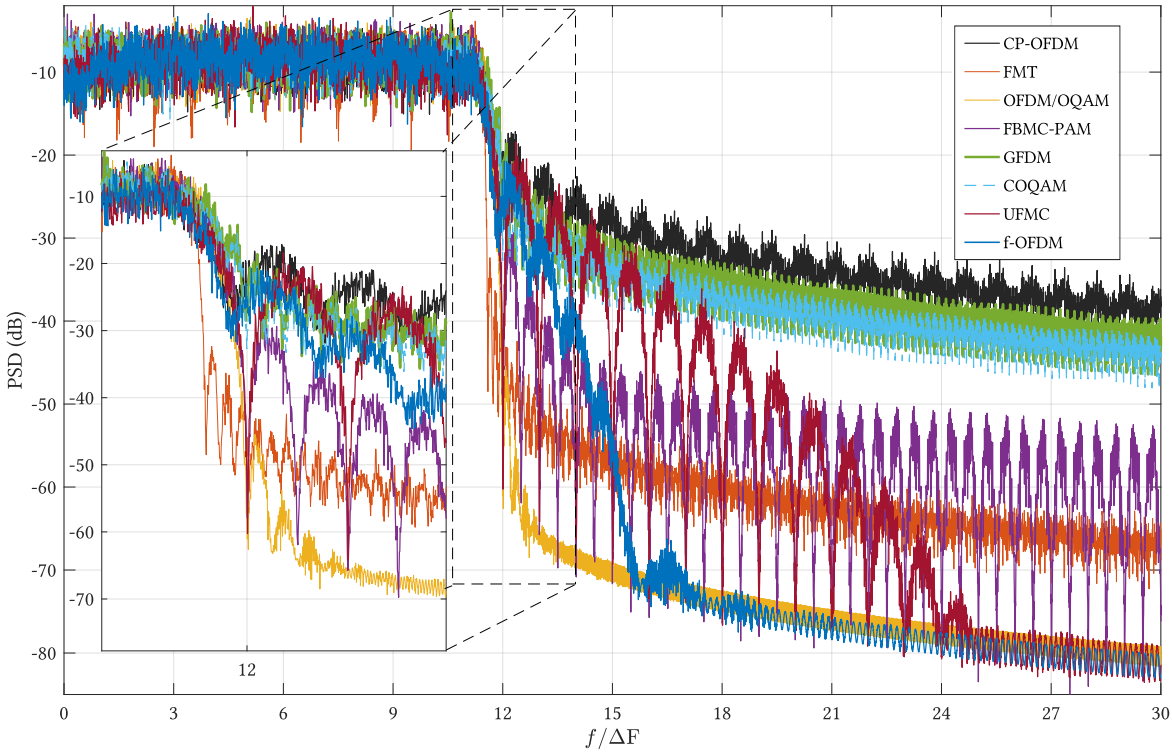


Figure 2.13: PSD of each studied waveform in a setup where 12 subcarriers are activated.

The set of waveform configurations listed in Table 2.2 gives a representative panel of the myriad of schemes that have been proposed in the literature. In the following, we review the performance of these waveforms according to a variety of different criteria.

### Spectral localization

Spectral localization is clearly the performance metric that has drawn the most attention in the course of the development of enhanced waveforms to replace OFDM. This is directly linked to the fact that the poor spectral localization of the latter has been identified as its main limiting factor. Therefore, the primary purpose of proposed waveforms is to achieve advantageous PSD characteristics. In Fig. 2.13, we represent the PSD achieved by each waveform in a setup in which 12 subcarriers are active. We see that all waveforms achieve better spectral localization than CP-OFDM. However, the gains achieved by circular FB-MC waveforms are only marginal, which is caused by the circular convolution they are based upon [99]. As we mentioned it previously, there have been a number of proposals to use additional filtering stages to improve the spectral localization of these waveforms [86, 88], but we leave these solutions out of our scope. On the other hand, linear FB-MC waveforms achieve very satisfying out-of-band rejection, in particular OFDM/OQAM. FMT and FBMC-PAM achieve improved performance, but they are outperformed by OFDM/OQAM. Finally, UFMC and

f-OFDM achieve the same rejection as OFDM/OQAM but their out-of band ripples exhibit a slower decay which is due to the fact that they use relatively short filters in time which are therefore characterized by a wider first sidelobe.

**Robustness to asynchronism in coexistence scenarios**

Though PSD is an important metric and allows one to quickly grasp the potential of a specific modulation scheme, it is not sufficient to fully understand the coexistence capabilities of each waveform. This is, in fact, an aspect that we will thoroughly investigate in this thesis. The coexistence between asynchronous users has drawn a lot of attention and a number of studies have investigated the performances of enhanced waveforms when coexisting users are misaligned in time and/or in frequency. Among all available works on the subject, [56] has stood out. In that work, the authors study separately through simulation the impact of TO and CFO on coexistence between two users that are based on either CP-OFDM, OFDM/OQAM, GFDM, COQAM or UFMC.

Here, to present the performance of each waveform when faced with TO and CFO, we adopt a similar approach as in [56]. We investigate a setup in which two users based on the different waveforms we study coexist on the same spectral band. They each use 12 subcarriers out of the 128 that compose the band. They use directly adjacent subbands, with two guard subcarriers between them. The normalized CFO and TO, expressed respectively in proportion of $\Delta$F and $\frac{1}{\Delta F}$ are varied separately to exhibit the sensitivity of each waveform setup we consider to both these effects.

In Fig. 2.14, we represent the NMSE of one user of interest when the relative TO and CFO between the two coexisting users are varied. We obtain results that are consistent with the literature [56]. First, we clearly identify that, if the timing offset is contained within the CP duration, CP-OFDM does not suffer from any interference. The same characteristic is observed for COQAM. For GFDM however, even if the timing offset is smaller than the duration of the CP it uses, some low level interference appears. This is because in our setup, the GFDM system performs a ZF detection [56]. When the timing offset goes beyond the CP though, CP-OFDM and circular FB-MC waveforms experience very high levels of interference. Even though GFDM and COQAM are approximately five times more resilient to timing offsets than CP-OFDM, they are largely outperformed by other waveforms. UFMC divides interference due to timing offset approximately by a factor ten compared to CP-OFDM. Furthermore, it exhibits a symmetric region around the perfect synchronization point in which interference is limited, which is the result of the filtering of the transmit signal. The performance of f-OFDM, which achieves even lower interference than UFMC on average, are shown to be completely independent from the value of the timing offset. In particular, even in the case where the two f-OFDM systems are perfectly synchronized, the user of interest suffers

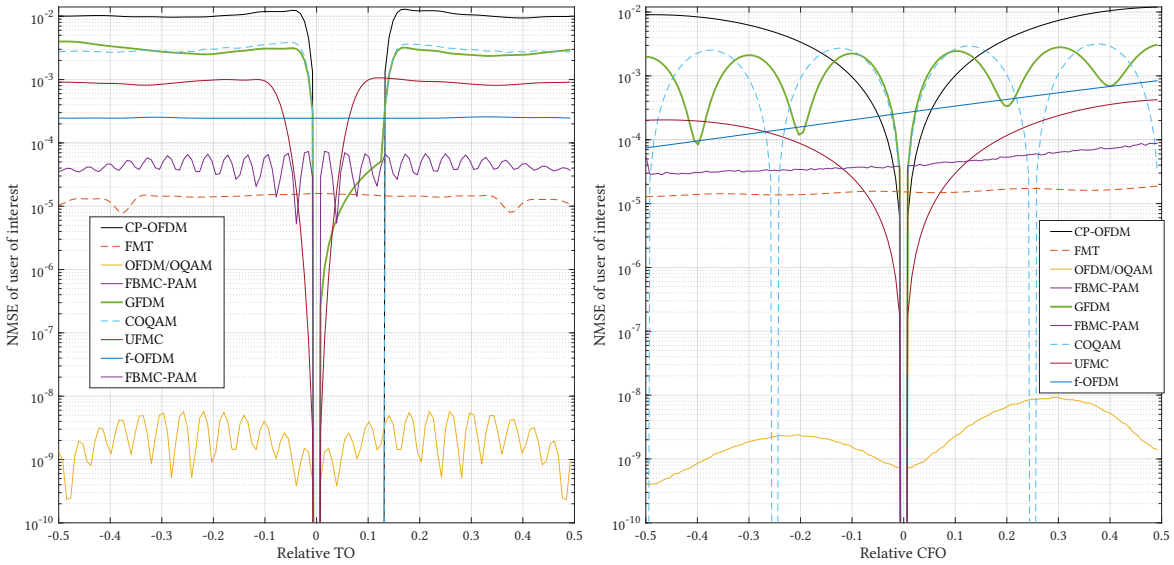


Figure 2.14: Sensitivity of enhanced multicarrier waveforms to (a) TO and (b) CFO.

from interference. This is because f-OFDM breaks orthogonality between subsequent symbols and adjacent subcarriers. The same observation applies to FMT. Both FMT and f-OFDM abandon orthogonality, but the filtering they perform ensures that their average robustness to timing offsets is increased. Out of all the studied waveforms, OFDM/OQAM exhibits the most resilient behaviour against timing offset as interference is close to non-existent. FBMC-PAM, which achieves null interference in the case where the two users are perfectly synchronized, achieves a satisfying average level of protection, but as it relies on prototype filters that are not as acutely spectrally localized than OFDM/OQAM or FMT, it suffers from higher levels of interference than both these waveforms.

In Fig. 2.14, we also represent the NMSE of the user of interest when both coexisting users exhibit some level of relative CFO. A first straightforward comment is that the interference experienced by the user of interest increases with the CFO. This is logical, as in the scenario investigated here, positive values of CFO correspond to situations where the coexisting users are brought closer together on the frequency axis. Here again, we see that even in the case where both users are perfectly synchronized, FMT and f-OFDM waveforms exhibit some interference as they break orthogonality between users. All other waveforms cancel interference between users when relative CFO is equal to 0. Once again, the best spectrally localized waveforms achieve the lowest values of interference, with OFDM/OQAM exhibiting insignificant levels of NMSE. The interference seen by FMT, FBMC-PAM and f-OFDM grows linearly with the CFO. UFMC exhibits a behavior similar to that of CP-OFDM, but at levels of interference more than ten times lower. GFDM and COQAM exhibit the same interesting

behavior, as NMSE of the user of interest achieves local minima for values of CFO that are multiples of $\frac{1}{N_b}$, which is once again consistent with [56].

### Time-spectral efficiency

Though spectral localization and robustness to asynchronism are essential characteristics, it would be useless to design waveforms that achieve acute spectral localization and are robust to asynchronism but sacrifice their time and spectral efficiency in the process, for example by using very wide guard subcarriers in the frequency domain or long guard intervals in time. Time-spectral efficiency is quite a simple concept to grasp: given a certain time and frequency band, how much of it is used to transmit useful and not redundant data? For example, the CP used in CP-OFDM incurs a loss in terms of time efficiency of $\frac{T_{\text{CP}}}{T+T_{\text{CP}}}$, which means that, with the parameters selected in Table 2.2, CP-OFDM achieves a time-spectral efficiency of $\frac{8}{9} = 88.8\%$. UFMC achieves the same exact efficiency as it uses the same guard interval time as CP-OFDM. Out of all the waveforms we consider, only OFDM/OQAM and FBMC-PAM, which do not rely on any guard interval, achieve a perfect time-spectral efficiency of 100%. However, these waveforms rely on linear filtering which incur a ramp-up and a ramp-down respectively at the beginning and the end of the transmission. Therefore, they do achieve full time-spectral efficiency for long transmission windows, but are inefficient for short bursty transmissions [66, 100]. Indeed, the ramp-up and down imposed by the linear convolution incur a fixed time efficiency loss that is independent of the amount of data transmitted. The same applies to f-OFDM, but with much lower impact given the relatively short filter it uses. Finally, GFDM and COQAM suffer from some efficiency loss due to their usage of a CP. Furthermore, GFDM and COQAM, due to their block structure, can only take advantage of transmission windows that are long enough to fit an integer number of blocks.

In details, given a certain transmission window of duration $T_{\text{Tx}}$, a waveform with optimal time-spectral efficiency (TSE) equal to 1 can transmit $\lfloor \Delta\text{F} T_{\text{Tx}} \rfloor$ multicarrier symbols. Based on the parameters listed in Table 2.2, the TSE of the multicarrier waveforms we consider in this thesis can be computed as follows:

- $\text{TSE}_{\text{CP-OFDM}} = \frac{\left\lfloor \Delta\text{F} T_{\text{Tx}} \frac{8}{9} \right\rfloor}{\lfloor \Delta\text{F} T_{\text{Tx}} \rfloor}$
- $\text{TSE}_{\text{FMT}} = \frac{\left\lfloor (\Delta\text{F} T_{\text{Tx}} \frac{8}{9} - 5) \right\rfloor^{+}}{\lfloor \Delta\text{F} T_{\text{Tx}} \rfloor}$
- $\text{TSE}_{\text{OFDM/OQAM}} = \frac{\lfloor \Delta\text{F} \left( T_{\text{Tx}} - \frac{3.5}{\Delta\text{F}} \right) \rfloor^{+}}{\lfloor \Delta\text{F} T_{\text{Tx}} \rfloor}$
- $\text{TSE}_{\text{FBMC-PAM}} = \frac{\lfloor \Delta\text{F} \left( T_{\text{Tx}} - \frac{1}{\Delta\text{F}} \right) \rfloor^{+}}{\lfloor \Delta\text{F} T_{\text{Tx}} \rfloor}$
- $\text{TSE}_{\text{GFDM}} = \frac{5 \left\lfloor \frac{\Delta\text{F} T_{\text{Tx}}}{5+1/8} \right\rfloor}{\lfloor \Delta\text{F} T_{\text{Tx}} \rfloor}$

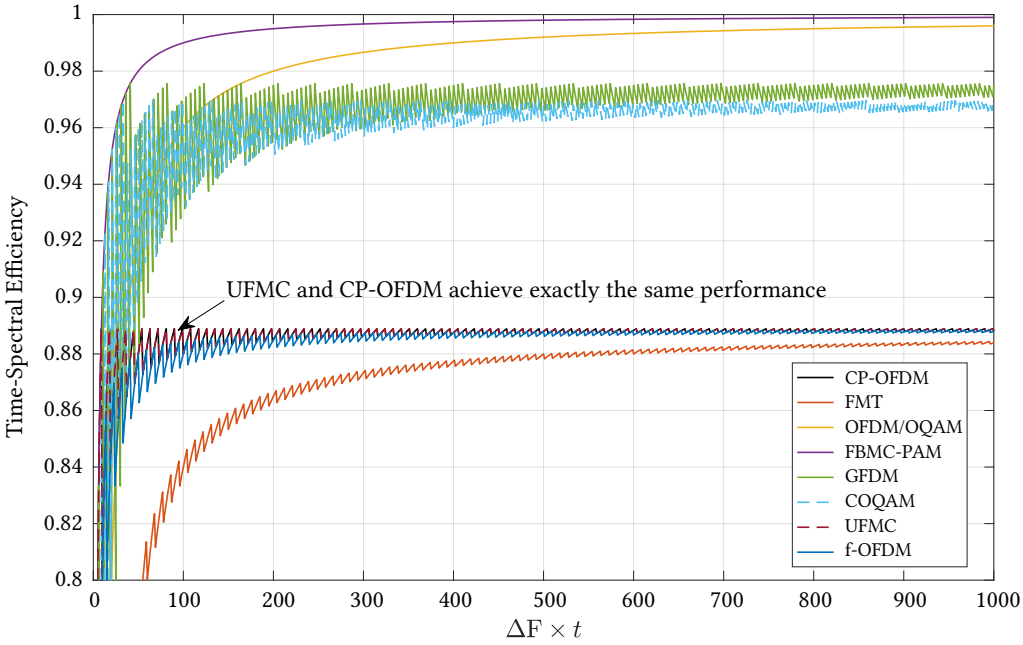


Figure 2.15: Time-spectral efficiency of enhanced multicarrier waveforms

– $\mathrm{TSE}_{\mathrm{COQAM}} = \frac{4\left\lfloor \frac{\Delta \mathrm{F} T_{\mathrm{Tx}}}{4+1/8} \right\rfloor}{\lfloor \Delta \mathrm{F} T_{\mathrm{Tx}} \rfloor}$

– $\mathrm{TSE}_{\mathrm{UFMC}} = \mathrm{TSE}_{\mathrm{CP\text{-}OFDM}}$

– $\mathrm{TSE}_{\mathrm{f\text{-}OFDM}} = \frac{\left\lfloor (\Delta \mathrm{F} T_{\mathrm{Tx}} - \frac{1}{2}) \frac{8}{9} \right\rfloor^{+}}{\lfloor \Delta \mathrm{F} T_{\mathrm{Tx}} \rfloor}$

The TSE of each waveform is reported in Fig. 2.15, which makes it easy to evaluate which waveform is more advantageous according to the duration of the transmission window considered. Clearly, FMT, which combines a CP and a long prototype filter achieves the smallest TSE of all waveforms. UFMC and CP-OFDM have exactly the same TSE and are closely followed by f-OFDM. GFDM and COQAM which use a shorter CP achieve asymptotically a higher TSE, but are out-performed by OFDM/OQAM and FBMC-PAM which are the only waveforms that asymptotically tend to a TSE of 1. Furthermore, FBMC-PAM uses a short prototype filter and therefore outperforms all other waveforms whatever he length of the transmission window. OFDM/OQAM on the other hand is more advantageous than CP-OFDM from $\Delta \mathrm{F} T_{\mathrm{Tx}} > 35$ on and than GFDM and COQAM from $\Delta \mathrm{F} T_{\mathrm{Tx}} > 125$.

### Raw BER performance

A metric of tremendous importance, the raw BER achievable by each waveform is of prime interest. Indeed, what would be the point of using highly spectrally localized waveforms if it

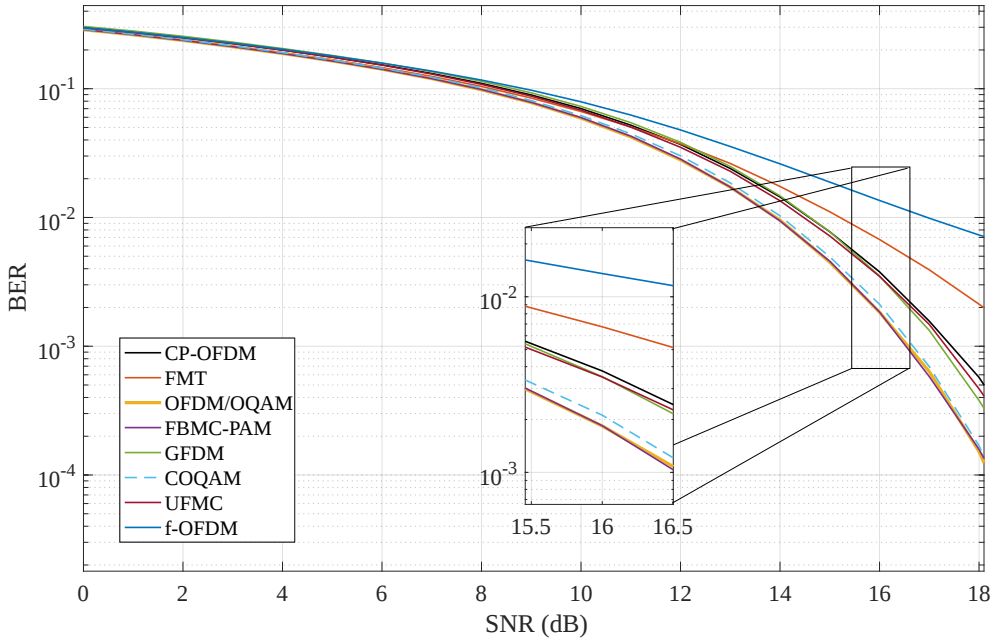


Figure 2.16: Uncoded BER achieved by studied waveforms on an AWGN channel for an uncoded 16-QAM constellation.

were at the cost of transmission quality ? We represent the BER of the different waveforms achieved on an AWGN channel in Fig. 2.16. The results reported in that figure show that CP-OFDM and UF-OFDM achieve the same BER. OFDM/OQAM and FBMC-PAM benefit from the fact that they do not use any CP: therefore, at a given symbol energy, OFDM/OQAM and FBMC-PAM achieve slightly better performance than CP-OFDM and UFMC which waste some energy in the CP transmission. COQAM shares the same advantage as the proportion of energy dedicated to the CP is smaller than in the case of CP-OFDM. GFDM, though it benefits from the same advantage as COQAM, sees its performance degraded by the ZF reception it performs to cancel ICI [101]. Finally, FMT and f-OFDM, which suffer from inherent ISI and ICI in the configurations we selected, exhibit poor raw BER performance. Nevertheless, this higher raw BER can be compensated for with appropriate coding and reception techniques which are out of the scope of this thesis.

### Other criteria

In addition to the criteria listed above which will be predominant in our analysis, it is important to mention other design criteria that are less relevant in the context of this thesis but that will play an important role in the choice of the waveform used by future wireless

communication systems. Therefore, though we will not directly study these criteria in this thesis, it is worth mentioning them here.

**Orthogonality and MIMO capability:** One of the key technologies that must be enabled by 5G communication networks is the use of multiple antenna techniques, a.k.a. MIMO. Indeed, MIMO promises to make it possible to scale up the rate achievable by communication systems by taking advantage of spatial diversity techniques. The detailed description of MIMO theoretical background is out of the scope of this thesis and we refer the reader to the relevant literature [102–104].

MIMO techniques such as Alamouti precoding mostly rely on the fact that transmitted symbols are orthogonal in the complex domain. This condition is sufficient to make virtually any MIMO technique designed for CP-OFDM work on top of another waveform. Therefore, MIMO techniques are directly applicable to f-OFDM and UFMC which maintain complex orthogonality between symbols [90, 91]. The same applies to circular FB-MC waveforms which preserve the CP-based structure of CP-OFDM [99]. Linear FB-MC waveforms, because of their inherently different structure, cannot natively support MIMO techniques with the exception of FMT [20]. In particular, OQAM based waveforms which only achieve orthogonality between symbols in the real domain real are not fit for direct MIMO transmission. However, it has been recently shown that, provided that appropriate precoding is performed, complex domain orthogonality can be retrieved and MIMO techniques made applicable [82, 83] at the cost of slightly increased complexity. Overall, all the waveforms we study can hence be considered as capable of supporting MIMO transmission techniques.

**Complexity:** One of the main reasons behind the commercial success of CP-OFDM is its very low complexity, as it only relies on an IFFT at the transmitter and a FFT at the receiver. Therefore, potential replacements of CP-OFDM should keep complexity within an acceptable range in order to be considered as credible alternatives to CP-OFDM. Complexity is an aspect that tends to be overlooked by the academic community, but it has to be noted that several works have recently investigated low complexity implementation schemes for enhanced multi-carrier waveforms. In particular, the authors in [47, 105] have shown that linear FB-MC techniques can be implemented with a complexity which is from 3 to 10 times that of CP-OFDM, and have successfully implemented OFDM/OQAM transmission on hardware platforms. Furthermore, circular FB-MC techniques have also been shown to be implementable with a complexity of less than 10 times that of CP-OFDM [87, 99], and even lower complexity increases are associated with band-filtered waveforms [90, 93, 94]. Given the constant improvements of hardware and the associated increase in computation capability, the rise in complexity associated with each of the studied waveform schemes is largely affordable, and complexity should therefore not be seen as a limiting factor.

**Peak to average power ratio (PAPR):** Though completely anecdotal in the context of this thesis, it is worth mentioning that PAPR might be an important design criterion for future networks. Indeed, the PAPR associated with each waveform is directly linked to the energy efficiency they make possible to achieve. In fact, the lower the PAPR, the closer to the saturation point of the high power amplifier the devices can operate without incurring any distortion to the transmit signal. Some works have claimed that some FB-MC waveforms could achieve lower PAPR than CP-OFDM [106]. However, these works usually do not perform fair comparison between FB-MC waveforms and CP-OFDM. In fact, the authors in [107] have proven that, at a given subcarrier spacing, CP-OFDM achieves the lowest PAPR among all FB-MC waveforms we study in this thesis. Overall, all waveforms proposed to replace CP-OFDM have shown to achieve similar PAPR. Recently, only some waveforms based on wavelet transforms have proven to achieve lower PAPR than CP-OFDM [107]. However, these solutions are out of the scope of this thesis.

#### Summary

In this section, we aimed to present some key results about the waveforms we will study in this thesis. All waveform schemes have different advantages but also shortcomings. Our study will focus on their coexistence capabilities in asynchronous networks, but other criteria will also be taken into account to evaluate the advantages of using a specific scheme for the applications of interest in our study.

## 2.5 Open research problems

In this chapter, we have briefly presented the structure of OFDM, the waveform used by most current-day wireless networks. In particular, we have detailed how it is applied in multiuser networks. We explained that wireless networks are both bound to be faced with coexistence issues in the coming years because of new applications like TVWS exploitation or D2D communication. In both these coexistence scenarios, we explained the shortcomings of OFDM which are the main motivation fueling research towards new multi-carrier waveforms with enhanced spectral localization. We then described the advantageous characteristics of these waveforms that make them very appealling in coexistence scenarios.

Based on this presentation, we see that new waveforms are a promising technique to be used by secondary users in the coexistence contexts we introduced in section 2.3. However, in both the TVWS and the D2D scenarios, secondary users will coexist with OFDM-based incumbent networks and, to the best of our knowledge, the coexistence between OFDM and 5G waveforms has not been thoroughly studied in the literature. In this thesis, we will therefore tackle this problem by answering the following questions:

- Given a setup in which a FB-MC and an OFDM based device coexist, how can we model the interference that arises between them ?
- Applying the answer to the previous question to a CR scenario in which the incumbent system is based on OFDM, what are the gains to expect if the secondary network relies on FB-MC instead of OFDM ?
- In a scenario such as D2D communication underlaying OFDM-based cellular networks in which there are multiple asynchronous secondary users, what gains are achievable through the use of FB-MC ?

In order to answer these three questions that we will tackle respectively in chapters 4,5 and 6, we review in the upcoming chapter 3 the works that are particularly relevant to our studies, in particular on the matter of interference modeling and coexistence between systems based on different waveforms.

# Chapter 3

# Related work and corresponding contributions

**Contents**



## 3.1 Introduction

In the previous chapter, we have laid out the main research questions that we propose to answer based on our review of the current state of wireless networks and their foreseen evolution. In particular, we have pointed out that the coexistence between enhanced multicarrier waveforms and CP-OFDM has not been well studied in the literature. In this chapter, we review the different approaches that are relevant to our work. In particular, we focus in section 3.2

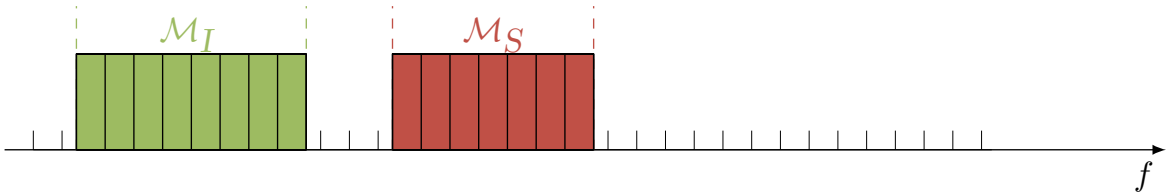


Figure 3.1: Spectral representation of the considered scenario. The incumbent and secondary systems coexist in the same spectral band, and each one is assigned a different subset of subcarriers. Because the systems are not coordinated, the secondary system may misalign its subcarriers with respect to the frequency basis of the incumbent by a frequency offset $\delta_{\mathrm{f}}$.

on the different ways that interference has been modeled in coexistence scenarios, and we identify two main approaches in the literature: a PSD-based approach on the one hand, and Asynchronous Interference Modeling (AIM) on the other hand. Furthermore, in section 3.3, we list the different experimental studies that address the problem of spectral coexistence between asynchronous users. In section 3.4 we review works that have studied the application of 5G waveforms for coexistence with OFDM-based networks, in particular in the context of CR and D2D communication. Finally, we conclude this chapter in section 3.5 by summarizing the key limitations and flaws of currently available studies. Based on this analysis, we detail the major contributions that we will present in the following of this thesis.

## 3.2 Interference modeling in coexistence scenarios

### 3.2.1 Spectral coexistence system model

Let us consider a scenario in which two systems, a secondary $\mathcal{S}$ and an incumbent $\mathcal{I}$, coexist in the same spectral band as is represented in Fig. 3.1 in which they use adjacent, non-overlapping spectral resources. In the following, parameters indexed as $\cdot_I$ and $\cdot_S$ refer to the incumbent and secondary system respectively. This setup is a canonical example of spectral coexistence and a vast amount of works have aimed at answering the question: “How can we model the interference caused by each user onto the other ?”. The first works addressing this question date back to the beginning of the century when the cognitive radio concept increasingly gained popularity after Mitola’s Ph.D. dissertation [32]. The need for a model of interference usable for cognitive radio deployments in spectral coexistence setups was soon identified by Haykin in [34] where he defined the term *interference temperature*. However, at that time, the research community did not identify clearly the links between this concept and the PHY layer problematics, especially the choice of waveform. It is only when Weiss and Jondral coined the term "spectrum pooling" in [108] that they defined a waveform-dependent model to compute interference between systems coexisting on the same spectral band. The model they defined went on to be known as the "PSD-based model" in the literature.

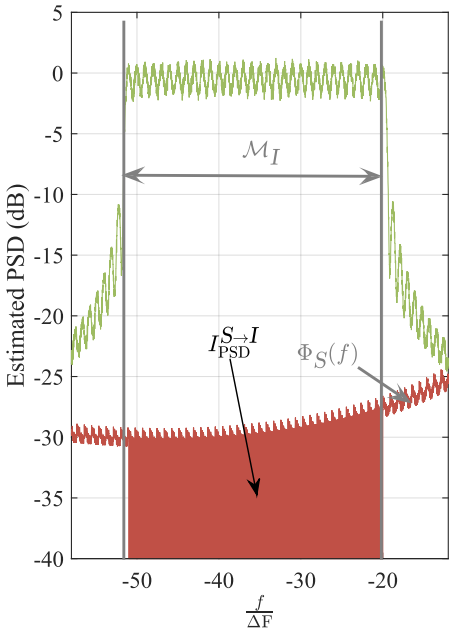


Figure 3.2: Principle of the PSD-based modeling of interference. Note that this representation is given in the case where the two signals arrive with the same power at the receiver, i.e. $P_S G_{SI} = P_I G_{II}$. The PSD-based modeling of interference consists in integrating the PSD of the interfering signal on the band of interest.

This model has then been extensively used to compute interference between secondary and incumbent users in cognitive radio scenarios in which both systems would utilize CP-OFDM [108, 109]. Because of the high OOB emissions of CP-OFDM, research works based on the PSD-based model that we will present later on showed that CP-OFDM is not well adapted for spectrum sharing between secondary and incumbent users [17]. As we mentioned it in the previous chapter, this observation was one of the many arguments that fostered the research of a new waveform able to replace CP-OFDM in 5G systems. Whatever the specific details of the aforementioned waveforms, they all achieve lower OOB emissions than CP-OFDM thanks to their inherent filtering of the transmitted symbols. Because of these advantageous PSD properties that we illustrated in Fig. 2.13, an important amount of research works have investigated the benefits of using these FB-MC waveforms for coexistence with legacy CP-OFDM incumbent users, for example [46, 109–112]. Given the wide adoption of the PSD-based model, we detail its principle in the following.

### 3.2.2 PSD-based modeling

#### Model definition

The PSD-based model consists in computing the leakage caused by users onto each other by integrating the PSD of the interfering signal on the band that suffers from the interference. Therefore, in the scenario that we described in Fig. 3.1, according to the PSD-based model, the interference caused by the secondary system onto the incumbent is simply obtained by integrating the PSD of the secondary signal on the band $\mathcal{M}_\mathrm{I}$ of the incumbent CP-OFDM system. Defining $I_{\mathrm{PSD}}^{\mathrm{S}\to\mathrm{I}}$ the interference injected by the secondary system onto the incumbent one according to the PSD based model, it is expressed as

$$I_{\mathrm{PSD}}^{S\to I} = P_S G_{SI} \int_{\mathcal{M}_I} \Phi_S(f)\,\mathrm{d}f, \tag{3.1}$$

where $\Phi_S$ represents the PSD of the secondary signal modulated by secondary system $S$, $P_S$ is the transmit power of the secondary and $G_{SI}$ is the gain associated with the channel $h_{SI}$.

Considering that the secondary system modulates i.i.d. symbols with unitary power on each subcarrier, its PSD is defined as

$$\forall f \in \mathbb{R}, \Phi_S(f) = \sum_{m\in\mathcal{M}_S} \Phi_m(f) = \sum_{m\in\mathcal{M}_S} \Phi_{\mathrm{WF},S}(f - m\Delta\mathrm{F}), \tag{3.2}$$

where $\Phi_{m,S}(f)$ is the PSD of the $m$th subcarrier of system $S$, and is directly obtained from $\Phi_{\mathrm{WF},S}$, the PSD of one subcarrier of the waveform used by the secondary system, as presented in Fig. 3.4. Therefore, it follows that, according to the PSD-based model,

$$I_{\mathrm{PSD}}^{S\to I} = \sum_{m_s\in\mathcal{M}_S} \sum_{m_i\in\mathcal{M}_I} I_{\mathrm{PSD}}^{S\to I}(m_s - m_i), \tag{3.3}$$

with

$$\forall l \in \mathbb{Z}, I_{\mathrm{PSD}}^{S\to I}(l) = P_S G_{SI} \int_{l\Delta\mathrm{F}-\frac{\Delta\mathrm{F}}{2}+\delta\mathrm{f}}^{l\Delta\mathrm{F}+\frac{\Delta\mathrm{F}}{2}+\delta\mathrm{f}} \Phi_{\mathrm{WF},S}(f)\,\mathrm{d}f. \tag{3.4}$$

With this notation, $I_{\mathrm{PSD}}^{S\to I}(l)$ corresponds to the amount of interference injected by a certain subcarrier $m_s$ of the secondary onto a subcarrier $m_i$ of the incumbent such that $m_s - m_i = l$.

Following the symmetric reasoning, the total interference caused by the incumbent system on the secondary is expressed, according to the PSD-based model, as

$$I_{\mathrm{PSD}}^{I\to S} = \sum_{m_s\in\mathcal{M}_S} \sum_{m_i\in\mathcal{M}_I} I_{\mathrm{PSD}}^{I\to S}(m_s - m_i), \tag{3.5}$$

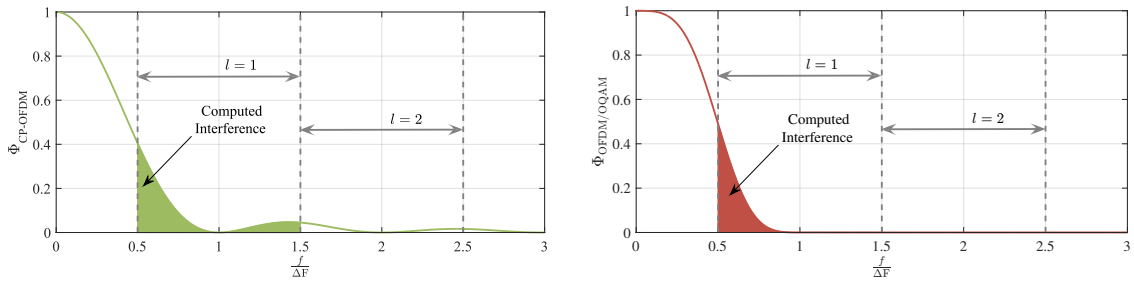


(a) (b)

Figure 3.3: Principle of PSD-based modeling of interference, applied to two waveforms. (a) : CP-OFDM, (b) : OFDM/OQAM. It applies in the exact same way to other FB-MC waveforms analyzed in this thesis.

$$\forall l \in \mathbb{Z}, I_{\text{PSD}}^{I \to S}(l) = P_I G_{IS} \int_{l-\frac{\Delta F}{2}}^{l+\frac{\Delta F}{2}} \Phi_{\text{WF},I}(f)\, \mathrm{d}f, \tag{3.6}$$

where $P_I$ is the transmit power of the incumbent and $G_{IS}$ the gain associated with channel $h_{IS}$.

An illustration of how the PSD-based model is used to compute the interference caused by the CP-OFDM and OFDM/OQAM waveforms is given in Fig. 3.3. We show that the interference caused by the subcarrier of index 0 onto the subcarrier of index $l$ is computed by integrating the PSD of subcarrier 0 on the width corresponding to subcarrier $l$. Note that this model applies exactly in the same way to the other FB-MC waveforms we analyze in this study.

### PSD-based model applied to FB-MC waveforms

In Fig. 3.4, we present the PSD of one subcarrier of the aforementioned waveforms with the chosen parameters. Note that, to achieve a fair comparison, we consider that not one, but two adjacent subcarriers of the FBMC-PAM system are active. The presented PSD curves can be used to compute the value of interference caused by each waveform at any given spectral distance according to the PSD-based model. Note that the PSD-based model is not applicable to subband-filtered waveforms, as it relies on the fact that all subcarriers have the same PSD. Therefore, it is only applicable to FB-MC waveforms which perform a per-subcarrier filtering. We present in Table 3.1 the values of $I_{\text{PSD}}^{S \to I}(l)$ obtained for all studied FB-MC waveforms in the case where $P_S G_{SI} = 0\ dB$ and $\delta \text{f} = 0$. As expected, we see that the PSD-based model predicts that waveforms with better spectral localization will inject the lowest amount of interference onto the incumbent CP-OFDM system. In details, we see

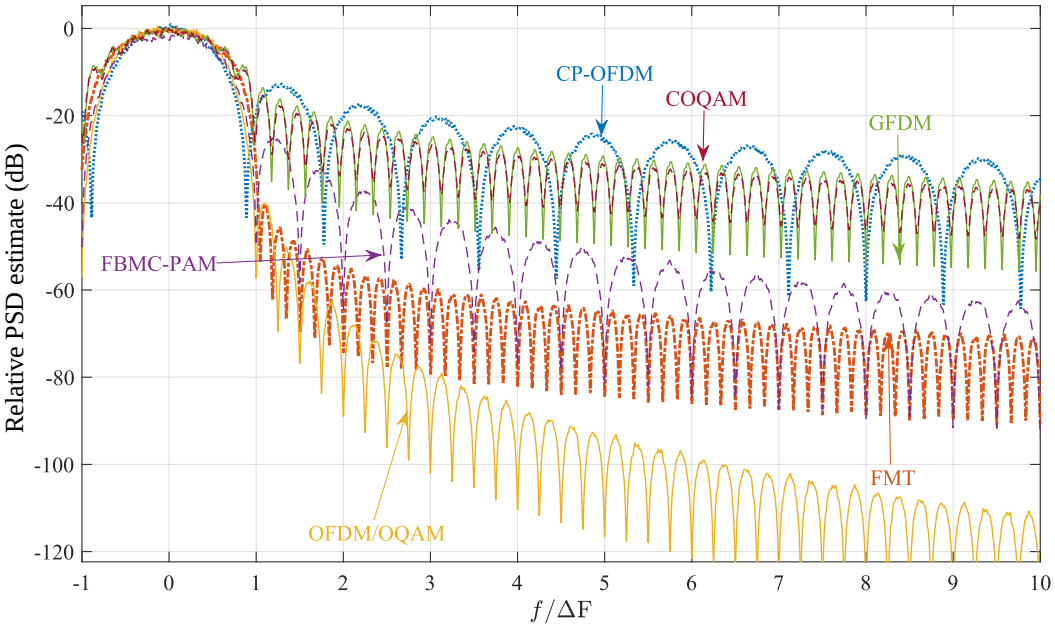


Figure 3.4: Welch estimate of the PSD level of studied waveforms with a Hanning Window of length $\frac{100}{\Delta F}$ and a frequential resolution of 500 points per subcarrier. PSD values are expressed relatively to their maximum.

Table 3.1: Interference tables in dB computed according to the PSD-based model for studied waveforms.

| $l$ | CP-OFDM | FMT | OFDM/ OQAM | FBMC- PAM | GFDM | COQAM |
|---|---|---|---|---|---|---|
| 0 | -1.28 | -1.26 | -0.99 | -2.64 | -1.59 | -1.47 |
| 1 | -12.3 | -10.8 | -12.3 | -13.1 | -10.0 | -10.3 |
| 2 | -20.1 | -57.2 | -65.4 | -37.2 | -24.1 | -24.7 |
| 3 | -23.9 | -62.7 | -80.7 | -45.3 | -28.1 | -28.9 |
| 4 | -26.4 | -65.7 | -89.6 | -50.6 | -30.8 | -31.5 |
| 5 | -28.0 | -68.0 | -96.1 | -54.6 | -32.8 | -33.4 |
| 6 | -29.2 | -70.0 | -101. | -58.0 | -34.2 | -35.0 |
| 7 | -30.3 | -71.0 | -105. | -60.6 | -35.5 | -36.2 |
| 8 | -31.4 | -72.2 | -109. | -63.0 | -36.7 | -37.4 |
| 9 | -32.6 | -73.2 | -112. | -65.1 | -37.8 | -38.5 |

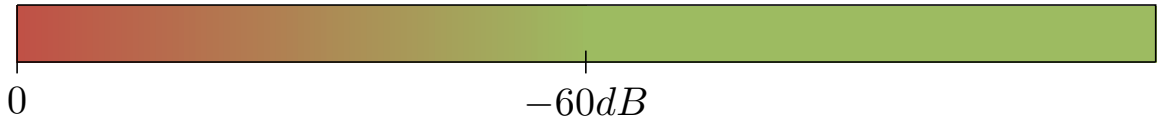

clearly that the PSD-based model predicts that OFDM/OQAM, FMT and FBMC-PAM can be used efficiently to coexist with CP-OFDM incumbent systems. On the contrary, GFDM and COQAM systems only reduce the interference onto incumbent systems by 5 dB compared to CP-OFDM based secondary systems. This is caused by the circular filtering which incurs steep variations in the transmit signal and therefore causes projections on the whole spectrum.

#### Limitations of the PSD-based model

Though the PSD-based model presented above is widely used in the literature, it suffers some limitations: in particular, being based purely on frequency considerations, it is unable to encompass phenomenons related to time synchronism. This was tackled by Medjahdi *et. al.* who showed in [113, 114] that the main drawback of the PSD-based model lies in the fact that it cannot encompass time asynchronism between coexisting systems. This is a major drawback that does not enable us to analyze the effects of the time misalignment between users. For example, the PSD-based model predicts that two coexisting CP-OFDM incumbent systems will interfere onto each other, even if they are synchronized within the CP, which is in contradiction with the results we presented if Fig. 2.14. In the following, we present alternative modeling approaches that enable one to take into account this asynchronism.

### 3.2.3 Asynchronous interference modeling

#### Model definition

Consider the system model of Fig. 2.1 and the spectral coexistence layout of Fig. 3.1. As there is no explicit synchronization between the coexisting systems, the secondary system $S$ may be desynchronized with a timing offset $\delta\mathrm{t}$ with regards to the incumbent system $I$. Not taking into account the effects of channel propagation and noise, the signal received at the incumbent receiver is expressed as

$$y_I(t) = s_I(t) + s_S(t - \delta\mathrm{t}). \tag{3.7}$$

Then, after demodulation, the interfering signal on the $n_0$-th symbol and $m_0$-th subcarrier of the incumbent system $I$ is obtained by computing the convolution product of the receive filter of the incumbent on subcarrier $m_0$ with the secondary signal $s_S(t - \delta\mathrm{t})$ as follows

$$\boldsymbol{\eta}_{I,m_0}[n_0] = \int_{-\infty}^{\infty} f_{n_0,\mathrm{R},I(t-n\Delta\mathrm{T})} s_S(t - \delta\mathrm{t}) e^{-j2\pi m_0(t-n\Delta\mathrm{T})}\,\mathrm{d}t. \tag{3.8}$$

Furthermore, given the expression of the multicarrier signal given in (4.2),

$$s_S(t-\delta\mathrm{t}) = \sum_{n\in\mathbb{Z}}\sum_{m\in\mathcal{M}_S} \mathbf{d}_{S,m}[n] f_{n,\mathrm{T},I}(t-\delta(t)) e^{j2\pi m(t-n\Delta\mathrm{T}-\delta\mathrm{t})}, \tag{3.9}$$

and therefore,

$$\boldsymbol{\eta}_{I,m_0}[n_0] = \sum_{m\in\mathcal{M}_S} \underbrace{\sum_{n\in\mathbb{Z}} \mathbf{d}_{S,m}[n] \int_{-\infty}^{\infty} f_{n,\mathrm{T},I}(t-\delta\mathrm{t}) f_{n_0,\mathrm{R},I(t-n\Delta\mathrm{T})} s_S(t-\delta\mathrm{t}) e^{j2\pi m(t-n\Delta\mathrm{T}-\delta\mathrm{t})} e^{-j2\pi m_0(t-n\Delta\mathrm{T})}\,\mathrm{d}t}_{\boldsymbol{\eta}_{I,m\to m_0}}, \tag{3.10}$$

where $\boldsymbol{\eta}_{I,m\to m_0}$ represents the share of interference that is caused by subcarrier $m$. Then, the average amount of interference caused by subcarrier $m$ onto subcarrier $m_0$ is expressed as

$$I(m,m_0) = E_{\delta\mathrm{t},\mathbf{d}_S}\left(|\boldsymbol{\eta}_{I,m\to m_0}|^2\right). \tag{3.11}$$

Furthermore, as Medjahdi states in [114], only the value difference $m-m_0$ affects the value of $\boldsymbol{\eta}_{I,m\to m_0}$. Therefore, defining $l=m-m_0$ as for the PSD-based model, we have

$$I^{S\to I}_{\mathrm{AIM}}(l) = E_{\delta\mathrm{t},\mathbf{d}_S}\left(|\boldsymbol{\eta}_{I,m\to m_0}|^2\right), \tag{3.12}$$

where AIM stands for asynchronous interference modeling. Note that this model can directly be extended to take into account frequency misalignement between user $\delta$f.

### Asynchronous interference modeling applied to FB-MC waveforms

In his thesis [114], Medjahdi applied the AIM approach he defined to compute interference between asynchronous users based on either CP-OFDM or OFDM/OQAM. In the case of CP-OFDM, he obtained closed-form expressions of $I^{S\to I}_{\mathrm{AIM}}(l)$ in the case where the timing offset between users $\delta$t is uniformly distributed. However, explicit closed-forms are more difficult to obtain in the case of OFDM/OQAM due to the more intricate expression of the used prototype filter. Nevertheless, it was shown in [115] that using this modeling approach yielded accurate evaluation of key metrics in asynchronous networks, such as SINR, BER or spectral efficiency.

Furthermore, this approach can be straightforwardly applied to any other FB-MC waveforms, as it only requires the knowledge of the transmit and receive prototype filters used by the considered systems. However, as for the PSD-based model, this approach is not applicable to UFMC and f-OFDM. Indeed, the AIM approach computes the interference created by one subcarrier onto another, whereas f-OFDM and UFMC apply filtering on groups of subcarriers. Overall, whereas it is feasible to design systematic interference models for FB-MC waveforms

because of the equivalence of each subcarrier, it is much more complicate to achieve the same for subband-filtered waveforms, in which different subcarriers are differently affected by the transmit and receive filter.

#### Limitations of the asynchronous interference model

Apart from its inapplicability to subband-filtered waveforms, the asynchronous interference modeling approach suffers a number of other shortcomings. In particular, the distribution followed by the interference signal is not clearly defined by this model, which only computes the average power of interference. The study in [114] assumes that the distribution of interference is Gaussian, but this has to be further validated. Furthermore, this approach has only been applied in homogeneous coexistence scenarios, in which the incumbent and secondary systems share the same waveform design. However, as we stated previously in this thesis, we are interested in studying heterogeneous coexistence deployments, in which only the secondary utilizes an enhanced waveform while the incumbent sticks to CP-OFDM. It is not yet clear how the AIM approach would apply in that particular context and this matter has to be investigated.

### 3.2.4 Summary

Given a spectral coexistence scenario in which two systems share the same spectral band, each of them transmitting on a subset of all available subcarriers, several approaches have been used to measure the level of interference that arises between them. The PSD-based approach has been widely used, as it gives a simple way to compute interference caused by the secondary system onto the incumbent by looking purely at the spectral localization of the secondary signal. However, because this model is based only on the properties of the transmit signal, it is inaccurate and a modeling approach that takes into account the receive operations by the incumbent system is necessary. In particular, the AIM approach has been proposed to take into account potential time offsets between the secondary transmitter and the incumbent receiver. This approach has proven to be much more accurate than the PSD-based model, but does not directly apply to the heterogeneous coexistence scenario we consider in which the secondary and the incumbent systems are based on different waveforms. The only work available on that topic so far is [116] in which the authors study the coexistence between UFMC and CP-OFDM. However, a thorough study of coexistence between FB-MC waveforms and CP-OFDM is still missing.

Based on these observations, we provide the following contributions in chapter 4:

1. We extend the AIM approach to our coexistence problem, and propose an EVM-based modeling of the interference between FB-MC and CP-OFDM users.

2. We carefully analyze the statistical distribution of the interference signal arising between FB-MC and CP-OFDM users.

3. We study the difference between the PSD-based model results and our modeling of interference.

4. We provide closed-form expressions of the interference caused by multiple FB-MC waveforms onto CP-OFDM users.

## 3.3 Experimental studies

In addition to theoretical and simulation-based studies cited here above, a number of experimental works have studied the coexistence between enhanced multicarrier waveforms and CP-OFDM. In [47], the authors present a hardware implementation of an OFDM/OQAM secondary system that they propose to use to coexist with DVB-T systems in TVWS setups. They show that the secondary system can transmit with more power if it uses OFDM/OQAM instead of CP-OFDM. However, this result is based on qualitative observation of the TV signal quality received by the incumbent systems, which makes it hardly reproducible. In [117, 118], the authors study the coexistence of multiple waveforms with legacy CP-OFDM based receivers. In details, they measure experimentally the layer 3 goodput of a LTE uplink receiver confronted with interference coming from an asynchronous secondary transmitter. They show that if the latter uses GFDM, it can transmit approximately with 3 dB more power than a secondary that would use CP-OFDM. However, this work is based on high-level metrics, and, in the case where the secondary is based on CP-OFDM, it assumes the worst case scenario in which the secondary and incumbent system have a CFO of half a subcarrier. Furthermore, in [119, 120], the authors measure the EVM and NMSE of a CP-OFDM receiver that faces interference from different enhanced waveforms. However, they do not properly compare the values that are achieved according to the waveform used by the secondary system, which makes it hard to use the results. Most recently in [121, 122], the authors have described an OFDM/OQAM overlay system that they used in the DySPAN 2017 spectrum contest to coexist with a CP-OFDM based incumbent network. However, their article only describes the architecture of the system and does not provide any insight on the gains obtained by using OFDM/OQAM instead of CP-OFDM. Overall, available experiments fail to provide low-level, reproducible results. At the end of chapter 4, we aim at solving this issue by presenting a software radio testbed of our own design that can accurately measure the interference caused by any FB-MC waveform on each subcarrier of a CP-OFDM receiver. The presented testbed can then be used to validate our theoretical analysis of interference.

## 3.4 Enhanced waveforms for coexistence with incumbent CP-OFDM systems

In the former section, we reviewed works that aim at precisely computing the level of interference created by the secondary user onto the primary system according to the waveform used by the former. Here, we summarize relevant works which do not focus on interference modeling but rather build up on available models to study the impact of the waveform used by the secondary system in different coexistence setups. First, we review some works addressing the impact of the used waveform in the field of CR. Then, we study the available literature addressing the use of enhanced multicarrier waveforms in the context of D2D communication.

### 3.4.1 CR context

There is a plethora of research on the topic of the applicability of enhanced waveforms in CR setups, and we will therefore not make a list of all available works on the topic. Rather, we select representative studies and we pay a close attention to the assumptions that are made on the waveform used by both the secondary and the incumbent systems. Works on this subject can be roughly classified in two approaches.

The first category of works focuses on the improved spectral localization associated with the use of enhanced multicarrier waveforms to investigate to what extent they can facilitate the insertion of a secondary system in a spectral hole. These works usually analyze the amount of subcarriers that can be turned on in a given spectral hole, or the width of the guard band that is necessary to protect the incumbent system given a certain spectral mask [46, 110, 123–127]. Overall, none of these works properly defines what waveform the incumbent system uses and they solely rely on the PSD of the transmit secondary signal to draw conclusions.

Another stream of research works has studied optimal resource and power allocation techniques for the secondary system [109, 128, 129]. These works usually rely on the PSD-based model to compute the level of interference that is injected by the secondary system onto the incumbent. Therefore, they do not take into account the specificities of the incumbent system either. On the other hand, some works explicitly study homogeneous coexistence scenario, in which both the incumbent and secondary systems utilize the same waveform [115, 130, 131] and rely on the AIM-based model to take into account the effects of time misalignements between the two systems. Overall, we therefore see that works on the application of enhanced waveforms in CR setups either overlook the impact of the waveform used by the incumbent system, or have only considered setups in which both systems use the same waveform. Thus, it is crucial to accurately study CR setups in which the secondary system uses an enhanced multicarrier waveform whereas the incumbent is based on CP-OFDM.

### 3.4.2 D2D context

As we have mentioned in chapter 2, enhanced waveforms look particularly appropriate in the realm of D2D communications given the fact that accurate synchronization between different D2D pairs, as well as between D2D pairs and cellular users, may be difficult or even impossible to achieve. Given the rising popularity of D2D in the latest years, some works have recently studied the potentials gains brought by the use of new waveforms in this new kind of communication setups. To the best of our knowledge, [58] has been the first work to address this topic. In that work, the authors study a setup in which OFDM/OQAM based D2D users underlay an OFDMA network. However, they fail to properly study the interference arising between CP-OFDM and OFDM/OQAM users, and rely once more on PSD-based measures of interference. It is in fact the only work available in the literature that explicitly studies the coexistence between CP-OFDM based cellular users and D2D systems based on another enhanced multicarrier waveform. Some other works [59–61, 132–135] have investigated the use of enhanced multicarrier waveforms for D2D communication, but either did not consider the presence of cellular users or assumed that both cellular systems and D2D users are based on the same waveform. Therefore, exactly as in the context of CR, we see that it is crucial to properly investigate scenarios of coexistence between D2D systems based on enhanced multicarrier waveforms and legacy CP-OFDM based users.

### 3.4.3 Summary

Both in the D2D and CR context, heterogeneous setups in which only the secondary system utilizes an enhanced waveform whereas the incumbent still relies on CP-OFDM have not been properly analyzed in the literature. In chapter 5, we therefore study typical CR setups and present the following contributions:

1. We use the interference model we will devise in chapter 4 to compute the width of the guard band that is necessary to protect a CP-OFDM incumbent user, in function of the waveform used by the secondary.

2. We analyze the optimal power distribution that can be assigned to FB-MC based secondary devices to maximize their capacity while limiting their interference to CP-OFDM based incumbent systems.

3. Taking into account the TSE of each waveform we introduced in chapter 2, we compare the amount of data they are capable of transmitting in a window of specific time and frequency dimensions.

Furthermore, in the context of D2D, we present the following contributions in chapter 6:

1. We study a mono-cellular setup in which D2D devices can use either CP-OFDM or OFDM/OQAM. Doing so, we demonstrate the interest of using enhanced multi-carrier waveforms for D2D transmission.

2. We extend this analysis to a multi-cellular setup and consider multiple enhanced waveforms for D2D transmissions. We investigate the performances of both the D2D and cellular systems for a variety of parameter values to better understand in what kind of deployments it is the most beneficial to change the waveform used by D2D systems.

## 3.5 Conclusion

In this chapter, we have reviewed works that address the potential use of enhanced multicarrier waveforms to facilitate coexistence with incumbent systems. We have identified several flaws in the works available so far in the literature which are mostly due to the fact that the impact of the waveform used by the incumbent system has been largely overlooked. In particular, we have pointed out that no proper modeling of the interference caused by enhanced waveforms on CP-OFDM receivers has been proposed. This lack for a precise interference model casts doubts on the validity of some results presented in the context of CR or D2D. Furthermore, we have also pointed out that experiments studying the coexistence between CP-OFDM incumbent systems and secondary devices based on enhanced waveforms provide either high-level or non-reproducible results that are difficult to exploit. All these observations serve as basis for our work and the contributions we present in the three following chapters of this thesis.

# Chapter 4

# Analysis of interference between CP-OFDM and FB-MC waveforms

## Contents

## 4.1 Introduction

Based on the review of the state of the art we provided in Chapters 2 and 3, the conclusion is clear: even though the research community has been extensively studying coexistence between enhanced waveforms and CP-OFDM with both simulation and experimental approaches, there is still no accurate analytical model of interference available in the literature to study these scenarios, with the exception of the work in [116] for UF-OFDM. Moreover, it has been noted that precise analysis of coexistence between CP-OFDM and FB-MC waveforms is an open issue that is important for various fields of research and that needs to be addressed [136]. In this chapter, we fill this gap by accurately analyzing the interference between any FB-MC waveform and CP-OFDM in spectral coexistence scenarios. More precisely, in our discussion, we point out that looking at the PSD of the interfering signal is not sufficient because it does not encompass the operations performed by the receiver, as PSD is measured before the input antenna of the receiver that suffers from interference. We recall that interference should be measured after the receiver operations, based on EVM measurement.

This chapter is organized as follows: in section 4.2, we lay out the system model we use. In section 4.3, we propose a new measure to rate interference with more accuracy in coexistence scenarios. In section 4.4, we derive analytical expressions of interference according to the newly proposed model, and we validate the latter through an experiment that we present in section 4.5. Finally, section 4.7 concludes this chapter. Note that this chapter details contributions that have been presented in three conference papers [137–139] and one journal article [140].

## 4.2 System model

Let us introduce a simple model that we will use in the following of this chapter to study the coexistence between one FB-MC secondary and one incumbent CP-OFDM system.

### 4.2.1 Coexistence setup

Let us lay out a simple system model consisting of a secondary system, $S$, and an incumbent system $I$, that coexist in a spectral band and both use a certain set of subcarriers, respectively $\mathcal{M}_S$ and $\mathcal{M}_I$, as is shown in Fig. 3.1. The incumbent system $I$ is composed of a pair of CP-OFDM users, whereas the users forming the secondary system $S$ are based on an alternative FB-MC waveform, as depicted in Fig. 4.1. We show that in each system, the vector $\mathbf{d}$ containing the symbols to be transmitted is fed to the waveform modulator. Then the signals transmitted by both systems are added in the wireless channel and received by both systems which demodulate the received signal and detect the vector of estimated symbols $\hat{\mathbf{d}}$.

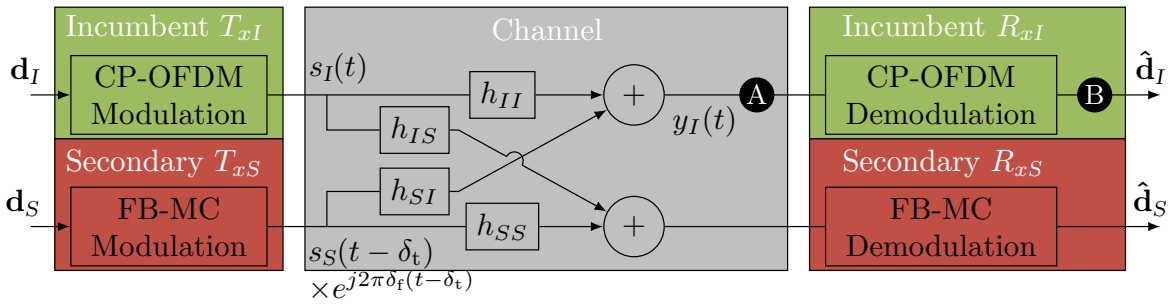


Figure 4.1: System model used to tackle the coexistence between the incumbent and secondary systems. White Gaussian noise is neglected to keep the focus on inter-system interference caused by the coexistence between the two systems. Timing and frequency misalignment factors are introduced to reflect the fact that there is no inter-system synchronization. We represent points A and B for future reference.

Therefore, each system may interfere on the other in function of the properties of the transmitted signals and the demodulation operations that are performed at the receive end. Two main specificities of the system model presented in Fig. 4.1 must be pointed out. In the first place, we do not take into account additive white Gaussian noise (AWGN). This is done deliberately to put the focus of this work on inter-system interference. Besides, as previously mentioned in this thesis, a core part of our analysis lies in the fact that the secondary and the incumbent users coexist without pursuing any collaboration and/or synchronization between them. Therefore, it is most likely that both systems will disagree on the time and frequency basis.

To encompass this effect, the system model defines the two following parameters :

i. **Time misalignment** $\delta_t$ : as the incumbent and secondary systems do not synchronize their transmission in time, we assume that the secondary system starts its transmission with a certain random delay $\delta_t$ with respect to the incumbent system.

ii. **Frequency misalignment** $\delta_f$ : local oscillators (LOs) of mobile terminals have a typical accuracy of ±1 ppm with respect to their nominal frequency [141]. For example, at a carrier frequency of 2 GHz, this can yield a misalignment between users of around $10^4$ Hz, which can become significant as it is close to the LTE subcarrier width of 15 kHz. Therefore, as the incumbent and secondary systems do not cooperate, we assume that the secondary system misaligns its carrier frequency of a factor $\delta_f$ with respect to the incumbent system. However, note that we consider that the transmitter and receiver in each separate system achieve perfect frequency synchronization.

Taking into account these two factors, the signal received at the input antenna of the incumbent CP-OFDM receiver is, as shown in Fig. 4.1,

$$y_I(t) = h_{II}(t) * s_I(t) + h_{SI}(t) * s_S(t - \delta_\mathrm{t}) e^{j2\pi\delta_\mathrm{f}(t-\delta_\mathrm{t})}, \tag{4.1}$$

in which $h_{II}$ is the channel between the incumbent transmitter and the incumbent receiver, whereas $h_{SI}$ is the channel between the secondary transmitter and the incumbent receiver. In our work, we will first consider flat channels and only take into account pathloss effects to keep the focus on the interference created by the reception of a FB-MC signal by a CP-OFDM receiver. Nevertheless, we will in a second step extend our study to multipath channels to take frequency fading into account in Section 4.4.

In order to build up on this system model, we recall in the following the signal models of the CP-OFDM and FB-MC waveforms that the incumbent and secondary systems can use.

### 4.2.2 Generic multicarrier waveform mathematical model

In line with the description of the multicarrier waveforms we gave in Chapter 2, we consider a multicarrier system with $M$ subcarriers, time spacing between symbols $\Delta\mathrm{T}$ and subcarrier spacing $\Delta\mathrm{F}$. Then, the time-domain continuous baseband signal that is transmitted by this system is written as

$$s(t) = \sqrt{P} \sum_{m=0}^{M-1} \underbrace{\sum_{n\in\mathbb{Z}} \mathbf{d}_m[n] f_{n,\mathrm{T}}(t - n\Delta\mathrm{T}) e^{j2\pi m\Delta\mathrm{F}(t-n\Delta\mathrm{T})}}_{s_m(t)}, \forall t \in \mathbb{R}, \tag{4.2}$$

where $P$ is the transmit power, $\mathbf{d}_m$ is the vector of unitary power symbols that are transmitted on the $m$th subcarrier, and $f_{n,\mathrm{T}}$ is the transmit filter used to transmit the $n$th symbol on each subcarrier by the multi-carrier system.

In our analysis, we assume perfect synchronization in both time and frequency between the transmitter and the receiver of the same system. Under this assumption, on a flat channel, the received signal $y(t)$ is expressed as

$$y(t) = \sqrt{G} s(t), \tag{4.3}$$

where $G$ is the channel gain. The obtained signal $y$ is then demodulated and the vector of estimated symbols on each subcarrier is expressed as

$$\hat{\mathbf{d}}_m[n] = \int_{-\infty}^{+\infty} f_{n,\mathrm{R}}(t - n\Delta\mathrm{T}) e^{-j2\pi m\Delta\mathrm{F}(t-n\Delta\mathrm{T})} y(t)\, \mathrm{d}t, \tag{4.4}$$

where $f_{n,\mathrm{R}}$ is the receive filter used on each subcarrier to demodulate the $n$th incoming symbol. Based on this generic model, we can describe any waveform, either CP-OFDM or FB-MC, by simply defining the parameters $f_{n,\mathrm{T}}$, $f_{n,\mathrm{R}}$, $\Delta\mathrm{T}$ and $\Delta\mathrm{F}$. In the following, we configure this generic model for the waveforms of interest to this thesis.

In our framework, CP-OFDM systems are classically defined by the following set of parameters:

- $\Delta\mathrm{T} = T + T_{\mathrm{CP}}$, $\Delta\mathrm{F} = \frac{1}{T}$
- $\forall n \in \mathbb{Z}, f_{n,\mathrm{T}}(t) = f_{\mathrm{T}}(t) = \begin{cases} \frac{1}{\sqrt{T}}, & t \in [-T_{\mathrm{CP}}, T] \\ 0, & \text{elsewhere} \end{cases}$
- $\forall n \in \mathbb{Z}, f_{n,\mathrm{R}}(t) = f_{\mathrm{R}}(t) = \begin{cases} \frac{1}{\sqrt{T}}, & t \in [0, T] \\ 0, & \text{elsewhere} \end{cases}$

As we explained in Chapter 2, each linear FB-MC waveform uses the following set of transceive filter, in which $g$ is the prototype filter they are based upon:

- $\forall n \in \mathbb{Z}, f_{n,\mathrm{T}}(t) = f_{\mathrm{T}}(t) = \begin{cases} g(t), & t \in \left[-\frac{T_g}{2}, \frac{T_g}{2}\right] \\ 0, & \text{elsewhere} \end{cases}$
- $\forall n \in \mathbb{Z}, f_{n,\mathrm{R}}(t) = f_{\mathrm{R}}(t) = \begin{cases} g(t), & t \in \left[-\frac{T_g}{2}, \frac{T_g}{2}\right] \\ 0, & \text{elsewhere} \end{cases}$

In FMT, we recall that the harmful inter-carrier interference introduced by prototype filter $g$ is countered by introducing a guard band of width $W_{\mathrm{GB}}$ between every subcarrier. Therefore, FMT systems use the following set of parameters : $\Delta\mathrm{T} = T$, $\Delta\mathrm{F} = \frac{1}{T} + W_{\mathrm{GB}}$

OFDM/OQAM, because it doubles the symbol rate, obeys the following set of parameters: $\Delta\mathrm{T} = \frac{T}{2}$, $\Delta\mathrm{F} = \frac{1}{T}$

FBMC-PAM which doubles the number of transmit subcarriers has the following parameters: $\Delta\mathrm{T} = T$, $\Delta\mathrm{F} = \frac{1}{2T}$

As we explained in Chapter 2, in GFDM, complex symbols are modulated per block of $N_{\mathrm{b}}$ and a CP of length $T_{\mathrm{CP}}$ is added between every subsequent block. Thus, GFDM systems utilize the following set of transceive filters and parameters:

- $\forall n \in \mathbb{Z}, f_{n,\mathrm{T}}(t) = \begin{cases} \tilde{g}_{n \mod N_{\mathrm{b}}}(t), & t \in [-T_{\mathrm{CP}}, N_{\mathrm{b}}T] \\ 0, & \text{elsewhere} \end{cases}$

– $\forall n \in \mathbb{Z}, f_{n,\mathrm{R}}(t) = f_{\mathrm{R}}(t) = \begin{cases} \tilde{g}_{n \mod N_\mathrm{b}}, & t \in [-T_{\mathrm{CP}}, N_\mathrm{b}T] \\ 0, & \text{elsewhere} \end{cases}$

– $\Delta\mathrm{T} = N_\mathrm{b}T + T_{\mathrm{CP}},\ \Delta\mathrm{F} = \frac{1}{T}$

COQAM is in all points equivalent to GFDM, except for the fact that real symbols are transmitted at half the symbol rate. Therefore, according to our model, $2N_\mathrm{b}$ prototype filters are defined from the original prototype filter $g$ as $\forall n \in [0, 2N_\mathrm{b} - 1]$,

$$\tilde{g}_n(t) = \begin{cases} g(t - n\frac{T}{2} \mod N_\mathrm{b}T), & t \in [-T_{\mathrm{CP}}, N_\mathrm{b}T] \\ 0 & \text{elsewhere.} \end{cases} \tag{4.5}$$

## 4.3 EVM-based measurement of interference

### 4.3.1 Why we need a new model

Consider the system model described in Fig. 4.1: it is clear that the interference computed by the PSD-based model $I_{\mathrm{PSD}}$ is measured **in the wireless channel**. This means that only the spectral properties of the interfering signal are taken into account. In other words, the PSD-based model computes the interference **at the input antenna** of the victim receiver, a point marked as Ⓐ in the system model scheme presented in Fig. 4.1. However, the values of interference that really matter are those experienced by the victim receiver after it demodulates the incoming signal, just before the decision, in other words at point Ⓑ in Fig. 4.1. Nevertheless, as we have extensively discussed in Chapter 3, in the literature, the PSD-based model has been used to evaluate the ability of FB-MC based systems to coexist with other systems potentially based on CP-OFDM. However, these studies should instead be based on measurements of the error vector magnitude (EVM) at the incumbent receiver that suffers from the adjacent transmission of the secondary system. This approach is indeed necessary to encompass both the properties of the transmitted secondary signal and the demodulation operations performed by the incumbent receiver. In fact, the PSD-based model only accounts for the properties of the transmitted secondary signal and omits the operations performed by the incumbent receiver. An illustration of the principle of the EVM-based measurement of interference is given in Fig. 4.2.

It is clear that the EVM-based approach is much more representative of the actual interference experienced by the incumbent receiver. In fact, the AIM approach of Medjahdi *et. al.* in [113] for homogeneous scenarios is very similar. However, in the heterogeneous scenario we study here, getting closed forms of the EVM may be challenging, as it involves much more intricate mathematical derivations than simply integrating the PSD. Therefore, it

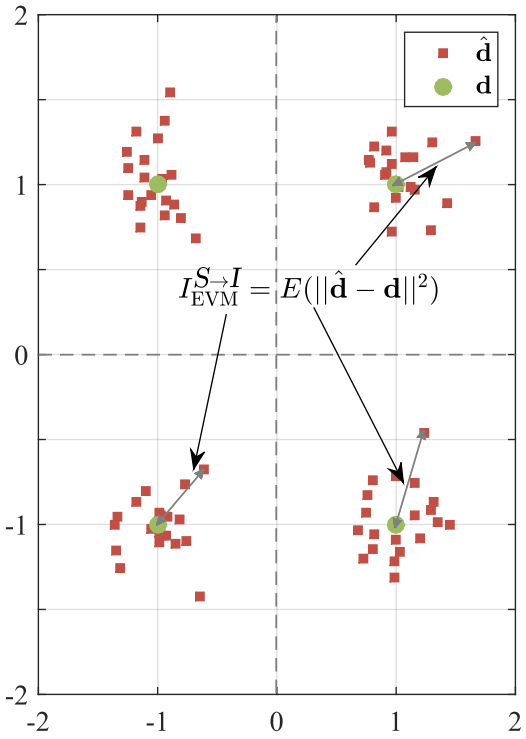


Figure 4.2: EVM-based measurement of interference at the level of the decoded constellation, just before the symbol decision.

would be tempting to stick to the PSD based approach in the hope that values given by this model are close enough to the actual EVM values. This is what we propose to (in)validate in the following section by comparing values of interference obtained with the PSD-based model to values obtained through numerical simulations of the EVM.

### 4.3.2 Principle of the EVM-based measure of interference

Consider the system model depicted in Fig. 4.1. According to (4.4) and the expression of the CP-OFDM receive filter given in Section 4.2.2, at point Ⓑ of Fig. 4.1, the demodulated symbol on the $n_I$th time slot and $m_I$th subcarrier of the incumbent is expressed as

$$\hat{\mathbf{d}}_{m_I}[n_I] = \frac{1}{\sqrt{T_I}} \int_{n_I(T_I+T_{\text{CP},I})}^{n_I(T_I+T_{\text{CP},I})+T_I} e^{-j2\pi \frac{m_I}{T_I}(t-n_I(T_I+T_{\text{CP},I}))} y(t)\,\mathrm{d}t \tag{4.6}$$

Recalling the expression of $y(t)$ given in (4.1), after some trivial derivations, we obtain

$$\hat{\mathbf{d}}_{m_I}[n_I] = \sqrt{P_I G_{II}}\mathbf{d}_{m_I}[n_I] + \boldsymbol{\eta}_{m_I}[n_I], \tag{4.7}$$

where $\boldsymbol{\eta}_{m_I}[n_I]$ represent the interference caused by the secondary FB-MC signal and is expressed as

$$\boldsymbol{\eta}_{m_I}[n_I] = \sqrt{\frac{P_S G_{SI}}{T_I}} \int_{n_I(T_I+T_{\mathrm{CP},I})}^{n_I(T_I+T_{\mathrm{CP},I})+T_I} e^{-j2\pi \frac{m_I}{T_I}(t-n_I(T_I+T_{\mathrm{CP},I}))} \times s_S(t-\delta_\mathrm{t}) e^{j2\pi\delta_\mathrm{f}(t-\delta_\mathrm{t})}\,\mathrm{d}t. \tag{4.8}$$

Then, inserting (4.2) in (4.8), and operating the change of variable $t \mapsto t - n_I(T_I + T_{\mathrm{CP},I})$, we obtain

$$\boldsymbol{\eta}_{m_I}[n_I] = \sum_{m_S \in \mathcal{M}_S} \sum_{n_S \in \mathbb{Z}} \mathbf{d}_{m_S}[n_S] \sqrt{\frac{P_S G_{SI}}{T_I}} \times \int_0^{T_I} \left[ f_{n_S,\mathrm{T}}(t-\tau(n_S,n_I)) e^{j2\pi[\nu(m_S,m_I,\delta_\mathrm{f})t + \phi(m_S,m_I,\delta_\mathrm{f},\delta_\mathrm{t})]} \right] \mathrm{d}t, \tag{4.9}$$

with

$$\tau(n_S, n_I) = n_S \Delta\mathrm{T}_S - n_I \Delta\mathrm{T}_I + \delta_\mathrm{t} \tag{4.10}$$

$$\phi(m_S, m_I, \delta_\mathrm{f}, \delta_\mathrm{t}) = -(m_S \Delta\mathrm{F}_S + \delta_\mathrm{f})(n_S \Delta\mathrm{T}_S - n_I \Delta\mathrm{T}_I) - \delta_\mathrm{f}\delta_\mathrm{t} \tag{4.11}$$

$$\nu(m_S, m_I, \delta_\mathrm{f}) = m_S \Delta\mathrm{F}_S - m_I \Delta\mathrm{F}_I + \delta_\mathrm{f} \tag{4.12}$$

Naming $C(m_S, m_I, n_S, n_I, \delta_\mathrm{f}, \delta_\mathrm{t})$ the integral term in (4.9), we have

$$\boldsymbol{\eta}_{m_I}[n_I] = \sum_{m_S \in \mathcal{M}_S} \underbrace{\sum_{n_S \in \mathbb{Z}} \mathbf{d}_{m_S}[n_S] \sqrt{\frac{P_S G_{SI}}{T_I}} C(m_S, m_I, n_S, n_I, \delta_\mathrm{f}, \delta_\mathrm{t})}_{\boldsymbol{\eta}_{m_S \to m_I}[n_I]} \tag{4.13}$$

Then, the interference injected by the $m_S$th subcarrier of the secondary system onto the $m_I$th subcarrier of the incumbent system during the $n_I$th time-slot is expressed, according to our EVM approach, as

$$\mathbf{I}_{\mathrm{EVM}}^{S\to I}(m_S, m_I, \delta_\mathrm{f}, \delta_\mathrm{t})[n_I] = E_{\mathbf{d}_S}\{|\boldsymbol{\eta}_{m_S\to m_I}[n_I]|^2\} \tag{4.14}$$

$$= \frac{P_S G_{SI}}{T_I} \sum_{n_S \in \mathbb{Z}} |C(m_S, m_I, n_S, n_I, \delta_\mathrm{f}, \delta_\mathrm{t})|^2 \tag{4.15}$$

Finally, in line with the approach in [113], we consider that $\delta_\mathrm{t}$ is a random variable that is uniformly distributed within the interval $[0, T_I + T_{\mathrm{CP},I}]$, in order to encompass the lack of synchronization and coordination between the secondary and incumbent systems. Note that we keep a fixed value of $\delta_\mathrm{f}$ as this parameter only shifts the secondary transmission in

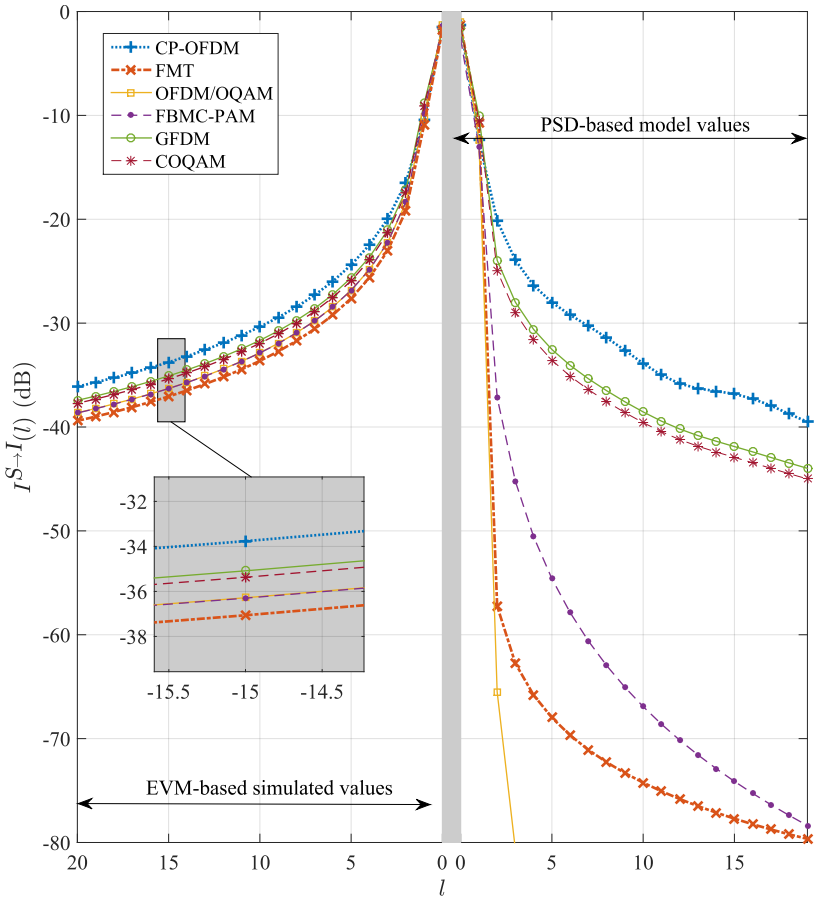


Figure 4.3: Interference caused onto a CP-OFDM based incumbent system by a secondary system based on multiple waveforms. Values predicted by the PSD-based model (right-hand side) are compared to those obtained through Monte-Carlo simulations of the average EVM at the incumbent CP-OFDM receiver according to (4.16) (left-hand side). Whatever the waveform used by the secondary system, EVM-based values are dramatically higher than those predicted by the PSD-based model. Results are shown for $P_S G_{SI} = 0dB$ and $\delta_\mathrm{f} = 0$. Note that any other value simply translates to a shift on the y-axis of all curves.

frequency. The final average value of measured interference is then obtained as the average EVM for all values of $n_\mathbf{I}$ and all possible realisations of $\delta_\mathrm{t}$ as

$$I_{\mathrm{EVM}}^{S\to I}(m_S, m_I, \delta_\mathrm{f}) = E_{\delta_\mathrm{t}}\left\{\overline{\mathbf{I}_{\mathrm{EVM}}^{S\to I}(m_S, m_I, \delta_\mathrm{f}, \delta_\mathrm{t})}\right\}. \tag{4.16}$$

### 4.3.3 Simulation setup and obtained results

Though the EVM-based modeling of interference we presented is much more rigorous than the PSD-based approach, it is also much more convoluted and far less practical. In order to check if it is necessary to pursue the EVM-based modeling of interference, we simulate values obtained according to the model defined in (4.16). To do so, we set $\delta_\mathrm{f} = 0$. Thus, as

in the PSD-based model, only the value of $m_S - m_I = l$ matters. For each waveform used by the secondary system, we measure the interference experienced on each subcarrier of the incumbent CP-OFDM system according to (4.16).

Obtained results are depicted in Fig. 4.3. Note that, in that figure, we plot both the results obtained with the EVM-based approach on the left side, and those obtained with the PSD-based model on the right side. Undeniably, the actual interference based on EVM measurements after the CP-OFDM demodulator is tremendously higher than what is predicted with the PSD-based model, at the input antenna of the incumbent receiver. The case of OFDM/OQAM based secondary systems gives a glaring example : at a subcarrier distance $l = 2$, the PSD-based model predicts that OFDM/OQAM will inject an interference power of $-65.4$ dB. In fact, simulated EVM values show that it is actually around $-18.4$ dB. This means that the PSD-based model underestimates more than 10 000 times some values of the interference experienced by the CP-OFDM incumbent system. Moreover, we see that the gains achieved by the secondary system if it uses FB-MC waveforms are dramatically reduced. Indeed, the interference caused onto the CP-OFDM incumbent receiver is only reduced by 1 to 3 dB if the secondary system uses a FB-MC waveform instead of CP-OFDM. Interestingly, the order of magnitude of this performance gap is quite in line with the results obtained by some of the experiments we cited in Chapter 3, in particular [117, 118]. This brings two conclusions:

1. The PSD-based model evaluates the interference to CP-OFDM systems poorly and gives misleading results. Though it gives an approximation of interference in the channel, it cannot be used to predict the performance of the incumbent receiver. In particular, it does not give any valid insight on the advantages of FB-MC for coexistence with CP-OFDM.

2. Opposed to the common way of thinking, FB-MC waveforms do not drastically facilitate coexistence with incumbent CP-OFDM based legacy systems.

So, why is the PSD-based model so inaccurate? The main reason is given in Fig. 4.4 : FB-MC systems rely on prototype filters that are longer than the time-symbol to achieve acute frequency localization. However, the CP-OFDM receiver filter is a rectangular window of length equal to the time-symbol. Therefore, it truncates the well-shaped prototype filter used to transmit the FB-MC secondary signal in parts that, on their own, are not particularly well frequency localized. As a result of this operation, the advantageous PSD properties of the FB-MC signals are lost by the CP-OFDM incumbent receiver. Note that this is a general result that can be extended to virtually any signal passing through a CP-OFDM receiver. Indeed, the latter acts exactly as a poor spectrum analyzer which outputs high frequency ripples even when fed a well localized signal.

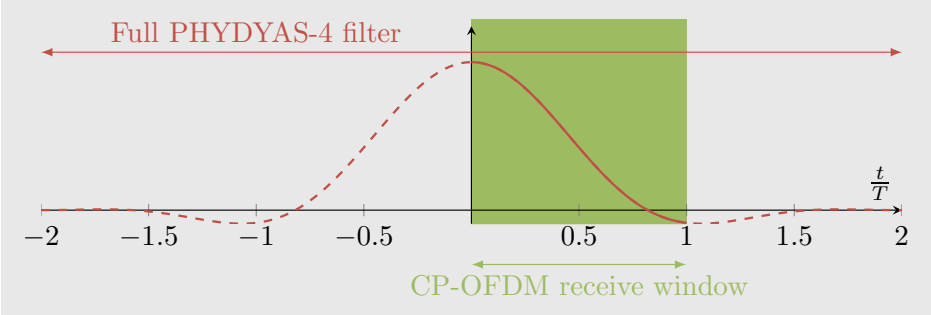


Figure 4.4: Key phenomenon explaining the difference between the EVM-based measurement of interference and the predictions of the PSD-based model: FB-MC waveforms use longer-than-$T$ filters to achieve high spectral localization, but these are cut by the $T$-long receive window of the incumbent CP-OFDM system. Figure shows the example of an OFDM/OQAM based secondary with PHYDYAS-4 filter, but the same applies for any other FB-MC waveform.We point out that this effect arises even if there is no time or frequency misalignment between users, i.e. in cases where $\delta_{\mathrm{t}} = \delta_{\mathrm{f}} = 0$.

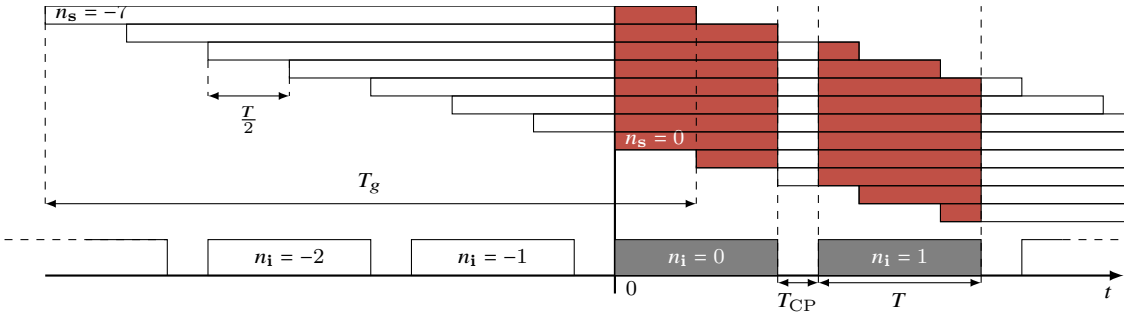


Figure 4.5: Time axis view of the interference caused by an OFDM/OQAM transmission on CP-OFDM receiving windows $n_{\mathrm{i}} = 0$ and $n_{\mathrm{i}} = 1$.

## 4.4 Analytical aspects

### 4.4.1 Statistics of interference signal

In the former section, we have shown that the PSD-based model fails to properly estimate the interference caused by FB-MC waveforms onto CP-OFDM receivers. Therefore, it is necessary to study the interference signal $\boldsymbol{\eta}$ defined in (4.9) in more accurate details. First and foremost, it is important to study its statistical distribution. Indeed, the power of the interfering signal is of course not sufficient to fully characterize it.

Reconsider the expression of $\boldsymbol{\eta}_{m_I}[n_I]$ given in (4.9): it is clear that its value is obtained as a weighted sum of the symbols modulated by the secondary system, where the weights associated with each term of the sum have deterministic values. This is further illustrated in Fig. 4.5 in which we represent how multiple OFDM/OQAM overlapping symbols interfere on a single reception window of a CP-OFDM receiver. Therefore, $\boldsymbol{\eta}_{m_S \to m_I}[n_I]$ can only take a

finite number of values. In details, for given values of $\delta_{\mathrm{t}}$ and $\delta_{\mathrm{f}}$, it can take $M_{c,S}^{N_{\mathrm{int}}}$ distinct values, where $M_{c,S}$ is the order of the constellation used by the secondary system and $N_{\mathrm{int}}$ is the number of symbols that interfere on the $n_I$-th symbol of the incumbent system. In order to model interference in a way that allows for practical computation of some metrics of interest, a common technique is to rely on Gaussian approximation of interference signals. However, this Gaussian approximation is only valid if the studied interference signal obeys the two following characteristics:

i. The interference signal is obtained as the sum of i.i.d. components.

ii. Enough components are summed to approach the asymptotic Gaussian distribution.

In the case we study here, condition i) is indeed respected as the components of the sum in the expression of $\boldsymbol{\eta}_{m_S \to m_I}[n_I]$ are i.i.d. because the values taken by vector $\mathbf{d}_{m_S}$ are themselves i.i.d.

As for condition ii), it is directly related to the factors $M_{c,S}$ and $N_{\mathrm{int}}$ introduced here above. To give an example of this, we represent in Fig. 4.6 the values taken by $\boldsymbol{\eta}_{m_S \to m_I}$ when the secondary system uses OFDM/OQAM, $m_S - m_I = 1$ and $\delta_{\mathrm{t}} = 0, \delta_{\mathrm{f}} = 0$. We give results obtained when the secondary system uses different constellation orders, namely 4-QAM, 16-QAM and 64-QAM. The results show that the Gaussian approximation of $\boldsymbol{\eta}_{m_S \to m_I}$ is abusive for small constellation orders, but starts being acceptable when high order constellations are used by the secondary system. Following the Gaussian approximation, we have

$$\boldsymbol{\eta}_{m_S \to m_I} \sim \mathcal{N}(0, I_{\mathrm{EVM}}(m_S, m_I, \delta_{\mathrm{f}})), \tag{4.17}$$

and therefore

$$\boldsymbol{\eta}_{m_I} \sim \mathcal{N}\left(0, \sum_{m_S \in \mathcal{M}_S} I_{\mathrm{EVM}}(m_S, m_I, \delta_{\mathrm{f}})\right). \tag{4.18}$$

To confirm that this Gaussian approximation is applicable in the cases that are of interest to us, we run the following simulation. We consider a setup in which the secondary uses OFDM/OQAM, and each system is active on 36 subcarriers, without any guard band between them. Then, we progressively increase the transmit power of the secondary and compute the BER of the incumbent. We run the simulation for a 4-QAM and a 64-QAM based secondary and each time compare the obtained BER with what is predicted by the Gaussian approximation. The results are reported in Fig. 4.7, where we show that the Gaussian approximation gives very good results, especially when the power of the secondary is important, i.e. when the secondary interference is the predominant source of error. Therefore, in the remaining of this thesis, we will follow the Gaussian approximation and model the

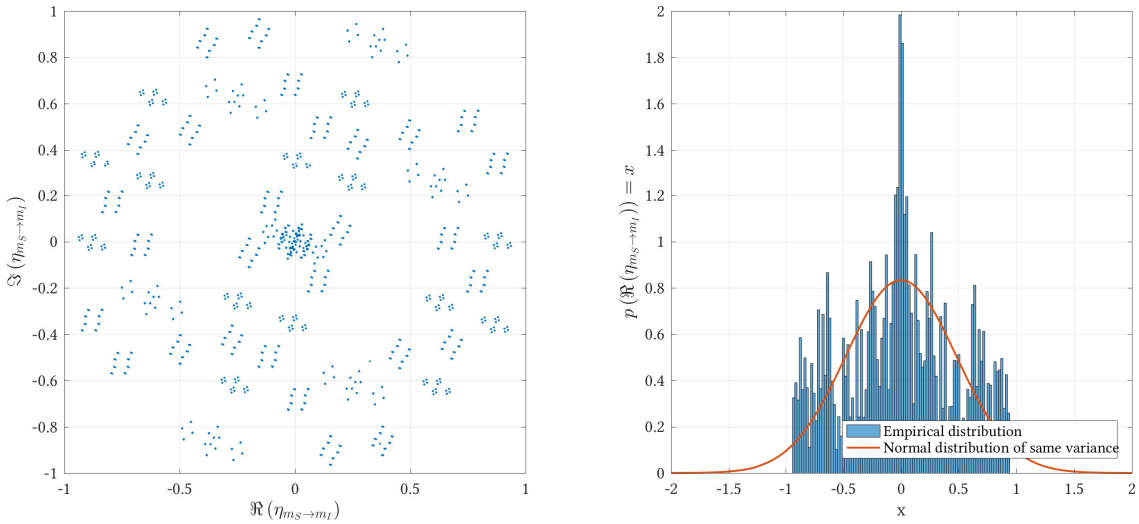


(a) 4-QAM

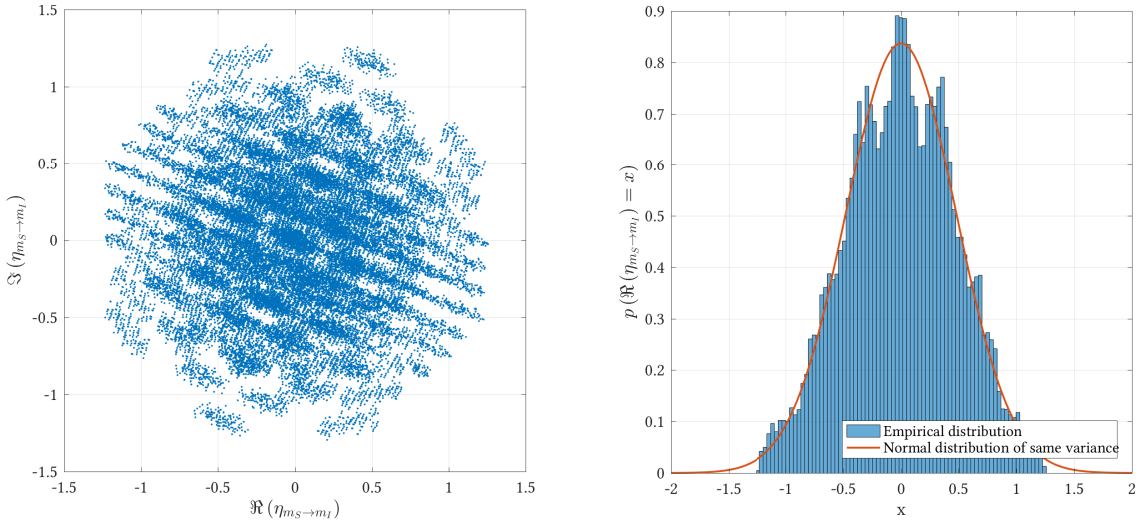


(b) 16-QAM

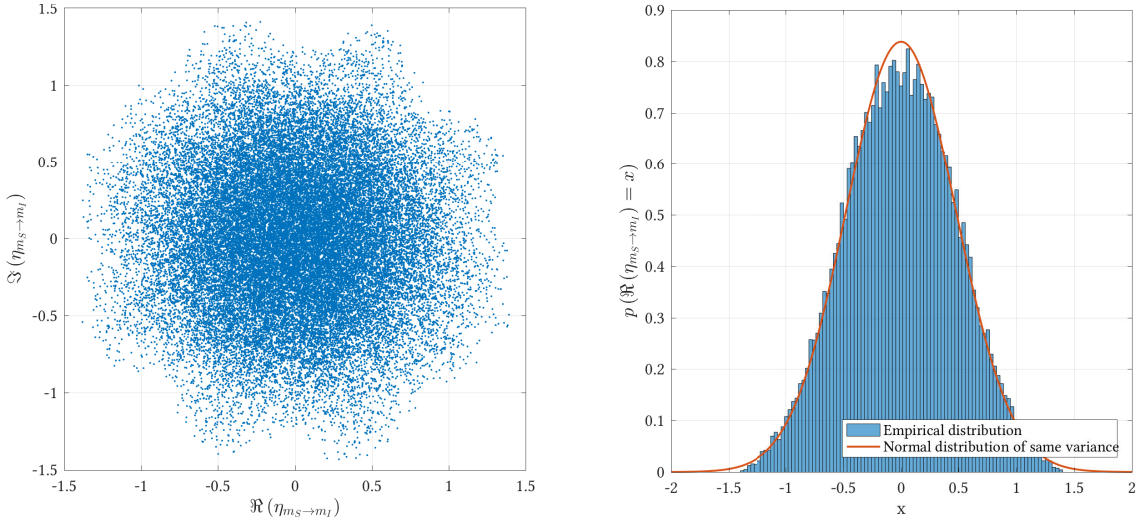


(c) 64-QAM

Figure 4.6: Representation of $\boldsymbol{\eta}_{m_S \to m_I}[n_I]$ for the considered parameters, when the secondary system uses different constellation orders. As the constellation order of the secondary grows, the central limit theorem applies and $\boldsymbol{\eta}_{m_S \to m_I}[n_I]$ can be approximated as a centered normal random variable.

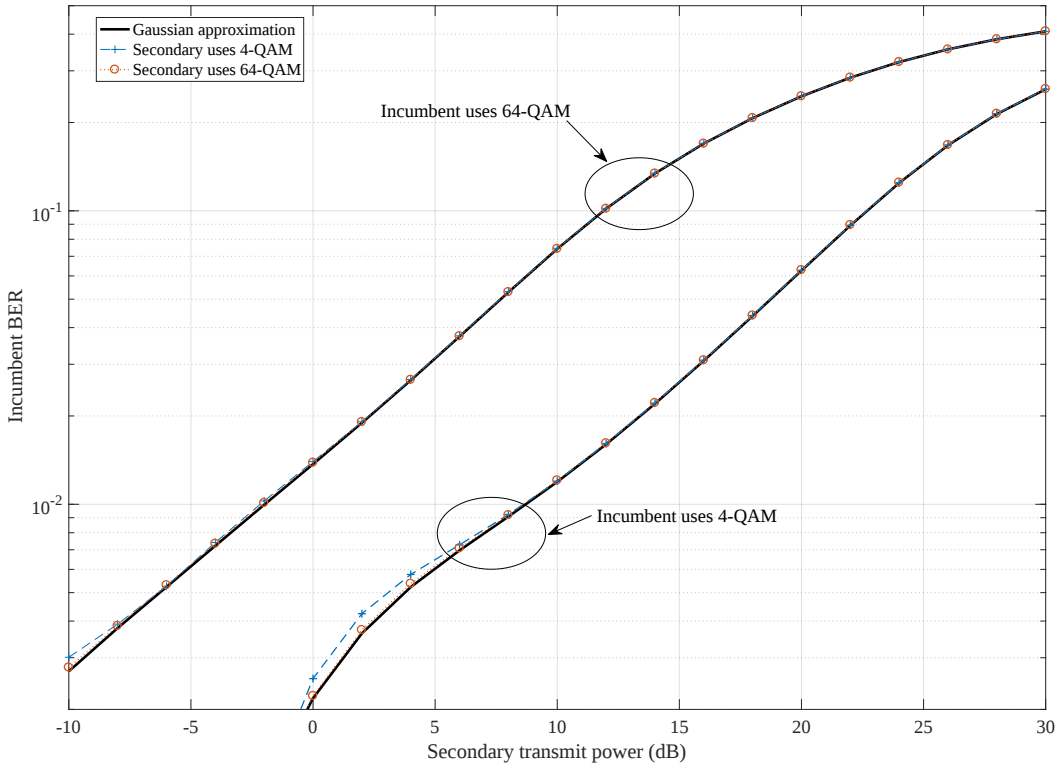


Figure 4.7: BER of the incumbent system for different constellation orders. The higher the constellation order of the secondary is, the more accurate the Gaussian approximation is. Nevertheless, even in the case where the secondary uses 4-QAM, the Gaussian approximation gives good results.

interference caused by the secondary system onto the incumbent as a centered normal random variable.

### 4.4.2 Closed-form expression of interference power

At this point of our discussion, we have shown that the interference caused by the secondary FB-MC signal can be modeled as a random normal variable. We have also shown that using the PSD-based model to predict the power of the latter gives inaccurate results. Therefore, in this section, we derive the mathematical analysis of the inter-system interference power according to the mathematical model laid out in Section 4.3.2. Let us fix $m_I$, $m_S$, $\delta_\mathrm{f}$ and $\delta_\mathrm{t}$. In (4.15), $I_{\mathrm{EVM}}^{S\to I}(m_S, m_I, \delta_\mathrm{f}, \delta_\mathrm{t})$ is written as the sum of specific values of the magnitude of the cross-ambiguity function between the transmit filter of the secondary and a rectangular window.

In the case where the secondary system is based on linear convolution FB-MC, we reminded in Section 2.4.2 that the transmit filter used to modulate each subsequent symbol is equal to the used prototype filter $g$. Therefore, we can show that $|C(m_S, m_I, n_S, n_I, \delta_\mathrm{f}, \delta_\mathrm{t})|$

can be expressed as the cross-ambiguity function $\left|A_{\Pi_{T_I},g}(\tau(n_S,n_I),\nu(m_S,m_I,\delta_\mathrm{f}))\right|$, between a rectangular window of length $T_I$ and the prototype filter $g$, with $\tau$ and $\nu$ following the expressions of (4.10),(4.12). The expression of $|A_{\Pi_T,g}|$ is given as

$$|A_{\Pi_{T_I},g}(\tau,\nu)| = \begin{cases} 0, & \tau > T_I + \frac{T_g}{2} \text{ or } \tau < -\frac{T_g}{2}. \\ \left|(\tau+\frac{T_g}{2})\sum\limits_{k\in\mathbb{Z}} G_k e^{j\pi\frac{k}{T_g}(\frac{T_g}{2}-\tau)}\mathrm{sinc}(\pi(\frac{k}{T_g}+\nu)(\frac{T_g}{2}+\tau))\right|, & -\frac{T_g}{2} \le \tau \le T_I - \frac{T_g}{2} \\ \left|(T_I-(-\frac{T_g}{2}+\tau))\sum\limits_{k\in\mathbb{Z}} G_k e^{j\pi\frac{k}{T_g}(-\frac{T_g}{2}-\tau+T_I)}\mathrm{sinc}(\pi(\frac{k}{T_g}+\nu)(T_I-(-\frac{T_g}{2}+\tau)))\right|, & \frac{T_g}{2} \le \tau \le T_I + \frac{T_g}{2} \\ \left|T_I\sum\limits_{k\in\mathbb{Z}} G_k e^{j\pi\frac{k}{T_g}(T_I-2\tau)}\mathrm{sinc}(\pi(\frac{k}{T_g}+\nu)T_I)\right|, & T_I - \frac{T_g}{2} \le \tau \le \frac{T_g}{2} \end{cases} \tag{4.19}$$

where the terms $G_k$ represent the Fourier coefficients of the prototype filter $g$ used by the secondary system. Developments leading to this expression are detailed in Appendix A. Therefore, (4.15) is rewritten as

$$\mathbf{I}^{S\to I}_{\mathrm{EVM}}(m_S,m_I,\delta_\mathrm{f},\delta_\mathrm{t})[n_I] = \frac{P_S G_{SI}}{T_I} \times \sum_{n_S\in\mathbb{Z}} |A_{\Pi_{T_I},g}(\tau(n_S,n_I),\nu(m_S,m_I,\delta_\mathrm{f}))|^2 \tag{4.20}$$

Putting (4.19) in this last expression, we see clearly that the power of interference caused by the secondary FB-MC waveform onto the incumbent CP-OFDM system slowly decays in frequency, following a weighted sum of sinc functions. This last expression can be used to rate the exact interference seen on the $n_I$th time slot of the incumbent system. This provides us with a closed-form expression of the interference seen on each symbol of the incumbent CP-OFDM system, for a particular value of time misalignment $\delta_\mathrm{t}$ between the two systems.

However, obtaining closed-form expressions of the average interference as expressed in (4.16) is impractical, because it involves taking the average value of the vector $\mathbf{I}^{S\to I}_{\mathrm{EVM}}(m_S,m_I,\delta_\mathrm{f},\delta_\mathrm{t})$, and then take the expected value of the result with respect to random variable $\delta_\mathrm{t}$. Moreover, the results presented in Fig. 4.3 reduce the appeal for closed-form expressions. The main point we want to show in this analysis is that the CP-OFDM reception causes high interference to the incumbent system , which is explained by the appearance of the sinc function in (4.19). In the following, we study the impact of $\delta_\mathrm{t}$ through simulations to see if it is possible to simplify the analysis.

Fig. 4.8 shows the interference that is injected by an active subcarrier with unitary power on 20 neighboring CP-OFDM subcarriers as a function of $\delta_\mathrm{t}$ for different waveforms. Interference caused by FBMC-PAM and OFDM/OQAM is weakly affected by the timing

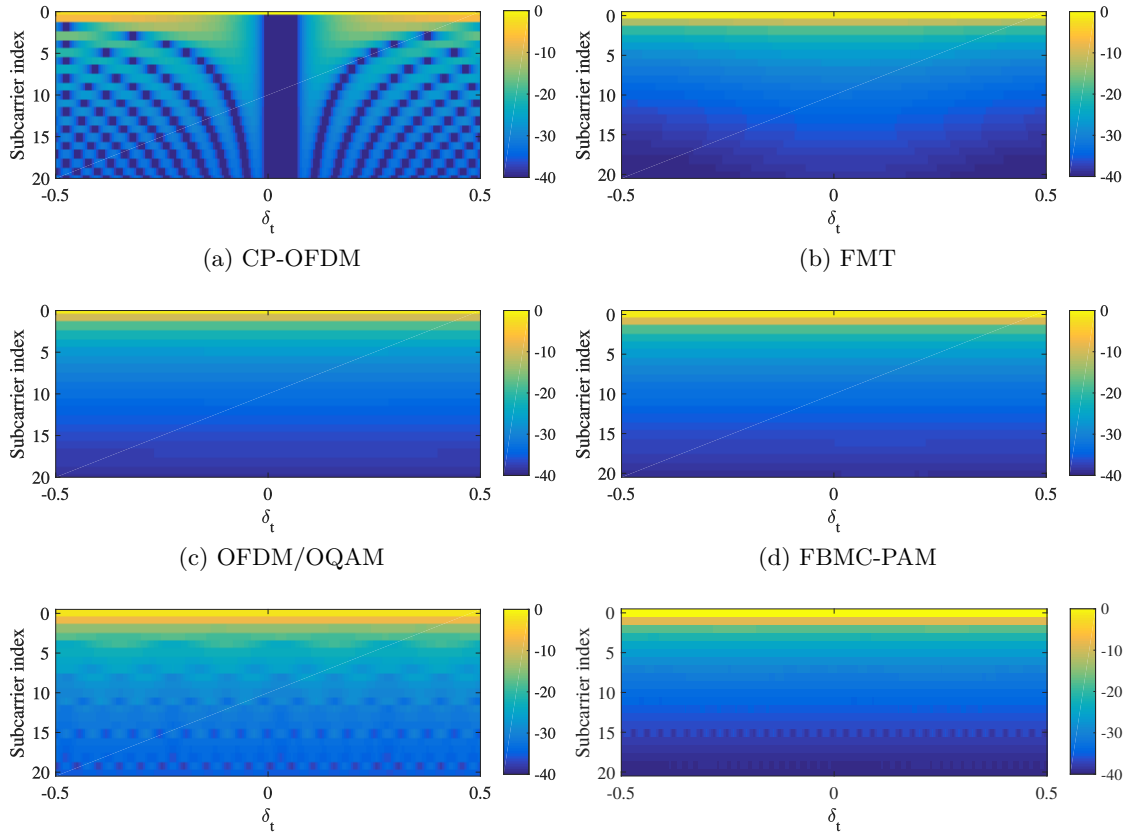


(a) CP-OFDM (b) FMT

(c) OFDM/OQAM (d) FBMC-PAM

(e) GFDM (f) COQAM

Figure 4.8: Interference in dB caused by an active subcarrier 0 on 20 neighboring CP-OFDM subcarriers of the incumbent in function of $\delta_t$ for different waveforms. Only CP-OFDM shows a figure significantly varying along the $\delta_t$ axis. For all FB-MC waveforms, perfect time synchronization does not significantly reduce injected interference, and the exact value of $\delta_t$ does not significantly affect the interference they cause onto the CP-OFDM receiver.

offset. GFDM, COQAM and FMT show very slight variations with respect to $\delta_t$. On the contrary, the figure for CP-OFDM shows high variations along the $\delta_t$ axis. We can therefore assert that the value of interference is in most cases only slightly dependent on the values of $n_I$ and $\delta_t$. Therefore, in order to offer tractable equations, it is possible to adopt the following approximation:

$$I_{\mathrm{EVM}}^{S\to I}(m_S, m_I, \delta_f) \approx \mathbf{I}_{\mathrm{EVM}}^{S\to I}(m_S, m_I, \delta_f, \delta_t = 0)[0] \tag{4.21}$$

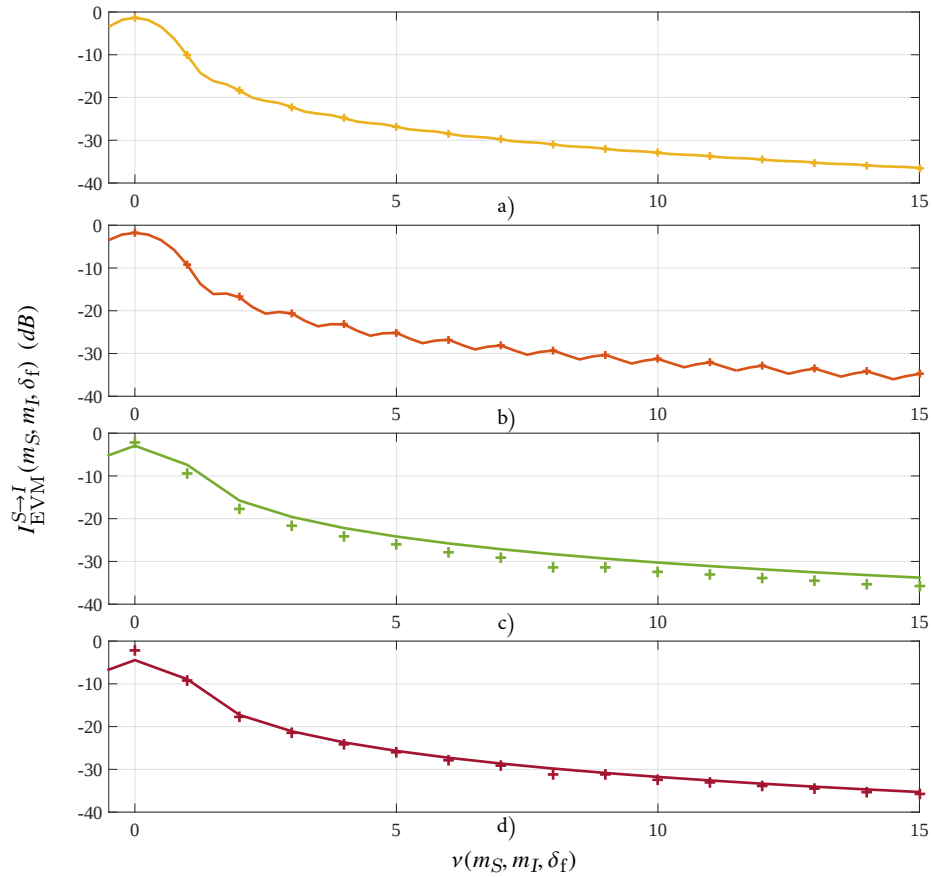


Figure 4.9: Comparison between simulated values of average interference based on EVM (crosses) and analytical approximation of (4.22) (solid line) for a) OFDM/OQAM, b) FMT, c) GFDM and d) COQAM.

With this approximated form, the expression of (4.16) simplifies into

$$I_{\mathrm{EVM}}^{S\to I}(m_S, m_I, \delta_f) \approx P_S G_{SI} T_I \sum_{n=0}^{\frac{T_g}{\Delta T_S}} \left| \sum_{k\in\mathbb{Z}} G_k e^{j\pi \frac{k}{T_g}(T_I - 2(n\Delta T_S))} \times \mathrm{sinc}(\pi(\frac{k}{T_g} + \nu)T_I) \right|^2 \tag{4.22}$$

Note that in the case where the secondary system uses circular convolution filter banks, the expression of (4.19) is not directly applicable. Indeed, because of the CP addition subsequent symbols pass through different filters that have slightly different Fourier coefficients. However, the main principle stays unchanged and (4.22) can be used as an approximation as well in the case of circular convolution FB-MC waveforms.

In Fig. 4.9, we compare the approximation of $I_{\mathrm{EVM}}^{S\to I}(m_S, m_I, \delta_f)$ given in (4.22) with results obtained through Monte-Carlo simulations for $P_S G_{SI} = 1$. We see that the proposed approximation matches perfectly the simulated values for linear filter banks but only approximates

the interference values in the case of circular filter banks, as predicted. Nevertheless, the obtained approximation is satisfying and shows well, for each waveform, that the interference to the CP-OFDM incumbent slowly decays, at approximately the same rate no matter what waveform is used by the secondary system. Note that we did not represent the curve for FBMC-PAM as it is clear from Fig. 4.3 that it interferes exactly as much as OFDM/OQAM.

### 4.4.3 Extension to multipath channels

All throughout our study so far, we have considered flat channels which only affect the received power of the transmit signal and we have not taken into account the effects of noise. This enabled us to precisely evaluate the interference caused by any FB-MC signal on a CP-OFDM receiver. In this section, we detail how the model we developed can be applied to evaluate the performance of the incumbent CP-OFDM systems in realistic setups in which the multipath channel and Gaussian noise come into play. We recall that the multi-path wireless channel can be modeled as a FIR filter as follows:

$$\forall t \in \mathbb{R},\ h(t) = \sqrt{G} \sum_{l=0}^{L-1} h_l \delta(t - \epsilon_l), \tag{4.23}$$

where $L$ is the number of paths, $h_l$ and $\tau_l$ are respectively the complex coefficient and delay associated with path $l$, and $\delta$ is the Dirac function. The coefficients $h_l$ are defined as follows:

$$h_l \sim \mathcal{N}(0, \sigma_l^2) \tag{4.24}$$

$$\sum_l \sigma_l^2 = 1 \tag{4.25}$$

As is commonly known, if the CP used by the CP-OFDM transmission is longer than the maximum delay incurred by the channel, there is neither inter-symbol interference nor inter-carrier interference and the signal received by the incumbent can be directly obtained through channel equalization in the frequency domain.

#### Zero Forcing (ZF) equalization

If the incumbent system performs zero-forcing equalization, the symbols demodulated by the CP-OFDM incumbent receiver are obtained as follows:

$$\hat{\mathbf{d}}_{m_I}[n_I] = \frac{\sqrt{P_I G_{II}} H_{II,m_I} \mathbf{d}_{m_I}[n_I] + \mathbf{w}_{m_I}[n_I]}{\hat{H}_{II,m_I}} + \boldsymbol{\eta}_{m_I}[n_I], \tag{4.26}$$

where $\mathbf{w}_{m_I}[n_I]$ is the additional white Gaussian noise of variance $\sigma_w^2$. $H_{II,m_I}$ is the channel response of channel $h_{II}$ on the $m_I$-th subcarrier of the incumbent and $\hat{H}_{II,m_I}$ the estimate

thereof. Classically, we can model the latter as

$$\hat{H}_{II,m_I} = H_{II,m_I} + \xi_{II,m_I}, \tag{4.27}$$

where $\xi_{II,m_I} \sim \mathcal{N}(0, \sigma^2_{\xi_{II,m_I}})$ represents the channel estimation error on subcarrier $m_I$. After trivial derivation steps, we obtain

$$\hat{\mathbf{d}}_{m_I}[n_I] = \sqrt{P_I G_{II}}\mathbf{d}_{m_I}[n_I] + \frac{\mathbf{w}_{m_I}[n_I]}{\hat{H}_{II,m_I}} + \boldsymbol{\rho}_{m_I}[n_I] + \boldsymbol{\eta}_{m_I}[n_I], \tag{4.28}$$

where $\boldsymbol{\rho}_{m_I}[n_I]$ is the part of error caused by imperfect channel estimation expressed as

$$\boldsymbol{\rho}_{m_I}[n_I] = -\frac{\xi_{II,m_I}\sqrt{P_I G_{II}}}{\hat{H}_{II,m_I}}\mathbf{d}_{m_I}[n_I]. \tag{4.29}$$

The effects of channel estimation errors are out of the scope of this study and we will therefore assume in the following that $\hat{H}_{II,m_I} = H_{II,m_I} \forall m_I$. The part of interference created by the secondary FB-MC signal that we are interested to model, $\boldsymbol{\eta}_{m_I}[n_I]$, is defined similarly as in (4.8) as

$$\begin{aligned}\boldsymbol{\eta}_{m_I}[n_I] = \frac{\sqrt{P_S}}{H_{II,m_I}\sqrt{T_I}} \int_{n_I(T_I+T_{\mathrm{CP},I})}^{n_I(T_I+T_{\mathrm{CP},I})+T_I} & e^{-j2\pi\frac{m_I}{T_I}(t-n_I(T_I+T_{\mathrm{CP},I}))} \\ & \times (h_{SI}(t) * s_S(t-\delta_\mathrm{t}))e^{j2\pi\delta_\mathrm{f}(t-\delta_\mathrm{t})}\,\mathrm{d}t.\end{aligned} \tag{4.30}$$

With the definition of the multipath channel given in (4.23), we see that

$$h_{SS}(t) * s_S(t-\delta_\mathrm{t}) = \sqrt{G_{SI}}\sum_{l=0}^{L-1} h_{SI,l}\, s_S(t-\delta_\mathrm{t}-\epsilon_{SI,l}). \tag{4.31}$$

Hence,

$$\begin{aligned}\boldsymbol{\eta}_{m_I}[n_I] = \frac{\sqrt{P_S G_{SI}}}{H_{II,m_I}\sqrt{T_I}} \sum_{l=0}^{L-1} h_{SI,l} \int_{n_I(T_I+T_{\mathrm{CP},I})}^{n_I(T_I+T_{\mathrm{CP},I})+T_I} & e^{-j2\pi\frac{m_I}{T_I}(t-n_I(T_I+T_{\mathrm{CP},I}))} \\ & \times s_S(t-\delta_\mathrm{t}-\tau_{SI,l})e^{j2\pi\delta_\mathrm{f}(t-\delta_\mathrm{t}-\tau_{SI,l})}\,\mathrm{d}t.\end{aligned} \tag{4.32}$$

This last equation is very interesting as we recognize a linear combination of the expression given in (4.8). Besides, if the channel $h_{SI}$ can be assumed flat on each subcarrier, as is the

case in most communication scenarios, (4.32) can be simplified to

$$\boldsymbol{\eta}_{m_I}[n_I] = \frac{\sqrt{P_S G_{SI}}}{H_{II,m_I}\sqrt{T_I}} H_{SI,m_I} \int_{n_I(T_I+T_{\mathrm{CP},I})}^{n_I(T_I+T_{\mathrm{CP},I})+T_I} e^{-j2\pi \frac{m_I}{T_I}(t-n_I(T_I+T_{\mathrm{CP},I}))} \times s_S(t-\delta_\mathrm{t}-\tau_{SI,l}) e^{j2\pi\delta_\mathrm{f}(t-\delta_\mathrm{t}-\tau_{SI,l})}\,\mathrm{d}t. \tag{4.33}$$

Then, following the exact same derivations as in the AWGN channel case, we can conclude that

$$I^{S\to I}_{\mathrm{EVM,ZF}}(m_S, m_I, \delta_\mathrm{f}) \approx \frac{P_S G_{SI} T_I |H_{SI,m_I}|^2}{|H_{II,m_I}|^2} \times \sum_{n=0}^{\frac{T_g}{\Delta \mathrm{T_S}}} \left| \sum_{k\in\mathbb{Z}} G_k e^{j\pi \frac{k}{T_\mathrm{g}}(T_I - 2(n\Delta \mathrm{T_S}))} \mathrm{sinc}(\pi(\frac{k}{T_\mathrm{g}}+\nu)T_I) \right|^2 \tag{4.34}$$

This last expression is very similar to (4.22) except for the factor $\frac{1}{|H_{II,m_I}|^2}$ which is due to the ZF equalization, and the factor $|\hat{H}_{SI,m_I}|^2$ which represents the gain of the interfering channel on subcarrier $m_I$.

### Minimum Mean Square Error (MMSE) equalization

In the case of MMSE equalization, following the same derivations as in the ZF case, we obtain the following expression, analog to (4.34):

$$I^{S\to I}_{\mathrm{EVM,MMSE}}(m_S, m_I, \delta_\mathrm{f}) \approx \frac{P_S G_{SI} T_I |H_{II,m_I} H_{SI,m_I}|^2}{\left||H_{II,m_I}|^2 + \frac{1}{\mathrm{SNR}_I}\right|^2} \times \sum_{n=0}^{\frac{T_g}{\Delta \mathrm{T_S}}} \left| \sum_{k\in\mathbb{Z}} G_k e^{j\pi \frac{k}{T_\mathrm{g}}(T_I - 2(n\Delta \mathrm{T_S}))} \mathrm{sinc}(\pi(\frac{k}{T_\mathrm{g}}+\nu)T_I) \right|^2, \tag{4.35}$$

where $\mathrm{SNR}_I$ is the SNR at the incumbent receiver. The derived expressions in the case of ZF and MMSE equalization show clearly that the model we developed on flat channel translates with very little modification to the multipath channel. In the following, we will demonstrate the validity of our model through simulations on multipath channels.

## 4.4.4 Case study

To demonstrate the validity of our approach, we consider a coexistence setup in which the secondary and the incumbent system are each allocated a band of 32 subcarriers. Furthermore, we consider that their active bands are directly adjacent such that $\mathcal{M}_S = \{0 \dots 31\}$ and

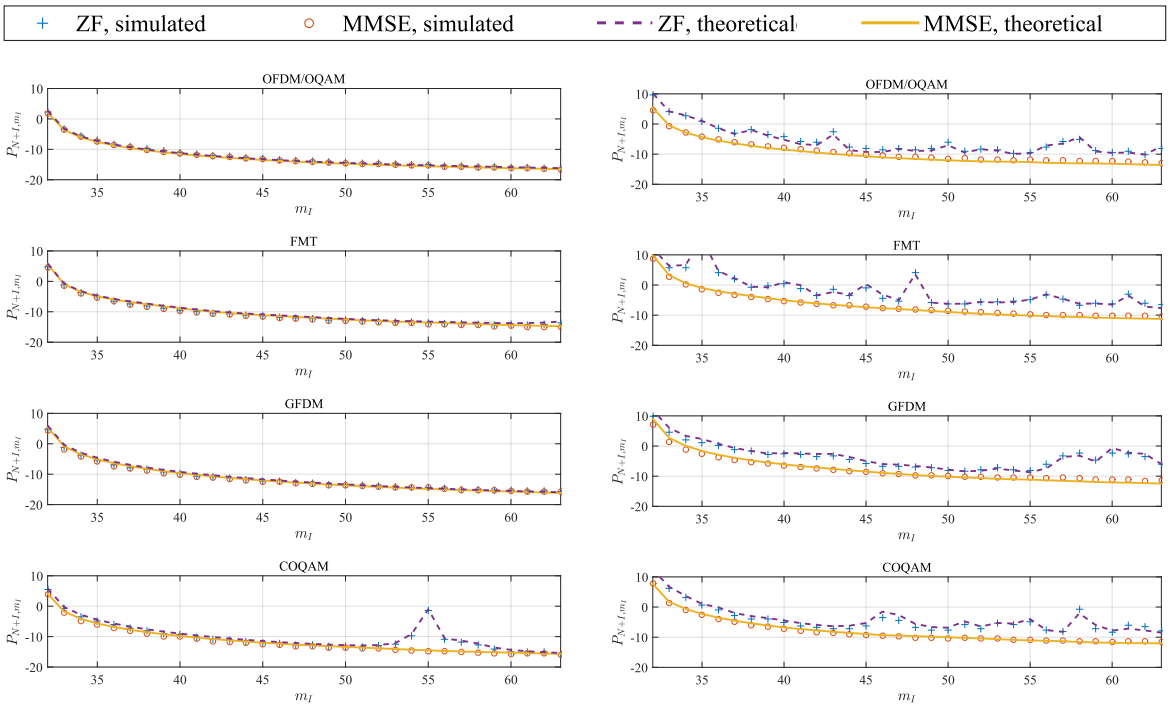


Figure 4.10: Average sum power of noise and interference in dB on each subcarrier $m_I$ of the incumbent CP-OFDM system. Results are averaged over 1000 realizations of the secondary and incumbent channels, following the EPA (a) and ETU (b) channel models.

$\mathcal{M}_I = \{32 \dots 63\}$. Moreover, we consider that the incumbent SNR, not accounting for the secondary interference, equals to $\frac{P_I G_{II}}{\sigma_w^2} = 20dB$. Besides, in order to put the focus on the effects of the interference caused by the secondary system, the secondary interfering transmitter is assumed to be closer to the incumbent receiver than the incumbent transmitter, so that $\frac{P_S G_{SI}}{P_I G_{II}} = 10dB$.

To verify the validity of our model in such a setup, we compute the average sum power of noise and interference on each subcarrier of the incumbent and compare it with the following predicted values in the case of ZF and MMSE equalization:

$$\text{ZF:} P_{N+I,m_I} = \frac{\sigma_w^2}{|H_{II,m_I}|^2} + \sum_{m_S \in \mathcal{M}_S} I^{S\to I}_{\text{EVM,ZF}}(m_S, m_I, \delta_f) \tag{4.36}$$

$$\text{MMSE:} P_{N+I,m_I} = \frac{\sigma_w^2 |H_{II,m_I}|^2}{\left(|H_{II,m_I}|^2 + \sigma_w^2\right)^2} + \sum_{m_S \in \mathcal{M}_S} I^{S\to I}_{\text{EVM,MMSE}}(m_S, m_I, \delta_f) \tag{4.37}$$

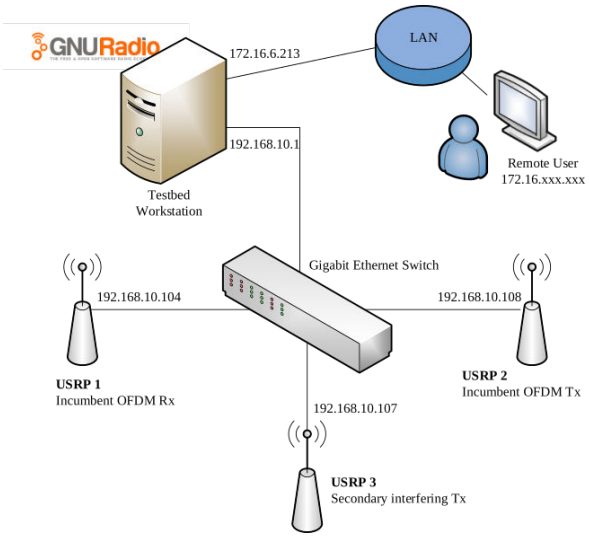


Figure 4.11: Experimentation setup : the three involved USRPs are in the same subnet and connected to the same gigabit ethernet switch as the testbed workstation. The latter acts as a gateway between the testbed subnet and the lab Local Area Network (LAN). Users can therefore access the workstation remotely and execute the GnuRadio application. Note that each USRP is also connected to an external clock source which is not represented in the figure.

In (4.36) and (4.37), the first term of the addition corresponds to the power of noise after equalization, which can be readily found in the literature, while the second term corresponds to the power of interference after equalization which we have characterized in (4.34) and (4.35) respectively. Results are shown in Fig. 4.10, in which we represent the simulated and predicted values of $P_{N+I,m_I}$ on each subcarrier of the incumbent for both the ZF and MMSE equalizers. Note that the presented results have been averaged over 1000 realizations of the incumbent and secondary channel. These results show that the proposed model estimates the performance of the incumbent CP-OFDM system in a satisfying manner.

## 4.5 Experimental Validation

### 4.5.1 Experimental setup

To confirm and conclude our analysis, we developed a software radio testbed to analyze the coexistence scenario corresponding to Fig. 4.1 and validate the analytical expressions derived in the former section. The experiment consists of three Ettus USRP N210. Two USRPs are used to implement the incumbent OFDM transmission, and one USRP acts as the interfering secondary transmitter. Note that the secondary receiver is not included in this experiment

as we focus on the interference caused by the secondary FB-MC system on the incumbent OFDM receiver.

The experiment is performed on the SCEE Testbed at CentraleSupélec that we describe extensively in appendix B. The two USRPs acting as the incumbent and secondary transmitters are both equipped with a SBX daughterboard and the incumbent receiver uses a WBX daughterboard. All USRPs are using a single VERT2450 antenna on their TX/RX RF frontend. To be able to control with ease the timing and frequency misalignements between all users, all USRPs are externally synchronized by an Ettus Research Octoclock-G which feeds each of them a reference 10 MHz clock and a pps signal. Moreover, all USRPs are connected to a gigabit ethernet switch and they are controlled by a workstation that is connected to the same switch. The experimentation software is written in python under the GnuRadio framework and executed on the workstation. The experiment is sketched in Fig. 4.11.

The communications take place in the 434 MHz ISM band. The CP-OFDM incumbent system uses 256 subcarriers of width 1500 Hz, which corresponds to a total band of 384 kHz. The CP-OFDM incumbent transmission is established on a subset of those 256 subcarriers, which is configurable at the initialization of the demonstration. In Fig. 4.13, we show an example in which the CP-OFDM incumbent transmission happens on the subcarriers 16 to 47, and the secondary system transmits on a directly adjacent band, from subcarriers -16 to 15. The CP-OFDM incumbent transmission is realized in real time through the use of custom GnuRadio CP-OFDM blocks, while the secondary system is emulated by playing signals generated with Matlab. The secondary transmit signal can be set to one of the following waveforms : CP-OFDM, FMT, OFDM/OQAM, FBMC-PAM, GFDM, COQAM. The transmit power of the secondary user can be dynamically varied at runtime.

It is well known that hardware impairments such as IQ imbalance or non-linearities of the high power amplifier can harmfully affect the theoretical spectral localization of the FB-MC waveforms we have shown in Fig. 3.4 [142]. However, these effects have been out of the scope of our study. Therefore, in our experimentation, we avoided these effects by precisely calibrating USRPs and ensuring that the high power amplifier was functioning in linear mode. To verify that we were able to transmit FB-MC waveforms with high spectral localization, we studied their spectral shape by plugging the output of the secondary USRP directly onto a spectrum analyzer. Results are represented in Fig. 4.12. We see clearly that, because the high power amplifier behaves linearly, the advantageous spectral shapes of the transmit FB-MC waveforms are preserved.

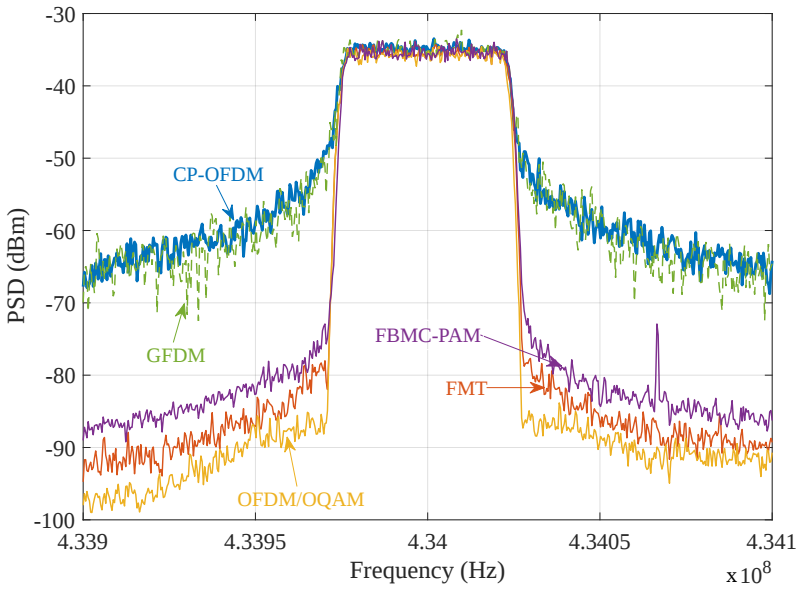


Figure 4.12: Comparison of the PSD of tested waveforms as seen on a spectrum analyzer. In our experiment, the high power amplifier functions almost perfectly linearly and we are therefore able to reproduce experimentally the theoretical spectral shapes of FB-MC signals.

### 4.5.2 Developed GUI, obtained results and discussion

To exploit the experimentation setup presented in Fig. 4.11, we developed a QT GUI on top of the GnuRadio application to dynamically manage the experiment and display results in real time. The workflow of each experimentation can be described with the following steps:

1. The CP-OFDM transmission is established, and sample synchronization is performed manually by finding the value for which no energy is leaked on inactive subcarriers.

2. Once sample synchronization is acquired, the CP-OFDM receiver performs a very simple channel equalization: indeed, in the first step of the experiment, the CP-OFDM transmitter is set to transmit only ones, so that the channel impulse response is equal to the received signal. The latter is simply inverted to perform ZF equalization of the channel.

3. Once sample synchronization and equalization have been performed, the CP-OFDM transmitter starts emitting random 4-QAM symbols. The power of noise and interference on each subcarrier of the CP-OFDM incumbent system is then plotted on the GUI, as is shown in Fig. 4.13.

4. We then start increasing the transmit power of the secondary interfering user so that the level of interference caused by the secondary system on the CP-OFDM incumbent is much higher than the Gaussian noise. This allows us to compare the measured values

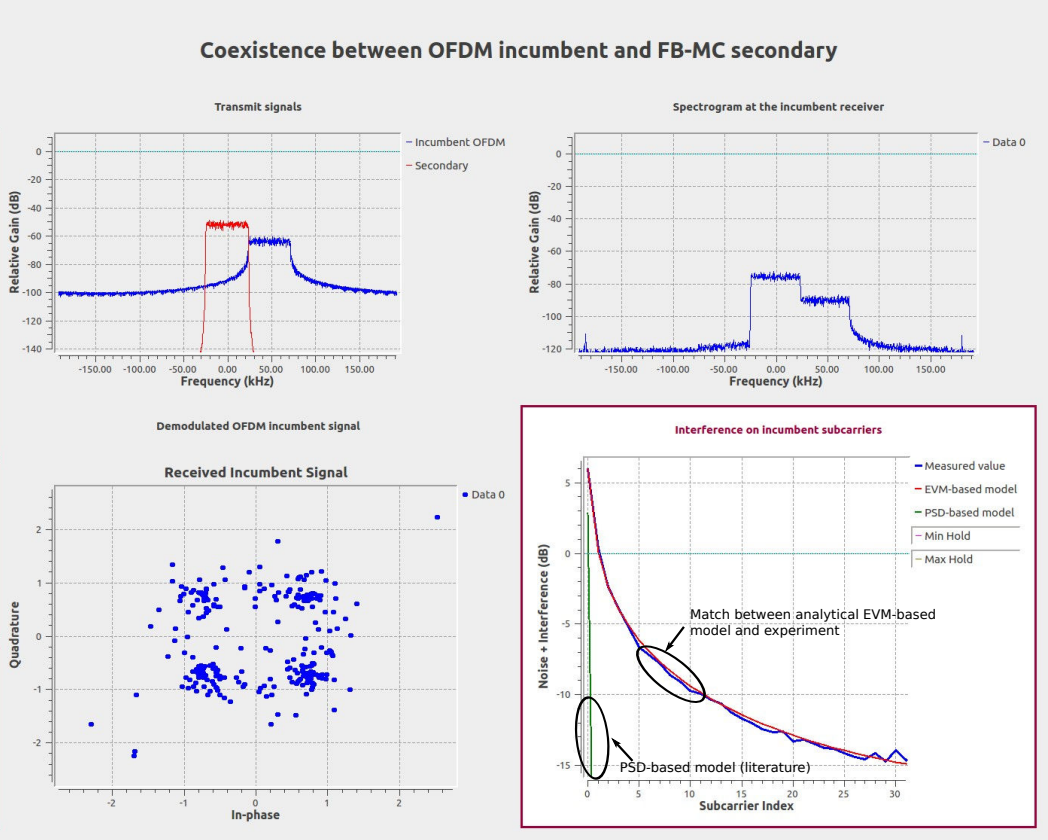


Figure 4.13: Developed GUI : the PSD of the FB-MC secondary signal (in red) and of the incumbent CP-OFDM signal (in blue) are displayed on the top left quarter. The spectral shape of the signal received by the incumbent receiver is represented on the top right, and the constellation of the demodulated CP-OFDM signal on the bottom left. The interference injected by the FB-MC transmitter on each subcarrier of the CP-OFDM incumbent signal is plotted on the bottom right (blue curve) and compared to the literature PSD-based model (green curve) and our EVM-based model (red curve), which exhibits perfect accuracy.

of interference with both the PSD-based model from the literature and the EVM-based model we developed in the former section.

Note that the synchronization and equalization procedures performed by the CP-OFDM incumbent system are deliberately kept simple. This is to keep the focus of our demonstration on the raw interference caused onto each subcarrier of the CP-OFDM incumbent receiver. If we had set the CP-OFDM transmission to use more advanced synchronization and equalization procedures based for example on pilot signaling, the interfering secondary signal may have altered the said pilot signals. As a result, the CP-OFDM incumbent transmission may have been entirely lost and it would have been infeasible to compare the experimental results with our theoretical model.

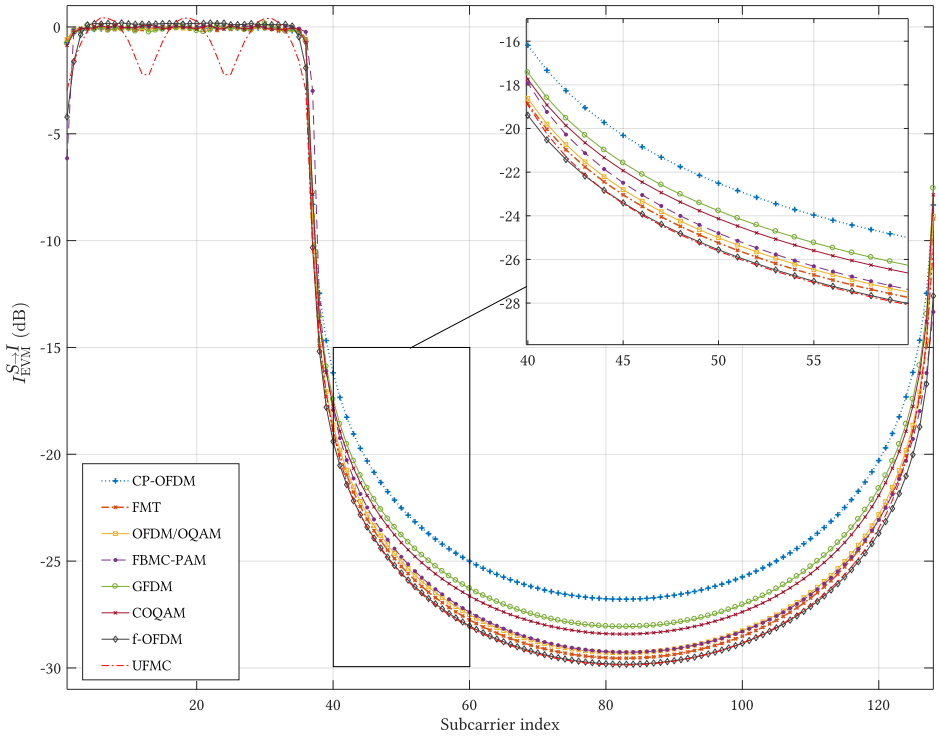


Figure 4.14: EVM on each subcarrier of the CP-OFDM incumbent receiver when a secondary user is transmitting on subcarriers 0 to 35 with different waveforms. f-OFDM and UFMC do not bring any significant advantage compared to analyzed FB-MC waveforms.

In Fig. 4.13, we present the developed GUI in the state which is achieved after steps 1 to 4 explained above have been performed. Note that in that example, the secondary FB-MC system is using OFDM/OQAM. Moreover, as explained above, the secondary system is set to transmit at high power so that the effect of gaussian noise is negligible compared to the level of interference caused by the secondary system onto the incumbent. In turn, we see on the bottom right of Fig. 4.13 a near-perfect match between the value of interference measured on each CP-OFDM incumbent subcarrier and the value predicted by the EVM-based model developed in this chapter. On the opposite, we see clearly that the PSD-based model fails to provide any valid estimation of the interference suffered by the incumbent. We observe similar results for FB-MC waveforms other than OFDM/OQAM.

## 4.6 Extension of the EVM-approach to subband-filtered waveforms

At this point of our discussion, we have made clear that all FB-MC waveforms fail to properly coexist with CP-OFDM incumbent systems, and shed light on the core analytical aspects that are responsible of this. Mainly, we have explained that the advantageous spectral properties of

FB-MC waveforms are drastically reduced when the long prototype filter is truncated by the rectangular window of the CP-OFDM receiver. However, a limitation of our work is that it is focused solely on FB-MC waveforms that perform a filtering per subcarrier. This was done on purpose to maintain a common mathematical model that would allow us to obtain tractable expressions. Indeed, as we explained it previously, the interference caused by each subcarrier of the secondary system can be computed separately only if those subcarriers are themselves filtered separately, which is not the case for subband-filtered waveforms. Therefore, one may wonder if the limitations shown in this chapter cannot be overcome if the secondary uses a subband filtered waveform such as UF-OFDM . Indeed, these waveforms use wider, hence shorter, filters. However, even with such a waveform, the CP-OFDM reception truncates the incoming signal with the same rectangular window and the same problem appears as for the FB-MC waveforms we have analyzed in that article. To make it clear, we present in Fig. 4.14 the EVM on each subcarrier of the CP-OFDM incumbent receiver when the secondary user is active on subcarriers 0 to 35. We compare all FB-MC waveforms analyzed in this article with a f-OFDM and a UFMC system. We show clearly that f-OFDM and FB-MC waveforms interfere to a similar extent on the CP-OFDM incumbent receiver. This shows once more that the limiting factor in the scenario we study is the CP-OFDM receiver, that truncates the incoming signal and outputs a poor spectral representation of it.

## 4.7 Conclusion

In this chapter, we investigated the coexistence on the same band of users utilizing FB-MC waveforms and legacy CP-OFDM incumbent devices. We first reminded that in these scenarios, interference between users with different physical layers is usually measured according to the PSD of the interfering signal. This PSD-based model, though practical, only encompasses the effects of interference in the channel, at the input antenna of the receiver that suffers from interference.

However, interference should actually be measured based on EVM after the demodulation operations, before the constellation decoding. We therefore compared values of interference measured at this stage with those predicted by the PSD-based model. We showed that there is a tremendous gap between the PSD-based and EVM-based model, and went on to explain that this is due to the fact that the CP-OFDM receiver truncates the incoming interfering signal, which destroys the advantageous PSD properties of FB-MC signals. We further validated these results through mathematical analysis and experimentation. The obtained results show that secondary users based on FB-MC waveforms interfere on CP-OFDM incumbent users in a similar extent as CP-OFDM based secondary users. Though the mathematical and analytical considerations behind this work are not particularly complex, they had been totally

omitted in a vast majority of the works available in the literature. We also showed that our analysis which focused on FB-MC waveforms also applies to subband-filtered waveforms.

Finally, the study carried out in this chapter shows that the in-band coexistence of new 5G communications with legacy CP-OFDM systems will only marginally be improved through the use of enhanced multicarrier waveforms. This improvement would be even more limited if signal impairments caused by the non-linear high power amplifier underlined for example in [142] came into play. Overall, based on the presented analysis, we can affirm that waveforms with sharp spectral localization do not efficiently reduce interference to CP-OFDM receivers. This results contradicts a number of studies that had been led so far in the field of CR. Therefore, in the following chapter, we propose to apply the interference model we derived in classical CR setups, in which the secondary system is based on FB-MC while the incumbent relies on CP-OFDM.

# Chapter 5

# Coexistence with CP-OFDM incumbent systems in CR setups

**Contents**



## 5.1 Introduction

In the former chapter, we have thoroughly analyzed the interference caused by enhanced multicarrier waveforms onto a CP-OFDM receiver. One of the key results we have established is that the PSD-based modeling of interference gives inaccurate results and dramatically underestimates the actual interference experienced by CP-OFDM incumbent systems. However, as we have extensively explained in Chapter 3, this PSD-based model has been widely used in the literature to investigate CR setups in which the incumbent system may be based

on CP-OFDM. Therefore, given the new insights we brought in Chapter 4, it is important to investigate some typical CR problems to understand what are the actual benefits of using enhanced waveforms for secondary transmission in cases where the incumbent relies on CP-OFDM.

In this chapter, we therefore investigate two CR problems that have been thoroughly discussed in the literature. First, in section 5.2 we compute the width of the guard band that is necessary between the two coexisting systems to ensure a given level of protection demanded by the incumbent system. Then, in section 5.3 assuming that the secondary and incumbent systems are assigned fixed bands to transmit, we analyze the optimal power distribution that the secondary system should follow to maximize its achievable rate.

Furthermore, in section 5.4, we apply these results in a particular setup in which the secondary system is only given a finite amount of time to transmit. Finally, section 5.5 concludes this chapter. Note that the results presented in this chapter have been presented in two conference papers: [143] and [138], and partially in [144].

## 5.2 Guard band dimensioning

### 5.2.1 System setup

Usually, in CR scenarios, the incumbent system defines a certain level of interference that it considers to be acceptable. In the following, we define this level as the *interference threshold* $I_{\text{th}}$ which corresponds to the amount of interference acceptable on each subcarrier of the incumbent system. One of the most studied problems in the CR literature consists in evaluating the width of the guard band that is necessary to ensure that the interference power level seen on each subcarrier of the incumbent CP-OFDM system is lower than $I_{\text{th}}$. Namely, this is the approach followed in [47, 110, 120, 124, 145].

In this section, we will study this problem in a CR setup in which a secondary device which uses 36 subcarriers to transmit coexists with a CP-OFDM incumbent system. Then, according to the waveform used by the secondary, we compute the number $N_G$ of guard subcarriers to ensure that the interference experienced on each subcarrier of the incumbent

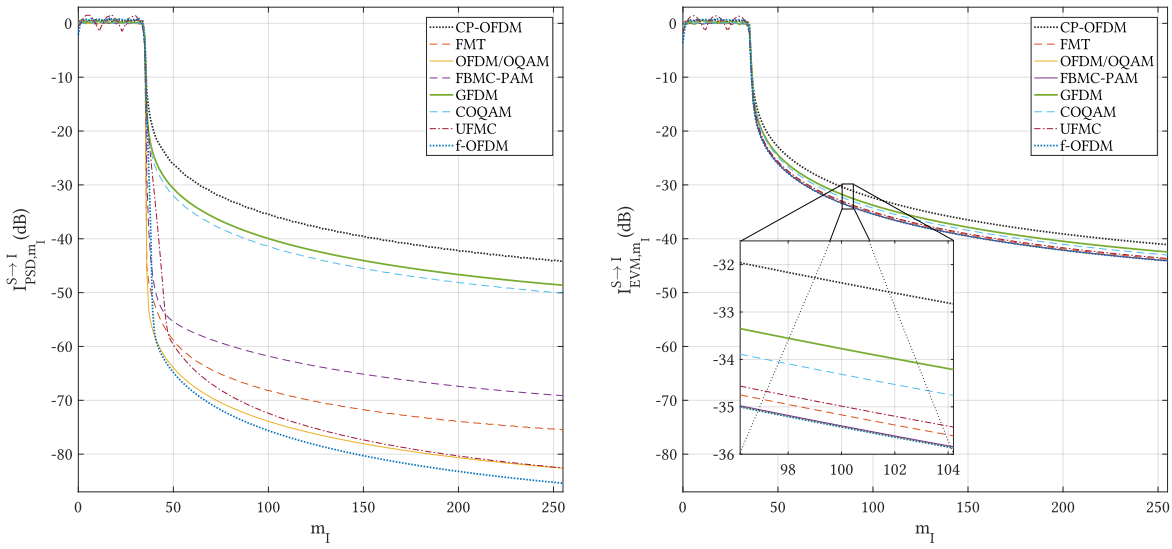


Figure 5.1: Interference seen on each subcarrier of the incumbent according to (a)the PSD-based model and (b)the EVM-based model presented in chapter 4.

is lower than $I_{\text{th}}$. In other words, we aim at resolving the following problem:

$$\text{Compute } N_G = \min_{m_S \in \mathcal{M}_S, m_I \in \mathcal{M}_I} |m_S - m_I - 1|$$

such that

$$\max_{m_I \in \mathcal{M}_I} \left( \underbrace{\sum_{m_S \in \mathcal{M}_S} I^{S\to I}(m_S, m_I)}_{I^{S\to I}_{m_I}} \right) < I_{\text{th}}.$$

### 5.2.2 Obtained results

Firstly, we compute the interference power on each subcarrier of the incumbent that would be seen at the input antenna according to the PSD-based model and present the obtained results in Fig. 5.1a. Then, we compare them with the interference that would be seen after the CP-OFDM demodulation, computed with the EVM-based approach we presented in chapter 4. Results are shown in Fig. 5.1b. Once again, this gives a glaring example of the discrepancy between the values obtained with the two approaches: while the PSD-based results show significant difference between the different waveforms according to their spectral

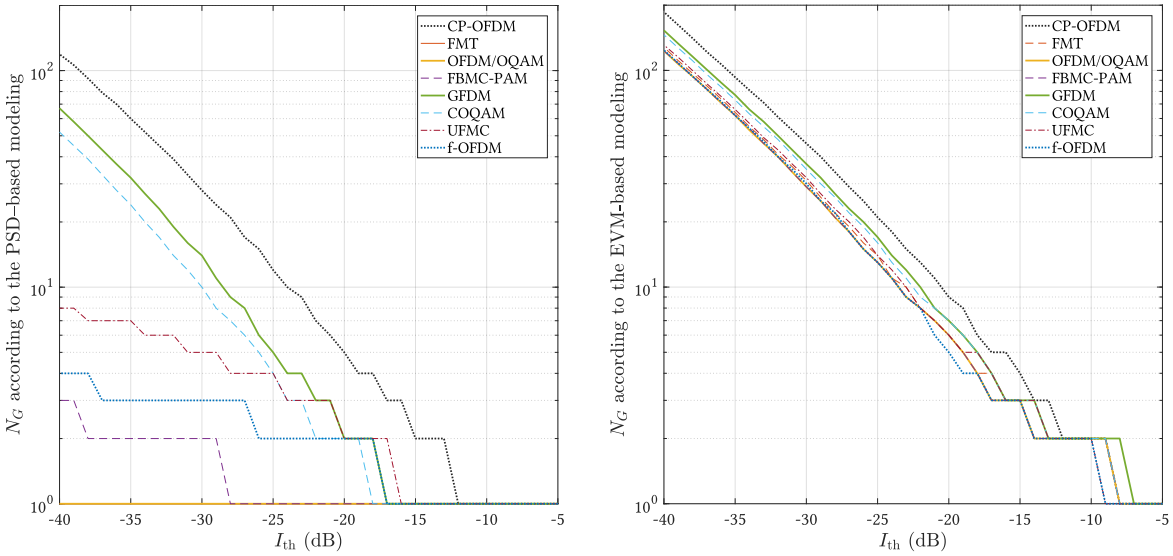


Figure 5.2: Number of guard subcarriers necessary to protect the incumbent as a function of its interference threshold per subcarrier $I_{\text{th}}$ according to (a) the PSD-based model of the literature and (b) our EVM-based modeling.

localization, the EVM-based ones demonstrate that all of them interfere equivalently onto the CP-OFDM incumbent receiver.

These values of interference can then be used to measure the amount of guard subcarriers that are needed between the two systems to protect the incumbent. To do so, one simply has to find on Fig. 5.1b and Fig. 5.1a the value of $m_I$ above which $I_{m_I}^{S\to I} < I_{\text{th}}$. The corresponding values are presented in Fig. 5.2. Once again, we present the results obtained by following the PSD-based modeling of the literature and those obtained with our much more accurate EVM-based approach.

Consistently with the results presented in Fig. 5.1, we see that the PSD-based model greatly underestimates the number of necessary subcarriers $N_G$. For example, for $I_{\text{th}} = -30$ dB, the PSD-based model predicts that only ones guard subcarrier is necessary if the secondary uses OFDM/OQAM instead of 28 if the latter was based on CP-OFDM. Our EVM-based approach shows on the opposite that for the same interference threshold, 46 guard subcarriers are necessary for CP-OFDM and 29 for OFDM/OQAM. Overall, while the PSD-based approach predicts a high variation in the results in function of the waveform used by the secondary system, actual results obtained with the EVM-based approach we proposed show that the number of necessary guard subcarriers is comparable with all waveforms tested. This result demonstrates that the insertion of secondary systems in spectral holes is not greatly facilitated by the sole adoption of enhanced multicarrier waveforms.

## 5.3 Optimal power allocation

### 5.3.1 System setup

The guard band dimensioning problem we have presented in the former section gives some insights on the gains brought by the use of enhanced waveforms in CR setups. However, it is insufficient. Indeed, it follows the idea of spectral masks and assumes that both systems transmit at equal power. However, one could imagine that a secondary system could transmit with more or less power according to the surrounding incumbent systems. Doing so, the secondary system tries to optimize its achievable rate while respecting the interference constraints set by the incumbent. This can be expressed as the following optimization problem:

$$\begin{aligned} P1: &\max_{P_{m_S}} \sum_{m_S \in \mathcal{M}_S} \log_2\left(1 + \frac{P_{m_S} G_{SS}}{\sigma_w^2 + \sigma_I^2}\right), \\ &\text{s.t.} \\ &\forall m_I \in \mathcal{M}_I,\ I_{m_I}^{S \to I} \leq I_{\text{th}}, \\ &\sum_{m_S \in \mathcal{M}_S} P_{m_S} \leq P_{\text{t}_S}, \\ &P_{m_S} \geq 0, \forall m \in \mathcal{M}_S. \end{aligned} \tag{5.1}$$

In the problem $P1$, the cost function to optimize is the rate achieved by the secondary system, expressed in function of the SINR at the secondary receiver. The first constraint expresses the interference threshold that should not be exceeded on each subcarrier of the incumbent system. The second constraint is related to the total power budget of the secondary system, i.e. how much power is available for the latter to communicate. Finally, the last constraint is straightforward and simply recalls that the power allocated on each subcarrier of the secondary system should be positive. Note that problem $P1$ can take different forms according to the waveform used by the secondary. Indeed, if the latter uses a subband-filtered waveform, it can only allocate the same power to every subcarrier and $P1$ is therefore changed into:

$$\begin{aligned} P2: &\max_{P_S} \log_2\left(1 + \frac{P_S G_{SS}}{\sigma_w^2 + \sigma_I^2}\right), \\ &\text{s.t.} \\ &\forall m_I \in \mathcal{M}_I,\ I_{m_I}^{S \to I} \leq I_{\text{th}}, \\ &P_S \leq P_{\text{t}_S}, \\ &P_S \geq 0. \end{aligned} \tag{5.2}$$

However, if the secondary system uses a FB-MC waveform, each subcarrier can be dealt with separately and get assigned a different power level. Furthermore, in this case, as we

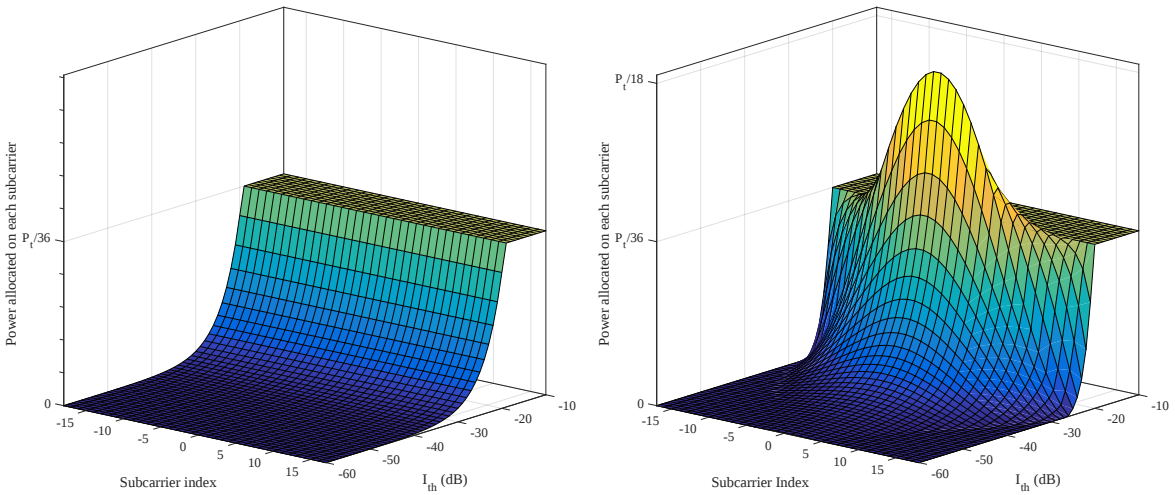


Figure 5.3: Power allocated on each subcarrier of the secondary system according to the interference threshold set by the incumbent for (a) UFMC and (b) OFDM/OQAM.

demonstrated in Chapter 4, the contribution of each subcarrier of the secondary to the total interference suffered by the incumbent can be computed separately. Therefore, for FB-MC waveforms, $P1$ turns into

$$
\begin{aligned}
P3: \max_{P_{m_S}} & \sum_{m_S \in \mathcal{M}_S} \log_2\left(1 + \frac{P_{m_S} G_{SS}}{\sigma_w^2 + \sigma_I^2}\right), \\
\text{s.t.} & \\
& \forall m_I \in \mathcal{M}_I, \sum_{m_S \in \mathcal{M}_S} I^{S \to I}(m_S, m_I) \leq I_{\text{th}}, \\
& \sum_{m_S \in \mathcal{M}_S} P_{m_S} \leq P_{\text{t}_S}, \\
& \forall m_S \in \mathcal{M}_S, P_{m_S} \geq 0,
\end{aligned}
\tag{5.3}
$$

with $I^{S \to I}(m_S, m_I)$ computed as depicted in chapter 4. Both $P2$ and $P3$ are convex optimization problems. Several works in the literature, such as [109], have studied these problems and proposed near-optimal low complexity algorithms to solve them. In this study, we are simply interested in studying the optimal solution for each of the studied waveforms and do not focus on any particular means to achieve the said optimum.

### 5.3.2 Obtained results

In the following, we study a scenario in which an incumbent system occupies a subset of a band composed of 512 subcarriers. In details, it uses the 144 subcarriers of the set

$\mathcal{M}_I = [-90 \dots -19] \cup [20 \dots 91]$, effectively leaving a spectral hole of 38 subcarriers in the middle of the band. Out of these 38 subcarriers, the secondary tries to use the 36 comprised in $\mathcal{M}_S = [-17 \dots 18]$, leaving one guard subcarrier on each side of its band. Furthermore, we consider that $G_{SS} = G_{SI}$, which corresponds to a case where the gain of the secondary channel and the interfering channel are similar. This is for example achieved when the secondary transmitter is at comparable distances of the incumbent and secondary receivers. The optimization problem $P2$ for UFMC and f-OFDM and $P3$ for other waveforms is solved by using CVX.

In Fig. 5.3, we represent the power that gets allocated on each subcarrier of the secondary system as the interference threshold $I_{\text{th}}$ set by the incumbent is varied. The results are shown both in the cases where the secondary uses UFMC and OFDM/OQAM. As we have explained in the previous subsection, when the secondary uses UFMC or f-OFDM, we are unable to perform per-subcarrier power allocation because of the subband-filtering. Therefore, the power that can be allocated on the whole secondary band is capped by the level that can be allocated at the edge of the band. Indeed, it is the subcarriers at the edge of the secondary band which cause the most interference to the incumbent. Finally, as the interference threshold increases, the power budget constraint becomes predominant and the power on each subcarrier is capped at $\frac{P_{tS}}{36}$. On the other hand, if the secondary uses a FB-MC waveform, the center subcarriers can be assigned more power. This is shown in Fig. 5.3 for OFDM/OQAM, in which we see clearly that the center subcarriers are allocated more power than those at the edge. However, when the interference constraint effects fades out, all subcarriers are assigned the same average power level. This shows that the subcarrier-granularity power allocation can be particularly beneficial in interference constrained setups.

Finally, in Fig. 5.4, we present the rate achievable by the secondary according to the waveform it uses. Note that the values we present do not account for the TSE of each waveform. Once more, we present the results obtained with the PSD-based modeling of interference and those predicted with our EVM-based approach. We can draw the same conclusions as for the results we have presented on the matter of guard band dimensioning. Indeed, the PSD-based model predicts that FMT, OFDM/OQAM and FBMC-PAM are almost never constrained by the interference constraint thanks to their enhanced spectral localization. In reality, the EVM-based results show that the rate all waveforms achieve is comparable, with OFDM/OQAM, FMT and FBMC-PAM performing only slightly better than GFDM and COQAM, the latter achieving slightly higher rate values than CP-OFDM. Interestingly, we see that the performance of f-OFDM and UFMC is quite disappointing. There are two reasons for this: first, as we have explained here above, f-OFDM and UFMC cannot perform subcarrier-wise power allocation, which is detrimental to the rate they can achieve in the interference constrained regime. Furthermore, in the scenario we have studied here, there is only one guard subcarrier between the secondary and the incumbent systems.

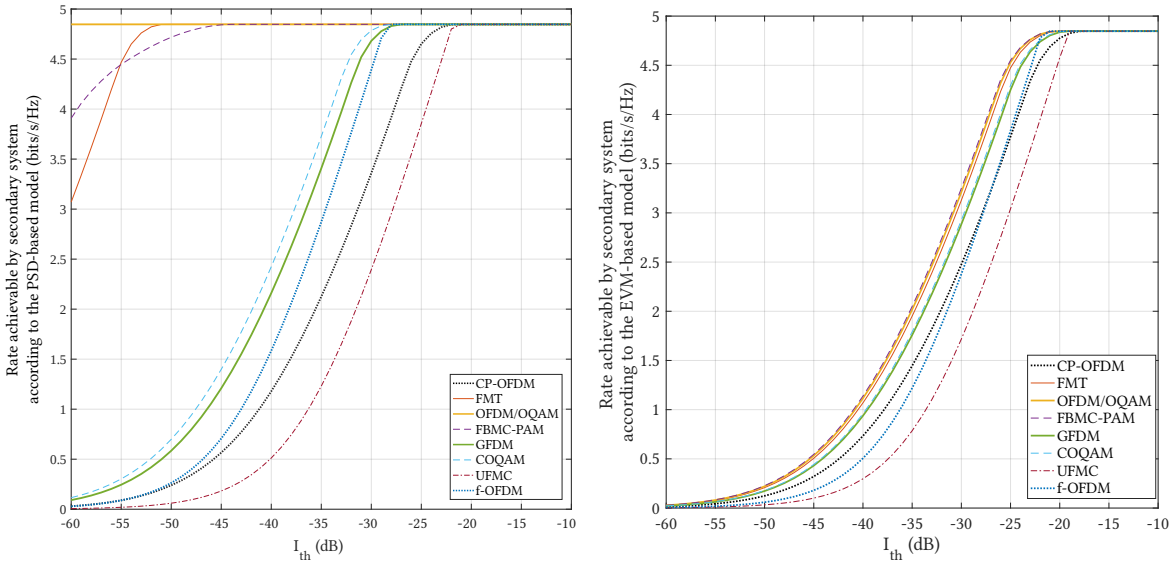


(a) (b)

Figure 5.4: Achievable rate (not accounting for TSE) by each studied waveform in the studied scenario as computed with (a) the PSD-based model and (b) our EVM-based approach.

However, as we have shown in chapter 2 in Fig. 2.13, the sidelobes of UFMC and f-OFDM decrease slower than those of FB-MC waveforms, which explains why even the results obtained with the PSD-based model are disappointing.

## 5.4 Optimal transmission in a given time frame

### 5.4.1 System setup

So far, the results we have shown, both in terms of necessary guard subcarriers and achievable rate, have demonstrated that there is little gain to expect from using enhanced waveforms for the secondary transmission when the incumbent is itself based on CP-OFDM. These results clearly contradict the relevant literature. In this last section of this chapter, we build on top of the power allocation study we have devised here above to study a CR setup in which the secondary tries to maximize the amount of data it can transmit in a given transmission window that is limited both in time and frequency. The corresponding system setup is sketched in Fig. 5.5. As a static interference constraint is assumed during the whole secondary transmission, we can simply compute the total number of bits that can be transmitted by the secondary system as

$$b_S = T_{\text{useful}} \times \sum_{m_S \in \mathcal{M}_S} \log_2\left(1 + \frac{P_{m_S} G_{SS}}{\sigma_w^2 + \sigma_I^2}\right), \tag{5.4}$$

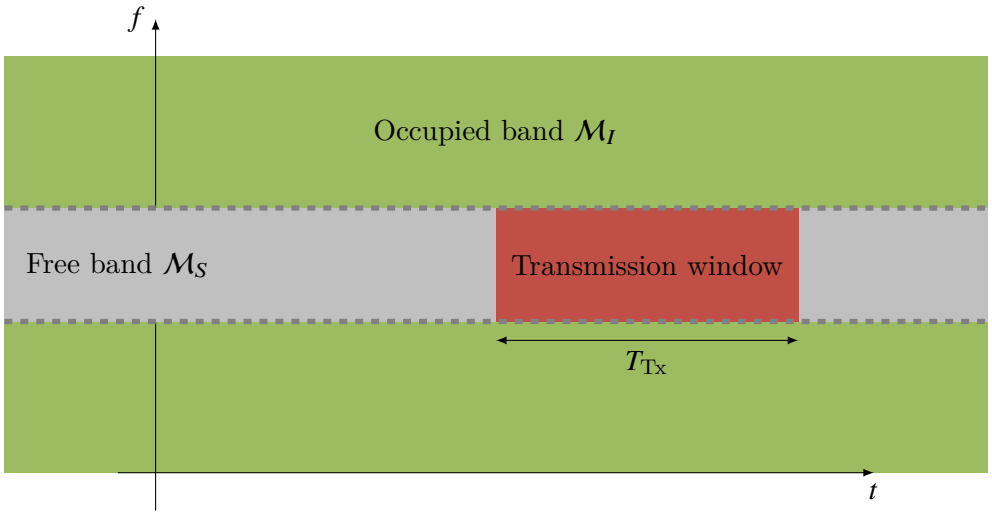


Figure 5.5: Considered system setup: the secondary device transmits in the free band $\mathcal{M}_S$ that it can use during $T_{\text{Tx}}$

where $T_{\text{useful}}$ is the duration in which useful symbols can transmitted. As we explained in section 2.4, this value depends on the TSE of the utilized waveform and is directly obtained as $T_{\text{useful}} = \lfloor TSE \times \Delta \text{F} T_{\text{Tx}} \rfloor$. In this equation, the value of $P_{m_S}$ is the one obtained by finding the optimal solution of the rate optimization problem discussed in the former section.

### 5.4.2 Obtained results

To stay consistent, we study the same spectral layout as in the former section, and therefore consider a scenario in which the band used by the secondary is composed of the 36 center subcarriers of the total available band, with one guard subcarrier on each side separating it from the band used by the incumbent. In the following, we present results that enable us to better understand the performance achieved by the secondary when it uses one of the waveforms we have studied.

Overall, the results of (5.4) depend only on two factors: the interference threshold $I_{\text{th}}$ set by the incumbent which influences the maximum achievable rate, and the available time to transmit $T_{\text{Tx}}$ which acts on the number of symbols the secondary is able to emit and receive. Therefore, we study the effects of these two factors in details. In Fig. 5.6, we present the value taken by $b_S$ as the time to transmit $T_{\text{Tx}}$ is increased. Furthermore, we present results obtained in the interference-constrained regime for $I_{\text{th}} = -40$ dB in Fig. 5.6a and in the power-constrained regime for $I_{\text{th}} = -10$ dB in Fig. 5.6b. These two figures give quite interesting teachings.

We see that when the interference constraint is predominant, the waveform used by the secondary plays a significant role. In particular, FBMC-PAM and OFDM/OQAM outperform

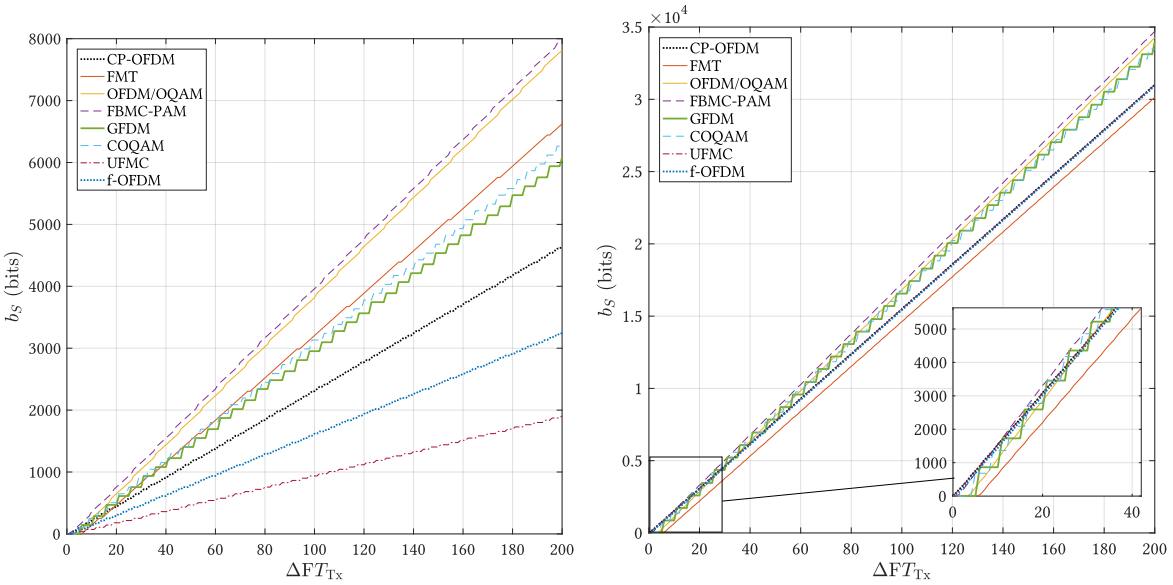


Figure 5.6: Total amount of transmittable data as a function of the available time to transmit $T_{\mathrm{Tx}}$ for a) $I_{\mathrm{th}} = -40$ dB and b) $I_{\mathrm{th}} = -10$ dB

all other waveforms. Interestingly, FBMC-PAM is constantly superior to OFDM/OQAM because of its shorter delay. Indeed, we have shown in Fig. 5.4 that these two waveforms achieve exactly the same rate, which is due to the fact that both interfere equally onto CP-OFDM as demonstrated in chapter 3. However, FBMC-PAM can start transmitting as soon as $\Delta F T_{\mathrm{Tx}} \geq 1$ whereas OFDM/OQAM can only transmit from $\Delta F T_{\mathrm{Tx}} \geq 3.5$ on because of its high filter delay. The advantage of FBMC-PAM over OFDM/OQAM is therefore particularly important for short transmission windows. Nevertheless, FBMC-PAM can constantly transmit approximately 100 bits more than OFDM/OQAM in the same transmit window. One should note, however, that this is not a significantly interesting gain in any realistic setup.

In the interference constrained regime and for long transmission windows, FMT follows directly OFDM/OQAM. However, it suffers from its very long delay and Gabor density inferior to 1 which make it difficulty applicable in short communications, where GFDM and COQAM tend to slightly outperform it. However, these two latter candidates suffer from their greater leakage and therefore lose their advantage over FMT as the transmission window grows longer. Interestingly, because interference is predominant in that case, CP-OFDM, UFMC and f-OFDM are always outperformed because of their poorer leakage. The performance of UFMC and f-OFDM is particularly poor, which is caused by the fact that they are unable to perform subcarrier-wise power loading as mentioned in the former section.

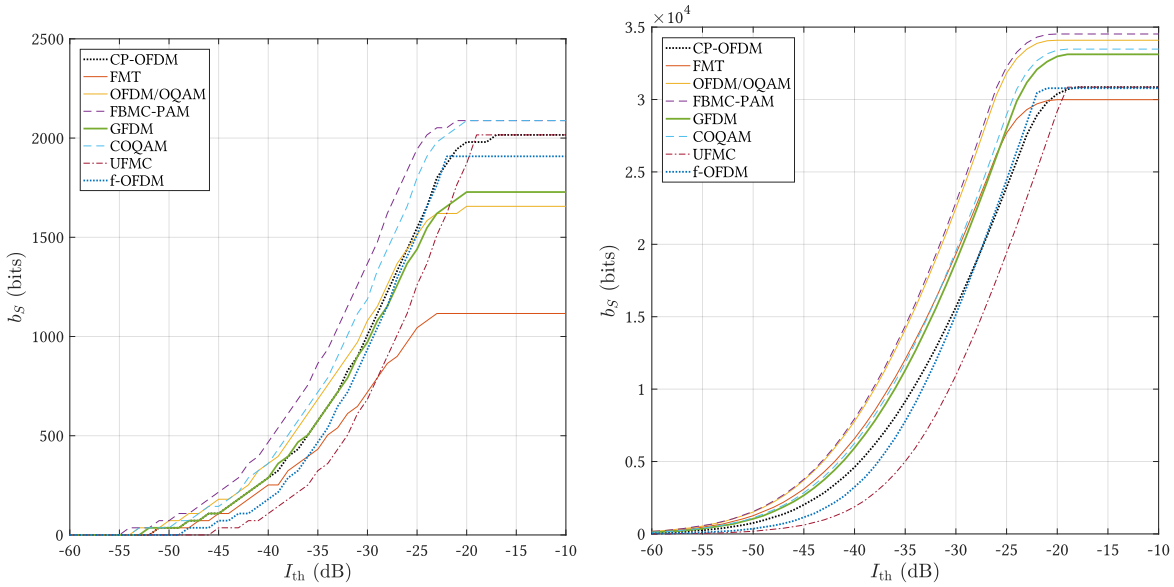


Figure 5.7: Total amount of transmittable data as a function of the interference constraint $I_{\text{th}}$ for a) a short transmission window $T_{\text{Tx}} = \frac{15}{\Delta F}$ equivalent to one LTE TTI and b) a long transmission window $T_{\text{Tx}} = \frac{200}{\Delta F}$.

In Fig. 5.6b, we take a closer look at the behavior exhibited by each waveform when the interference constraint becomes negligible. In that case, all waveforms can achieve the same rate and only their TSE can differentiate between them. We observe once more the superiority of FBMC-PAM. GFDM and COQAM closely follow OFDM/OQAM. Finally, CP-OFDM, UFMC and f-OFDM achieve the exact same performance, while FMT lags behind because of its poor TSE.

In Fig. 5.7, we investigate the effects of $I_{\text{th}}$ for two kinds of transmission windows. Firstly, we investigate a very short transmission window $T_{\text{Tx}} = \frac{15}{\Delta F}$ which corresponds approximately to one time transmission interval (TTI) in the LTE standard. As is represented in Fig. 5.7a, in those very short transmission windows, OFDM/OQAM and FMT cannot achieve interesting performance because of their long prototype filters. Interestingly, FBMC-PAM keeps its lead, as it benefits from both reduced leakage and good TSE. COQAM follows just behind, which shows that the available time to transmit is the predominant factor in this case. This is further confirmed by the surprisingly good performance of CP-OFDM, UFMC and f-OFDM. We also note that GFDM performs quite poorly. Note that this is caused by its block structure, which allows it to transmit only a very limited number of symbols compared to other waveforms.

On the opposite, we represent in Fig. 5.7b the total amount of data that can be transmitted by the secondary in a long window of duration $T_{\text{Tx}} = \frac{200}{\Delta F}$. We observe, once again, that

FBMC-PAM and OFDM/OQAM lead the race, with a slight advantage to the former. GFDM and COQAM achieve medium performance whatever the value of $I_{\text{th}}$. FMT competes with FBMC-PAM and OFDM/OQAM for very stringent interference constraints but is rapidly limited by its low TSE and is less efficient than CP-OFDM, UFMC and f-OFDM when the interference constraint becomes insignificant.

All these results give interesting insights on the relative importance of the factors $I_{\text{th}}$ and $T_{\text{Tx}}$. However, it is important to put back the numerical values of the results we have presented into perspective: when the interference constraint is relaxed, enhanced multicarrier waveforms can only benefit of their improved TSE over CP-OFDM. However, this results in quite low gains of approximately 12.5% which correspond to the proportion of the CP wasted by CP-OFDM. Some relatively higher gains are demonstrated when the interference constraint set by the incumbent is predominant, as FBMC-PAM and OFDM/OQAM have been shown to be able to transmit around 1.7 times as much data as CP-OFDM in the same transmit window.

## 5.5 Conclusion

In this chapter, we have studied under different angles a CR setup in which a secondary system based on an enhanced multicarrier waveform coexists with a legacy CP-OFDM based incumbent system. Overall, the results we presented have shown that there is little gain to be achieved from using an enhanced waveform for the secondary transmission. In particular, we have shown that the gains that can be expected are insignificant in comparison with some that had been previously advertised in the literature. Realistically, the gains we have exposed make it difficult to justify the hassle associated with a change in the waveform used by secondary devices. Nevertheless, we have only studied setups in which there is only one secondary device that uses a waveform other than CP-OFDM. In reality, legacy networks will coexist will multiple secondary devices; if the latter are all to use enhanced multicarrier waveforms, they could bring important advantages. Therefore, in the following chapter, we focus on this type of setups. In particular, we apply our analysis in a D2D communication scenario, which is both timely and relevant to our study.

# Chapter 6

# Asynchronous D2D operation in 5G networks

**Contents**



## 6.1 Introduction

In this chapter, we thoroughly analyze scenarios that involve the coexistence of D2D communications with legacy cellular networks. Following the taxonomy of CR, D2D pairs can be seen as secondary systems, while cellular devices play the role of incumbent. However, as we explained it in chapter 2, it is unlikely that D2D pairs can achieve perfect synchronization between themselves. Thus, D2D pairs are bound to interfere one onto another as well. We are therefore interested to study scenarios in which D2D systems based on enhanced multi-carrier waveforms coexist with legacy CP-OFDM cellular users. In order to study this type of setups,

we follow the approach hereafter. First, in section 6.2, we study a single cell setup, in which one cluster of D2D devices coexists with cellular users in one cell. We study the optimal rate achievable by D2D pairs given a certain interference constraint set by cellular systems. Furthermore, we compare the results achieved by the D2D according to the waveform they use, either CP-OFDM or OFDM/OQAM. The results we show enable us to demonstrate the interest of adopting an alternative waveform for D2D communication. We therefore investigate this idea in more details in section 6.3, in which we lead thorough network-level simulations that enable us to investigate a more realistic scenario, composed of multiple cells and multiple D2D clusters. We investigate, for a large variety of waveforms, the effects of different parameters such as the cell radius or the amount of asynchronism on the performance achieved by the D2D and cellular users. Our study reveals that there are important gains to be expected from the use of enhanced multicarrier waveforms for D2D communications and paves the way for more advanced work in this area. We finally discuss concluding remarks in section 6.4. The work presented in this chapter has been published in one conference paper [146] and one journal article under review [147]. It is the fruit of a close collaboration with Conor Sexton, Ph.D. student at CONNECT, Trinity College Dublin, who is the first author on both papers cited here above.

## 6.2 Preliminary mono-cellular analysis

### 6.2.1 System Model

In this section, we investigate an OFDMA based network in which D2D pairs are permitted to reuse the uplink resources of the incumbent cellular users in an underlay fashion, subject to interference constraints. We stay consistent with the literature and consider uplink resource sharing for two reasons. Firstly, in the uplink, all of the interference imposed by the D2D users onto the cellular users is experienced at the base station (BS), enabling this type of interference to be mitigated through BS coordination. Secondly, and most importantly, some of the pilot information broadcast in the downlink is crucial and should not be interfered with.

Fig. 6.1 illustrates a simplified scenario in which D2D communication underlays an OFDMA network in the uplink. In a more general scenario, $N_D$ D2D pairs coexist with $N_C$ CUs, and reuse the uplink spectral resources. $\mathcal{C} = \{1, \ldots, N_C\}$ denotes the set of incumbent (cellular) users and $\mathcal{D} = \{1, ..., N_D\}$ denotes the set of D2D pairs. The useful and interference channels in Fig. 6.1, shown as solid and dashed lines, respectively, are presented in Table 6.1. CUs do not interfere with each other as we assume they are perfectly synchronized by the BS. Therefore, there are three main interference types requiring consideration:

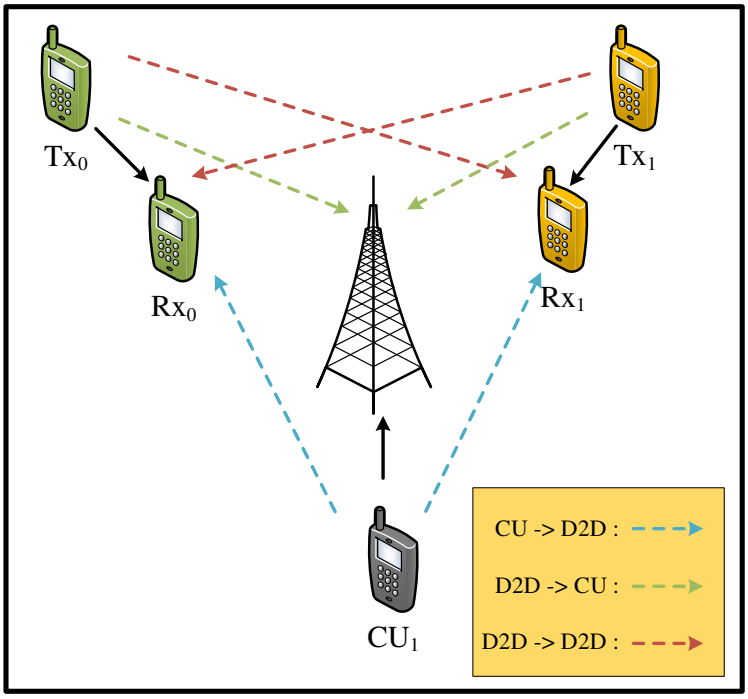


Figure 6.1: Simplified diagram showing two D2D pairs and one cellular user with both interference channels (dashed lines), and useful channels (solid black lines) outlined.

1. The D2D pairs interfere with the incumbents' transmissions. Since we are investigating uplink resource sharing, this interference is observed at the base station.

2. Conversely, the incumbents interfere with the D2D pairs at D2D receivers.

3. D2D pairs interfere with each other (inter-D2D interference).

In each type, we consider both co-channel and adjacent-channel interference. The D2D pairs can choose to operate using either OFDM/OQAM or CP-OFDM, while the cellular users are restricted to using CP-OFDM. The reason to consider the use of OFDM/OQAM for D2D operation lies in its high spectral containment and its low sensitivity to asynchronism in the multi-user context that we have extensively documented in this thesis, which is expected to decrease the interference both between different D2D pairs and between D2D and cellular users. The idea of this section is therefore to see if OFDM/OQAM, which is the waveform exhibiting the best spectral localization, can bring gains in a simple single-cell D2D coexistence context.

We consider an OFDMA micro-cell with parameters selected based on the 3GPP LTE standard, as outlined in Table 6.2 in Section 6.2.3. We assume that the cell is fully loaded with each CU assigned a single uplink RB. D2D devices underlay the OFDMA cell by reusing

Table 6.1: Useful and interference channels for Fig. 6.1

| **Useful Channels** | | |
|---|---|---|
| $cu_1 \rightarrow eNb$ | $Tx_0 \rightarrow Rx_0$ | $Tx_1 \rightarrow Rx_1$ |
| **Interference Channels** | | |
| $cu_1 \rightarrow Rx_0$ | $Tx_0 \rightarrow eNb$ | $Tx_1 \rightarrow eNb$ |
| $cu_1 \rightarrow Rx_1$ | $Tx_0 \rightarrow Rx_1$ | $Tx_1 \rightarrow Rx_0$ |

a single uplink RB. In our channel model, we are primarily concerned with pathloss, since we wish to evaluate the performance of both waveforms as we vary several distance related parameters such as cluster size, or distance from the BS. As explained in Chapter 2, we use the WINNER II channel models [24] to provide us with a distance based pathloss, which also incorporates the probability of line-of-sight. Specifically, we use scenario B1 - *urban micro-cell*.

### 6.2.2 Interference Model and Problem Formulation

#### Interference Model

The main measure that we base our analysis upon is the SINR experienced by incumbent CUs and D2D pairs. To rate the latter with accuracy, it is necessary to use models of interference that properly estimate the leakage that two asynchronous users inject onto each other. As mentioned in chapters 2 and 3 of this thesis, to the best of our knowledge, most studies on D2D underlay operation do not consider leakage between adjacent frequency resource blocks. On the other hand, papers that do consider leakage, as in [58], rely on the Power Spectral Density (PSD)-based model, the shortcomings of which we have demonstrated in Chapter 4.

Note that we have extensively analyzed and precisely modeled the leakage between asynchronous users operating on different parts of the spectrum band, and derived interference tables that we will build our analysis upon. Our previous developments in Chapter 4 allow us to rate the value of $I\{\text{A} \rightarrow \text{B}\}(l)$, which corresponds to the interference injected by a subcarrier of waveform A to a subcarrier of waveform B at spectral distance $l$.

In this analysis, we use the interference table shown in Fig. 6.2. This figure shows that the use of OFDM/OQAM for D2D operation will only marginally reduce the interference between cellular and D2D users, as $I\{\text{OFDM/OQAM} \rightarrow \text{CP-OFDM}\}$ is only slightly less than $I\{\text{CP-OFDM} \rightarrow \text{CP-OFDM}\}$. This has been thoroughly explained in chapter 4. However, the interference between asynchronous D2D users will be drastically reduced if they use

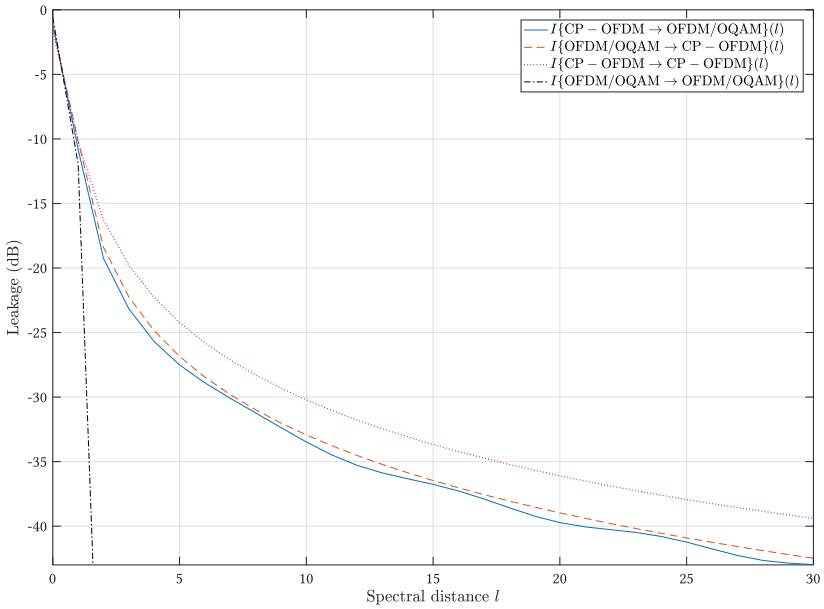


Figure 6.2: Interference tables measuring the value of interference injected between different couples of waveforms according to Chapter 4 and [113].

OFDM/OQAM instead of OFDM, since $I\{\text{OFDM/OQAM} \rightarrow \text{OFDM/OQAM}\}$ is considerably lower than $I\{\text{CP-OFDM} \rightarrow \text{CP-OFDM}\}$ .

### Optimization Problem Formation

We wish to improve the performance of the cellular network using underlay D2D communication. A D2D pair is allowed to transmit when the interference introduced on the incumbent network does not prevent the incumbent CUs from satisfying their minimum SINR constraints. The D2D transmissions affect the SINR experienced at the BS and hence the CUs suffer from adjacent channel interference. The SINR of the CU indexed by $i$ can therefore be expressed as

$$\gamma_i = \frac{P_i h_{iB}}{\sigma_w^2 + \sum_{j \in \mathcal{D}} \sum_{r \in \mathcal{R}} \sum_{m \in b_r} \omega_{jr} h_{jB} \Omega_{mi}^{\mathrm{D}}}, \tag{6.1}$$

where $P_i$ is the transmit power of the $i^{\text{th}}$ CU, $h_{iB}$ is the channel gain between the $i^{\text{th}}$ CU and the BS, $\sigma_w^2$ is the AWGN variance, $r$ indexes the resource blocks (RB) across the entire band, $m$ indexes the subcarriers in a particular RB band $b_r$, $\omega_{jr}$ is a resource reuse indicator where $\omega_{jr} = 1$ when D2D pair $j$ reuses RB $r$, and $\omega_{jr} = 0$ otherwise. Finally, $\Omega_{mi}^{\mathrm{D}}$ is the interference introduced by the $m^{\text{th}}$ subcarrier onto the RB used by the $i^{\text{th}}$ CU. $\Omega_{mi}^{D}$ is given by

$$\Omega_{mi}^{\mathrm{D}} = \sum_{k \in b_i} \frac{P_m}{P_0} I(k - m), \tag{6.2}$$

where $k$ indexes the subcarriers in the incumbent band $b_i$ used by user $i$, and $I(k-m)$ is the appropriate interference table $I\{\mathrm{A} \rightarrow \mathrm{B}\}$ in Fig. 6.2, depending on the waveform being used by the D2D pairs.

A D2D receiver will experience two types of interference: i) interference from CUs, and ii) interference from other D2D pairs. The SINR experienced on subcarrier $m$ at the D2D receiver of pair $j$ is given by

$$\gamma_{jm} = \frac{P_{jm} h_j}{\sigma_w^2 + I_{\mathrm{cu}} + I_{\mathrm{D2D}}}, \tag{6.3}$$

where $P_{jm}$ is the power of the $j^{\mathrm{th}}$ D2D pair on subcarrier $m$. $I_{\mathrm{cu}}$ is the interference injected on the $m^{\mathrm{th}}$ subcarrier from cellular users using CP-OFDM in the incumbent band, and $I_{\mathrm{D2D}}$ is the interference from other D2D users. $I_{\mathrm{cu}}$ is defined as

$$I_{\mathrm{cu}} = h_{ij} \sum_{i \in C} \Omega_{im}^{\mathrm{C}}, \tag{6.4}$$

where $\Omega_{im}^{\mathrm{C}}$ is the interference introduced by the $i^{\mathrm{th}}$ CU onto the $m^{\mathrm{th}}$ subcarrier of D2D pair $j$, and is specified in a similar fashion to equation (6.2). Finally, $I_{\mathrm{D2D}}$ is the interference from other D2D links given by

$$I_{\mathrm{D2D}} = \sum_{d \in \mathcal{D}, d \neq j} \sum_{r \in \mathrm{R}} \sum_{n \in b_r} \omega_{dr} h_{jd} \Omega_{nm}^{\mathrm{D}}\,, \tag{6.5}$$

where $\Omega_{nm}^{\mathrm{D}}$ is the interference injected by the $n^{\mathrm{th}}$ subcarrier of the $d^{\mathrm{th}}$ D2D user onto the $m^{\mathrm{th}}$ subcarrier of $j^{\mathrm{th}}$ D2D user.

Using the above SINR expressions, we can formulate the optimization problem $P1$, in which the objective is to maximize the sum rate of D2D pairs, subject to a minimum SINR constraint for each CU.

$$\mathrm{P1}: \max_{P_m, \omega_{jr}} \sum_{j \in \mathcal{D}} \sum_{r \in \mathcal{R}} \sum_{m \in b_r} \omega_{jr} \log(1 + \gamma_{jm}), \tag{6.6}$$

subject to

$$\omega_{jr} \in \{0,1\}, \forall j, r, \tag{6.6a}$$

$$\sum_{j \in \mathcal{D}} \omega_{jr} \leq 1, \forall r \in \mathcal{R}, \tag{6.6b}$$

$$\sum_{r \in \mathcal{R}} \omega_{jr} = 1, \forall j \in \mathcal{D}, \tag{6.6c}$$

$$\gamma_i \geq \mathrm{SINR}^{\mathrm{C}}_{\mathrm{min}}, \forall i \in \mathcal{C}, \tag{6.6d}$$

$$P_j = \sum_{m \in b_j} P_m < P^{\mathrm{D}}_{\mathrm{max}}, \tag{6.6e}$$

where $\mathrm{SINR}^{\mathrm{C}}_{\mathrm{min}}$ is the minimum acceptable SINR that a CU must achieve.

Optimization problem P1 is a mixed integer non-linear programming (MINLP) problem from which it is difficult to obtain the solution directly. Accordingly, we split the optimization problem into two sub-problems. First, we perform RB assignment, which is a discrete optimization problem. Once RBs have been assigned, we perform power-loading for the D2D pairs.

Even after splitting P1 into two simpler problems, solving them remains complicated due to the inclusion of inter-D2D interference. The main source of this complexity lies in the fact that $I_{\mathrm{D2D}}$ (6.5) is a function of the power assigned to each subcarrier of each D2D transmitter, as shown in (6.3). Furthermore, incorporating inter-D2D interference into the RA scheme would assume that every D2D pair is able to obtain information regarding the interference contribution from every other D2D pair. This is an unrealistic assumption, requiring an exchange of information between D2D pairs before any resource is assigned. We are instead motivated to develop alternative methods to mitigate inter-D2D interference other than through resource allocation (RA), namely through the use of OFDM/OQAM.

Accordingly, in the following, we aim to demonstrate that if D2D pairs use OFDM/OQAM, then there is no significant performance loss incurred by performing RA and power loading without taking into account the inter-D2D interference. Hence, we do not consider the effects of inter-D2D interference when performing both RB assignment and power-loading. This greatly reduces the complexity of the RA schemes and ensures that the power-loading objective function is convex. It is also more realistic as it makes no assumptions regarding the information a D2D pair possesses about every other D2D pair in the cluster. Therefore, we consider a simplification of P1 (6.6) where the SINR $\gamma_{jm}$ (6.3) is reduced to

$$\gamma'_{jm} = \frac{P_m h_j}{\sigma^2_w + I_{\mathrm{cu}}}. \tag{6.7}$$

Given the above simplifications, the two intermediate problems to be solved can be rewritten as follows.

**RB Assignment:** We assume each cellular user is assigned a single RB and that there are as many CUs as RBs. Since we only consider pathloss in our channel model, RBs can be randomly assigned to CUs. We then want to assign one RB to each D2D pair such that the interference experienced by each D2D pair from the CUs is minimized. The interference experienced by D2D pair $j$ on RB $r$ is given by

$$I_{jr} = \sum_{i \in C} \sum_{m \in b_i} \sum_{k \in b_r} \frac{P_m}{P_0} h_{ji} I(k-m). \tag{6.8}$$

The RB assignment problem can be specified as follows

$$\text{P2} : \min_{\omega_{jr}} \sum_{j \in \mathcal{D}} \omega_{jr} \phi_{jr}, \tag{6.9}$$

subject to

$$\omega_{jr} \in \{0,1\}, \forall j, r, \tag{6.9a}$$

$$\sum_{j \in \mathcal{D}} \omega_{jr} \leq 1, \forall r \in \mathcal{R}, \tag{6.9b}$$

$$\sum_{r \in \mathcal{R}} \omega_{jr} = 1, \forall j \in \mathcal{D}, \tag{6.9c}$$

where $\phi_{jr}$ is the interference from CUs experienced by D2D pair $j$ on RB $r$. Problem P2 is a combinatorial optimization problem, made complicated by the fact that multiple D2D users may have the same optimal RB assignment. In line with the literature [51, 148, 149], we utilize the well-known Kuhn-Munkres algorithm (commonly known as the Hungarian method), to solve the uplink resource assignment problem for D2D pairs.

**Power-loading:** Having assigned a RB to each D2D pair, power-loading can now be performed. The power-loading optimization problem is similar to P1, with the discrete constraints (6.6a-6.6c), which relate to RB assignment, removed. Since RB assignment has already been performed, the objective function of optimization P1, i.e., equation (6.6), can be simplified as follows

$$\max_{P_m} \sum_{j \in \mathcal{D}} \sum_{m \in b_j} \log(1 + \gamma'_{jm}). \tag{6.10}$$

The resulting problem is clearly convex and similar to others in the literature, for example [109]. The solution can be readily obtained using an appropriate software package.

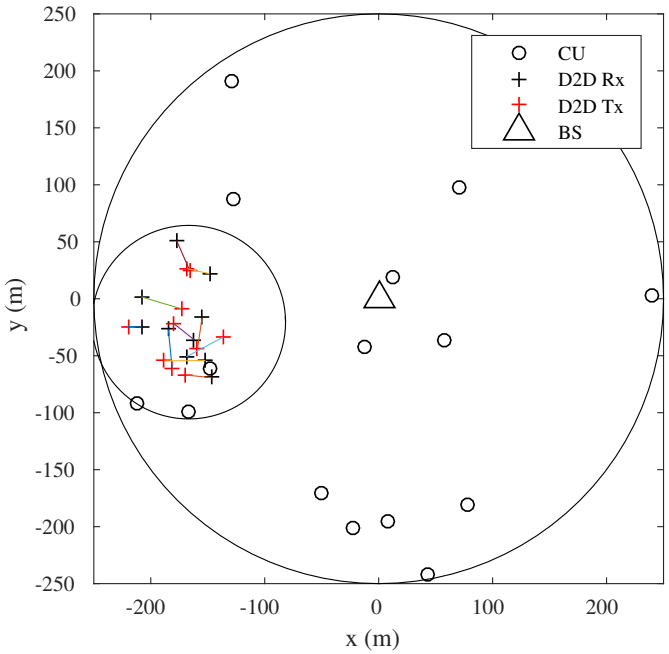


Figure 6.3: Example of clustered scenario consisting of 10 D2D pairs.

### 6.2.3 Obtained Results

In the following, we perform simulations to investigate the co-existence of OFDM/OQAM and CP-OFDM, presenting a broad set of results. Cellular users are uniformly distributed over the coverage area of the encompassing OFDMA cell. In the clustered scenario, the cluster centre is chosen according to a uniform distribution within the cell area and D2D pairs are uniformly distributed within the cluster area. Fig. 6.3 illustrates an example of a clustered scenario with 10 D2D pairs.

Table 6.2 describes the key simulation parameters. After distributing both the CUs and D2D pairs within the cell, we then perform RB assignment and power-loading as described previously. The average rate per D2D pair is used as the main output metric from simulations. This metric is calculated for two different cases using the SINR expressions described in the previous section:

1. Case 1: D2D pairs use CP-OFDM, CUs use CP-OFDM.
2. Case 2: D2D pairs use OFDM/OQAM, CUs use CP-OFDM.

In both cases, we compare the predicted average rate per D2D pair calculated using $\gamma'_{jm}$ (which does not take into account inter-D2D interference), with the actual average rate per D2D pair calculated using $\gamma_{jm}$ (which takes into account inter-D2D interference).

Table 6.2: Simulation parameters

| Parameter | Value |
|---|---|
| inter-site distance (ISD) | 500 m |
| macro-cell radius | 250 m |
| carrier frequency | 700 MHz |
| subcarrier spacing | 15 kHz |
| number of RBs | 15, 25 |
| number of CUs | 15, 25 |
| scenario type | clustered or non-clustered |
| maximum cluster radius | ISD/5 m |
| minimum cluster radius | ISD/10 m |
| maximum D2D Tx. Rx. distance | (cluster radius) × 2/3 |
| pathloss model | WINNER II scenario B1 |
| CU minimum SINR | 10 dB |
| noise power per subcarrier [1] ($\sigma_\nu^2$) | -127 dBm |
| maximum transmit power | 24 dBm |
| number of iterations | 40000 |

**Effects of inter-D2D interference for both OFDM/OQAM and CP-OFDM:** In the first set of results, we generate the empirical cumulative distribution function (CDF) for the average rate per D2D pair for both the clustered (Fig. 6.4a) and non-clustered (Fig. 6.4b) scenarios in order to demonstrate the effects of inter-D2D interference for both OFDM/OQAM and OFDM.

In the clustered scenario in Fig. 6.4a, we observe that when inter-D2D interference is not taken into account when calculating the rate (which is not representative of reality), there appears to be very little advantage to using OFDM/OQAM over CP-OFDM. OFDM/OQAM does demonstrate some negligible improvement over CP-OFDM due to the fact that it receives less interference from CUs, since the projected interference from CP-OFDM to OFDM/OQAM is slightly less than that from CP-OFDM to CP-OFDM, as shown in Fig. 6.2. However, the actual average rate per D2D pair, accounting for inter-D2D interference, shows that OFDM/OQAM provides significant improvement over CP-OFDM. In fact, the average rate per D2D pair when using OFDM/OQAM is very similar to the case when inter-D2D interference is not considered.

[1] Noise power per subcarrier is calculated using the expression $-174\text{dBm/Hz}+10\log_{10}(15\text{kHz})$, where $-174$dBm/Hz is the background noise and 15kHz is the LTE subcarrier spacing.

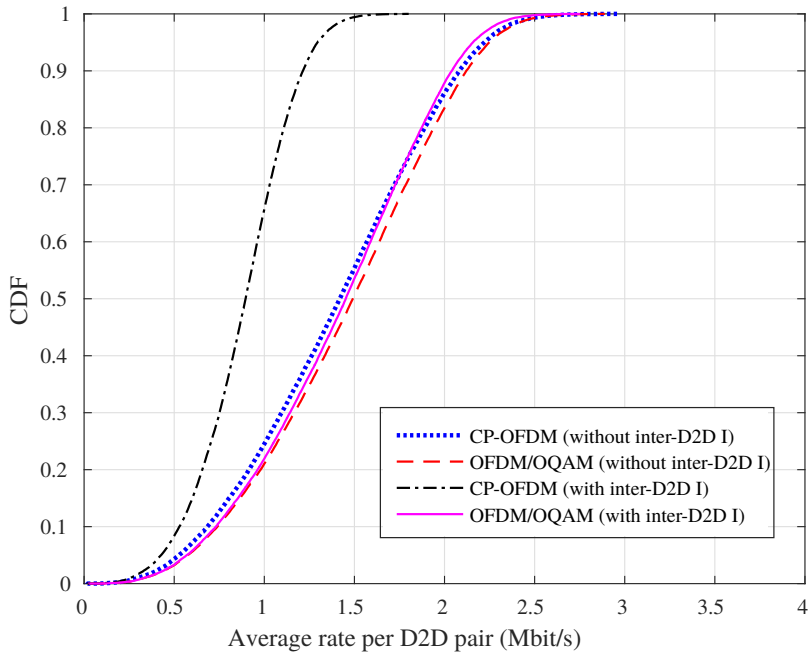


(a)

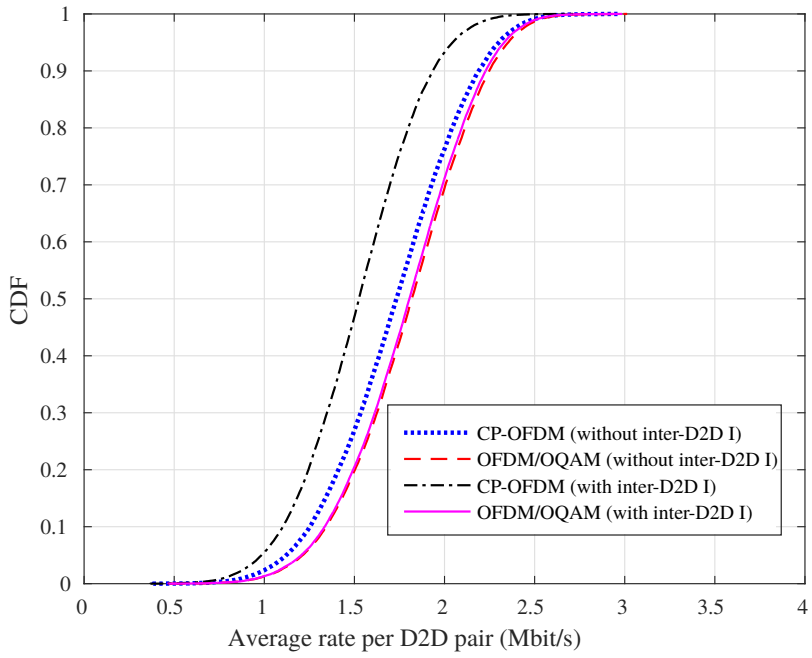


(b)

Figure 6.4: (a) Clustered and (b) non-clustered scenario consisting of 10 D2D pairs.

In the non-clustered scenario in Fig. 6.4b, we observe that the advantage of using OFDM/OQAM, even when inter-D2D interference is taken into account, is less than the corresponding clustered scenario. This is intuitive, as D2D pairs are farther apart in the

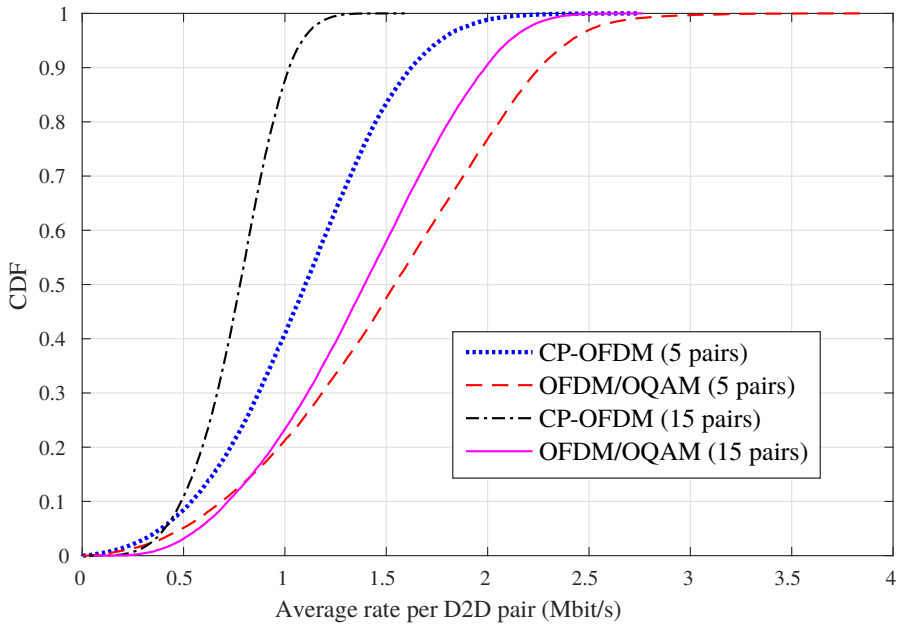


Figure 6.5: Average rate per D2D pair for different numbers of D2D pairs.

non-clustered scenario and, hence, inter-D2D interference does not play such a significant role.

Hence, we make two observations. First of all, inter-D2D interference plays a significant role in clustered D2D underlay communication. Second, we observe that when OFDM/OQAM is used, the actual values of achieved average rate per D2D pair are very close to those calculated without taking inter-D2D interference into account. Thus, OFDM/OQAM successfully mitigates inter-D2D interference. Conversely, when CP-OFDM is used, the gap between the actual and predicted values of rate (calculated using $\gamma_{jm}$ and $\gamma'_{jm}$ respectively) is significantly larger. Therefore, Fig. 6.4a and Fig. 6.4b show that permitting D2D users to use OFDM/OQAM can significantly facilitate the resource allocation process in the considered scenarios.

Fig. 6.5 reinforces our observations. We display the actual average rate per D2D pair, calculated using $\gamma_{jm}$ when inter-D2D interference is considered, in a clustered scenario for 5 D2D pairs and 15 D2D pairs. We first observe that the average rate for both CP-OFDM and OFDM/OQAM decreases as the number of D2D pairs increases, since each D2D transmitter must now use a lower transmit power in order to satisfy the interference constraint specified by (6.6d). We also observe that the benefit attributed to using OFDM/OQAM increases as the number of D2D pairs increases, i.e. the gap between the OFDM/OQAM and CP-OFDM curves grows larger as the number of D2D pairs increases. This is due to inter-D2D interference becoming more significant as the number of D2D pairs is increased, despite the fact that pairs must now use less power.

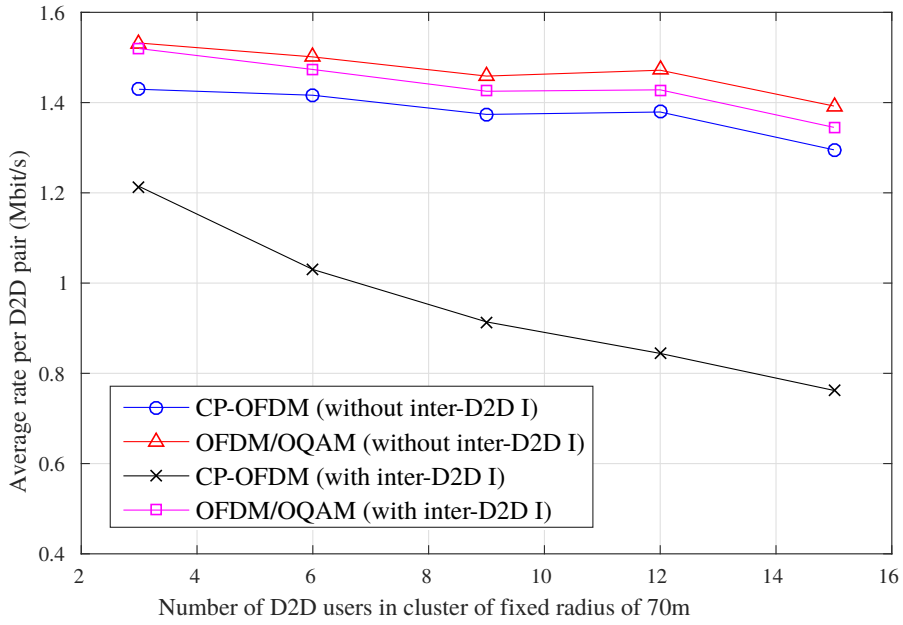


Figure 6.6: Average rate per D2D pair versus number of D2D users in a cluster of fixed radius of 70m.

**OFDM/OQAM and CP-OFDM performance in varying scenario set-ups:** In this subsection, we examine the performance of OFDM/OQAM and CP-OFDM as we vary several parameters of the simulation. We are interested in determining the scenarios that are best suited to the adoption of OFDM/OQAM, i.e. in which OFDM/OQAM offers a significant advantage. We first examine the effect that cluster density has on the relative performance of both waveforms. Cluster density can be varied in two manners: i) the cluster radius can be held constant and the number of D2D pairs in the cluster can be altered, or ii) the number of users can be fixed and the cluster radius can be altered. We point out that a small cluster with few users and a large cluster with many users may have similar densities but represent two different types of scenario. Hence, we investigate the effects of density for both of the aforementioned cases. We also investigate the effect that the distance from the cluster centre to the BS has on performance.

Fig. 6.6 shows the effect of varying the density of a cluster by fixing the cluster radius at 70 m and varying the number of D2D pairs in the cluster. OFDM/OQAM only seems to offer a small improvement in comparison with CP-OFDM when the rate is calculated without consideration for inter-D2D interference. However, it is the improvement that OFDM/OQAM offers over the actual D2D rate, which takes into account inter-D2D interference, that interests us. As the cluster density is increased by adding additional D2D pairs, the throughput gain that OFDM/OQAM offers over OFDM also increases. OFDM/OQAM is, therefore, most

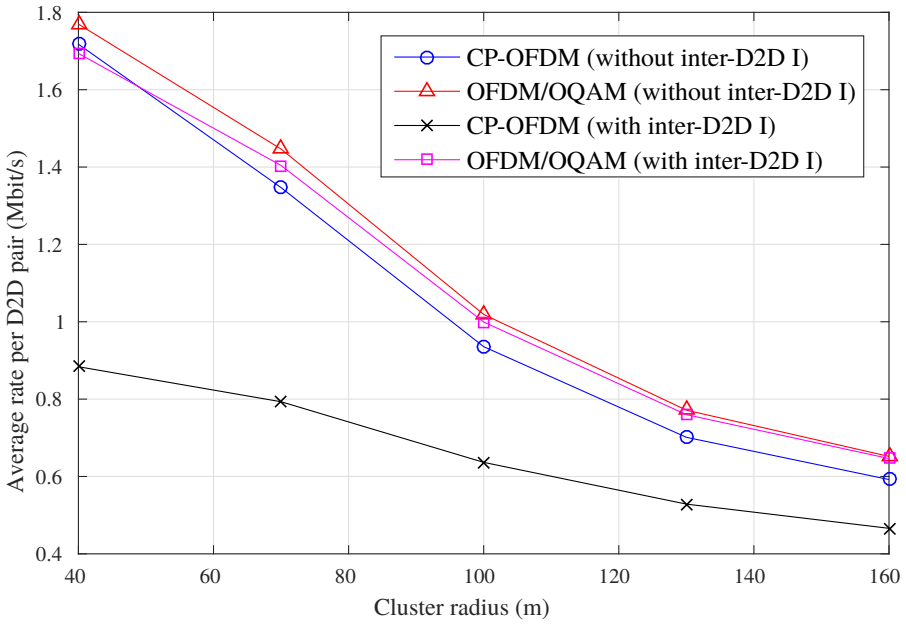


Figure 6.7: Average rate per D2D pair versus cluster radius for a fixed number of D2D pairs.

effective in dense clusters, consisting of many users, in which inter-D2D interference has a significant impact on the SINR of D2D devices.

Fig. 6.7 demonstrates the effect of cluster size on the average rate per D2D pair. In effect, we are varying the cluster density by fixing the number of D2D pairs, while changing the cluster radius. In order to achieve greater densities, we use a scenario consisting of 25 RBs, 25 CUs, and 20 D2D pairs. As the cluster radius is decreased, we observe that the D2D pairs are able to achieve higher rates as the pathloss between a D2D transmitter and receiver also decreases. We also note that the inter-D2D interference becomes more significant, as is shown by the increasing gap between the curve representing the rate achieved using CP-OFDM when inter-D2D is taken into account, and the rate achieved using OFDM/OQAM. At a cluster radius of 40 meters, the benefit obtained from using OFDM/OQAM is significant. Based on the results presented in Figs. 6.6 and 6.7, we conclude that OFDM/OQAM is best suited to scenarios consisting of small, dense D2D clusters.

Fig. 6.8 demonstrates the effect of varying the distance from the cluster centre to the BS. We make three observations with respect to Fig. 6.8. First, we note that the average D2D rate increases as the cluster distance from the BS increases. Indeed, since the interference imposed by D2D pairs onto CUs is observed at the BS, D2D transmitters belonging to clusters that are at a greater distance from the BS are permitted to use higher transmit powers. Second, we note that the benefit of using OFDM/OQAM is greater when the cluster is near the cell edge. This can be attributed to the fact that inter-D2D interference increases, and hence becomes more significant, when D2D pairs are permitted to transmit using higher power

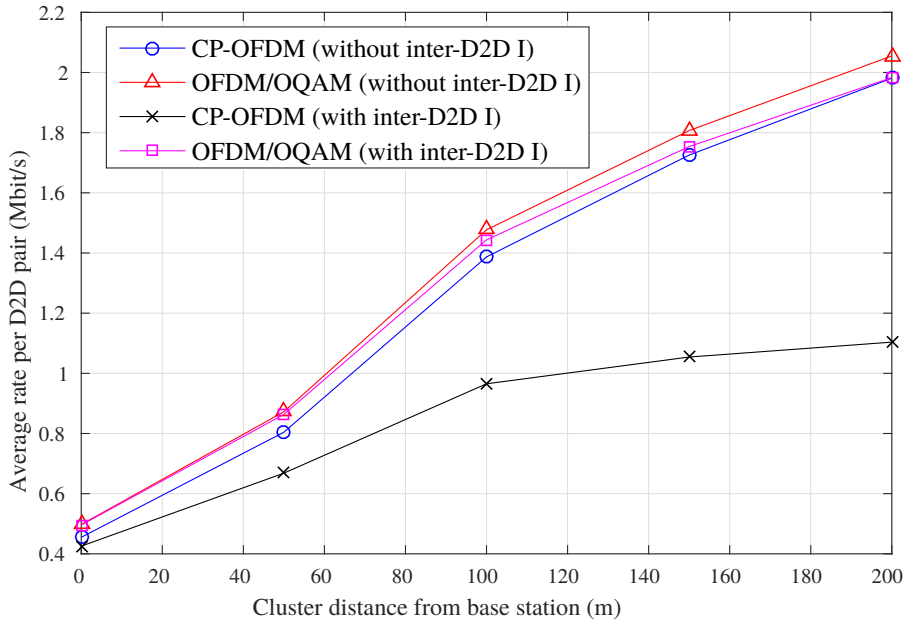


Figure 6.8: Average rate per D2D pair versus distance from cluster centre to BS.

values. Finally, we note that the average rate per D2D user increases less rapidly as the distance from the BS increases, particularly after a distance of 100 m. This is as a result of increased interference from cell-edge CUs, which compensate their pathloss to the BS by using higher transmit powers. It should be pointed out that these results were obtained for a single cell scenario. In a multi-cell scenario, we would expect clusters located near the macro-cell edge to experience increased interference from neighbouring cells.

### 6.2.4 Summary of the study

Overall, the results obtained in this preliminary study tend to show that using an enhanced multicarrier waveform for D2D communication can bring some interesting advantages in some particular setups. Without surprise, we show that the waveform used by the D2D system does not affect the interference they cause directly onto the CP-OFDM based cellular users; this is in line with all results presented so far in this thesis. However, we have shown that - as expected - the waveform used by D2D can significantly affect the inter-D2D interference. Thus, in setups where this type of interference might be preponderant compared to D2D to cellular interference, changing the waveform used by D2D devices makes perfect sense. In particular, we have shown that using a waveform with high spectral localization (OFDM/OQAM here) can significantly facilitate the network management in setups where D2D pairs are distributed in dense clusters. Therefore, in the following, we focus on this particular type of setups, and evaluate the gains that can be achieved if D2D devices use one of the enhanced waveforms we study in this thesis.

## 6.3 Network level study

### 6.3.1 System Model

In this section, we expand upon the previous study and consider clustered deployments of D2D systems underlaying a legacy LTE-A network. Our study, which is application-agnostic can find applications in a number of scenarios: intelligent process control, autonomous manufacturing systems, smart factories, and self-organising warehouses are but a few examples of 5G use cases which require high-rate inter-machine communication in a spatially clustered environment.

#### Network Set-up

As in our preliminary study, we stay consistent with the literature and consider uplink resource sharing for two reasons. Firstly, and most importantly, D2D user equipments (DUEs) should not interfere with crucial pilot information broadcast in the downlink. Secondly, for uplink resource sharing, DUE to CU equipment (CUE) interference occurs centrally at the base station. Therefore, the BS possesses full knowledge of this type of interference and can attempt to coordinate and mitigate it through resource allocation schemes [150].

We consider an OFDMA network with parameters selected based on the 3GPP LTE standard, as outlined in Table 6.4 in Subsection 6.3.2. Cells are modeled as hexagons, with the network consisting of a central cell of interest and two rings of neighboring cells (totaling nineteen cells). We assume that each cell is fully loaded, with each CUE assigned a single uplink RB. DUEs underlay the OFDMA cell by reusing a single uplink resource block (RB). In reality, LTE networks actually use SC-FDMA in the uplink. However, as explianed in Chapter 2, SC-FDMA is simply OFDMA in which users apply DFT precoding to their transmit signal. In the scope of our study, this precoding is inconsequential and we therefore do not consider it.

CUEs are distributed throughout the entire network according to a Poisson point process (PPP). DUEs are employed in high-rate spatially clustered applications such as process control, robotics control, or machine-to-machine communications. In order to capture this clustering effect in our model, we distribute DUE transmitters in the network using a Matérn point process which generates clusters according to a two-step process. In the first step, a PPP is used to generate a set of parent points. In the second step, a Poisson distributed number of child points is uniformly distributed around each parent point within a disk of a given radius. The rate of occurrence of clusters (i.e. parent points), DUE transmitters per clusters (i.e. child points per parent point), and the cluster radii can be configured in the simulation parameters. For each DUE transmitter, we distribute a receiver at a distance $d$

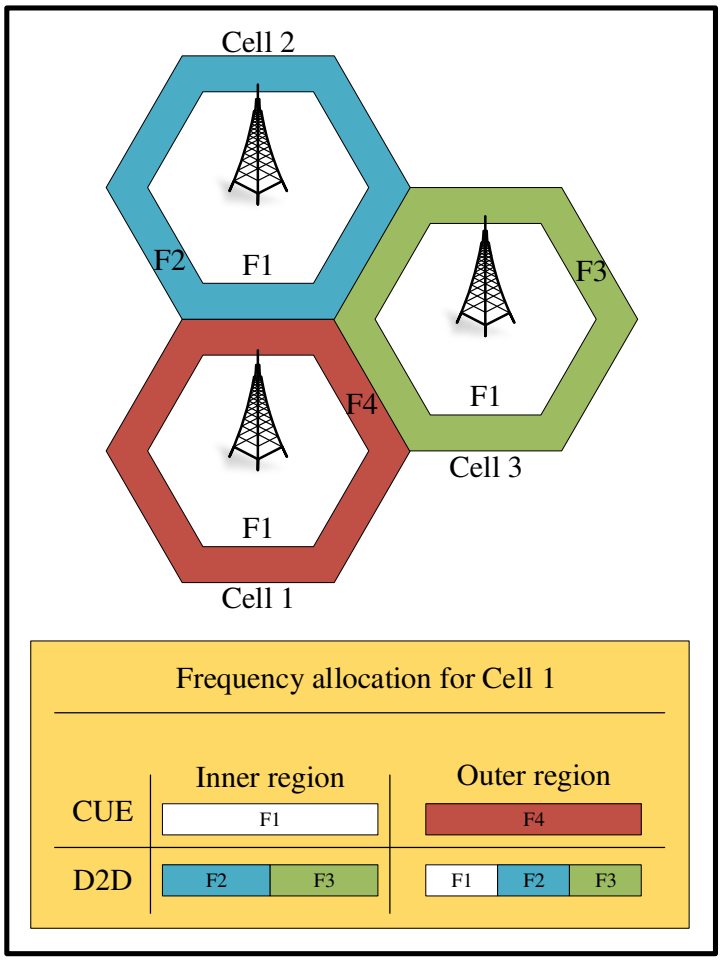


Figure 6.9: The inner region of each cell uses the same set of sub-bands, while reuse three is employed in the outer regions. CUEs and DUEs are allocated sub-bands in a manner that aims to reduce interference between them.

according to a uniform random variable $U_{[a,b]}$, with $a$ and $b$ representing the minimum and maximum distance, respectively.

When multiple cells are considered, harmful inter-cell interference occurs. However, its effects can be lowered through the use of adapted frequency reuse schemes, in which devices in different cells are assigned different frequency bands. In particular, fractional frequency reuse (FFR) [151] has drawn a lot of attention in the recent years. Therefore, in this study, we consider the use of strict FFR. Fig. 6.9 illustrates the division of sub-bands between cells. The CUEs in the inner region of each cell are provisioned using a common set of sub-bands. Frequency reuse three is employed for the outer regions of the cells, with cell-edge CUEs in these regions provisioned from one of three sets of sub-bands. DUEs are permitted to reuse the spectral resources of cellular users according to the scheme outlined in [152] for D2D communication underlaying a network employing strict FFR. Hence, DUEs in the inner

region of a cell may reuse the spectral resources assigned to CUEs in the outer regions of neighbouring cells. DUEs in the outer region of a cell may use any spectral resource, except the set assigned to CUEs in the same region.

The ratio of the radius of the inner region ($R_{\text{inner}}$) to the radius of the cell ($R_{\text{cell}}$) is an important parameter in strict FFR systems and influences how sub-bands are divided between regions. We follow the approach used in [153], and choose the ratio $R_{\text{inner}}/R_{\text{cell}}$ to be 0.65, which was shown in [154] to maximise the average network throughput for uniformly distributed CUEs. Given $N_{\text{band}}$ available sub-bands in the system, we can determine the number of resources allocated to each region as follows [154]

$$N_{\text{inner}} = \left[ N_{\text{band}} \left( \frac{R_{\text{inner}}}{R_{\text{cell}}} \right)^2 \right], \tag{6.11}$$

$$N_{\text{outer}} = [(N_{\text{band}} - N_{\text{inner}})/3]. \tag{6.12}$$

**Resource Allocation**

RBs are assigned under the condition that an RB may only be assigned to a single CUE, and reused by a single DUE, in a given cell. CUEs transmit on the physical uplink shared channel (PUSCH) and use a power control procedure that assigns each CUE a power level that results in acceptable signal reception at the base station. The power control procedure [155] for a CUE transmitting during subframe $i$ is described by the formula

$$P(i) = P_{\text{O\_PUSCH}} + 10\log_{10}(M_{\text{PUSCH}}(i)) + \Delta_{\text{TF}}(i) + \alpha L + f(i),$$

where $P_{\text{O\_PUSCH}}$ is the power that the base station expects to receive over a single resource block, $M_{\text{PUSCH}}(i)$ is the number of resource blocks on which the device is transmitting, $\Delta_{\text{TF}}(i)$ is an optional adjustment for higher modulation orders and coding rates, $L$ is the estimation of downlink path loss, $\alpha$ is a weighting factor to reduce the impact of changes in path loss, and $f(i)$ relates to power control commands from the base station. As previously stated, we assume that each CUE uses only a single RB, implying that $10\log_{10}(M_{\text{PUSCH}}(i)) = 0$. The maximum power at which a CUE may transmit is also capped at $P_{\text{cmax}}$. Therefore, the transmit power of a CUE operating during subframe $i$ is given by

$$P_{\text{CUE}}(i) = \min(P(i), P_{\text{cmax}}). \tag{6.13}$$

Our focus in this study is on evaluating the relative performance of the waveforms under consideration for direct communication between devices in spatially clustered use cases, not on proposing a new resource allocation scheme. Hence, in order to avoid bias towards any

particular scheme, we consider a simple power allocation scheme for DUEs where DUEs are permitted to transmit at maximum power, which is capped by the controlling base station.

### Channel Modelling

CUEs in the same cell do not interfere with each other, as we assume they are perfectly synchronized by the BS. Therefore, there are four main interference types requiring consideration:

1. DUE pairs interfere with the CUEs' transmissions. Since we are investigating uplink resource sharing, this interference is observed at base stations.
2. Conversely, the CUEs interfere with the DUE pairs at DUE receivers.
3. DUEs interfere with each other (inter-DUE interference).
4. CUEs in different cells are not synchronized and, hence, interfere with each other (inter-CUE interference).

As in our preliminary study, we employ the WINNER II channel models [24] to provide us with a distance based path loss, which also incorporates the probability of line-of-sight. Distinct path loss models are used for the different types of links in the system in order to represent the network in a realistic manner. Path loss models employed for D2D channels have been modified so that both transceivers in a D2D link are the same height above the ground. The distribution of shadow fading is log-normal, with the standard deviation specified by the Winner II channel models for each scenario.

### Performance Measures

Below, we present several metrics and details of their formulation that we will use to evaluate the performance of the system. All metrics are evaluated for DUEs and CUEs in the central cell, which represents the cell of interest.

**SINR:** The SINR of a CUE $j$ in the central cell $o$ using RB $k$ is given by:

$$\gamma_{j_o}^k = \frac{P_{j_o}^k h_{j_o B}^k}{\sigma_w^2 + I_{\mathrm{C_N}} + I_{\mathrm{D_N}} + I_{\mathrm{D_S}}}, \tag{6.14}$$

where $P_{j_o}^k$ is the transmit power of the CUE (given by Eq. (6.13)), $h_{j_o B}$ is the channel gain between the $j^{\mathrm{th}}$ CUE and the BS of the central cell $o$, and $\sigma_w^2$ is the AWGN variance. $I_{\mathrm{C_N}}$ is

the interference from CUEs in neighbouring cells and is given by

$$I_{\mathrm{C_N}} = \sum_{n \in \mathcal{N}} \sum_{c_n \in \mathcal{C}_n} \sum_{r \in \mathcal{R}} P^r_{c_n} h^r_{c_n B} \Omega_{\mathrm{wf}_{c_n} \to \mathrm{wf}_{j_o}}(|r-k|, \delta_\mathrm{t}, \delta_\mathrm{f}), \tag{6.15}$$

where $n$ indexes the set of neighbouring cells $\mathcal{N}$, $c_n$ indexes the CUEs in the set $\mathcal{C}_n$ of CUEs in the $n^{\mathrm{th}}$ neighbouring cell, and $r$ indexes the set of resource blocks $\mathcal{R}$ available to the system. $P^r_{c_n}$ is the transmit power of the $c_n^{\mathrm{th}}$ CUE operating on RB $r$ (given by Eq. (6.13)), $h^r_{c_n B}$ is the channel gain between the $c_n^{\mathrm{th}}$ CUE and the BS of the central cell. If the $c_n^{\mathrm{th}}$ CUE is not operating on RB $r$, then $P^r_{c_n}$ is 0. Finally, $\Omega_{\mathrm{wf}_{c_n} \to \mathrm{wf}_{j_o}}(|r-k|, \delta_\mathrm{t}, \delta_\mathrm{f})$ is the fraction of power injected by CUE $c_n$ using waveform $\mathrm{wf}_{c_n}$ and resource block $r$ onto CUE $j_o$ using waveform $\mathrm{wf}_{j_o}$ and resource block $k$, at a timing offset of $\delta_\mathrm{t}$ and CFO $\delta_\mathrm{f}$. For synchronous communication, both $\delta_\mathrm{t}$ and $\delta_\mathrm{f}$ can be set to 0.
$I_{\mathrm{D_N}}$ is the interference from DUEs in the neighbouring cells and is given by

$$I_{\mathrm{D_N}} = \sum_{n \in \mathcal{N}} \sum_{d \in \mathcal{D}_n} \sum_{r \in \mathcal{R}} P_\mathrm{D} h^r_{d_n B} \Omega_{\mathrm{wf}_{d_n} \to \mathrm{wf}_{j_o}}(|r-k|, \delta_\mathrm{t}, \delta_\mathrm{f}), \tag{6.16}$$

which is defined in a similar fashion to Eq. (6.15), where $\mathcal{D}_n$ represents the set of DUEs in the $n^{\mathrm{th}}$ neighbouring cell, and $P_\mathrm{D}$ is the transmit power of DUE devices. Finally, $I_{\mathrm{D_S}}$ represents the interference from DUEs in the same cell, i.e. the central cell, and is formulated in a similar fashion to Eq. (6.16).

The SINR of a DUE $d$ in the central cell $o$ operating on RB $r$ is given by:

$$\gamma^r_{d_o} = \frac{P_\mathrm{D} h^r_{d_o}}{\sigma^2_w + I_{\mathrm{C_N}} + I_{\mathrm{C_S}} + I_{\mathrm{D_S}} + I_{\mathrm{D_N}}}, \tag{6.17}$$

where $P_\mathrm{D}$ is the transmit power of the DUE devices, $h^r_{d_o}$ is the channel gain between the transmitter and receiver of the $d^{\mathrm{th}}$ DUE using RB $r$, and $\sigma^2_w$ is the AWGN variance. $I_{\mathrm{C_S}}$ and $I_{\mathrm{C_N}}$ represent the aggregate interference from CUEs in the same cell and neighbouring cells, respectively. $I_{\mathrm{D_S}}$ and $I_{\mathrm{D_N}}$ represent the aggregate interference from DUEs in the same cell and neighbouring cells respectively. The expressions for each of the above aggregate interference terms are similar to Eqs. (6.15) and (6.16), with the channel gain $h$ considered between the interfering device and the DUE receiver.

**Achieved Rate:** We are also interested in the rate achieved by devices, after the bandwidth efficiency of each waveform has been taken into account. The rate of a device using a waveform wf can be calculated as

$$b = \rho_{\mathrm{wf}} B \log_2(1+\gamma)[b/s], \tag{6.18}$$

Table 6.3: Bandwidth Efficiency of Waveforms

| **Waveform** (wf) | **Bandwidth Efficiency** ($\rho_{\text{wf}}$) |
|---|---|
| CP-OFDM | 8/9 |
| FMT | 8/9 |
| GFDM | 5/(5 + 1/8) |
| OFDM/OQAM | 11/12 |
| FBMC-PAM | 11/12 |
| f-OFDM | $8/9 * 11/12$ |
| UFMC | 8/9 |

where $\boldsymbol{B}$ is the bandwidth of an LTE resource block, and $\rho_{\text{wf}}$ is the TSE of waveform wf that we have evaluated in section 2.4. Here, we use the asymptotic value of their TSE when the time to transmit is infinite, which therefore does not encompass the low efficiency of linear FB-MC for short time frames. Furthermore, we consider a setup in which OFDM/OQAM, FBMC-PAM and f-OFDM only use 11 subcarriers out of the 12 that are available in a RB in order to absorb interference between two asynchronous users that would be transmitting on directly adjacent RBs. The value of $\rho_{\text{wf}}$ achieved by each waveform is presented in Table 6.3. Note that we exclude COQAM of this study to keep our results readable; furthermore, we have seen earlier in this thesis that COQAM achieves approximately the same results as GFDM.

### Interference Model

To model interference between users using each of the waveforms we consider, we follow the EVM-based approach proposed in Chapter 4. However, whereas our previous analyses were based on interference tables with a spectral granularity of one subcarrier spacing, we base the present system-level analysis on interference tables that are defined at the RB level. This is necessary to be able to carry out system level studies, as resource allocation and other procedures of the upper layers operate with a minimum granularity of one RB. Besides, whereas most studies on asynchronous networks rely on average values of interference [61, 113], we compute the interference between given pairs of waveforms for specific values of timing offset $\delta$t. Moreover, we also take into account CFO. We therefore generate three-dimensional interference tables which give the interference value at a given RB distance for each possible value of the timing offset, $\delta$t, and CFO, $\delta$f. We consider that the timing offset and CFO

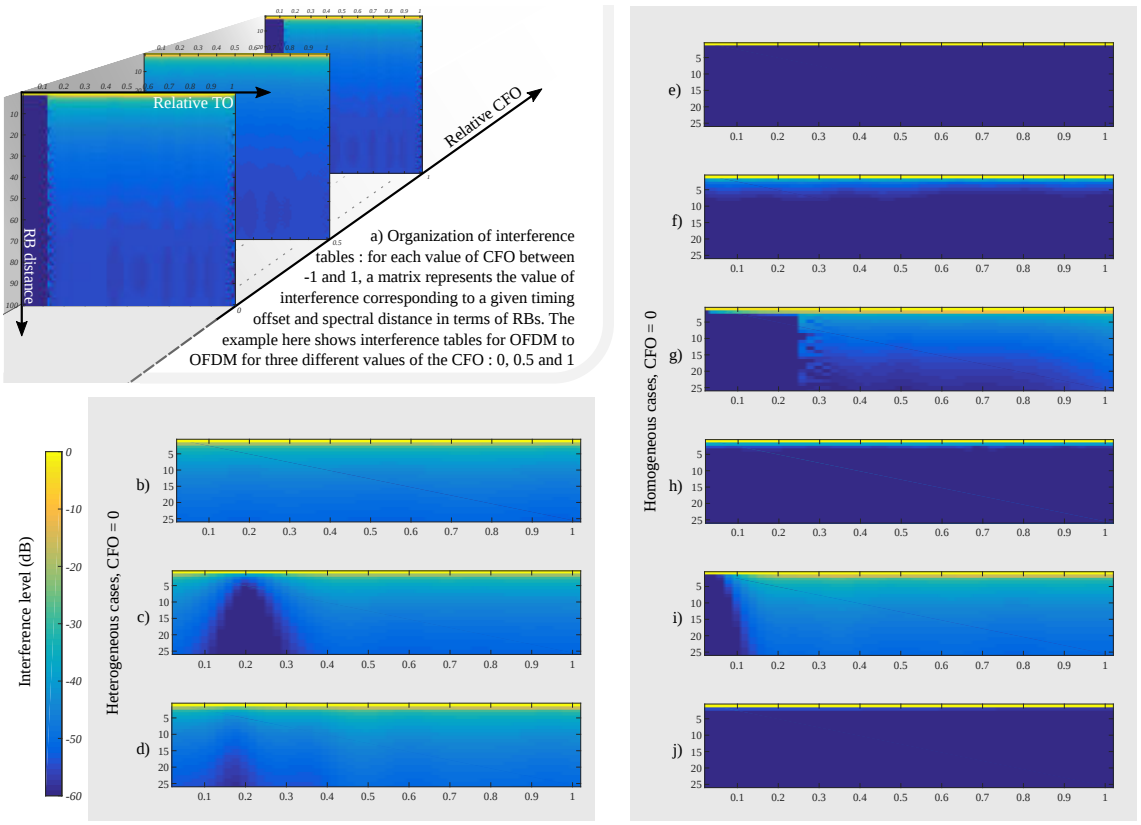


Figure 6.10: Representative examples of interference tables. Timing offset is expressed in proportion of $T + T_{\mathrm{CP}}$ of a reference CP-OFDM configuration and CFO is expressed relative to ΔF. Values lower than −60 dB appear in dark blue.
a) Organization of interference tables and CP-OFDM to CP-OFDM example.
b) OFDM/OQAM to CP-OFDM – c) f-OFDM to CP-OFDM – d) UFMC to CP-OFDM.
e) OFDM/OQAM to OFDM/OQAM f) FBMC-PAM to FBMC-PAM – g) GFDM to GFDM – h) FMT to FMT – i) UFMC to UFMC – j) f-OFDM to f-OFDM.

between users are uniformly distributed in a given interval so that $\delta \mathrm{t} \sim U_{[-\delta \mathrm{t}^{\max}, \delta \mathrm{t}^{\max}]}$ and $\delta \mathrm{f} \sim U_{[-\delta \mathrm{f}^{\max}, \delta \mathrm{f}^{\max}]}$.

In order to present our interference model, we display in Fig. 6.10 some of the interference tables that are available in our system-level simulator. In particular, we present in Fig. 6.10-a the structure of the interference tables as they are represented in our system level simulator. For each value of $\delta_{\mathrm{t}}$ and $\delta_{\mathrm{f}}$, our tables provide the corresponding level of interference, up to a maximum spectral distance of 100 RBs. Note that we consider heterogeneous scenarios in which DUEs use an alternative waveform and CUEs employ OFDM, and more advanced homogeneous scenarios in which both CUEs and DUEs use an alternative waveform. To model the interference between different users in these different set-ups, we therefore need to generate homogeneous interference tables, from a given waveform to the same waveform, and heterogeneous ones, from a given waveform to OFDM and from OFDM to a given waveform.

In Fig. 6.10, for each table *Waveform A* to *Waveform B*, an interfering user using *Waveform A* is active on an RB of index 0, and we show the interference power seen by a victim user using *Waveform B* at a given spectral distance specified in number of RBs, and for given values of the timing offset $\delta_t$. Note that, due to space limitations, we present interference tables only in the case where there is no CFO, i.e. $\delta_f = 0$, and only for spectral distances lower than 25 RBs.

Fig. 6.10-b shows the interference table from OFDM/OQAM to CP-OFDM. Consistent with the results presented in Chapter 4, we show that the interference to the CP-OFDM receiver decreases very slowly in frequency and does not exhibit any particular behaviour related to the timing offset. As presented earlier in this thesis, this twofold observation holds true for interference from any FB-MC waveform to a CP-OFDM receiver or from a CP-OFDM transmitter to any FB-MC receiver. However, for waveforms that are filtered per block of subcarriers, such as f-OFDM and UFMC, the interference experienced by a CP-OFDM receiver achieves a minimum point for specific values of the timing offset, as can be seen in Fig. 6.10-c and Fig. 6.10-d, respectively. This is due to the similarity of these waveforms to the CP-OFDM scheme. Note that this observation is consistent with the analysis of Ahmed *et al.* in [116].

More diverse and interesting behaviours can be observed in homogeneous cases; as is commonly known, coexisting CP-OFDM systems will not interfere with each other provided that they are synchronized within the CP duration, which is verified in Fig. 6.10-a for $\delta_f = 0$. This statement also applies almost directly to GFDM systems, which achieve quasi-orthogonality even if the timing offset is contained within the CP duration, as can be seen in Fig. 6.10-g. For both CP-OFDM and GFDM systems, interference between users dramatically increases if their relative asynchronism goes beyond the cyclic prefix. On the other hand, linear FB-MC waveforms (Fig. 6.10-e,f,h) achieve good coexistence capabilities, with the injected interference dropping rapidly along the frequency axis irrespective of the timing offset value. As we can see in Fig. 6.10-e, the best performance is achieved by the OFDM/OQAM waveform, as almost no interference leaks onto adjacent resource blocks.

f-OFDM (see Fig. 6.10-j) exhibits similar behaviour owing to its filtering at both the transmitter and the receiver. In contrast, UFMC (Fig. 6.10-h) only achieves good containment for timing offset values that are lower than the duration of the used filter. Outside of this interval, interference rapidly increases, which is consistent with what we observed in Fig. 2.14. This is because the particular implementation of UFMC considered here does not involve any windowing at the receiver. We highlight that the performance of certain waveforms, in particular GFDM and UFMC, could be improved by the use of additive windowing techniques at the transmitter and/or the receiver side. However, we intentionally do not implement these techniques in order to keep the focus on the intrinsic filtering properties offered by the

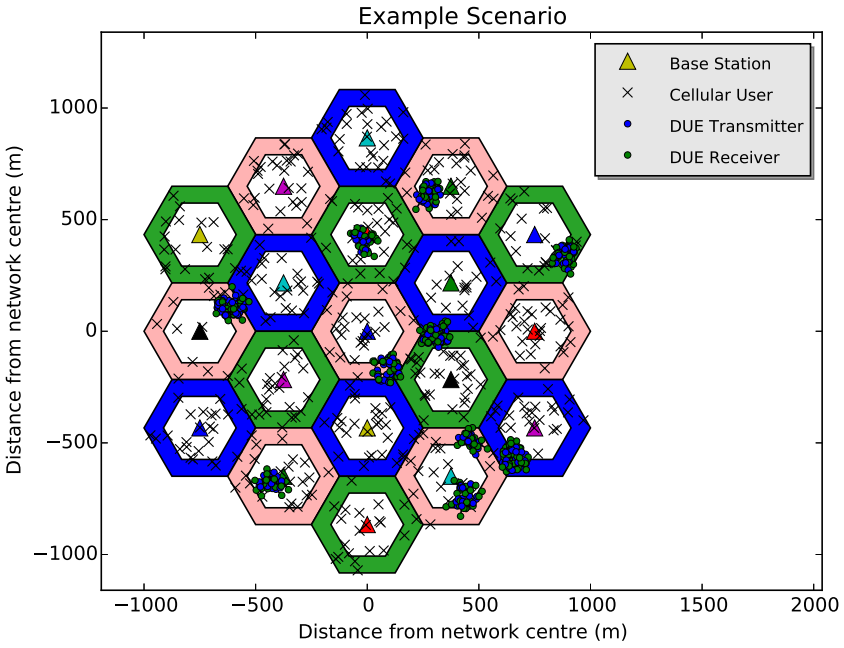


Figure 6.11: Example scenario consisting of 19 cells, with each region coloured according to the spectral resources permitted for use. Each cross represents an ordinary cellular user, whereas DUEs involved in direct communication are clustered in groups.

waveforms under study. This is important as every additional filtering operation increases the overall complexity of the system.

### 6.3.2 Evaluation of System Performance

#### Scenario Under Investigation

We first present detailed results for the scenario defined by the parameters listed in Table 6.2. We then examine how the performance of the system changes depending on the scenario by varying a key parameter of interest while maintaining the other parameters as per their value in Table 6.2. For each set of results, we compare the asynchronous performance of all waveforms under consideration, and use the performance of synchronous CP-OFDM as a baseline for comparison.

For the synchronous CP-OFDM baseline case, we assume quasi-orthogonality in which all timing offsets are absorbed by the CP. We also do not consider CFO in this case for two reasons. First, the scenario that we are considering typically consists of low mobility, resulting

[1]Noise power per RB is calculated using the expression $-174\text{dBm/Hz}+10\log_{10}(180\text{kHz})$, where $-174$dBm/Hz is the thermal noise and 180kHz is the bandwidth of an LTE RB.

Table 6.4: Simulation parameters

| **Parameter** | **Value** | **Parameter** | **Value** |
|---|---|---|---|
| Number RBs in system | 50 | $P_{\text{O\_PUSCH}}$ | -96 dBm |
| Cell Radius | 250 m | $\alpha$ | 1 |
| Inner Radius | 163 m | Max Tx Power CUE | 24 dBm |
| Number of Cells | 19 | Max Tx Power DUE | -5 dBm |
| CUEs Per Square Km | 200 | BS Antenna Gain | 15 dBi |
| DUEs Per Cluster | 30 | UE Antenna Gain | 0 dBi |
| Clusters Per Square Km | 3 | BS Noise Figure | 5 dB |
| Average Cluster Radius | 60 m | UE Noise Figure | 9 dB |
| Average Tx-Rx Distance | Uniformly distributed in the range [10, 50] m | Max Timing Offset | $T + T_{CP}$ |
| Carrier Frequency | 2 GHz | Max Local Oscillator (LO) Inaccuracy | 2.5 ppm |
| Subcarrier Spacing ($\Delta$F) | 15 kHz | Waveforms | CP-OFDM, FMT, OFDM/OQAM, FBMC-PAM, GFDM, f-OFDM, UFMC |
| Noise Per RB [1] ($\sigma_\nu^2$) | -116 dBm | Number of Iterations | 5000 |

in negligible Doppler shifts and frequency offsets. Secondly, the 3GPP standards specify stringent frequency errors for UEs of less than +/- 0.1 parts per million (ppm)[156] compared to the carrier frequency received from the BS. In contrast, for asynchronous scenarios, we consider timing offsets uniformly distributed in the range of 0 to $T + T_{CP}$, where $T$ is the length of an OFDM symbol and $T_{CP}$ is the length of the CP. We also consider less stringent hardware-related frequency error requirements, with local oscillator (LO) inaccuracies of +/- 2.5 ppm[2] permitted.

The cell radius value of 250m is based on the 3GPP LTE system scenarios [157], representing an urban macro-cell environment. The antenna gain values, noise figures, and the carrier frequency value are also based on [157]. The values for the maximum CUE transmit power, subcarrier spacing, and number of resource blocks are based on the LTE standard, with 50 resource blocks corresponding to a bandwidth of 10MHz. The maximum DUE transmit power of -5 dBm was chosen as we found through experimentation that it yielded good results. The effects of varying the maximum DUE transmit power will be discussed later in this section.

Fig. 6.11 shows an example of our simulation scenario. We explore the case whereby each macro-cell is fully loaded, with all available resource blocks being utilised, and hence consider a large number of CUEs per square kilometre to ensure this. The parameters relating to the size and frequency of occurrence of clusters are scenario dependant. A cluster of radius 60m, containing 30 inter-communicating devices and with an average of 3 clusters per square

[2]Generally, strict frequency error requirements require more accurate and expensive clocks. 2.5ppm is the stated frequency accuracy of the NI USRP-292x range of devices.

kilometre might, for example, represent a factory in an urban area with moderate industrial activities.

For each of the candidate waveforms, we initially investigate two cases:

1. Case 1: DUEs pairs deploy waveforms from the pool of waveforms under study, CUEs use CP-OFDM.
2. Case 2: Both DUE pairs and CUEs deploy waveforms from the pool of waveforms under study.

We also examine the effects of the timing offset on the relative performance of all waveforms, ranging from perfectly synchronised to fully asynchronous communication. An analogous investigation is performed for CFO by varying LO inaccuracies.

**System Performance**

For the SINR and rate metrics, we present our findings using box plots which allow us to present the results for each waveform in a single plot in a manner that is easily readable. A box plot is a convenient way of representing a distribution using a box that spans from the first quartile (bottom edge) to the third quartile (top edge). A solid horizontal line in the box represents the median, while the mean is marked with a dashed horizontal line.

The span of the box, from the top edge to the bottom edge, is known as the inter-quartile range (IQR). Whiskers, the lines extending from either end of the box, denote the maximum and minimum values. Values lying outside the whiskers are marked individually and classified as outliers. A value is considered to be an outlier if it is either $1.5 \times \text{IQR}$ or more above the third quartile or $1.5 \times \text{IQR}$ or more below the first quartile.

**DUE SINR Performance:** Fig. 6.12 presents box plots summarizing the SINR distribution for DUEs according to each considered waveform couple. The baseline CP-OFDM case, assuming no timing or frequency offsets, performs quite well and achieves an average SINR value of approximately 22dB. This, however, reduces to approximately 13dB when asynchronous communication is considered, with UFMC and GFDM exhibiting similar average values. When both CUEs and DUEs employ an alternative waveform in the set {OFDM/OQAM, FMT, FBMC-PAM, f-OFDM}, performance comparable to the baseline case is achieved even though communication is asynchronous. Interestedly, this same set of waveforms performs quite well in the coexistence scenarios in which CUEs use CP-OFDM and DUEs use an alternative waveform, with averages values approximately 3dB less than the baseline case, but almost 6dB greater than asynchronous CP-OFDM in some cases.

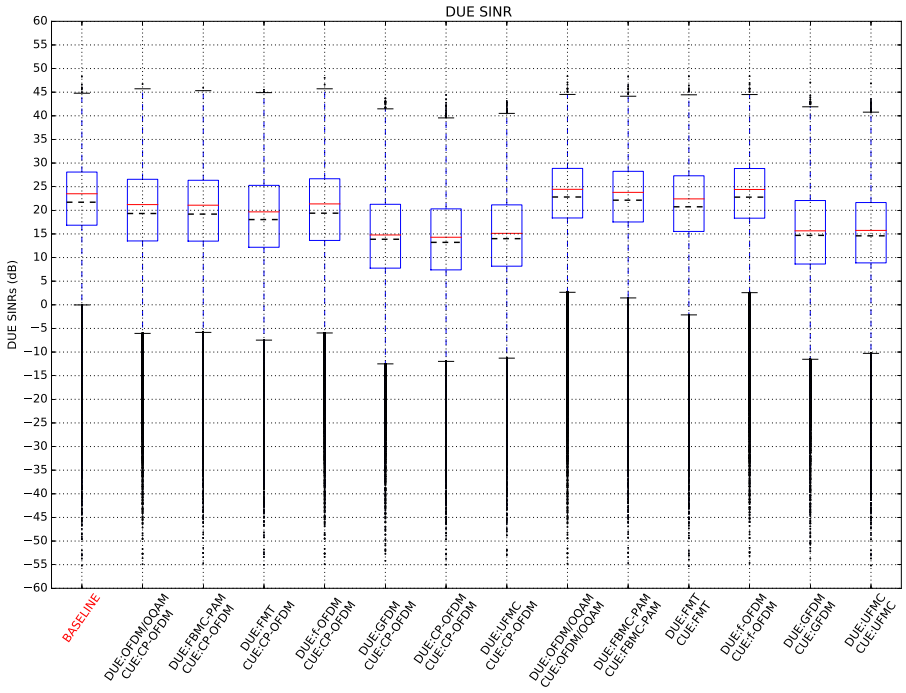


Figure 6.12: The box plots of DUE SINR show that a large performance increase can be obtained by choosing an appropriate alternative waveform.

We note that the number of outliers is relatively small (approx. 2.2%) compared to the number of DUEs in the data set. The presence of outliers is not unusual; while the majority of DUEs will experience a similar SINR to one another, especially favourable or unfavourable channel conditions will inevitably result in DUEs with SINRs that are considerably higher or lower than average. As stated previously, our aim is to compare the relative performance of waveforms, not to propose a specific resource allocation technique for DUEs. Employing a more intelligent RA scheme for DUEs that accounts for interference coordination and fairness could result in less outliers and better performance equality among DUEs, but is not within the scope of this study.

**DUE Rate Performance:** We also wish to show the achieved rate of DUEs, taking into account the bandwidth efficiency of each modulation scheme. Fig. 6.13 shows the achieved rate of DUE pairs for each waveform. The greatest performance is achieved when both CUEs and DUEs use OFDM/OQAM, closely followed by FBMC-PAM. The baseline synchronous CP-OFDM case yields the next highest achieved rate. The variation in achieved rate, despite each of the aforementioned cases exhibiting similar SINR values, can be attributed to the different bandwidth efficiencies of the waveforms, listed in Table 6.3.

In the coexistence scenarios, in which CUEs use CP-OFDM and DUEs use an alternative waveform, both OFDM/OQAM and FBMC-PAM exhibit the best performance. In particular,

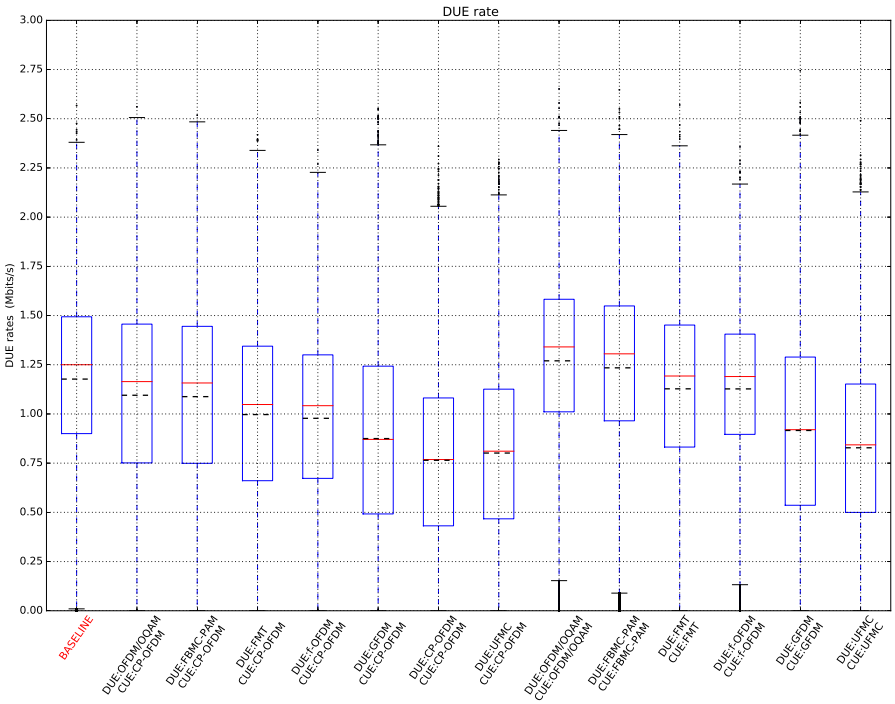


Figure 6.13: Rate performance of DUEs taking into account bandwidth efficiency.

in the scenario in which OFDM/OQAM is used by DUEs, the achieved rate is just 7.0% less than the synchronous CP-OFDM baseline case, but 43.3% greater than the asynchronous CP-OFDM case. This is an encouraging result, as DUEs could enjoy the benefits that asynchronous communication would allow without suffering a large degradation in performance. It also allows for the possibility that 5G will permit multiple waveforms, whereby different services employ the waveform that is best suited to them.

**CUE Performance:** It is imperative that CUE performance is not significantly degraded by the inclusion of DUEs in the network. Interference in this case comes from two sources. First, CUEs will experience interference from DUEs operating on the same resource block as them. Secondly, CUEs will be affected by interference leakage from DUEs on different resource blocks, resulting from the misaligned communications. Fig. 6.14 demonstrates that the average DUE to CUE interference is quite low. This can be attributed to two factors: the low transmit power of DUEs (-5dB) and the use of strict FFR.

In the baseline case, the average DUE to CUE interference is less than -120dBm. In cases where both CUEs and DUEs use an alternative waveform from the set {OFDM/OQAM, FMT, FBMC-PAM, f-OFDM}, the interference experienced by CUEs is lower than the baseline case. In all other cases, the interference is comparable to the noise per RB.

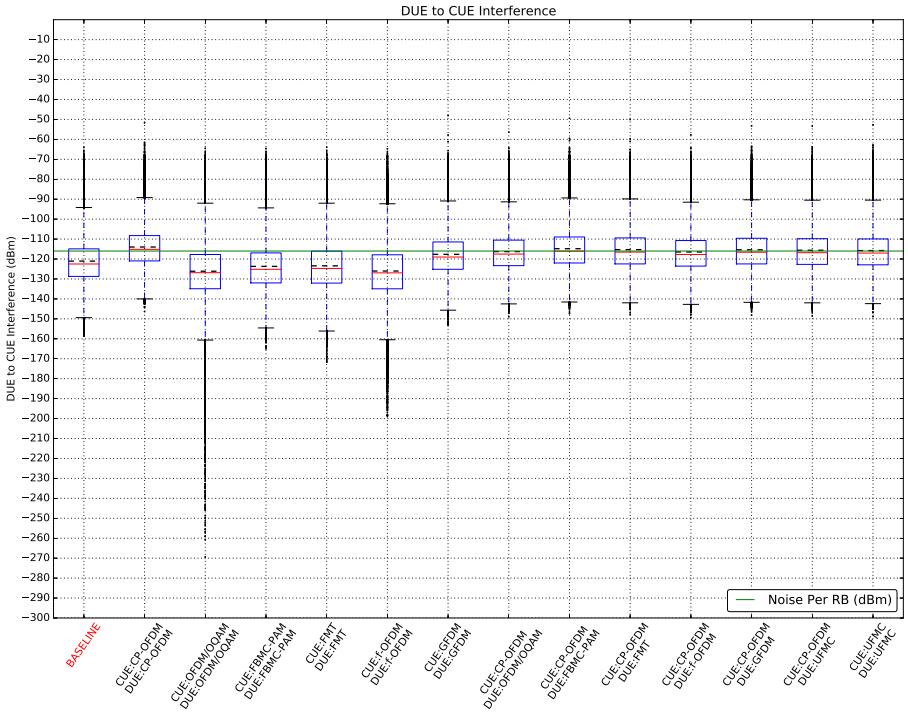


Figure 6.14: The DUE to CUE interference is similar to the value of noise per resource block for coexistence cases.

In the synchronous baseline case, CUEs will still suffer slightly from leakage interference from DUEs, owing to the fact that different cells in LTE are misaligned in time. Hence, the use of an appropriate alternative waveform by both sets of users can assist in reducing the interference that CUEs experience from DUEs. However, if CUEs use CP-OFDM, then employing an alternative waveform for DUEs has little effect on CUEs; its main benefit is to increase the performance of the DUEs themselves. For CUEs, the interference from DUEs using the same RB will generally be a greater factor than leakage. In contrast, for DUEs, leakage interference from other DUEs in close proximity is the dominant type of interference, and hence they can benefit from adopting a waveform with better spectral localization than CP-OFDM.

Although the DUE to CUE interference is quite low, it is not negligible and requires attention, particularly in the asynchronous coexistence cases. In particular, the presence of outliers suggests that while the majority of CUEs suffer little degradation to their performance, a small number of users suffer a large reduction in performance. These users are victims of the specific spatial distribution of transmitting users at that instant, in which strict FFR and the low transmit power of DUEs fail to offer sufficient protection.

Fig. 6.14 demonstrates that employing a different waveform for DUEs, while CUEs continue to use CP-OFDM, does little to mitigate DUE to CUE interference, which is

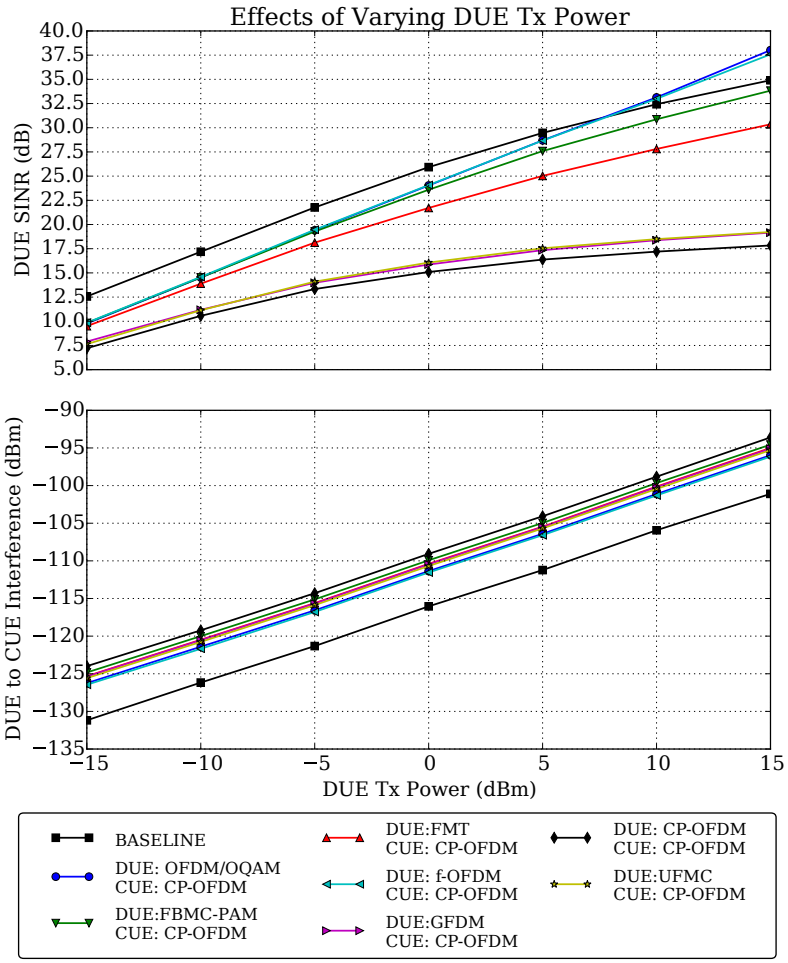


Figure 6.15: Increasing DUE transmit power results in an increase in DUE SINR at the cost of increased interference to CUEs.

consistent with our preliminary analysis of section 6.2 and the interference study detailed in chapter 4. In these cases, additional protection is needed to ensure that interference to CUEs is kept at an acceptable level and that the minority of users who suffer significant degradation can also obtain adequate performance. This may take the form of intelligent resource allocation schemes that aim to protect vulnerable CUEs by assigning resources in a manner that reduces DUE to CUE interference. As stated previously, such schemes are not within the scope of this study as we are solely interested in demonstrating the effect on performance of employing different waveforms.

### DUE Transmit Power

We investigate the effect that DUE transmit power has on system performance by varying the DUE transmit power from -15dBm to 15dBm in 5dBm increments, while holding all other parameters at the same value as in Table 6.4. We do not include cases in which both CUEs and DUEs use an alternative waveform, as we are more interested in the coexistence cases. Fig. 6.15 provides insight into how the DUE SINR performance and the interference experienced by CUEs changes according to different DUE transmit powers. The upper sub-plot shows average DUE SINR, while the lower sub-plot shows the average DUE to CUE interference.

As intuition suggests, increasing the DUE transmit power will increase DUE SINR at the cost of increased interference to CUEs. The case in which DUEs employ CP-OFDM for asynchronous communication exhibits the worst performance while the synchronous baseline case achieves the greatest performance for transmit powers below 7.5dBm, at which point it is overtaken by both OFDM/OQAM and f-OFDM. Leakage interference from D2D pairs in other cells will be present even in the synchronous case as neighbouring cells do not achieve time alignment. While OFDM/OQAM and f-OFDM successfully mitigate this type of leakage interference, it becomes significant at high transmit powers for synchronous CP-OFDM and, hence, the curve representing the baseline case begins to taper as the transmit power is increased.

In particular, we draw the readers' attention to two points.

1. First, for the case in which DUEs do not use an alternative waveform from the set {OFDM/OQAM, FMT, FBMC-PAM, f-OFDM}, successively higher transmit powers provide increasingly diminishing returns since increasing DUE transmit power will also increase the inter-DUE leakage interference. This is evident in Fig. 6.15, in which the set of curves at the bottom of the upper sub-plot gradually begin to level off as the DUE transmit power is increased. In contrast, the curves at the top of the upper sub-plot, representing scenarios in which DUEs employ a waveform from the set {OFDM/OQAM, FMT, FBMC-PAM, f-OFDM}, increase almost linearly with DUE transmit power since inter-DUE leakage interference is effectively negligible in these cases.

2. Secondly, the benefit to DUEs of using an alternative waveform will be greater at higher values of DUE transmit power since inter-DUE leakage will be more prominent. However, as the DUE transmit power is increased, there is a linear increase in the interference experienced by CUEs.

The main consequence of these observations is that higher DUE transmit powers provide increasingly diminishing returns unless an alternative waveform that adequately mitigates

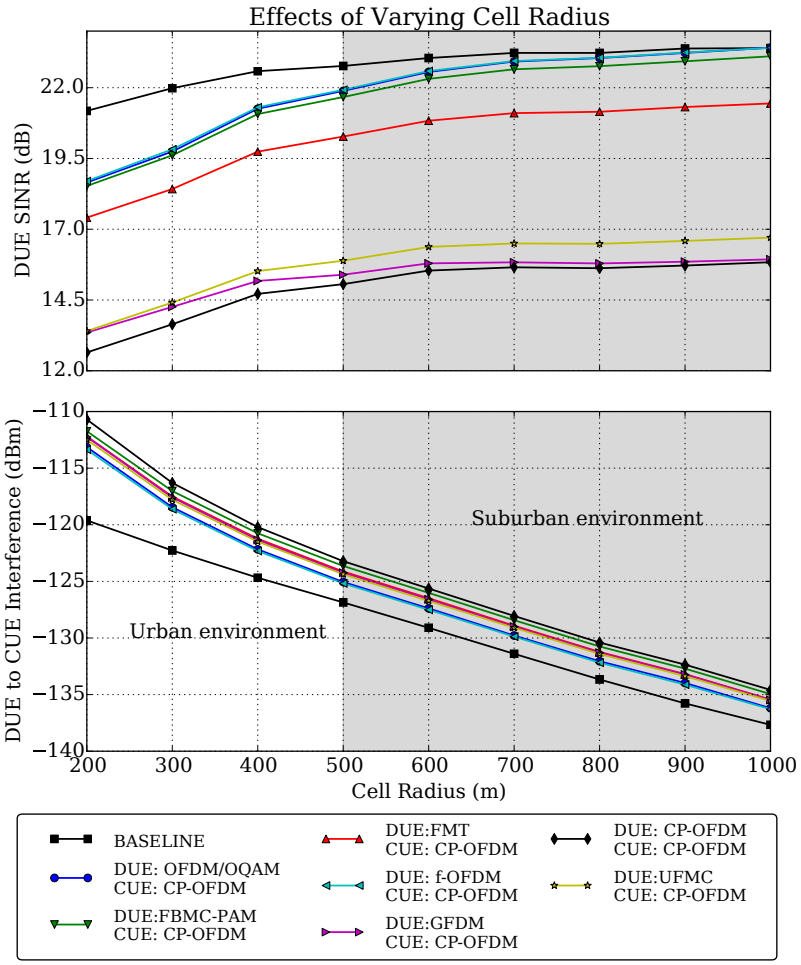


Figure 6.16: As the cell radius increases, DUE SINR increases and reduction in CUE SINR decreases.

leakage interference is employed. A maximum permissible transmit power should be chosen for DUEs that achieves a balance between adequate average DUE SINR and an acceptable level of interference to CUEs. The value of -5dBm chosen in Table 6.2 reasonably achieves this, with DUEs achieving a SINR close to 20dB when they employ OFDM/OQAM while limiting interference to CUEs to approximately the noise value per RB. We also note that we can trade off some DUE performance for reduced interference to CUEs. We observe, however, that the DUE to CUE interference is at a minimum for the synchronous baseline case.

### Cell Radius

In this subsection, we investigate the influence that cell size has on performance by varying the cell radius from 200m to 1000m in 100m increments while holding all other parameters

at the same value as in Table 6.4. We display the results in Fig. 6.16: for cell radii under 500m, we consider an urban environment and use the appropriate pathloss models for this scenario, while for cell radii greater than 500m, we consider a suburban environment.

At the smallest cell radius considered (200m), average DUE SINR is at its lowest and average DUE to CUE interference is at its greatest. This is understandable, and readily explained. According to the strict FFR scheme employed, DUEs reuse the resources of CUEs in neighbouring reuse regions. At small cell sizes, the average distance between devices in neighbouring reuse regions is reduced. This results in greater CUE to DUE interference and reduces DUE SINR. As the cell radius increases, so too does the distance between reuse regions, and DUE SINR increases. This increase is mainly observed at smaller cell sizes; at large cell sizes, CUE to DUE interference is almost negligible and further increases to cell radius exhibit little or no increase in DUE SINR.

DUE to CUE interference, on the other hand, occurs at base stations. In small cells, the average distance between clusters and the base stations serving neighboring reuse regions is shorter, resulting in higher DUE to CUE interference. This is shown in the lower sub-plot in Fig. 6.16, in which we observe that the average DUE to CUE interference decreases as the cell radius increases.

Therefore, as the cell size increases, average DUE to CUE interference decreases and average DUE SINR increases. Essentially, the greater the cell size the more protection strict FFR offers against the various types of interference, as the reuse regions are further apart.

We note at the maximum cell radius considered (1000m), f-OFDM, FBMC-PAM, and OFDM/OQAM each offer approximately a 7dB improvement in the coexistence scenario over the asynchronous CP-OFDM case. At large cell sizes, even further gains are achievable as DUEs could transmit at a higher power without affecting CUEs. Unfortunately, at the other end of the scale, DUEs in very small cells might not be able to transmit at a power level that allows them to obtain the required data rates without interfering too much with CUEs. In these cases, additional measures may need to be developed and deployed to enable DUE communication, such as advanced resource allocation schemes that minimize the interference from DUEs to CUEs. Failing that, DUE communication may only be permitted to underlay sufficiently large cells.

Over the range of cell radii considered, synchronous CP-OFDM provides the best performance and asynchronous CP-OFDM provides the worst. However, as the cell radius increases, the interference from CUEs in neighbouring reuse regions to DUEs is reduced and the performance of several alternative waveforms approaches that of synchronous OFDM. As observed in previous plots, the baseline synchronous OFDM case results in the least amount of interference to CUEs, although this interference is quite low in all cases as the cell radius increases.

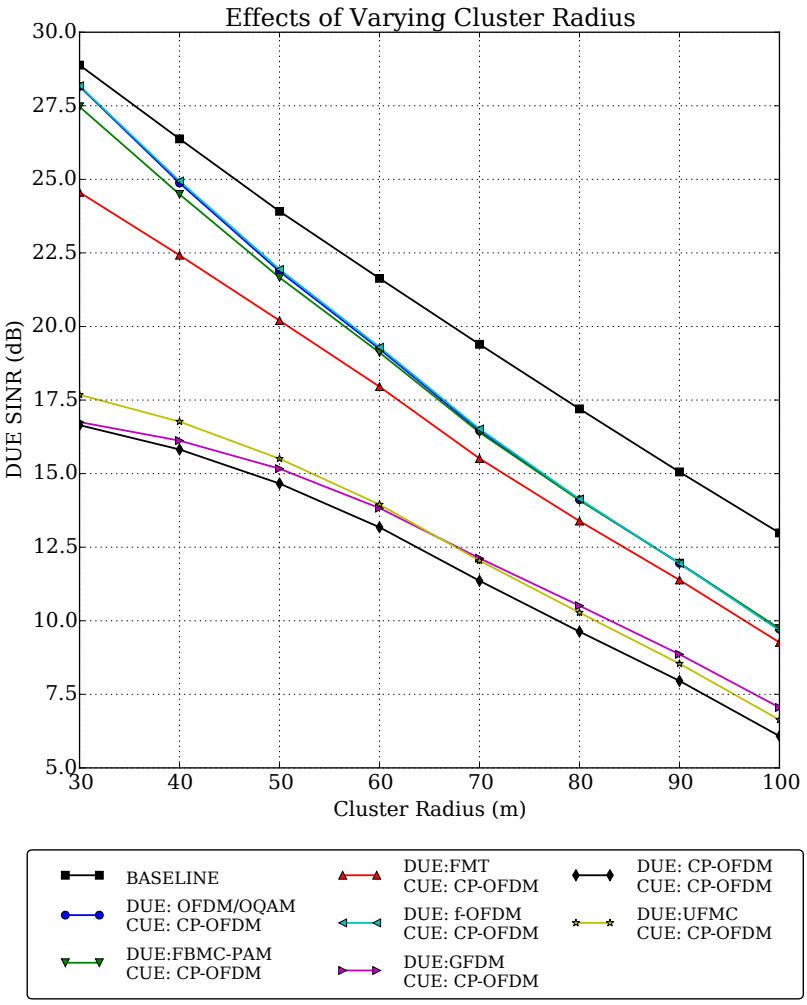


Figure 6.17: Employing an appropriate alternative waveform for DUEs yields the greatest benefit in small clusters in which inter-DUE leakage interference is most significant.

### Cluster Radius

We study the impact that cluster radius has on performance. We present the results in Fig. 6.17, varying the cluster radius from 30m to 100 m in 10 m increments. Reducing the cluster radius necessitates a corresponding change in the distance between a DUE transmitter and receiver, which we modeled using a uniform random variable. Accordingly, we choose the parameters $a$ and $b$, representing the minimum and maximum Tx-Rx distances, respectively, of the uniform random variable $U_{[a,b]}$ as follows: $a$ = 5m; $b$ = (cluster radius) – 10m.

Increasing the cluster radius has two opposing influences on DUE SINR. On the one hand, it results in reduced inter-DUE interference, which should boost the SINR. On the other hand, it also results in reduced received signal power, which should cause the SINR to

decrease. This makes it difficult to predict how the average SINR will change. In Fig. 6.17, we see that the reduction in received power is more influential and DUE SINR decreases as cluster radius increases. We concede, however, that this is somewhat dependant on how the distance between DUE transmitters and receivers is modelled (such as the parameters $a$ and $b$), as this affects by how much the received power will decrease. We also note that for small cluster sizes, and in cases where DUEs do not use a waveform in the set {OFDM/OQAM, FMT, FBMC-PAM, f-OFDM}, SINR decreases slowly at first as the reduction in inter-DUE interference is almost significant enough to counter-act the effect of lower received signal powers.

Reducing the cluster radius increases the density of DUEs in the cluster, resulting in greater inter-DUE interference. Hence, employing an appropriate alternative waveform for DUEs yields the greatest benefit in dense clusters in which inter-DUE leakage interference is most significant. The synchronous baseline case again performs the best; however, the performance for cases where DUEs use a waveform in the set {OFDM/OQAM, FBMC-PAM, f-OFDM} approach that of the baseline for small cluster sizes. This can be attributed to reduced leakage interference from CUEs in the same reuse region, as smaller clusters are less likely to encompass CUEs in the same cell.

### Amount of Time and Frequency Misalignment between Devices

The final parameters whose influence on performance interests us are the maximum permitted timing offset and CFO. Both CFO and TO affect DUE performance similarly, and so it makes sense to isolate them when studying their effects on performance. Hence, when examining the effect of timing offset on DUE performance, we consider a case involving no CFO. Similarly, when investigating the effects of CFO, we consider devices to be perfectly aligned in time.

**Maximum Possible Timing Offset:** As expressed in Section 6.3.1, rather than relying on average values of interference like many papers in the literature [113], we employ a more realistic approach of assigning specific values of timing offset $\delta_{\mathrm{t}}$ to individual DUEs using a uniform random variable.

We vary the maximum permissible timing offset as a fraction of the time spacing between two OFDM symbols from 0 (full synchronism) to 1 (full asynchronism) in 0.1 increments. Limiting the maximum permissible timing offset corresponds to a case in which coarse alignment has been obtained; for example, 0.2 would correspond to the case in which devices are synchronized to within 20% of an OFDM symbol time.

Fig. 6.18 illustrates the results. The black line representing the case whereby both DUEs and CUEs use CP-OFDM will be our baseline for comparison, and it can be seen that SINR

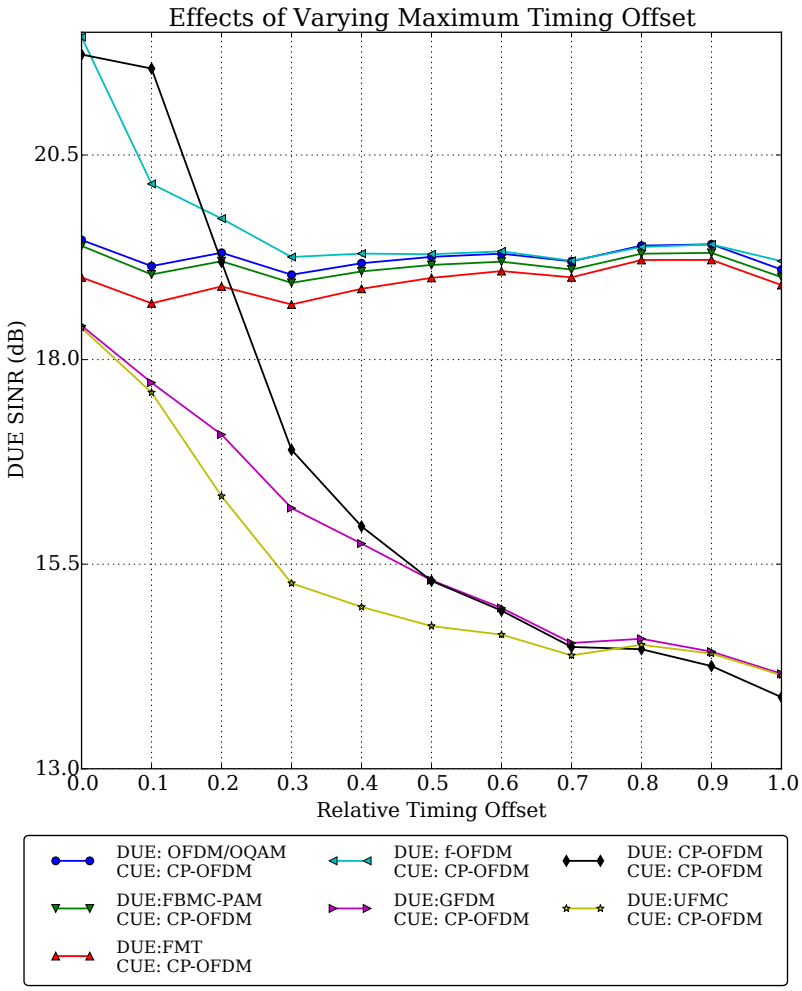


Figure 6.18: DUE SINR performance as the maximum permitted timing offset is varied.

drops rapidly when the timing offset is greater than the cyclic prefix. The cyclic prefix duration $T_{\mathrm{CP}}$ for CP-OFDM is 12.5% of the symbol duration $T$. We can divide the rest of the graph into two scenarios:

i) *Scenario in which DUEs use a waveform in the set {GFDM, UFMC}, and CUEs use CP-OFDM*: These curves become quite similar as the maximum permissible timing offset increases, and are out-performed by our baseline OFDM-OFDM case. This seems surprising at first glance, but can be explained. Indeed, we saw in Fig. 6.10 that, with the chosen parameters, UFMC and GFDM still cause a significant amount of interference between coexisting users in homogeneous links in which both users are deploying one of these waveforms; thus, inter-DUE interference is quite important if DUEs use either GFDM or UFMC. Moreover, CP-OFDM based users are orthogonal with one another

as long as $\delta$t is contained in the CP duration. However, GFDM or UFMC users never achieve orthogonality with OFDM users, which explains that if CUEs use OFDM, CUE to DUE interference is on average more significant if DUEs use UFMC or GFDM than if they also employ OFDM.

ii) *Coexistence scenario in which DUEs use a waveform in the set {OFDM/OQAM, FBMC-PAM, f-OFDM, FMT} and CUEs use OFDM*: As the timing offset increases, the curves exhibit similar performance. At a maximum timing offset, the benefit to using one of these alternative waveforms for DUEs is considerable. With the exception of f-OFDM, the performance of these waveforms varies little according to the timing offset, and they are outperformed by the baseline CP-OFDM case for very low timing offsets (< 20%). f-OFDM has an interesting behaviour, as it is the only waveform that is affected differently by CP-OFDM according to the value of $\delta_{\mathrm{t}}^{\mathrm{max}}$. This is due to the fact that for small timing offsets, f-OFDM and OFDM achieve quasi-orthogonality, which is then lost as $\delta$t increases.

**Maximum Possible CFO:** Having investigated the effect of TO, we now examine the relative performance of the waveforms under various levels of CFO. The LO inaccuracy is varied from 0ppm to 3.5ppm in increments of 0.5, corresponding to frequency offsets of 0kHz to +/- 7kHz in 1kHz increments at a carrier frequency of 2GHz.

In Fig. 6.19, for the case in which CP-OFDM is used by both sets of users, we observe that the average DUE SINR reduces as the frequency offsets become greater. This is in line with the sensitivity to asynchronism of CP-OFDM we have illustrated in chapter 2. In a similar fashion to the study on the effects of TO, we again take the case in which both sets of users employ CP-OFDM to be our baseline case, and divide the rest of Fig. 6.19 into two scenarios:

i) *Scenario in which DUEs use a waveform in the set {GFDM, UFMC}, and CUEs use CP-OFDM*: When DUEs employ GFDM or UFMC, DUE SINR decreases as the maximum possible LO inaccuracy is increased; however, the decrease occurs at a lower rate than for CP-OFDM. For low LO inaccuracies, the baseline OFDM case outperforms the scenarios in which CUEs use CP-OFDM and DUEs use either UFMC or GFDM. While CP-OFDM users achieve near orthogonality at low CFOs, GFDM or UFMC users never achieve orthogonality with CP-OFDM users. However, as the LO inaccuracy is increased, CP-OFDM suffers from increasingly large interference leakage and the waveform choices involving UFMC or GFDM begin to outperform the baseline CP-OFDM case.

ii) *Coexistence scenario in which DUEs use a waveform in the set {OFDM/OQAM, FBMC-PAM, f-OFDM, FMT} and CUEs use CP-OFDM*: The waveform choices involving

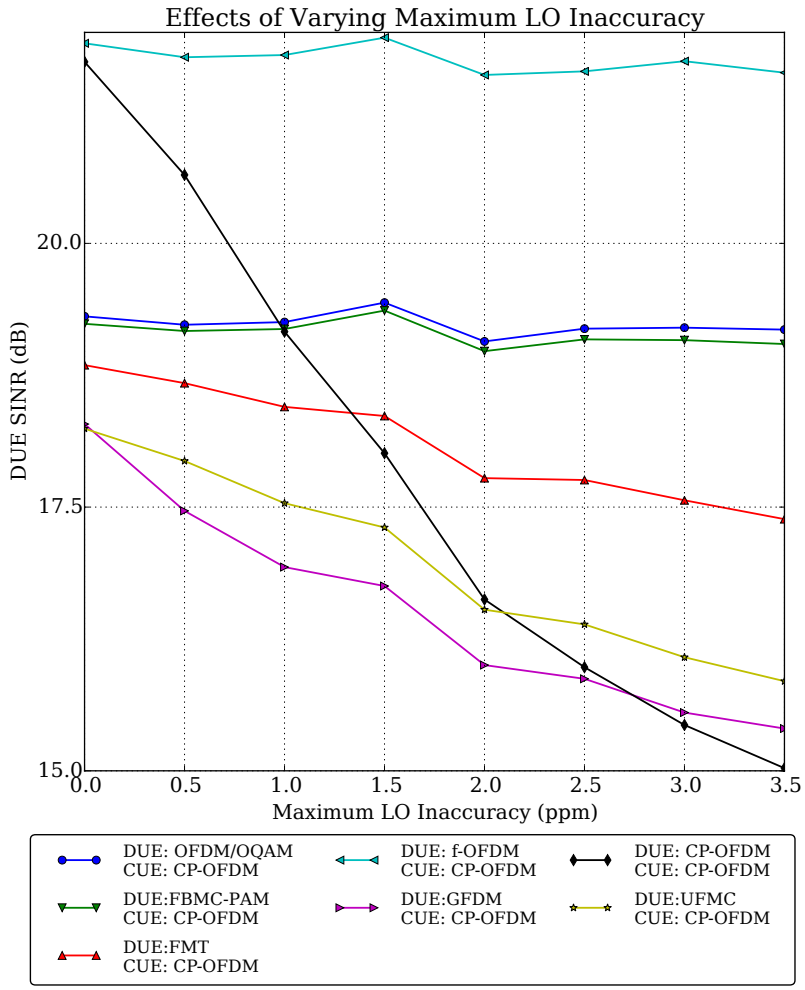


Figure 6.19: DUE SINR performance as the maximum CFO is varied.

OFMC/OQAM, FBMC-PAM, and f-OFDM are largely unaffected by varying CFO, as made evident by the horizontal lines in Fig. 6.19. At the LO inaccuracies considered, frequency offsets are contained within +/- half a subcarrier. Given that these schemes use a guard band of half a subcarrier at either side of an RB, and that leakage is confined within a similar range for these alternative waveforms, it is not surprising that very little variation in performance is observed as the CFO is increased. FMT, on the other hand, uses 12 subcarriers per RB. Hence, we observe that the SINR performance of DUEs using FMT reduces as the maximum possible LO inaccuracy is increased. Out of the waveform couples considered in this scenario, f-OFDM exhibits the best performance and is never outperformed by the baseline CP-OFDM case. The waveform choices involving FBMC-PAM and OFDM/OQAM only begin to outperform the baseline OFDM case after approximately 1ppm. For DUE users using FMT, improvements in SINR over the

baseline case are only observed after a maximum LO inaccuracy of 1.3ppm (based on an interpolated value).

### 6.3.3 Concluding Remarks

When only the SINR metric is considered, the best results are obtained when either synchronous OFDM is used, or both sets of users use a waveform from the set {FBMC/OQAM, FMT, FBMC-PAM, f-OFDM}. However, when the achieved rate is considered instead, taking bandwidth efficiency into account, the case in which DUEs operate asynchronously and both sets of users employ FBMC/OQAM achieves the greatest performance.

Promisingly, we also showed that good performance can be obtained when DUEs operate asynchronously and use a different waveform to CUEs, paving the way for the possibility of the coexistence of waveforms in 5G for different use cases, which represents a paradigm shift from previous generations. In particular, when FBMC/OQAM is used by DUEs, the achieved rate is just 7.0% less than the synchronous OFDM baseline case, but 43.3% greater than the asynchronous OFDM case. We also note that these figures are conservative, as they assume perfect synchronisation in the baseline case. They also do not take into account the additional gains that asynchronous communication could offer, as symbols previously required to achieve time alignment could instead be used for data.

We highlight, however, that the decision of whether to use synchronous or asynchronous communication is multifaceted and should not be made solely based on performance metrics such as SINR and achieved rate. There are many reasons why an operator may decide to employ asynchronous communication for the scenario under consideration. As mentioned, the cost of achieving and maintaining synchronous communication for DUEs may be unattractive. Removing the synchronisation procedure for DUEs could help to reduce the latency experienced by these devices. Asynchronous DUE communication also removes several duties of control from the base station, potentially enabling the network operator to treat resource allocation for high-rate clustered D2D scenarios in a different manner than for CUEs. Finally, if DUEs use a waveform with better spectral localization than CP-OFDM, then the stringent requirements on the accuracy of local oscillators in equipment could be relaxed.

Obtained results indicate that the biggest drawback of asynchronous D2D communication is the increased interference to cellular users. Unfortunately, employing a different waveform for DUEs does little to reduce this type of interference, which is consistent with the findings presented in Chapters 4 and 5. We note, however, that interference can typically be kept low through the use of strict FFR and low DUE transmit powers. Furthermore, as we were primarily interested in comparing the relative performance of waveforms, we used simple RA schemes in our study and assumed fully loaded cells. In reality, inter-cell interference coordination schemes are employed to mitigate inter-cell interference, resulting in RBs in

each cell that are deliberately not used. Similar schemes have the potential to minimize the interference from DUEs to CUEs but, as noted several times throughout the chapter, this is out of scope in this study. To conclude, we have shown that it may be feasible for cellular networks to serve clustered 5G use-cases using asynchronous D2D communication. In particular, we highlighted the benefits to DUEs of using an alternative waveform to reduce leakage interference.

## 6.4 Conclusion

In this chapter, we have studied the application of enhanced multicarrier waveforms in scenarios in which D2D systems coexist with cellular networks. We have first investigated a simple scenario in which a cluster of D2D pairs underlays an OFDMA cell. In that simple scenario, we have established that the use of enhanced multicarrier waveforms for D2D communications can be highly beneficial, even if the cellular users still use CP-OFDM. Motivated by this finding, we have evaluated the performance of a more realistic network setup, comprised of multiple cells and multiple D2D clusters. Even though the numerical results we have obtained based on our simulation campaigns are dependant on the exact waveform setups we have considered, they do reveal some interesting insights. In particular, we are able to conclude that the birth of new applications involving clustered communication in which a significant number of devices transmit with little synchronization in a relatively small area can be facilitated by the adoption of waveforms alternative to CP-OFDM. Furthermore, our study tends to show that MNOs could readily implement these use cases in the spectral bands so far dedicated to cellular communications and therefore optimize the usage of the latter.

# Chapter 7

# Conclusions and perspectives

**Contents**



## 7.1 General conclusion

### 7.1.1 Context of the study

The works presented in this thesis fit into a wide body of studies that have been searching for alternative waveforms to CP-OFDM in order to overcome the shortcomings of the latter. Indeed, even if CP-OFDM has been applied with success in LTE cellular networks, its poor spectral localization and high sensitivity to asynchronism raises question regarding its potential to enable foreseen 5G use cases. Therefore, a large number of new waveforms that achieve better spectral localization than CP-OFDM have been proposed in the literature.

However, as we demonstrated in Chapter 4, the literature studying the coexistence between legacy systems based on CP-OFDM on the one hand and newly introduced devices based on alternative waveforms on the other hand is rather weak. This is nevertheless an important issue, as technological progress is intrinsically incremental. Therefore, should new waveforms be deployed in future devices, all currently CP-OFDM based systems would not be shut down yet. Thus, it is very likely that, at least for some years, CP-OFDM legacy

networks would coexist with new devices employing whichever waveform would be selected for 5G.

In this thesis, we have therefore been committed to thoroughly studying such heterogeneous coexistence setups. To do so, we have first carefully analyzed the interference arising between one device using CP-OFDM and one device using an alternative waveform. Then, we have built upon our results to study CR setups and finally have applied our analysis in D2D deployment scenarios.

### 7.1.2 Main results and findings of the thesis

#### Analysis of interference between CP-OFDM and FB-MC waveforms

We presented a generic framework that can be used to analyze the interference caused by FB-MC waveforms onto CP-OFDM receivers. We showed that the PSD-based model which was the only tool available in the literature to study this problem is inaccurate. In extenso, we have shown that it underestimates the interference suffered by the CP-OFDM receiver because it does not take into account the operations performed by the latter. In particular, we have demonstrated that the long prototype filters used by FB-MC are cut by the short receive window of the CP-OFDM receiver, which destroys the advantageous spectral properties of the FB-MC signal. Our results show that all waveforms proposed in the literature are not orthogonal with CP-OFDM receivers and therefore highly interfere on the latter despite their advantageous spectral properties. Based on our analysis, we were able to demonstrate that the interference suffered by the CP-OFDM receiver is well approximated by a Gaussian distributed signal and derived closed-form expressions of the interference power. Furthermore, we validated our theoretical analysis through experiments which confirmed our results.

#### Coexistence with CP-OFDM incumbent systems in CR setups

The PSD-based model the limitations of which we have demonstrated has been used in a number of works of the literature to investigate CR setups in which the secondary system, based on an enhanced waveform, tries to reuse spectral holes left free by the incumbent network. We have therefore applied our improved interference model to revise some results of the literature. In particular, for all the waveforms we have considered in this thesis, we have answered the following questions:

1. How wide should the guard band between the secondary and incumbent system be in order to sufficiently protect the latter ?

2. Given a fixed spectral distribution of users, what is the optimal power loading the secondary system should follow to maximize its capacity while respecting the interference constraint set by the incumbent system ?

3. In a CR setup in which the incumbent system has limited time to transmit data, what is the best waveform to use according to the duration of its transmission window?

Overall, the results we obtained tend to show that the gains of using enhanced multicarrier waveforms to coexist with CP-OFDM incumbent systems are limited or even insignificant, at least when compared with the results predicted in the literature.

#### Asynchronous D2D operation in 5G networks

Finally, we have studied setups in which D2D pairs utilizing enhanced multicarrier waveforms coexist with CP-OFDM based cellular users. In line with the results we obtained in CR setups, we have shown that the use of waveforms with high spectral localization for D2D communication only does not directly reduce interference to CP-OFDM cellular users. However, these waveforms successfully limit interference between D2D users themselves. We have shown that this has interesting consequences on the network management procedures. In particular, we have demonstrated that if D2D users utilize waveforms with high spectral localization, the inter-D2D interference can be neglected during the resource allocation procedure, which can be highly beneficial as it greatly facilitates the scheduling procedure. Furthermore, we have investigated the effect of different parameters on the performance of the network according to the waveform used by the D2D pairs. Overall, our results have shown that it is worth using a multicarrier scheme other than CP-OFDM for D2D transmission, in particular when D2D pairs are clustered in small areas.

## 7.2 Perspectives for future work

In this thesis, we have investigated a problem that had been highly overlooked in the literature, namely the coexistence of legacy CP-OFDM based systems with new users utilizing enhanced multicarrier waveforms. The results we have obtained raise some questions, that we list as potential perspectives for future work in the following.

**Accurate study of the interference distribution:** In chapter 4, we have shown that the interference suffered by the CP-OFDM incumbent systems can be approximated by a Gaussian distributed signal. However, this is just that: an approximation. It would be valuable to dispose of more accurate statistical descriptions of this signal. Indeed, this knowledge would enable us to better predict the performance of the incumbent system.

**Design of precoders for incumbent protection:** This point is directly related to the former one. In this thesis, we have constantly considered that the symbols sent by the secondary system are i.i.d. and we have evaluated the average interference caused to the incumbent. However, it may be possible, provided that the secondary system is able to acquire knowledge of the channel between them and the incumbent, to precode transmit symbols in order to reduce the interference suffered by the latter.

**Analysis of channel coding effects:** Another limitation of our work lies in the fact that we did not take into account the channel coding used by the incumbent system in the evaluation of the performance of the latter. It would be interesting to take this into account. Indeed, we have shown in chapter 4 that the average interference caused by FB-MC waveforms onto a CP-OFDM receiver can be 2 to 3 dB lower than that caused by CP-OFDM. This is not a tremendous gain, however it might be greatly increased by the channel coding of the incumbent system which could multiply it.

**Taking into consideration the synchronization procedures of the incumbent:** In our study, we have completely overlooked the synchronization procedures performed by the incumbent CP-OFDM system. However, this is a crucial step which affects the quality of the whole transmission. Therefore, evaluating the impact of the secondary transmission on the quality of the synchronization procedures performed by the incumbent is crucial.

**Taking into account hardware impairments:** As we have mentioned it in chapter 4 when we presented our software radio demonstrator, all the results we presented in this thesis assume that the RF components of every considered system behave perfectly linearly. However, in real systems, the high power amplifier does not necessarily function in its linear area, which incurs harmful distortions on the transmit signal. This usually results in an increase of the out of band emissions. Therefore, it is to be expected that the rather limited gains obtained by using enhanced waveforms we have shown would be even smaller when the nonlinearities caused by hardware impairments are taken into account.

**Taking into account potential bandpass filtering at the incumbent:** All throughout our study, we have considered that the secondary signal is fed directly to the DFT processing block of the CP-OFDM incumbent receiver. However, in certain spectral coexistence setups, the incumbent might be performing a band-pass filtering on top of the CP-OFDM reception, which should be accounted for in future works.

**Extending our analysis to coexisting systems with different subcarrier widths:** In this thesis, we have limited our analysis to coexistence setups in which the incumbent

and secondary systems use the same subcarrier width. It may be potentially interesting to study the effects that a discrepancy between the subcarrier widths of each system may have. However, we do not expect obtained results to be drastically different from those we have presented in this report.

**Extending the FB-MC formalism to subband-filtered waveform:** A major obstacle we have encountered in this work lies in the fact that different waveforms hardly fit into the same mathematical model. In particular, the FB-MC mathematical model does not directly apply to subband-filtered waveforms. This has made it impossible to apply the same developments to all waveforms studied in this thesis. In particular, the analysis we have devised in chapter 4 is focused on FB-MC only, even if we have shown that similar results are observed for subband-filtered waveforms. Furthermore, the lack of a per-subcarrier interference measure for subband-filtered waveforms makes it impossible to perform power loading on the latter, as demonstrated in chapter 5. The need for a unified multicarrier model that could be parameterized to encompass any waveform proposed to replace CP-OFDM is growing, and some works in the literature have tackled this issue [158]. However, no practical approach has achieved unanimity yet, and more efforts are needed in that direction.

**Correction of the Gaussian approximation in network simulations:** In the network simulations we have led in chapter 6 to evaluate the coexistence of D2D systems with a cellular network, we have evaluated the sum interference on each device by summing the average interference power coming from each interferer, which means that we have performed a Gaussian approximation of the interference. However, Wu *et. al.* in [135] have demonstrated that this approach is not entirely accurate in D2D setups in which there is usually one main interferer. Future studies should therefore take this into account to update the results we have presented.

**Study of metrics other than SINR in network simulations:** SINR is the only metric that we have evaluated in our study. However, network simulations usually rely on higher level metrics such as block or frame error rate. However, to be able to evaluate such metrics, a fastidious link to system level mapping procedure has to be performed for each considered waveform. Nevertheless, it is necessary to lead this analysis in order to be able to give more meaningful results at the network level.

**Evaluating the impact of Full Duplex technology on the led studies:** Full Duplex is a technology that allows a device to both transmit and receive at the same time and on the same frequency. Recent developments in hardware technologies have made Full Duplex

applicable and it is particularly appealing in the context of D2D communications. Including it in our system model is therefore an interesting track to follow.

**Comparing the gains brought by new waveforms with those achieved by multi-antenna techniques:** Overall, in this thesis, we have focused solely on enhanced multicarrier waveforms. However, it is not the only means to facilitate coexistence between asynchronous systems. Namely, MIMO techniques and in particular beamforming can serve the same purpose. The results we have evaluated in this thesis should therefore be compared with those that can be achieved by a proper use of beamforming. Given the results we have presented, it is likely that the latter technique may outperform enhanced waveforms in a large number of scenarios of interest.

**Adopting a simulation-driven approach to wireless networks management:** Let's end up on a somewhat futuristic note. Wireless networks, because they are composed of more and more various user types, become ever more complex and intricate. To use an example from this thesis, finding the optimal resource allocation in a system composed of both cellular and D2D users is a very challenging task and most analytical-based studies use some simplifications to make the problem tractable. This kind of complex setups will multiply in the coming years as wireless networks undergo an important densification. Therefore, finding optimal management techniques only through analytical tools will become hopeless. At the same time, our computational power is constantly increasing and it becomes possible to simulate entire communication networks with great accuracy and at high speed. Therefore, the same way AlphaGo has practiced its technique over millions of games before beating a human opponent, we could design software capable of learning how to best manage communication networks by simulating millions of possible network deployments - for example on a much improved version of the network simulator we used in chapter 6 - before being deployed in real network infrastructure. We are not there just yet; the needed computation power to enable such applications is so far not available to any operator. But in some years, this kind of approach will not only become affordable: it will become necessary to optimally exploit the complex and heterogeneous networks of the future. In any case, this is for sure an exciting track to explore.

## 7.3 Final words

In this thesis, we have focused our study on the use of enhanced multicarrier waveforms to enable smoother coexistence of new communication services with legacy networks. The results we have presented clearly put back into question the relevance of this approach as we demonstrated that the achievable gains are far less significant than what was expected

in the literature. Besides, one is forced to admit that despite decades of research on this topic, the scientific community has had a hard time to reach a consensus on a particularly advantageous waveform scheme. The myriad of similar studies on the subject has made it difficult to convince the industrials of the interest of replacing CP-OFDM. Namely, the 3GPP has recently made it clear that the PHY of 5G, called New Radio (NR), will not include any radical changes and will most certainly rely on CP-OFDM, possibly with some additional filtering procedures. With this decision, all hope of seeing some FB-MC waveform massively adopted in the immediate future has vanished.

So what ? Should we wait for 6G for the works on waveforms alternative to OFDM finally pay off ? This kind of wait-and-see approach could well end up lasting forever. Thus, it is crucial that all stakeholders investigate why enhanced waveforms have attracted so little attention from the industrial and commercial operators. Indeed, theoretically, the technology is ready: for most enhanced multicarrier schemes, all technological obstacles related to classical communication systems, such as synchronization, equalization or MIMO applicability have been overcome. However, CP-OFDM works just as well, and so far, the scientific community has failed to justify its replacement. This is mainly due to the fact that the kind of highly asynchronous coexistence scenarios in which CP-OFDM starts to fail do not exist yet. Will they exist one day ? Certainly. However, plenty of other technologies that are currently being developed might perfectly fit the new needs they will bring. For example, the mastery of mm-wave communications makes the spectrum shortage issue obsolete, and may well make some of the scenarios we have investigated in this thesis meaningless.

These observations do not make for an optimistic conclusion. However, given the current level of adoption of enhanced waveforms and the so-called "hype cycle" massive MIMO and mm-wave technologies, among others, have entered, it is quite likely that all the waveform schemes we have studied will end up in the graveyard of beautiful theories; unless they can be proven to be particularly efficient in very specific use-cases. Among other examples, FMT has been successfully adopted for PLC networks, OFDM/OQAM seems to raise some interest for underwater or very high speed communications, and GFDM is studied for application in optical front-haul networks. Nothing is lost entirely; however, unless proven otherwise, civil cellular communications will continue to work just well with CP-OFDM.

# Appendix A

# Derivation of $A_{\Pi_T,g}(\tau,\nu)$

Consider a rectangular window of length $T$, noted $\Pi_T$ and a filter $g$ of length $T_g$. We assume that $g$ respects the following properties: it is equal to 0 anywhere except for $t \in [a,\ a+T_g]$ and is Lebesgue integrable on its non null area. Note that this is not a strong assumption and that filters commonly used in the literature respect it. We also add the condition that $T_g > T$. Under these assumptions, it is possible to define $g$ as a truncation of a periodic signal $g_\infty(t)$ defined as

$$g_\infty(t) = g(\frac{t-a}{T_g}), \forall t \in \mathbb{R}. \tag{A.1}$$

With this definition, $g_\infty(t)$ is a $T_g$-periodic signal which is Lebesgue integral on one period. Therefore, it can be decomposed in Fourier series as

$$g_\infty(t) = \sum_{k\in\mathbb{Z}} G_k e^{j2\pi k \frac{t}{T_g}}, t \in \mathbb{R} \tag{A.2}$$

where $G_k$ are the Fourier coefficients of $\tilde{g}$. Therefore, the cross-ambiguity function of $g$ and a rectangular window of length $T$ is equal to

$$A_{\Pi_T,g}(\tau,\nu) = \int_0^T g(t-\tau)e^{j2\pi t\nu}dt, \tag{A.3}$$

$$= \sum_{k\in\mathbb{Z}} G_k e^{-j2\pi k\frac{\tau}{T_g}} \int_0^T e^{j2\pi t(\frac{k}{T_g}+\nu)}dt \tag{A.4}$$

which simplifies into different expressions according to the values of $\tau$.

**$T_g \geq T$ case**

Here, we consider the case $T_g \geq T$.

**Case I:** $\tau > T - a$ or $\tau < -(a + T_g)$.

In that case, $g(t-\tau)$ does not overlap the rectangular window and

$$A_{\Pi_T,g}(\tau,\nu) = 0 \tag{A.5}$$

**Case II:** $-(a + T_g) \leq \tau \leq T - (a + T_g)$

In that case, only a small part of the filter overlaps the beginning of the rectangular window and

$$A_{\Pi_T,g}(\tau,\nu) = \sum_{k\in\mathbb{Z}} G_k e^{-j2\pi k\frac{\tau}{T_g}} \int_0^{a+\tau+T_g} e^{j2\pi t(\frac{k}{T_g}+\nu)} dt \tag{A.6}$$

**Case III:** $-a \leq \tau \leq T - a$

In that case, only a small part of the filter overlaps the end of the rectangular window and

$$A_{\Pi_T,g}(\tau,\nu) = \sum_{k\in\mathbb{Z}} G_k e^{-j2\pi k\frac{\tau}{T_g}} \int_{a+\tau}^{T} e^{j2\pi t(\frac{k}{T_g}+\nu)} dt \tag{A.7}$$

**Case IV:** $T - (a + T_g) \leq \tau \leq -a$

In that case, the filter $g$ overlaps with the whole rectangular window and

$$A_{\Pi_T,g}(\tau,\nu) = \sum_{k\in\mathbb{Z}} G_k e^{-j2\pi k\frac{\tau}{T_g}} \int_0^{T} e^{j2\pi t(\frac{k}{T_g}+\nu)} dt \tag{A.8}$$

In order to give a simplified expression of $A_{\Pi_T,g}(\tau,\nu)$ in all the listed cases, we derive in the following lines the generic expression of $I_b^c = \int_b^c e^{j2\pi t(\frac{k}{T_g}+\nu)}$.

$$I_b^c = \frac{e^{j2\pi c(\frac{k}{T_g}+\nu)} - e^{j2\pi b(\frac{k}{T_g}+\nu)}}{j2\pi(\frac{k}{T_g}+\nu)} \tag{A.9}$$

$$= (c-b)e^{j\pi(\frac{k}{T_g}+\nu)(b+c)}\operatorname{sinc}\left(\pi(\frac{k}{T_g}+\nu)(c-b)\right) \tag{A.10}$$

Putting ($A$.10) into ($A$.5) – ($A$.8), we obtain the expression of (A.11) for $A_{\Pi_T,g}(\tau,\nu)$.

$$A_{\Pi_T,g}(\tau,\nu) =$$

$$\begin{cases} 0, & \tau > T-a \text{ or } \tau < -(a+T_g). \\ (a+\tau+T_g)e^{j\pi\nu(a+\tau+T_g)} \sum\limits_{k\in\mathbb{Z}} G_k e^{j\pi\frac{k}{T_g}(a-\tau+T_g)} \operatorname{sinc}(\pi(\frac{k}{T_g}+\nu)(a+\tau+T_g)), & -(a+T_g) \le \tau \le T-(a+T_g) \\ (T-(a+\tau))e^{j\pi\nu(a+\tau+T)} \sum\limits_{k\in\mathbb{Z}} G_k e^{j\pi\frac{k}{T_g}(a-\tau+T)} \operatorname{sinc}(\pi(\frac{k}{T_g}+\nu)(T-(a+\tau))), & -a \le \tau \le T-a \\ Te^{j\pi\nu T} \sum\limits_{k\in\mathbb{Z}} G_k e^{j\pi\frac{k}{T_g}(T-2\tau)} \operatorname{sinc}(\pi(\frac{k}{T_g}+\nu)T), & T-(a+T_g) \le \tau \le -a \end{cases} \tag{A.11}$$

# Appendix B

# SCEE Testbed

Testbeds are becoming an increasingly important part of research on wireless communication. Indeed, given the increasing complexity of communication networks, it is not always feasible to tackle all aspects of a problem through theoretical analysis only. Therefore, a large number of research groups have constituted testbeds with different capabilities. Famous examples include the Iris testbed at Trinity College Dublin[1] [159], the 5G USRP testbed at KU Leuven described in [160][2] and the CorteXlab at INSA Lyon in France [161][3].

## B.1 Testbed presentation and layout

The SCEE Testbed is a software radio platform that has been designed, built and managed by the different PhD students of SCEE research team at CentraleSupelec. The aforementioned testbeds offer remote access to a variety of hardware components and important software capabilities. However, it is sometimes necessary to have access to these tools on-site as the remote access does not necessarily enable users to obtain the hardware configurations they desire, which is why we decided to build the SCEE Testbed, which is much less ambitious than previously mentioned platforms but is more convenient to use on a day-to-day basis. Its goal is to provide the students and professors of the research team, as well as undergrad students interested in wireless communications, with a simple to access, hassle-free radio experimentation platform. The experiment presented in chapter 4 has been performed on top of this testbed. Here, we present its architecture in more details.[4]

[1] https://iris-testbed.connectcentre.ie/

[2] http://www.esat.kuleuven.be/telemic/research/NetworkedSystems/networked-systems-infrastructure

[3] http://www.cortexlab.fr

[4] Videos of most experiments that are run on top of the SCEE testbed can be found on SCEE youtube channel: https://goo.gl/8XeJqs

Table B.1: USRPS available in SCEE Testbed

| Model | Mounted daughter-board | Transmit frequencies | Bandwidth | Quantity | Comment |
|---|---|---|---|---|---|
| N210 | SBX | 400 MHz - 4.4 GHz | 40 MHz | 10 | Used for most day-to-day experiments |
| X310 | UBX-160 × 2 | 10 MHz - 6 GHz | 160 MHz | 1 | Used for FPGA reconfiguration applications |
| E110 | WBX | 50 MHz - 2.2 GHz | 40MHz | 2 | Standalone USRP equipped with an embedded processor. |
| B210 | N/A | 70 MHz - 6 GHz | 56 MHz | 1 | USB powered, small form-factor convenient USRP easily usable by students |

The testbed structure itself simply consists of a wooden shelf composed of 5 levels. The two upper levels as well as the two bottom levels are composed of five casings which can each house one USRP. In total, the structure can therefore house twenty USRPs. The center level on the other hand is supposed to house larger instrumentation such as the gigabit ethernet switch and the clock distribution module. Furthermore, gaps between the different levels of the structure have been designed to allow for easy and elegant cabling.

## B.2 Available hardware material

We list the USRPs that are available in the SCEE testbed in Table B.1. Most day-to-day experiments and demonstrations are run with N210 USRPs that are available in a large amount. Other experimentations with specific needs can be performed on either the available X310, E110 or B210 USRPs. All additional material is referenced in Table B.2, where we have referenced the different network components, antennas and spare daughterboards available at the testbed. Note that we have not drawn an extensive list of all SMA, ethernet or MIMO cables but they are of course available in sufficient quantity.

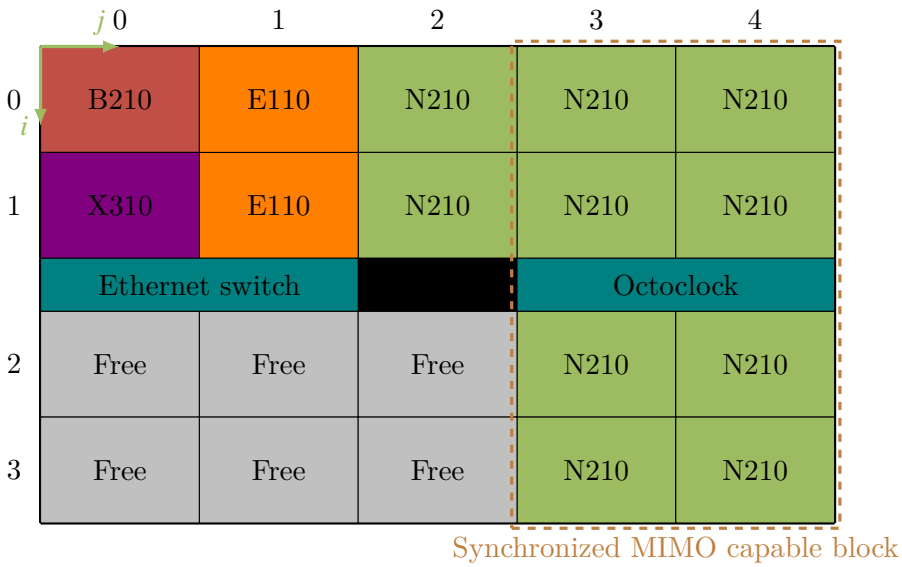


Figure B.1: Testbed organization and USRP identification

## B.3 Testbed organization and network architecture

The testbed is organized as a (4,5) matrix, and each USRP is identified by its id $5i+j+1$ where $i$ indexes rows and $j$ columns. Note that index start at 0. The grid indexation and USRP identification method is detailed in Fig. B.1. For example, according to our identification scheme, the USRP B210 has id 1 and the 2 USRP E110 have respectively ids 2 and 7. In Fig. B.1, we also show that the 8 USRP N210 hosted in columns 3 and 4 compose a fully synchronized block. Indeed, each of them is connected to the octoclock. Furthermore, they are connected in pairs via MIMO cables, which makes it possible to perform $4 \times 4$ MIMO transmission and reception. In details, the USRPs are connected in pairs as follows: (4,9), (5, 10), (14, 19) and (15, 20). Note that 6 compartments are still free and can be used in the future to make the testbed evolve.

In Fig.B.2, we represent the ethernet cabling plan of the testbed. As we see, the Gb ethernet switch disposes of 24 ports. 20 of them are therefore dedicated to USRP communication and we have represented on each of them the id of the testbed compartment it should be connected to. The 4 ports on the left side are each assigned a specific purpose: one is reserved for administration purpose and is therefore left free. Just beneath the latter is the port to which the testbed workstation is connected. The octoclock is also connected to one port of the switch. Finally, the port labeled as "local access" can be used to directly plug one's personal computer, which allows anyone to bypass the workstation and execute experimentation software directly on their laptop.

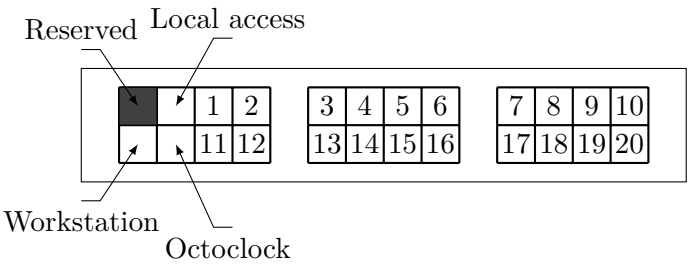


Figure B.2: Ethernet switch cabling

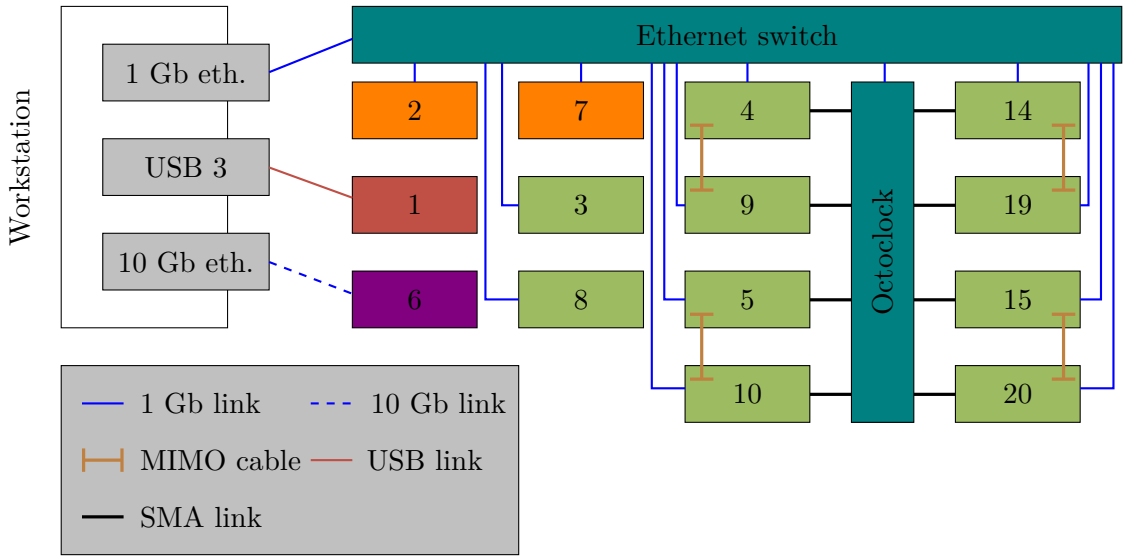


Figure B.3: Detailed cabling diagram of all testbed components. USRPs are represented via their id.

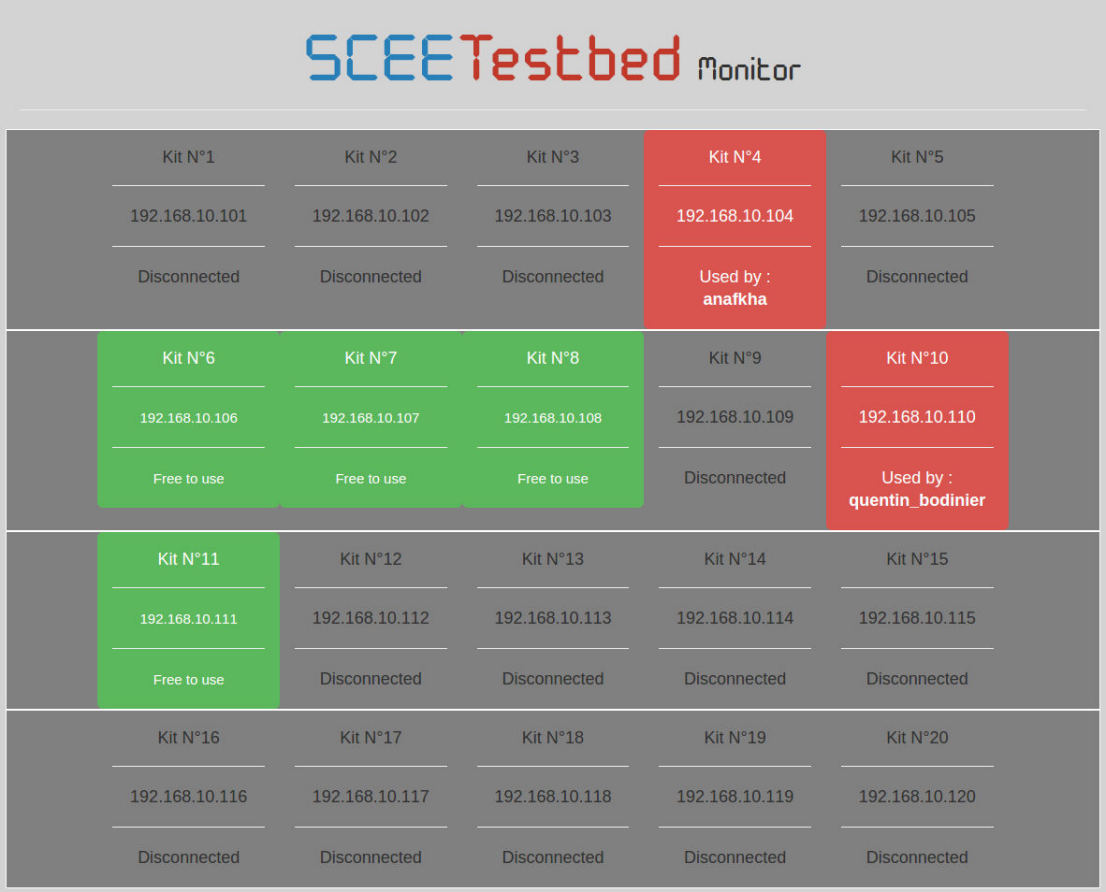


Figure B.4: Interface of the SCEE testbed monitor. This example was captured with a prior testbed configuration that does not correspond to the one we have presented. Here, two different USRPs are used by two different persons, and the monitoring software has successfully detected it.

Note that even if a port of the switch is reserved for each compartment of the testbed, not all USRPs are connected to the former. Indeed, the B210 and X310 USRPs do not have a Gb ethernet interface. The former is plugged onto a USB port of the workstation, while the latter is directly connected to it through a 10 Gb ethernet interface. All these different cablings are summarized in Fig. B.3. All USRPs connected to the ethernet switch are addressed in the same subnet and assigned the ip address 192.168.10.1xx where xx is replaced by their id. For example, USRP 7 is addressed as 192.168.10.107.

## B.4 Usage monitoring

The main goal of this testbed is to make it easy for multiple people to access it and run experiments at the same time. Therefore, multiple people could try to access the same USRP

at the same time. Unfortunately and quite surprisingly, no locking mechanism is implemented by the USRP drivers, so that it is impossible to prevent an USRP from being preempted by someone while it is used in an experiment. Therefore, we have implemented a usage monitor which makes it possible, via a web application, to see in real time what USRPs are used and by whom.

The software, available online at https://goo.gl/6FAHLU, is based on a Python Flask web server. The application itself functions by monitoring all UDP and TCP sockets that are opened from the workstation to any of the IP addresses corresponding to the testbed USRPs. If it detects a relevant socket, the software then retrieves the associated pid which enables it to find who is using the USRP in question. This process is executed at a customizable frequency. Once the state of each monitored IP has been retrieved, the web server updates the interface. A snapshot of the said interface is shown in Fig. B.4. This monitoring system has proven to be quite easy to use and is an efficient way to share resources fairly between all persons accessing the testbed. Furthermore, it can be adapted quite easily to any USRP testbed architecture.

Table B.2: Other hardware

| **Hardware material** | |
|---|---|
| Designation | Details |
| Dell Inspiron T5810 Workstation | Workstation used to access all USRPs<br>*OS:* Ubuntu 16.04.2 LTS<br>*CPU:* Intel Xeon E5-1650 v4 @ 3.6 GHz<br>*Memory:* 4 × 8 Go DDR4 SDRAM<br>*Network interfaces:* Gb ethernet × 2, 10Gb ethernet × 2 |
| Gb Ethernet Switch | 24-ports Switch used to connect all USRPs and the workstation |
| OctoClock-G CDA-2990 | 8-Channel clock distribution module |

| **Spare daughterboards** | | | |
|---|---|---|---|
| Model | Transmit Frequencies | Bandwidth | Quantity |
| WBX | 50 MHz - 2.2 GHz | 40 MHz | 4 |
| CBX | 1.2 GHz - 6 GHz | 40 MHz | 1 |

| **Antennas** | | | |
|---|---|---|---|
| Model | Transmit Frequencies | Details | Quantity |
| Vert2450 | Dual-band,<br>2.4 - 2.48 GHz &<br>4.9 - 5.9 GHz | omni-directional,<br>3dBi Gain | 28 |
| Vert900 | Dual-band,<br>824 - 960 MHz &<br>1710 - 1990 MHz | omni-directional,<br>3dBi Gain | 5 |
| Vert400 | Tri-band,<br>144 MHz,<br>400 MHz &<br>1200 MHz | omni-directional | 28 |
| LP0965 | Log-periodic,<br>850 MHz - 6.5 GHz | Directional antenna,<br>5-6 dBi gain | 1 |
| LP0410 | Log-periodic,<br>400 MHz - 1 GHz | Directional antenna,<br>5-6 dBi gain | 1 |

# Appendix C

# Network-level simulator

Network and system-level simulators, just like testbeds, make it feasible to investigate network deployments that are too complex to be thoroughly analyzed with theoretical tools only. In the field of wireless communications, two major network simulators are used. First, ns-3[1] is a discrete-event network simulator for Internet systems, that can be used to simulate the whole OSI stack. However, because it is based on discrete-event simulations, it requires the communication process to be very precisely detailed. Another alternative is the Vienna LTE-A simulator[2] which is designed specifically to simulate LTE-A networks. However, it suffers from a limited documentation and community and therefore from a quite long learning curve. For all these reasons, we have decided to implement our own network simulator to run the simulation campaigns presented in the network level study of section 6.3. It is not the purpose of this manuscript to present a detailed documentation of the developed software, but we describe its organization and some key elements in the following.

## C.1 Simulator description

The network simulator has been developed in Python 2 and follows an object-oriented paradigm. The simplified class diagram is presented in Fig. C.1, in which we show that the simulator is organized in 4 distinct packages. Note that attributes and methods are not displayed in order to keep the diagram readable. The 4 packages are as follows:

– **Network Physical Description:** this package contains classes that represent the different elements of the network. The Network is composed of Cells, that are themselves composed of Sectors. In each Sector, there are a number of D2DPairs and CUs.

[1] https://www.nsnam.org/

[2] https://www.nt.tuwien.ac.at/research/mobile-communications/vccs/vienna-lte-a-simulators/

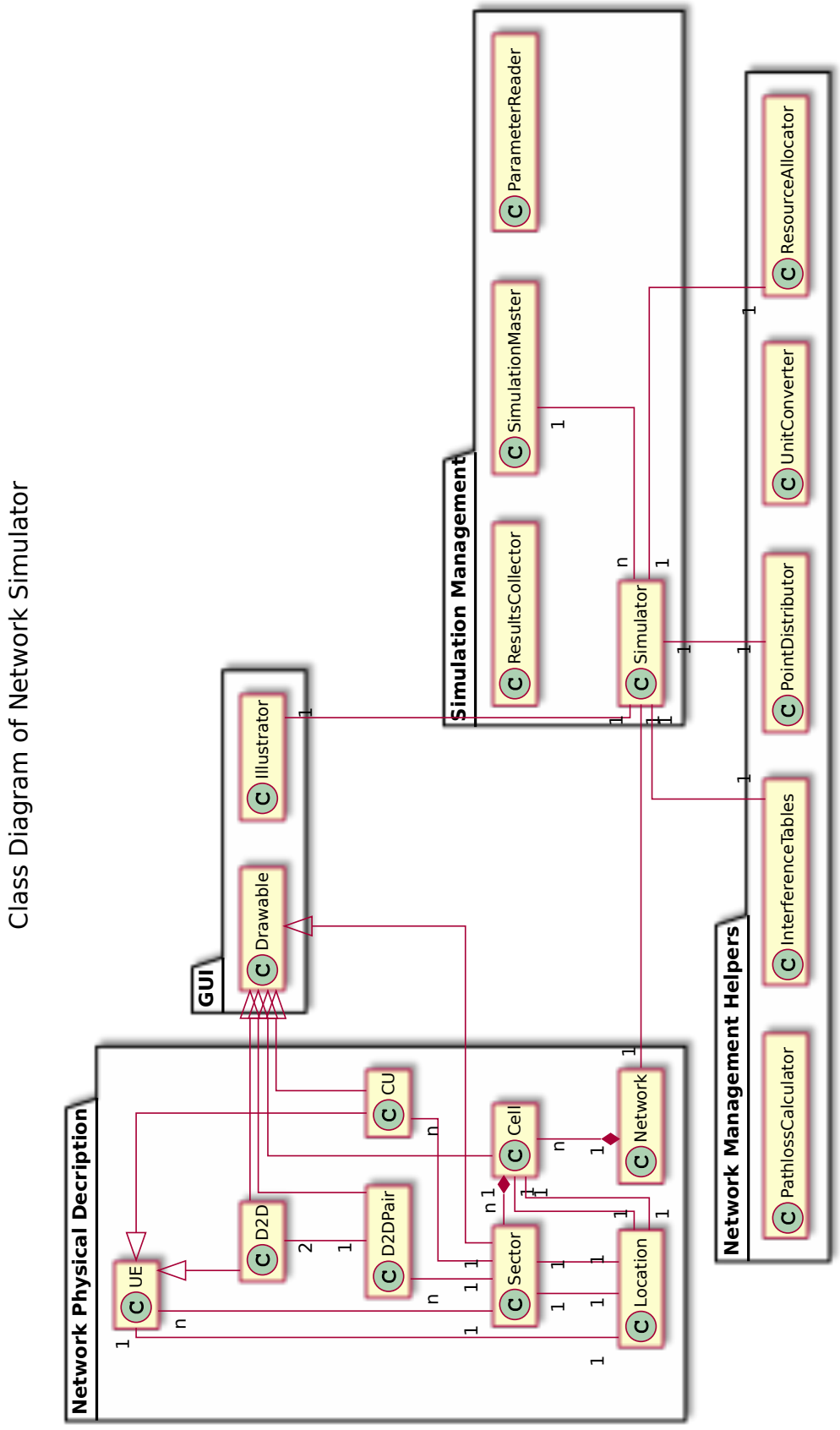


Figure C.1: Class diagram of the Network Simulator

D2DPairs are composed of two D2D users. D2D and CU classes extend the UE class. Furthermore, UEs, Sectors and Cells have a Location.

- **Network Management Helpers:** this package contains classes that provide methods necessary to manage the network and measure its performance. First, the PathlossCalculator class provides static methods that can be used to compute the Pathloss between different elements of the Network. The PointDistributor is in charge of distributing the locations of users according to different point processes. The ResourceAllocator allocates resources according to the specified policies. The InterferenceTables class is used to access leakage interference tables related to the waveform used by each device. Finally, the UnitConverter is a helper class that provides static methods that can be used to convert values, for example from linear to log scales.
- **Simulation Management:** this package is in charge of managing the simulation process. The Simulator class is the cornerstone of the software, as it simulates the Network with the help of the Network Management Helper classes. The SimulationMaster class is the entry point of the software. It reads the simulation parameters file thanks to the ParameterReader class. It then creates $n$ instances of the Simulator class that run simulations in parallel. The ResultsCollector class is used, as its name indicates, to collect results generated by each Simulator.
- **GUI:** the GUI package is in charge of the graphical display of the simulator. In particular, the Illustrator class handles the plotting of the different network elements. Note that only Classes that extend the Drawable class correspond to elements that can be drawn. This includes the classes CU, D2D, D2DPair, Sector and Cell.

## C.2 Simulation parameters

A variety of parameters can be fed to the simulator via the use of a configuration file. Here is a typical configuration file:

```
[SystemSettings]
SectorRadius: 500
InnerRadius: 325
NumCellRings: 2
CUsPerSquareKm: 200
D2DsPerSquareKm: 30
D2DsPerCluster: 30
ClustersPerSquareKm: 3
AverageClusterRadius: 60
MinTxRxDistance: 5
MaxTxRxDistance: 50
```

```
D2DPointProcess: matern
D2DRbAllocator: random:unique
D2DPowerAllocator: max
CuRbAllocator: random:unique
CuPowerAllocator: openloop
IndoorDUEtoDUEPathlossModel: B3
OutdoorDUEtoDUEPathlossModel: C4m
IndoorUEtoBSPathlossModel: C4
OutdoorUEtoBSPathlossModel: C2
IndoorCUEtoDUEPathlossModel: B3
OutdoorCUEtoDUEPathlossModel: C4m
CarrierFrequency: 2e9
NoisePerRB: -116
ICIon: True
FR: 3
FFR: strict
ResultsType: sinr
MaxTO: 1
MaxLOppm: 2.5
InterfMode: spec

[CellSettings]
NumRBs: 50
NumSectors: 1
PPusch: -96
Alpha: 1

[UESettings]
MaxTxPowerCU: 24
MaxTxPowerD2D: 0
CuMinSINR: 10
Waveforms: OFDM, FMT, FBMCOQAM, FBMCPAM, GFDM, fOFDM, UFMC
```

The parameters in the section SystemSettings specify system-wide parameters as follows:

- SectorRadius: The radius of each sector in m.
- InnerRadius: The radius of the inner section of each sector in m, in the case where FFR is used.
- NumCellRings: Indicates the number of cell rings to consider. If put equal to 0, only the center cell of interest is generated and considered in the simulation. If it is equal to 1, the cells directly adjacent to the center cell are also considered. It is preferable to

set NumCellRings=2 in order to simulate two rings of adjacent cells (19 cells in total) to fully grasp the effects if inter-cell interference.

- CUsPerSquareKm: density of CUs in the network
- D2DsPerSquareKm: density of D2Ds in the network in the case where D2DPointProcess is set to poisson
- D2DsPerCluster and ClustersPerSquareKm: density of cluster centers and number of D2DsPerCluster in the case where D2DPointProcess=matern which corresponds to the case where D2D users are distributed in clusters.
- AverageClusterRadius: average radius of the D2D clusters. The actual radius of each cluster is drawn from a normal distribution with the set average and a variance equal to one tenth of the set average.
- MinTxRxDistance and MaxTxRxDistance: minimum and maximum distance between two members of a D2D pair. The actual distance is drawn uniformly between these two bounds
- D2DPointProcess: can be set to poisson to distribute D2D pairs uniformly or matern to use a clustered distribution.
- D2DRbAllocator: sets the resource allocation strategy used by DUEs. Can be:
  - random : assign RBs completely randomly to DUEs.
  - random:unique : assign one random RB only to each D2Dpair while making sure that each RB is assigned to only one D2D pair.
  - random:fullyloaded : assign RBs randomly to DUEs while making sure that all RBs are used.
  - min:interference : finds the optimal RB allocation that minimizes the total interference created by CUs on D2D pairs.
  - greedy : each D2D pair selfishly selects the RB allocation that minimizes the interference it suffers from CUs.
- D2DPowerAllocator : sets the power allocation strategy used by DUEs. Can be:
  - max : assigns maximum allowed transmit power to DUEs
  - openloop : use openloop power control to set DUEs transmit power
- CuRbAllocator: sets the resource allocation strategy used by CUEs. Can be:
  - random : assign RBs completely randomly to CUEs.

  - random:unique : assign one random RB only to each CUE while making sure that each RB is assigned to only one CUE.
  - random:fullyloaded : assign RBs randomly to CUEs while making sure that all RBs are used.

- CUPowerAllocator : sets the power allocation strategy used by CUEs. Can be:
  - max : assigns maximum allowed transmit power to CUEs
  - openloop : use openloop power control to set CUEs transmit power
- TypeOfLinkPathlossModel: pathloss model associated with the considered TypeOfLink. Can be chosen from the different Winner pathloss models.
- CarrierFrequency: value of the carrier frequency in Hz.
- NoisePerRB: noise power per RB in dBm.
- ICIon: can be True or False. Used to specify if the inter-cell interference should be taken into account.
- FR: Frequency Reuse Factor. Can be 1 or 3.
- FFR: can be set to strict or soft.
- ResultsType: specify the type of results to return after simulations. Can be SINR, rate or rx_pow (received power).
- MaxTO: maximum timing offset value relative to $\frac{1}{\Delta F}$.
- MaxLOppm: maximum LO inacurracy in ppm.
- InterfMode: specifies the way that values are drawn from interference tables. Can be:
  - spec: uniformly draw a specific value of timing offset and CFO in the intervals set by MaxTO and MaxLOppm.
  - mean: always use the average values of interference in the timing offset and CFO intervals set by MaxTO and MaxLOppm.
  - max: always use the maximum values of interference in the timing offset and CFO intervals set by MaxTO and MaxLOppm.

The parameters in the sections CellSettings and UESettings specify cell-specific and UE parameters as follows:

- NumRBs: number of RBs in the frequency band.

- NumSectors: number of sectors in each cell
- PPusch and Alpha: parameters related to the openloop power control
- MaxTxPowerCU and MaxTxPowerD2D: maximum transmit power of each type of user in dBm
- CuMinSINR: Minimum SINR required by cellular users
- Waveforms: set of waveforms to be tested

## C.3 Simulation Workflow

In order to run a simulation batch, one has to call the script `run.py` which is used as follows:

```
usage: run.py [-h] [-f CONF_FILE] [-p] [-d] [-t] [-n ITERATIONS_NUMBER]
              [-j PARALLEL_JOBS] [-o OUTPUT_FOLDER]

optional arguments:
  -h, --help            show this help message and exit
  -f CONF_FILE, --conf_file CONF_FILE
                        input configuration file with simulation parameters
  -p, --profile         enable profiling
  -d, --disable-graphics
                        disable graphics outputs
  -t, --time            simple measure of execution time
  -n ITERATIONS_NUMBER, --iterations-number ITERATIONS_NUMBER
                        number of Monte Carlo iterations to process
  -j PARALLEL_JOBS, --parallel-jobs PARALLEL_JOBS
                        Number of jobs run in parallel
  -o OUTPUT_FOLDER, --output-folder OUTPUT_FOLDER
                        Output Folder
```

When the script starts, it creates an instance of the SimulationMaster class. The latter parses the configuration file thanks to the ParameterReader class. It then creates multiple objects Simulator objects and calls their method `Simulator.run` which is in charge of running the simulation on one network realization. The workflow of the `Simulator.run` method is as follows: first, the cells and sectors of the network are generated according to the specified parameters. Then, CUEs and DUEs are generated and distributed according to the specified densities. Afterwards, spectral resources are allocated to users according to the selected policies. At this point, two directed graphs representing the interfering and useful links of the

network are generated. In these graphs, each edge is weighted with its associated pathloss. These graphs are used as an input to assign the transmit power to every user. Then, the SINR (or whatever result type has been specified in the configuration file) of each UE is computed. The results of each simulation are fetched asynchronously by the SimulationMaster through an instance of the ResultsCollector class. The SimulationMaster then appends them to a CSV file which gathers the results from all iterations of the simulation. The obtained file can then be parsed to analyze and plot the results.

# Appendix D

# Publications and Involvement in R&D Projects

## Publications related to the thesis

The contributions related to the works presented in this manuscript are listed here:

### Journal articles

[J1] Conor Sexton, Quentin Bodinier, Arman Farhang, Nicola Marchetti, Faouzi Bader, and Luiz A. DaSilva. "Coexistence between D2D and Cellular Communications Using Multiple Waveforms in 5G". *IEEE Trans. Vehicular Tech.* (2017 (submitted))

[J2] Q. Bodinier, F. Bader, and J. Palicot. "On Spectral Coexistence of CP-OFDM and FB-MC Waveforms in 5G Networks". *IEEE Access* 5 (2017), pp. 13883–13900. DOI: 10.1109/ACCESS.2017.2723822

### International conferences

[C1] C. Sexton, Q. Bodinier, A. Farhang, N. Marchetti, F. Bader, and L. A. DaSilva. "Coexistence of OFDM and FBMC for Underlay D2D Communication in 5G Networks". *2016 IEEE Globecom Workshops (GC Wkshps)*. 2016, pp. 1–7. DOI: 10.1109/GLOCOMW.2016.7848863

[C2] Q. Bodinier, F. Bader, and J. Palicot. "Coexistence in 5G: Analysis of Cross-Interference between OFDM/OQAM and Legacy Users". *IEEE Globecom Workshops (GC Wkshps)*. 2016, pp. 1–6. DOI: 10.1109/GLOCOMW.2016.7848862

[C3] Q. Bodinier, F. Bader, and J. Palicot. “Coexistence of filter banks and CP-OFDM: What are the real gains?” *International Symposium on Wireless Communication Systems (ISWCS)*. 2016, pp. 628–632. DOI: 10.1109/ISWCS.2016.7600980

[C4] Q. Bodinier, F. Bader, and J. Palicot. “Modeling interference between OFDM/OQAM and CP-OFDM: Limitations of the PSD-based model”. *23rd International Conference on Telecommunications (ICT)*. 2016, pp. 1–7. DOI: 10.1109/ICT.2016.7500462

[C5] Q. Bodinier, A. Farhang, F. Bader, H. Ahmadi, J. Palicot, and L. A. DaSilva. “5G waveforms for overlay D2D communications: Effects of time-frequency misalignment”. *IEEE International Conference on Communications (ICC)*. 2016, pp. 1–7. DOI: 10.1109/ICC.2016.7511285

[C6] A. Bourrous, L. Iacobelli, M. Pischella, R. Zakaria, A. Dziri, A. Untersee, O. Rousset, Q. Bodinier, and F. Bader. “ACCENT5: a Vision for D2D Communications within 5G Networks”. *14th International Symposium on Wireless Communication Systems (ISWCS)*. 2017

### Demonstrations

[D1] Q. Bodinier, M. Zhang and F. Bader, "Coexistence of systems based on 5G waveforms with legacy OFDM devices", *12th EAI International Conference on Cognitive Radio Oriented Wireless Networks (CROWNCOM)*, 2017.

### Technical deliverables

[TR1] French ANR-funded project ACCENT5, D1.2 : "Advanced FB-MC for D2D Communications", *technical contribution*

[TR2] French ANR-funded project ACCENT5, D2.2 : "Energy efficient power controls and interference mitigation (second issue)", *technical contribution and lead edition*

### Talks without proceedings

[T1] Q. Bodinier, "Coexistence of Communication Systems based on Heterogeneous Waveforms in 5G Wireless Networks", *SCEE research team seminar*, 2017

## Publications indirectly related to this thesis

During my Ph.D., I have had the opportunity to work on broader research aspects indirectly related to this thesis, in the fields of waveform design, energy-efficient techniques for wireless networks, and Full Duplex techniques. The relevant published works are listed here.

### International conferences

[C7] M. Caus, A. I. Perez-Neira, A. Kliks, Q. Bodinier, and F. Bader. "Capacity analysis of WCC-FBMC/OQAM systems". *IEEE International Conference on Acoustics, Speech and Signal Processing (ICASSP)*. 2016, pp. 3916–3920. DOI: 10.1109/ICASSP.2016.7472411

[C8] M. Naoues, Q. Bodinier, and J. Palicot. "Cognitive Green Radio for Energy-Aware Communications". *URSI Scientific Days*. 2016

[C9] T. Vial, A. Lefevre, M. Le Penven, and Q. Bodinier. "A Short Review of Current Challenges and Potential Applications of Full Duplex in Wireless Networks". *32nd International Union of Radio Science General Assembly & Scientific Symposium (URSI GASS)*. 2017

### Demonstrations

[D2] M. Naoues, Q.Bodinier, and J. Palicot, "WiFi-Based Platform for Energy Saving in Wireless Networks", *11th EAI International Conference on Cognitive Radio Oriented Wireless Networks (CROWNCOM)*, 2016.

[D3] M. Naoues, H. Noureddine, Q.Bodinier, H.Zhang and J. Palicot, "WiFi-Based Platform for Energy Saving in Wireless Networks", *IEEE Online GreenComm*, 2014.

### Technical deliverables

[TR3] European project Newcom #, D13.3 : "Overall assessment of selected techniques on energy and bandwidth-efficient communications", *technical contribution*

### Talks without proceedings

[T2] Q. Bodinier, "Can mankind achieve green communications while chasing Pokemon ?", *4th International Workshop on Next Generation Green Wireless Networks (Next-GWiN), Ph.D. Student Challenge (Winner)*, 2016, Dublin.

# Involvement in R&D Projects

## ACCENT5

ACCENT5 is a French project funded by the ANR under Grant agreement ANR-14-CE28-0026. Its goal is to study the coexistence of D2D and cellular communications in future 5G networks. My role in this project has been to study the impact of the waveform used by the two kinds of users on their coexistence capabilities. The results of this research have been largely presented in this manuscript. Publications [C1-C6] and [J1] directly contribute to this project. Furthermore, I actively participated in the project by taking part in most technical meetings (4 per year) and contributing in several deliverables [TR1, TR2] including one as lead editor [TR2].

## NEWCOM #

NEWCOM #[1] was a European project (project code: FPT-ICT-318306) that aimed at fostering research collaboration among institutions from different countries and pursuing research on topics seen as strategic by the European Commission. One of the actions undertaken by NEWCOM # consists in promoting the mobility of young researchers by attributing mobility grant on a competitive basis. I have been the recipient of one of those grants, which funded a mobility of one month at the Centre Tecnològic Telecomunicacions Catalunya (CTTC) in Barcelona, Spain. The research works undertaken during this mobility have led to the publication of [C7] and were included in one of Newcom # deliverables [TR3]. Furthermore, some discussions I had with researchers there during this visit were instrumental to the later publication of [C3].

## PHC ULYSSES

Partenariats Hubert Curien (PHC) are bilateral mobility funding schemes that are handled by the French ministry for foreign affairs. ULYSSES is the PHC which funds collaborative research between French and Irish institutions. We succesfully applied for this funding scheme together with CONNECT Research Centre back in 2014. The obtained grant (code 34151SA) enabled me to visit CONNECT twice during the year 2015. These visits gave birth to [C5] and, more broadly speaking, to a collaboration that is still going on today, as [C1] and [J1] are joint works between our team SCEE and the researchers at CONNECT.

[1] http://www.newcom-project.eu

# Bibliography


[1] J. G. Andrews et al. "What Will 5G Be?" *IEEE J. Sel. Areas Commun.* 32.6 (2014), pp. 1065–1082. ISSN: 0733-8716. DOI: 10.1109/JSAC.2014.2328098.

[2] Gerhard Wunder and Ivan Simoes Gaspar. *5GNOW - 5G Cellular Communications Scenarios and System Requirements*. Tech. rep. 5GNOW Project Consortium, 2013.

[3] *White Paper - 5G Use Cases and Requirements*. Tech. rep. Nokia.

[4] S. E. Elayoubi et al. "5G service requirements and operational use cases: Analysis and METIS II vision". *European Conference on Networks and Communications (EuCNC)*. 2016, pp. 158–162. DOI: 10.1109/EuCNC.2016.7561024.

[5] *TR 36.802 V1.0.0: NB-IoT Technical Report for BS and UE radio transmission and reception*. Tech. rep. 3GPP.

[6] *TRP-150492, 3GPP Work Item on Further LTE Physical Layer Enhancements for MTC*. Tech. rep. 3GPP.

[7] C. Sexton et al. "5G: Adaptable Networks Enabled by Versatile Radio Access Technologies". *IEEE Commun. Surveys Tuts.* PP.99 (2017), pp. 1–1. ISSN: 1553-877X. DOI: 10.1109/COMST.2017.2652495.

[8] A. Gupta and R. K. Jha. "A Survey of 5G Network: Architecture and Emerging Technologies". *IEEE Access* 3 (2015), pp. 1206–1232. ISSN: 2169-3536. DOI: 10.1109/ACCESS.2015.2461602.

[9] R. Zhang et al. "LTE-unlicensed: the future of spectrum aggregation for cellular networks". *IEEE Wireless Commun. Mag.* 22.3 (2015), pp. 150–159. ISSN: 1536-1284. DOI: 10.1109/MWC.2015.7143339.

[10] L. Doyle et al. "Spectrum Without Bounds, Networks Without Borders". *Proc. of the IEEE* 102.3 (2014), pp. 351–365. ISSN: 0018-9219. DOI: 10.1109/JPROC.2014.2302743.

[11] Ian F. Akyldiz et al. "NeXt generation/dynamic spectrum access/cognitive radio wireless networks: A survey". *Computer Networks* 50 (2006), pp. 2127–2159. ISSN: 13891286. DOI: 10.1016/j.comnet.2006.05.001.

[12] M. Lopez-Benitez, A. Umbert, and F. Casadevall. "Evaluation of Spectrum Occupancy in Spain for Cognitive Radio Applications". *VTC Spring - IEEE 69th Vehicular Technology Conference*. 2009, pp. 1–5. DOI: 10.1109/VETECS.2009.5073544.

[13] M. Wellens and P. Mahonen. "Lessons learned from an extensive spectrum occupancy measurement campaign and a stochastic duty cycle model". *5th International Conference on Testbeds and Research Infrastructures for the Development of Networks Communities and Workshops*. 2009, pp. 1–9. DOI: 10.1109/TRIDENTCOM.2009.4976263.

[14] A. Al-Dulaimi et al. "5G Communications Race: Pursuit of More Capacity Triggers LTE in Unlicensed Band". *IEEE Veh. Technol. Mag.* 10.1 (2015), pp. 43–51. ISSN: 1556-6072. DOI: 10.1109/MVT.2014.2380631.

[15] T. Pollet, M. Van Bladel, and M. Moeneclaey. "BER sensitivity of OFDM systems to carrier frequency offset and Wiener phase noise". *IEEE Trans. Commun.* 43.2/3/4 (1995), pp. 191–193. ISSN: 0090-6778. DOI: 10.1109/26.380034.

[16] Babar Aziz, Inbar Fijalkow, and Myriam Ariaudo. "Intercarrier interference in uplink OFDMA systems with carrier frequency offset". *21st Annual IEEE International Symposium on Personal, Indoor and Mobile Radio Communications* (Sept. 2010), pp. 746–751. DOI: 10.1109/PIMRC.2010.5671922.

[17] H. Mahmoud, T. Yucek, and H. Arslan. "OFDM for cognitive radio: merits and challenges". *IEEE Wireless Commun. Mag.* 16.April (2009), pp. 6–15. ISSN: 1536-1284. DOI: 10.1109/MWC.2009.4907554.

[18] Leonardo G. Baltar, Dirk S. Waldhauser, and Josef A. Nossek. "Out-Of-Band Radiation in Multicarrier Systems: A Comparison". *Multi-Carrier Spread Spectrum 2007*. Vol. 1. Springer Netherlands, 2007, pp. 107–116. ISBN: 978-1-4020-6128-8. DOI: 10.1007/978-1-4020-6129-5.

[19] P. Banelli et al. "Modulation Formats and Waveforms for 5G Networks: Who Will Be the Heir of OFDM?: An overview of alternative modulation schemes for improved spectral efficiency". *IEEE Signal Process. Mag.* 31.6 (2014), pp. 80–93. ISSN: 1053-5888. DOI: 10.1109/MSP.2014.2337391.

[20] B. Farhang-Boroujeny. "OFDM Versus Filter Bank Multicarrier". *IEEE Signal Process. Mag.* 28.3 (2011), pp. 92–112. ISSN: 1053-5888. DOI: 10.1109/MSP.2011.940267.

[21] M Bellanger. *FBMC physical layer: a primer*. Tech. rep. Project PHYDYAS, 2010.

[22] M. Renfors and X. Mestre and E. Kofidis and F. Bader, ed. *Orthogonal Waveforms and Filter Banks for Future Communication Systems*. Elsevier Academic Press, 2017. ISBN: 9780128103845.

[23] CE Shannon. "A mathematical theory of communication". *Bell System Technical Journal* 27 (1948).

[24] Pekka Kyösti et al. *IST-4-027756 WINNER II D1.1.2 V1.2 - WINNER II Channel Models*. Tech. rep. WINNER II Consortium, 2008.

[25] Vincent Savaux. "Contributions to multi-paths channel estimation in OFDM context". PhD thesis. Supélec, 2013.

[26] Raj Jain. "Channel models: A tutorial". *WiMAX forum AATG*. 2007, pp. 1–6.

[27] S. Weinstein and P. Ebert. "Data Transmission by Frequency-Division Multiplexing Using the Discrete Fourier Transform". *IEEE Trans. Commun. Technol.* 19.5 (1971), pp. 628–634. ISSN: 0018-9332. DOI: 10.1109/TCOM.1971.1090705.

[28] Babar Aziz. "Frequency synchronization for carrier allocation in uplink OFDMA systems". PhD thesis. Université de Cergy Pontoise, Dec. 2011.

[29] Stefania Sesia, Matthew Baker, and Issam Toufik. *LTE-the UMTS long term evolution: from theory to practice*. John Wiley & Sons, 2011. ISBN: 978-0-470-66025-6.

[30] G. Auer et al. "How much energy is needed to run a wireless network?" *IEEE Wireless Commun. Mag.* 18.5 (2011), pp. 40–49. ISSN: 1536-1284. DOI: 10.1109/MWC.2011.6056691.

[31] Q. Zhao and A. Swami. "A Survey of Dynamic Spectrum Access: Signal Processing and Networking Perspectives". *2007 IEEE International Conference on Acoustics, Speech and Signal Processing - ICASSP '07*. Vol. 4. 2007, pp. IV–1349–IV–1352. DOI: 10.1109/ICASSP.2007.367328.

[32] Joseph Mitola. "Cognitive radio: An integrated agent architecture for software defined radio". PhD thesis. Royal Institute of Technology (KTH), 2000. ISBN: 9780471742449.

[33] C. Moy and J. Palicot. "Software radio: a catalyst for wireless innovation". *IEEE Commun. Mag.* 53.9 (2015), pp. 24–30. ISSN: 0163-6804. DOI: 10.1109/MCOM.2015.7263342.

[34] S. Haykin. "Cognitive radio: brain-empowered wireless communications". *IEEE J. Sel. Areas Commun.* 23.2 (2005), pp. 201–220. ISSN: 0733-8716. DOI: 10.1109/JSAC.2004.839380.

[35] Ian F. Akyildiz, Brandon F. Lo, and Ravikumar Balakrishnan. "Cooperative spectrum sensing in cognitive radio networks: A survey". *Phys. Comm.* 4.1 (Mar. 2011), pp. 40–62. ISSN: 18744907. DOI: 10.1016/j.phycom.2010.12.003.

[36] Z. Khan et al. "Autonomous Sensing Order Selection Strategies Exploiting Channel Access Information". 12.2 (2013), pp. 274–288. ISSN: 1536-1233. DOI: 10.1109/TMC.2011.257.

[37] Michele Morelli, C.-C. Jay Kuo, and Man-On Pun. "Synchronization Techniques for Orthogonal Frequency Division Multiple Access (OFDMA): A Tutorial Review". *Proc. of the IEEE* 95.7 (July 2007), pp. 1394–1427. ISSN: 0018-9219. DOI: 10.1109/JPROC.2007.897979.

[38] Gerhard Wunder et al. *5GNOW - 5G Waveform Candidate Selection*. Tech. rep. 5GNOW Project Consortium, 2013.

[39] FCC. *FCC, ET Docket 03-222, Notice of proposed rule making and order, December 2003*. Tech. rep.

[40] *FCC Third Memorandum Opinion and Order in the matter of unlicensed operation in the TV Broadcast Bands*. Tech. rep. FCC, 2012.

[41] S.J. Shellhammer, A.K. Sadek, and Wenyi Zhang. "Technical challenges for cognitive radio in the TV white space spectrum". *2009 Inf. Theory Appl. Work.* (2009), pp. 323–333. DOI: 10.1109/ITA.2009.5044964.

[42] Chittabrata Ghosh, Sumit Roy, and Dave Cavalcanti. "Coexistence challenges for heterogeneous cognitive wireless networks in TV white spaces". *IEEE Wireless Commun. Mag.* 18.4 (2011), pp. 22–31. ISSN: 15361284. DOI: 10.1109/MWC.2011.5999761.

[43] Michael Fitch et al. "Wireless service provision in TV white space with cognitive radio technology: A telecom operator's perspective and experience". *IEEE Commun. Mag.* 49.3 (2011), pp. 64–73. ISSN: 01636804. DOI: 10.1109/MCOM.2011.5723802.

[44] Tuncer Baykas et al. "Developing a standard for TV white space coexistence: Technical challenges and solution approaches". *IEEE Wireless Commun. Mag.* 19.1 (2012), pp. 10–22. ISSN: 15361284. DOI: 10.1109/MWC.2012.6155872.

[45] Office of Communications. *Implementing TV White spaces*. Tech. rep. February. 2015.

[46] Dominique Noguet, Matthieu Gautier, and Vincent Berg. "Advances in opportunistic radio technologies for TVWS". *EURASIP J. Wirel. Commun. Netw.* 2011.1 (2011), pp. 1–12. ISSN: 1687-1499. DOI: 10.1186/1687-1499-2011-170.

[47] Vincent Berg, Jean-Baptiste Doré, and Dominique Noguet. "A flexible radio transceiver for TVWS based on FBMC". *Microprocessors and Microsystems* 38.8, Part A (2014). 2013 edition of the Euromicro Conference on Digital System Design (DSD 2013), pp. 743 –753. ISSN: 0141-9331. DOI: 0.1016/j.micpro.2014.05.010.

[48] Vincent Berg et al. *QoSMOS Flexible PHY concepts for white spaces – Final Report*. 2009.

[49] Arash Asadi, Qing Wang, and Vincenzo Mancuso. "A survey on device-to-device communication in cellular networks". *IEEE Commun. Surv. Tutorials* 16.4 (2014), pp. 1801–1819. ISSN: 1553877X. DOI: 10.1109/COMST.2014.2319555. arXiv: 1310.0720.

[50] Klaus Doppler et al. "Device-to-device communication as an underlay to LTE-advanced networks". *IEEE Commun. Mag.* 47.12 (2009), pp. 42–49. ISSN: 01636804. DOI: 10.1109/MCOM.2009.5350367.

[51] Daquan Feng et al. "Device-to-device communications underlaying cellular networks". *IEEE Trans. Commun.* 61.8 (2013), pp. 3541–3551. ISSN: 00906778. DOI: 10.1109/TCOMM.2013.071013.120787.

[52] Pavel Mach, Zdenek Becvar, and Tomas Vanek. "In-Band Device-to-Device Communication in OFDMA Cellular Networks: A Survey and Challenges". *IEEE Communications Surveys & Tutorials* XX.XX (2015), pp. 1–1. ISSN: 1553-877X. DOI: 10.1109/COMST.2015.2447036.

[53] Xingqin Lin et al. "An overview of 3GPP device-to-device proximity services". *IEEE Commun. Mag.* 52.4 (2014), pp. 40–48. ISSN: 01636804. DOI: 10.1109/MCOM.2014.6807945. arXiv: 1310.0116.

[54] Mark J. Cannon. "On the design of D2D synchronization in 3GPP Release-12". *2015 IEEE Int. Conf. Commun. Work. ICCW 2015* (2015), pp. 633–638. DOI: 10.1109/ICCW.2015.7247252.

[55] 3GPP TR36.843. *Study on LTE device to device proximity services; Radio aspects (Release 12)*. Tech. rep. 2014.

[56] A. Aminjavaheri et al. "Impact of timing and frequency offsets on multicarrier waveform candidates for 5G". *IEEE Signal Processing and Signal Processing Education Workshop (SP/SPE)*. 2015, pp. 178–183. DOI: 10.1109/DSP-SPE.2015.7369549.

[57] Mohammad Ghadir Khoshkholgh et al. "Connectivity of Cognitive Device-to-Device Communications Underlying Cellular Networks". *IEEE Journal on Selected Areas in Communications* PP.99 (2014), pp. 1–1. ISSN: 0733-8716. DOI: 10.1109/JSAC.2014.2369611.

[58] Hongnian Xing and Markku Renfors. "Investigation of filter bank based device-to-device communication integrated into OFDMA cellular system". *International Symposium on Wireless Communications Systems (ISWCS)*. 2014, pp. 513–518.

[59] P. Wu, P. C. Cosman, and L. B. Milstein. "Resource Allocation for Multicarrier Device-to-Device Video Transmission: Symbol Error Rate Analysis and Algorithm Design". *IEEE Trans. Commun.* PP.99 (2017), pp. 1–1. ISSN: 0090-6778. DOI: 10.1109/TCOMM.2016.2623313.

[60] Mylene Pischella, Rostom Zakaria, and Didier Le Ruyet. "Resource Block level power allocation in asynchronous multi-carrier D2D communications". *IEEE Commun. Lett.* 21.4 (2016), pp. 1–1. ISSN: 1089-7798. DOI: 10.1109/LCOMM.2016.2640273.

[61] Mylene Pischella, Rostom Zakaria, and Didier Le Ruyet. "Weighted sum rate maximization with filtered multi-carrier modulations for D2D underlay communications". *IEEE Int. Symp. Pers. Indoor Mob. Radio Commun. PIMRC*. 2016. ISBN: 9781509032549. DOI: 10.1109/PIMRC.2016.7794592.

[62] David Garcia-Roger et al. "Hardware testbed for sidelink transmission of 5G waveforms without synchronization". *IEEE Int. Symp. Pers. Indoor Mob. Radio Commun. PIMRC* 1 (2016), pp. 0–5. DOI: 10.1109/PIMRC.2016.7794739.

[63] A. Sahin, I. Guvenc, and H. Arslan. "A Survey on Multicarrier Communications: Prototype Filters, Lattice Structures, and Implementation Aspects". *IEEE Communications Surveys Tutorials* 16.3 (2014), pp. 1312–1338. ISSN: 1553-877X. DOI: 10.1109/SURV.2013.121213.00263.

[64] J. Bazzi et al. "Design and Performance Tradeoffs of Alternative Multi-Carrier Waveforms for 5G". *2015 IEEE Globecom Workshops (GC Wkshps)*. 2015, pp. 1–6. DOI: 10.1109/GLOCOMW.2015.7414010.

[65] P. Guan et al. "5G Field Trials: OFDM-Based Waveforms and Mixed Numerologies". *IEEE J. Sel. Areas Commun.* 35.6 (2017), pp. 1234–1243. ISSN: 0733-8716. DOI: 10.1109/JSAC.2017.2687718.

[66] Mathieu Van Eeckhaute et al. "Performance of emerging multi-carrier waveforms for 5G asynchronous communications". *EURASIP J. Wirel. Commun. Netw.* 2017.1 (2017), p. 29. ISSN: 1687-1499. DOI: 10.1186/s13638-017-0812-8. URL: 10.1186/s13638-017-0812-8.

[67] Y. Liu et al. "Waveform Design for 5G Networks: Analysis and Comparison". *IEEE Access* PP.99 (2017), pp. 1–1. ISSN: 2169-3536. DOI: 10.1109/ACCESS.2017.2664980.

[68] Jean-Baptiste Doré et al. "Waveform contenders for 5G: Description, analysis and comparison". *Phys. Commun.* (2017). ISSN: 1874-4907. DOI: 10.1016/j.phycom.2017.05.004.

[69] M. Shafi et al. "5G: A Tutorial Overview of Standards, Trials, Challenges, Deployment, and Practice". *IEEE J. Sel. Areas Commun.* 35.6 (2017), pp. 1201–1221. ISSN: 0733-8716. DOI: 10.1109/JSAC.2017.2692307.

[70] Z. Ankarali, B. Pekoz, and H. Arslan. "Flexible Radio Access Beyond 5G: A Future Projection on Waveform, Numerology Frame Design Principles". *IEEE Access* PP.99 (2017), pp. 1–1. ISSN: 2169-3536. DOI: 10.1109/ACCESS.2017.2684783.

[71] M. Renfors et al. *D2.1 - FB-MC and Enhanced OFDM Schemes*. Tech. rep. Project Metis, 2015.

[72] P. Popovski et al. *D2.4 - Proposed solutions for new radio access*. Tech. rep. Project Metis, 2015.

[73] R. Balian. "Un principe d'incertitude fort en théorie du signal ou en mécanique quantique (French)". *C.R. Acad. Sc. Paris.* 292 (1981), pp. 1357–1362.

[74] F. Low. "Complete Sets of Wave Packets". *A Passion for Physics: Essays in Honor of Geoffrey Chew*. World Scientific Publishing Co Pte Ltd, 1986.

[75] R. W. Chang. "High-Speed Multichannel Data Transmission with Bandlimited Orthogonal Signals". *Bell Syst. Tech. J* 15.6 (1966), pp. 1775–1796.

[76] B. Saltzberg. "Performance of an Efficient Parallel Data Transmission System". *IEEE Trans. Commun. Technol.* 15.6 (1967), pp. 805–811. ISSN: 0018-9332. DOI: 10.1109/TCOM.1967.1089674.

[77] Andrea M. Tonello. "Performance limits for filtered multitone modulation in fading channels". *IEEE Trans. Wireless Commun.* 4.5 (2005), pp. 2121–2135. ISSN: 15361276. DOI: 10.1109/TWC.2005.853872.

[78] Markku Renfors et al. *D2.1 : FB-MC and Enhanced OFDM Schemes*. Tech. rep. EU Project ICT-EMPHATIC, 2013.

[79] Pierre Siohan, Cyrille Siclet, and Nicolas Lacaille. "Analysis and design of OFDM / OQAM systems based on filterbank theory". *IEEE Trans. Signal Process.* 50.5 (2002), pp. 1170–1183. ISSN: 1053587X. DOI: 10.1109/78.995073.

[80] C. Lélé et al. "Channel estimation methods for preamble-based OFDM/OQAM modulations". *European Transactions on Telecommunications* 19.7 (2008), pp. 741–750. ISSN: 1541-8251. DOI: 10.1002/ett.1332.

[81] Vincent Savaux, Faouzi Bader, and Yves Louet. "A Joint MMSE Channel and Noise Variance Estimation for OFDM/OQAM Modulation". *IEEE Trans. Commun.* 6778.c (2015), pp. 1–1. ISSN: 0090-6778. DOI: 10.1109/TCOMM.2015.2476798.

[82] A. I. Pérez-Neira et al. "MIMO Signal Processing in Offset-QAM Based Filter Bank Multicarrier Systems". *IEEE Trans. Signal Process.* 64.21 (2016), pp. 5733–5762. ISSN: 1053-587X. DOI: 10.1109/TSP.2016.2580535.

[83] R. Nissel, S. Schwarz, and M. Rupp. "Filter Bank Multicarrier Modulation Schemes for Future Mobile Communications". *IEEE J. Sel. Areas Commun.* PP.99 (2017), pp. 1–1. ISSN: 0733-8716. DOI: 10.1109/JSAC.2017.2710022.

[84] M. Bellanger, D. Mattera, and M. Tanda. "A filter bank multicarrier scheme running at symbol rate for future wireless systems". *Wireless Telecommunications Symposium (WTS)*. 2015, pp. 1–5. DOI: 10.1109/WTS.2015.7117247.

[85] Gerhard Fettweis, Marco Krondorf, and Steffen Bittner. "GFDM-generalized frequency division multiplexing". *IEEE Vehicular Technology Conference Sping*. 2009, pp. 1–4. ISBN: 9781424425174.

[86] Nicola Michailow et al. "Generalized Frequency Division Multiplexing for 5th Generation Cellular Networks". *IEEE Trans. Commun.* 62.9 (2014), pp. 3045–3061. ISSN: 0090-6778. DOI: 10.1109/TCOMM.2014.2345566.

[87] A. Farhang, N. Marchetti, and L. E. Doyle. "Low-Complexity Modem Design for GFDM". *IEEE Trans. Signal Process.* 64.6 (2016), pp. 1507–1518. ISSN: 1053-587X. DOI: 10.1109/TSP.2015.2502546.

[88] Hao Lin and Pierre Siohan. "Multi-carrier modulation analysis and WCP-COQAM proposal". *EURASIP J. Adv. Signal Process.* 2014.1 (2014), p. 79. ISSN: 1687-6180. DOI: 10.1186/1687-6180-2014-79.

[89] M. Caus et al. "Capacity analysis of WCC-FBMC/OQAM systems". *IEEE International Conference on Acoustics, Speech and Signal Processing (ICASSP)*. 2016, pp. 3916–3920. DOI: 10.1109/ICASSP.2016.7472411.

[90] J. Abdoli, M. Jia, and J. Ma. "Filtered OFDM: A new waveform for future wireless systems". *2015 IEEE 16th International Workshop on Signal Processing Advances in Wireless Communications (SPAWC)*. 2015, pp. 66–70. DOI: 10.1109/SPAWC.2015.7227001.

[91] T. Wild, F. Schaich, and Y. Chen. "5G air interface design based on Universal Filtered (UF-)OFDM". *19th International Conference on Digital Signal Processing*. 2014, pp. 699–704. DOI: 10.1109/ICDSP.2014.6900754.

[92] Vida Vakilian et al. "Universal-filtered multi-carrier technique for wireless systems beyond LTE". *IEEE Globecom Workshops (GC Wkshps)* (Dec. 2013), pp. 223–228. DOI: 10.1109/GLOCOMW.2013.6824990.

[93] T. Wild and F. Schaich. "A Reduced Complexity Transmitter for UF-OFDM". *IEEE 81st Vehicular Technology Conference (VTC Spring)*. 2015, pp. 1–6. DOI: 10.1109/VTCSpring.2015.7145643.

[94] M. Matthe et al. "A Reduced Complexity Time-Domain Transmitter for UF-OFDM". *IEEE 83rd Vehicular Technology Conference (VTC Spring)*. 2016, pp. 1–5. DOI: 10.1109/VTCSpring.2016.7504101.

[95] X. Zhang et al. "Filtered-OFDM - Enabler for Flexible Waveform in the 5th Generation Cellular Networks". *IEEE Global Communications Conference (GLOBECOM)*. 2015, pp. 1–6. DOI: 10.1109/GLOCOM.2015.7417854.

[96] P. Weitkemper et al. "On Regular Resource Grid for Filtered OFDM". *IEEE Commun. Lett.* 20.12 (2016), pp. 2486–2489. ISSN: 1089-7798. DOI: 10.1109/LCOMM.2016.2572183.

[97] M. Renfors et al. "Fast-convolution filtered OFDM waveforms with adjustable CP length". *IEEE Global Conference on Signal and Information Processing (GlobalSIP)*. 2016, pp. 635–639. DOI: 10.1109/GlobalSIP.2016.7905919.

[98] S. Wang, J. S. Thompson, and P. M. Grant. "Closed-Form Expressions for ICI/ISI in Filtered OFDM Systems for Asynchronous 5G Uplink". *IEEE Trans. Commun.* PP.99 (2017), pp. 1–1. ISSN: 0090-6778. DOI: 10.1109/TCOMM.2017.2698478.

[99] B. Farhang-Boroujeny and H. Moradi. "OFDM Inspired Waveforms for 5G". *IEEE Commun. Surveys Tuts.* 18.4 (2016), pp. 2474–2492. ISSN: 1553-877X. DOI: 10.1109/COMST.2016.2565566.

[100] D. Qu et al. "Improving Spectral Efficiency of FBMC-OQAM Through Virtual Symbols". *IEEE Trans. Wireless Commun.* 16.7 (2017), pp. 4204–4215. ISSN: 1536-1276. DOI: 10.1109/TWC.2017.2693277.

[101] Nicola Michailow et al. "Bit Error Rate Performance of Generalized Frequency Division Multiplexing". *IEEE Vehicular Technology Conference Fall*. Sept. 2012, pp. 1–5. ISBN: 978-1-4673-1881-5. DOI: 10.1109/VTCFall.2012.6399305.

[102] Siavash M Alamouti. "A simple transmit diversity technique for wireless communications". *IEEE J. Sel. Areas Commun.* 16.8 (1998), pp. 1451–1458.

[103] Thomas L Marzetta. "Noncooperative cellular wireless with unlimited numbers of base station antennas". *IEEE Trans. Wireless Commun.* 9.11 (2010), pp. 3590–3600.

[104] Rostom Zakaria. "Transmitter and receiver design for inherent interference cancellation in MIMO filter-bank based multicarrier systems". PhD thesis. Conservatoire national des arts et metiers - CNAM, Nov. 2012.

[105] Vincent Berg, Jean-Baptiste Dore, and Dominique Noguet. "A flexible FS-FBMC receiver for dynamic access in the TVWS". *Cognitive Radio Oriented Wireless Networks and Communications (CROWNCOM), 2014 9th International Conference on*. 2014, pp. 285–290.

[106] N. Michailow and G. Fettweis. "Low peak-to-average power ratio for next generation cellular systems with generalized frequency division multiplexing". *International Symposium on Intelligent Signal Processing and Communication Systems*. 2013, pp. 651–655. DOI: 10.1109/ISPACS.2013.6704629.

[107] M. Chafii et al. "A Necessary Condition for Waveforms With Better PAPR Than OFDM". *IEEE Trans. Commun.* 64.8 (2016), pp. 3395–3405. ISSN: 0090-6778. DOI: 10.1109/TCOMM.2016.2584068.

[108] T. A. Weiss and F. K. Jondral. "Spectrum pooling: an innovative strategy for the enhancement of spectrum efficiency". *IEEE Commun. Mag.* 42.3 (2004), S8–14. ISSN: 0163-6804. DOI: 10.1109/MCOM.2004.1273768.

[109] Musbah Shaat and Faouzi Bader. "Computationally Efficient Power Allocation Algorithm in Multicarrier-Based Cognitive Radio Networks: OFDM and FBMC Systems". *EURASIP J. Adv. Signal Process.* 2010.1 (2010), p. 528378. ISSN: 1687-6180. DOI: 10.1155/2010/528378.

[110] Alexandre Skrzypczak, Jacques Palicot, and Pierre Siohan. "OFDM/OQAM modulation for efficient dynamic spectrum access". *International Journal of Communication Networks and Distributed Systems* 8.3-4 (2012), pp. 247–266. DOI: 10.1504/IJCNDS.2012.046360.

[111] Yenming Huang, Borching Su, and I-Kang Fu. "Heterogeneous LTE downlink spectrum access using embedded-GFDM". *IEEE International Conference on Communications Workshops (ICC)*. 2016, pp. 474–479. DOI: 10.1109/ICCW.2016.7503832.

[112] N. Michailow et al. "Integration of a GFDM secondary system in an OFDM primary system". *2011 Future Network Mobile Summit*. 2011, pp. 1–8.

[113] Yahia Medjahdi et al. "Interference tables: a useful model for interference analysis in asynchronous multicarrier transmission". *EURASIP J. Adv. Signal Process.* 2014.54 (2014), pp. 1–17. ISSN: 1687-6180. DOI: 10.1186/1687-6180-2014-54. arXiv: 1006.4278.

[114] Yahia Medjahdi. "Interference modeling and performance analysis of asynchronous OFDM and FBMC wireless communication systems". PhD thesis. Conservatoire National des Arts et Métiers - CNAM, 2012.

[115] Yahia Medjahdi et al. "Performance analysis in the downlink of asynchronous OFDM / FBMC based multi-cellular networks". *IEEE Trans. Wireless Commun.* 10.8 (2011), pp. 2630–2639. ISSN: 15361276. DOI: 10.1109/TWC.2011.061311.101112.

[116] R. Ahmed, T. Wild, and F. Schaich. "Coexistence of UF-OFDM and CP-OFDM". *2016 IEEE 83rd Vehicular Technology Conference (VTC Spring)*. 2016, pp. 1–5. DOI: 10.1109/VTCSpring.2016.7504169.

[117] F. Kaltenberger et al. "Experimental analysis and simulative validation of dynamic spectrum access for coexistence of 4G and future 5G systems". *Networks and Communications (EuCNC), 2015 European Conference on*. 2015, pp. 497–501. DOI: 10.1109/EuCNC.2015.7194125.

[118] F. Kaltenberger et al. "Experimental analysis of 5G candidate waveforms and their coexistence with 4G systems". *Joint NEWCOM/COST Workshop on Wireless Communications (JNCW), October 14-15, 2015*. Barcelona, Spain, Oct. 2015.

[119] Keysight Technologies. *Sub-6 GHz Coexistence between 5G and 4G Waveforms*. Accessed Sep. 4, 2016. 2015. URL: http://goo.gl/6yOxMR.

[120] Greg Jue and Sangkyo Shin. *Implementing a Flexible Testbed for 5G Waveform Generation and Analysis - White Paper*. Tech. rep. Keysight Technologies, 2015.

[121] F. Wunsch et al. "A cognitive overlay system based on FBMC". *IEEE International Symposium on Dynamic Spectrum Access Networks (DySPAN)*. 2017, pp. 1–2. DOI: 10.1109/DySPAN.2017.7920782.

[122] F. Wunsch et al. "DySPAN Spectrum Challenge: situational awareness and opportunistic spectrum access benchmarked". *IEEE Transactions on Cognitive Communications and Networking* PP.99 (2017), pp. 1–1. DOI: 10.1109/TCCN.2017.2745682.

[123] M. Bellanger. "Physical layer for future broadband radio systems". *IEEE Radio and Wireless Symposium (RWS)*. 2010, pp. 436–439. DOI: 10.1109/RWS.2010.5434093.

[124] R. Datta et al. "FBMC and GFDM Interference Cancellation Schemes for Flexible Digital Radio PHY Design". *2011 14th Euromicro Conference on Digital System Design*. 2011, pp. 335–339. DOI: 10.1109/DSD.2011.48.

[125] Z. Kollár and P. Horváth. "Modulation schemes for cognitive radio in white spaces". *Radioengineering* 19.4 (2010), pp. 511–517.

[126] Hanna Bogucka, Paweł Kryszkiewicz, and Adrian Kliks. "Dynamic spectrum aggregation for future 5G communications". *IEEE Commun. Mag.* 53.5 (2015), pp. 35–43.

[127] Malte Schellmann et al. "FBMC-based air interface for 5G mobile: Challenges and proposed solutions". *Cognitive Radio Oriented Wireless Networks and Communications (CROWNCOM), 9th International Conference on*. 2014, pp. 102–107.

[128] Sener Dikmese et al. "Spectrum sensing and resource allocation for multicarrier cognitive radio systems under interference and power constraints". *EURASIP J. Adv. Signal Process.* 2014.1 (2014), p. 68.

[129] H. Zhang et al. "Noncooperative Multicell Resource Allocation of FBMC-Based Cognitive Radio Systems". *IEEE Trans. Veh. Technol.* 61.2 (2012), pp. 799–811. ISSN: 0018-9545. DOI: 10.1109/TVT.2011.2180743.

[130] H Zhang et al. "Spectral Efficiency Comparison of OFDM/FBMC for Uplink Cognitive Radio Networks". *EURASIP J. Adv. Signal Process.* 2010.1 (2010), p. 621808. ISSN: 1687-6180. DOI: 10.1155/2010/621808.

[131] H. Zhang et al. "Uplink Capacity Comparison of OFDM / FBMC Based Cognitive Radio Networks". *IEEE International Conference on Communications*. 2010, pp. 1–5. DOI: 10.1109/ICC.2010.5502008.

[132] Y. Li, X. Sha, and L. Ye. "Downlink Resource Sharing for D2D Communications in a Filtered OFDM System". *IEEE 83rd Vehicular Technology Conference (VTC Spring)*. 2016, pp. 1–6. DOI: 10.1109/VTCSpring.2016.7504201.

[133] Mithun Mukherjee et al. "Joint power and reduced spectral leakage-based resource allocation for D2D communications in 5G". *Lect. Notes Comput. Sci. (including Subser. Lect. Notes Artif. Intell. Lect. Notes Bioinformatics)*. Ed. by Guojun Wang et al. Vol. 9531. Cham: Springer International Publishing, 2015, pp. 244–258. ISBN: 9783319271392. DOI: 10.1007/978-3-319-27140-8_18.

[134] T. Haddadin et al. "An underlay communication channel for 5G cognitive mesh networks: Packet design, implementation, analysis, and experimental results". *IEEE International Conference on Communications Workshops (ICC)*. 2016, pp. 498–504. DOI: 10.1109/ICCW.2016.7503836.

[135] P. Wu, P. C. Cosman, and L. B. Milstein. "Subcarrier Assignment and Power Allocation for Device-to-Device Video Transmission in Rayleigh Fading Channels". *IEEE Transactions on Wireless Communications* PP.99 (2017), pp. 1–1. ISSN: 1536-1276. DOI: 10.1109/TWC.2017.2717823.

[136] J. Wang et al. "Nonlinear Inter-Band Subcarrier Intermodulations of Multi-RAT OFDM Wireless Services in 5G Heterogeneous Mobile Fronthaul Networks". *J. Lightw. Technol.* 34.17 (2016), pp. 4089–4103. ISSN: 0733-8724. DOI: 10.1109/JLT.2016.2584621.

[137] Q. Bodinier, F. Bader, and J. Palicot. "Modeling interference between OFDM/OQAM and CP-OFDM: Limitations of the PSD-based model". *23rd International Conference on Telecommunications (ICT)*. 2016, pp. 1–7. DOI: 10.1109/ICT.2016.7500462.

[138] Q. Bodinier et al. "5G waveforms for overlay D2D communications: Effects of time-frequency misalignment". *IEEE International Conference on Communications (ICC)*. 2016, pp. 1–7. DOI: 10.1109/ICC.2016.7511285.

[139] Q. Bodinier, F. Bader, and J. Palicot. "Coexistence in 5G: Analysis of Cross-Interference between OFDM/OQAM and Legacy Users". *IEEE Globecom Workshops (GC Wkshps)*. 2016, pp. 1–6. DOI: 10.1109/GLOCOMW.2016.7848862.

[140] Q. Bodinier, F. Bader, and J. Palicot. "On Spectral Coexistence of CP-OFDM and FB-MC Waveforms in 5G Networks". *IEEE Access* 5 (2017), pp. 13883–13900. DOI: 10.1109/ACCESS.2017.2723822.

[141] D. Richard III Brown and Andrew G. Kelin. "Synchronization Concepts". *Coordinated Multi-Point in Mobile Communications: From Theory to Practice*. Ed. by Patrick Marsch and Gerhard P. Fettweis. Cambridge Univeristy Press, 2011. Chap. 8.1, pp. 161–170.

[142] M. Renfors, J. Yli-Kaakinen, and M. Valkama. "Power Amplifier Effects on Frequency Localized 5G Candidate Waveforms". *22th European Wireless Conference*. 2016, pp. 1–5.

[143] Q. Bodinier, F. Bader, and J. Palicot. "Coexistence of filter banks and CP-OFDM: What are the real gains?" *International Symposium on Wireless Communication Systems (ISWCS)*. 2016, pp. 628–632. DOI: 10.1109/ISWCS.2016.7600980.

[144] A. Bourrous et al. "ACCENT5: a Vision for D2D Communications within 5G Networks". *14th International Symposium on Wireless Communication Systems (ISWCS)*. 2017.

[145] T. Ihalainen, A. Viholainen, and M. Renfors. "On spectrally efficient multiplexing in cognitive radio systems". *Wireless Pervasive Computing, 2008. ISWPC 2008. 3rd International Symposium on*. 2008, pp. 675–679. DOI: 10.1109/ISWPC.2008.4556295.

[146] C. Sexton et al. "Coexistence of OFDM and FBMC for Underlay D2D Communication in 5G Networks". *2016 IEEE Globecom Workshops (GC Wkshps)*. 2016, pp. 1–7. DOI: 10.1109/GLOCOMW.2016.7848863.

[147] Conor Sexton et al. "Coexistence between D2D and Cellular Communications Using Multiple Waveforms in 5G". *IEEE Trans. Vehicular Tech.* (2017 (submitted)).

[148] J Han et al. "Bipartite matching approach to optimal resource allocation in device to device underlaying cellular network". *Electron. Lett.* 50.3 (2014), pp. 212–214. ISSN: 0013-5194.

[149] L Wang and H Wu. "Fast Pairing of Device-to-Device Link Underlay for Spectrum Sharing With Cellular Users". *IEEE Commun. Lett.* 18.10 (2014), pp. 1803–1806. ISSN: 1089-7798.

[150] Gábor Fodor et al. "Design aspects of network assisted device-to-device communications". *IEEE Commun. Mag.* 50.3 (2012), pp. 170–177. ISSN: 01636804. DOI: 10.1109/MCOM.2012.6163598.

[151] T. D. Novlan et al. "Analytical Evaluation of Fractional Frequency Reuse for OFDMA Cellular Networks". *IEEE Transactions on Wireless Communications* 10.12 (2011), pp. 4294–4305. ISSN: 1536-1276. DOI: 10.1109/TWC.2011.100611.110181.

[152] H. S. Chae et al. "Radio resource allocation scheme for device-to-device communication in cellular networks using fractional frequency reuse". *Proc. of The 17th Asia Pacific Conference on Communications (APCC)*. Kota Kinabalu, Oct. 2011, pp. 58–62.

[153] Nazmus Saquib, Ekram Hossain, and Dong Kim. "Fractional frequency reuse for interference management in LTE-advanced hetnets". *IEEE Wireless Commun. Mag.* 20.2 (Apr. 2013), pp. 113–122.

[154] Thomas Novlan et al. "Comparison of Fractional Frequency Reuse Approaches in the OFDMA Cellular Downlink". *Proc. of 2010 IEEE Global Communications Conference (Globecom)*. Miami, Dec. 2010, pp. 1–5.

[155] Christopher Cox. "An introduction to LTE: LTE, LTE-advanced, SAE and 4G mobile communications". John Wiley & Sons, 2012. Chap. 8.8.1, pp. 157–158.

[156] *Universal Mobile Telecommunications System (UMTS); User Equipment (UE) radio transmission and reception (FDD)*. Tech. rep. TS 25.101 V14.0.0. 3GPP, May 2017.

[157] *LTE; Evolved Universal Terrestrial Radio Access (E-UTRA); Radio Frequency (RF) system scenarios*. Tech. rep. TR 36.942 V14.0.0. 3GPP, Apr. 2017.

[158] Konstantinos N. Maliatsos, Eleftherios Kofidis, and Athanasios G. Kanatas. "A Unified Multicarrier Modulation Framework". *CoRR* abs/1607.03737 (2016). URL: http://arxiv.org/abs/1607.03737.

[159] L. E. Doyle et al. "Experiences from the Iris Testbed in Dynamic Spectrum Access and Cognitive Radio Experimentation". *2010 IEEE Symposium on New Frontiers in Dynamic Spectrum (DySPAN)*. 2010, pp. 1–8. DOI: 10.1109/DYSPAN.2010.5457835.

[160] C. M. Chen et al. "Exploration of User Separation Capabilities by Distributed Large Antenna Arrays". *2016 IEEE Globecom Workshops (GC Wkshps)*. 2016, pp. 1–6. DOI: 10.1109/GLOCOMW.2016.7848903.

[161] A. Massouri et al. "CorteXlab: An open FPGA-based facility for testing SDR amp; cognitive radio networks in a reproducible environment". *2014 IEEE Conference on Computer Communications Workshops (INFOCOM WKSHPS)*. 2014, pp. 103–104. DOI: 10.1109/INFCOMW.2014.6849176.

[162] M. Naoues, Q. Bodinier, and J. Palicot. "Cognitive Green Radio for Energy-Aware Communications". *URSI Scientific Days*. 2016.

[163] T. Vial et al. "A Short Review of Current Challenges and Potential Applications of Full Duplex in Wireless Networks". *32nd International Union of Radio Science General Assembly & Scientific Symposium (URSI GASS)*. 2017.